

Analysis Note for “Coherent diffractive photoproduction of ρ^0 mesons on gold nuclei at RHIC”

R. Debbe, S. Klein

February 22, 2016

Abstract

This note is a compilation of a set of documents related to the run 10 analysis of ρ^0 meson production and the measurement of a diffraction pattern off the Au nuclei. The analysis that produced the paper is described in details for each item listed in the “Contents” section. This is mainly a reference document and the authors expect the reader to approach it with specific queries and to use the Content section as guidance, otherwise the document may appear too extended.

Contents

1	Paper title	3
2	Introduction	4
2.1	A compilation of relevant physics for this work	4
2.2	Layout of this note	12
3	Data collection and triggering	12
4	Datasets	14
4.1	Raw data and MuDst	14
4.2	Monte-Carlo sets	14
4.3	UPC output pico DST	15
5	Offline production of pico DST with StPeCMaker	16
5.1	Vertex selection with StPeCMaker	20
6	Luminosity	24
7	Full Chain correction with embedded events	26
7.1	Private embedding process summary	27
7.2	Official embedding process at pdsf	27
7.3	Reading the mixed embedding MuDst	28
7.4	TOF geometry, alignment, detector response and veto use in trigger	33
7.5	BBC geometry, detector response and veto use in trigger	41
7.6	Track TOF matching extracted from embedding and from data	42
7.6.1	Introduction	42
7.6.2	Matching tracks to TOF hits	43
7.7	Extraction of efficiencies from the Mixed embedding	47
8	Analysis	53
8.1	Data (2010) pico DST location	53
8.2	Mixed Embedding (SL10k_embed + .DEV2) pico DST location	53
8.3	Performance monitoring throughout the run	53
8.4	UPC_Main definition and XnXn cross section	57
8.5	Comparison between data and the RELDIS event generator	60
8.5.1	Comparison of all collected UPC_Main events and RELDIS generated events	60
8.5.2	Reducing background with selected events with an exclusive ρ^0 meson	64
8.5.3	Extrapolation of data from 1-4 neutrons to 1-14 neutrons	69
8.5.4	Correction from UPC_Main to XnXn cross sections using STARlight	70
8.6	Number of events analyzed	72

8.7	The processData analysis macro	73
8.8	Information extracted from the Mixed embedding project	77
8.9	Relative t resolution	78
9	Results	82
9.1	Cross-section $d\sigma/dM$ as function of pion pair mass	82
9.1.1	The phase of the ω meson production amplitude	86
9.2	Cross-section $d\sigma/dy$ in rapidity	89
9.3	Correction to event loss due to vertex finder track assignement to vertices	89
9.4	Diffraction pattern $d\sigma/dt$	94
9.5	Fits to coherent and incoherent portions of the cross section	95
9.6	Comparison of integrated cross sections	96
10	Systematic Uncertainties discussion	107
10.1	Procedure	107
10.2	Systematic uncertainties in invariant mass distributions	107
10.3	Systematic uncertainties in the ω meson phase	116
10.4	Systematic uncertainties in rapidity distributions	118
10.5	Systematic uncertainties in -t distribution	124
10.6	Summary of all systematic uncertainties identified for the ρ^0 diffraction paper	127
10.6.1	Common uncertainties	127
10.6.2	Point-to-point uncertainties for Figure 3	128
10.6.3	Systematic uncertainties in the ω meson phase	135
10.6.4	Point-to-point uncertainties for Figure 4	137
10.6.5	Point-to-point uncertainties for Figure 6	137
11	Appendix	140
11.1	Enhancing f2 and ρ' signal with pair p_T cuts	140
12	Appendix 2: Reconstruction efficiency (first embedding request)	147

1 Paper title

Coherent diffractive photoproduction of ρ^0 mesons on gold nuclei at RHIC

The paper start with a description of the physics in Ultra-Peripheral Collisions and a brief survey models available to describe them. The data collection and the analysis are then described in detail followed by a discussion of the Mutual Electromagnetic dissociation that accompany the ρ^0 photoproduction as it is studied with our triggers based on the response of both ZDC detectors. One of the results presented in this paper is based on the fit to the invariant mass distribution of selected pion pairs. The fit include the interplay of three of the photon states, non resonant pion pairs, the ρ^0 meson and the ω meson as well. Rapidity distribution of coherent ρ^0 mesons are presented as extracted from the so called 1n1n events where one neutron is required in both ZDCs. We then use the STARlight event generator to scale it to the distribution for XnXn events and compare that rapidity distribution to previous STAR measurement (2007). Fully corrected differential cross sections as function of the third Mandelstam invariant t are them formed for both 1n1n and XnXn events. These distributions show clearly the presence of coherent and incoherent components. The incoherent tail at high t is fit with an standard function called “dipole form factor”. The fit is then subtracted from the total differential cross section to isolate the coherent component. The coherent component for 1n1n and XnXn is another main result presented in this paper. These distribution are dominated by a first peak which decays exponentially, followed by a well defined first dip and hints of more dips, specially in the 1n1n distribution. We have applied a Fourier-Bessel transform to extract a density distribution in the transverse plane. All results are presented with systematic uncertainties.

2 Introduction

Starting with the 2010 run, which collided Au ions at 200 GeV in the center of mass, the RHIC program started its gradual evolution into its high intensity program labelled RHIC II. The STAR UPC program collected 38 million with its main trigger. Analysis of data set of such size has the extraction of a diffraction pattern as the ρ^0 scatters off one of the Au ions. The first public presentation of such result occurred on October 2011 at the DNP meeting. A second version of that analysis, which included tracking and acceptance corrections obtained from an embedding project as well as a tentative trigger efficiency extracted from data, was presented in April of 2012 at the 28th Winter Workshop on Nuclear Dynamics together with a proceedings contribution: [arXiv:1209.0743](https://arxiv.org/abs/1209.0743) Further work to prepare for a publication made it clear that extracting a value for the trigger efficiency from data would not be the appropriate way because of uncertainties introduced by the use of different vertex finding algorithm in the data set used made it necessary to redefine the basic approach to analyze these data. The diffraction pattern presented publicly has not changed but its normalization needs a complete redo.

2.1 A compilation of relevant physics for this work

From section 15.4 (page 719) of Classical Electrodynamics (J.D. Jackson (Second edition): Weizacker-Williams method of virtual quanta: The flux of photons as shown in Fig. 1:

$$dI_1/d\omega \sim |E_2(\omega)|^2$$

(completely longitudinal) and

$$dI_2/d\omega \sim |E_2(\omega)|^2 \sim 1/\gamma^2$$

The duration of the I_1 pulse is: $\Delta t \sim b\gamma/v$ where b is the impact parameter, γ and v are the Lorentz factor and velocity of the charged particle in a frame where the target is at rest. In colliders, the target is also highly relativistic and the connection to the collider Lorentz factor $\gamma = 2\gamma_{collider}^2 - 1$. At RHIC $\gamma_{collider} = 108$ which makes the value of γ as high as 23327 The I_2 flux can then be neglected because of the $1/\gamma^2$ term.

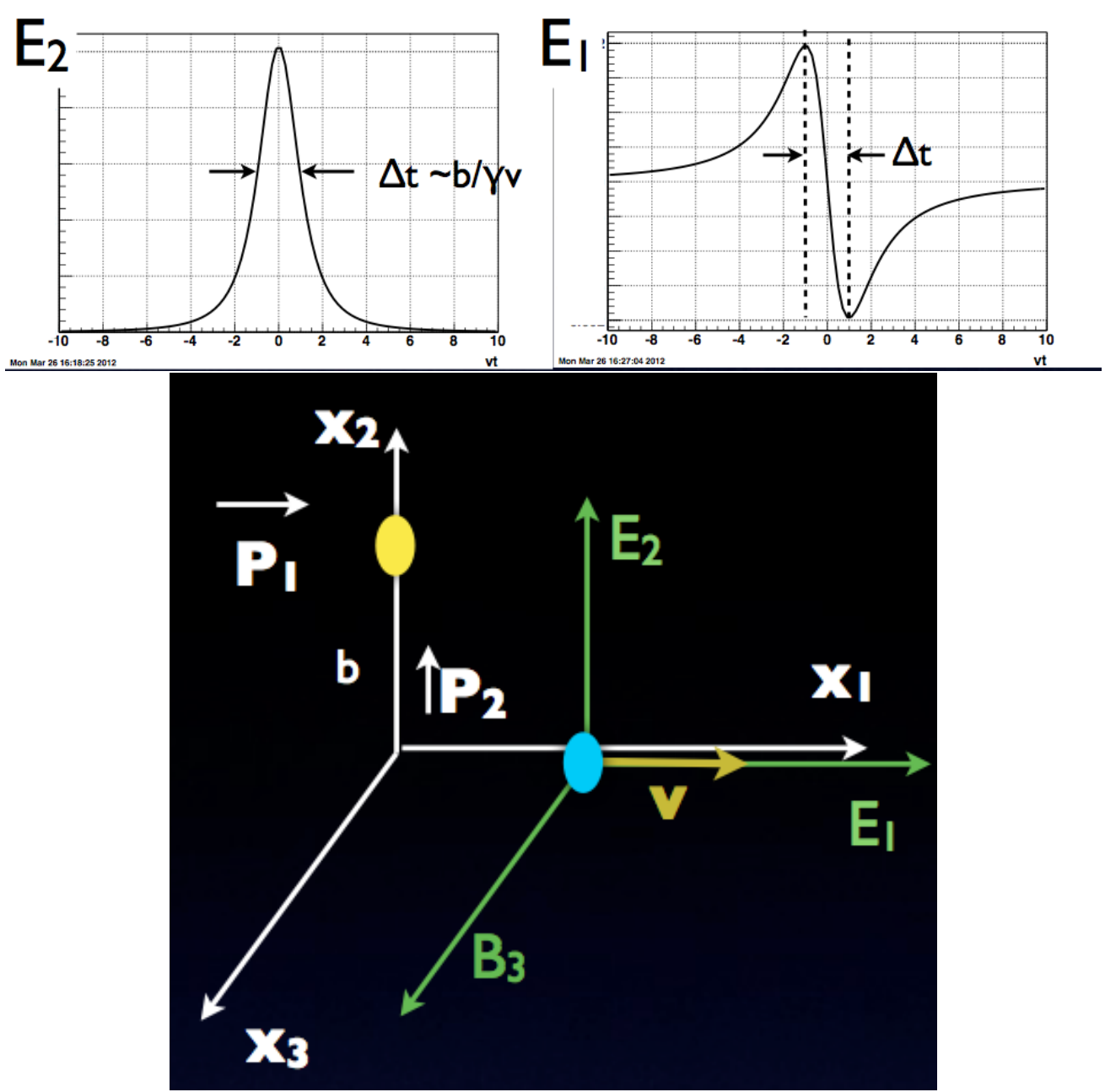


Figure 1: Top panels show outlines of the Lorentz contracted electric fields centered at the position of the target. The particle producing these fields moves with velocity v at an impact parameter b , as indicated in the lower panel.

A Fourier transformation from t to energy for a narrow pulse in time will produce a flat distribution in frequency with a maximum $\hbar\omega = \hbar/\Delta t = \gamma\hbar c/b$ which translates into a 382 GeV photon on the target rest frame.

Accelerator	Ions	Max. Energy per nucleon pair (CM)	Luminosity	Max. γp	Max. $\gamma\gamma$ energy
CERN SPS	Pb+Pb	17 GeV	—	3.1 GeV	0.8 GeV
RHIC	Au+Au	200 GeV	$4 \times 10^{26} \text{ cm}^{-2} \text{ s}^{-1}$	<u>24 GeV</u>	6.0 GeV
RHIC	p+p	500 GeV	$6 \times 10^{30} \text{ cm}^{-2} \text{ s}^{-1}$	79 GeV	50 GeV
LHC	Pb+Pb	5.6 TeV	$10^{27} \text{ cm}^{-2} \text{ s}^{-1}$	705 GeV	178 GeV
LHC	p+p	14 TeV	$10^{34} \text{ cm}^{-2} \text{ s}^{-1}$	3130 GeV	1400 GeV
Tevatron	p+ \bar{p}	20 TeV	$5 \times 10^{31} \text{ cm}^{-2} \text{ s}^{-1}$	320 GeV	200 GeV

Figure 2: Table compiled in Bertulani et al. summarizes UPC environment achievable at different accelerators.

The following is just cut and paste from Spencer's recent review [7]

"One nucleus emmits a photon, which fluctuates into a quark-antiquark pair , which then scatters elastically (but hadronically) emerging as a real vector meson; the cross-section depends on the size of the (qq) dipole. This occurs via meson (at low energies) and Pomeron (in modern terms. a gluon ladder) exchange. In perturbative QCD, the cross-section depends on the gluon density g of the target nucleus, $\sigma \propto g^2(x, Q^2 \sim m_q^2)$ where m_q is the quark mass. The Bjorken-x of the gluon is determined by kinematics, $\gamma x M_p = M_v/2\exp(\pm y)$, where M_p is the proton mass, M_v is the vector meson mass, and y is its rapidity. Here, γ is the Lorentz boost of one nucleus, in the lab frame. The \pm is because of the ambiguity as to which nucleus emitted the photon and which is the target." This translates on access to x ranging from 0.001 up to 0.01 for $-1 < y < 1$.

The claim the UPC events at RHIC involve the elastic scattering of vector mesons of the target nuclei through the exchange of a Pomeron relies on a compilation of cross sections measured at HERA shown in Fig. ??.

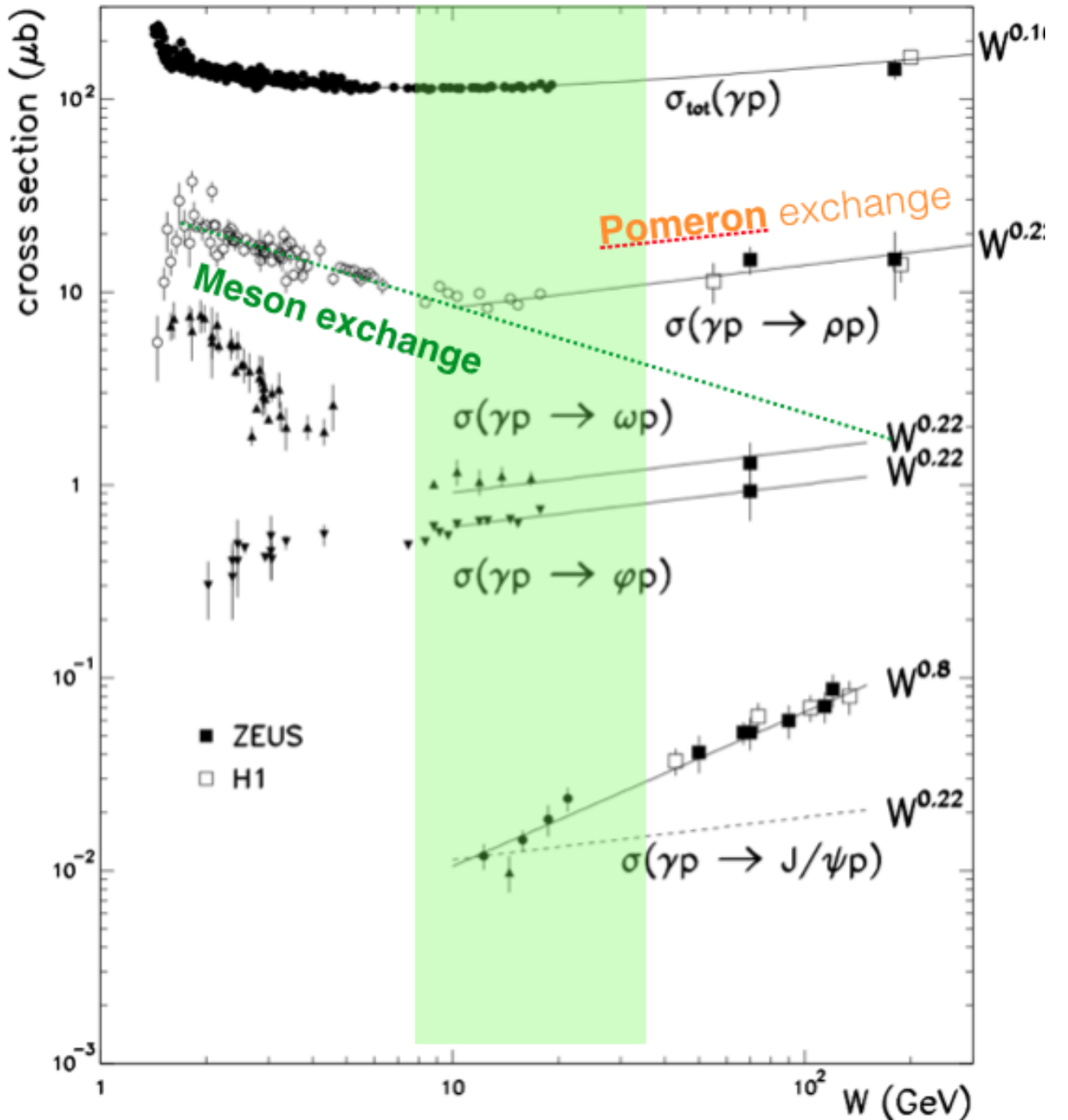


Figure 3: Cross-sections for exclusive vector meson photoproduction at HERA compiled by J.A. Crittenden. A clear switch is visible for all mesons included in the review at the same value of W the photon-nucleon center of mass energy around 7 GeV. The negative slope part below that value is well described within the context of a Regge exchange (pion, pion pairs, sigma mesons). At higher energies the slope turns positive and the cross-sections grow slowly as a power of W , this region is well described with the so called Pomeron object or a gluon ladder with vacuum quantum numbers. The region covered by STAR $|y| < 0.7$ is shown with the green band.

I insert here a document produced by Boris. The green band showing the RHIC reach in photon-nucleon center of mass has been calculated using equations from that document: To get the lower photon-nucleon center of mass energy we used Boris' equation 4 with $y=-0.7$ and have the value $W_{min} = 8.8$ GeV. To find the maximum photon-nucleon energy that can be achieved at RHIC we need to first find the highest photon energy in the lab. frame with equation 16 ($k_{max}^{lab} = 3.0$ GeV/c). In the lab frame the invariant photon-nucleon center of mass energy is written: $(E_\gamma + E_N)^2 - (k - P)^2$ which can also be written as $m_N^2 + Q^2 + 2(E_\gamma E_N + kP)$ with $Q^2 = E - \gamma^2 - k^2$. The assumption that m_N and Q^2 are small compared to the other terms, which implies that $E_\gamma = k$ and $E_N = P + \sqrt{s_{NN}}$ produced the final value: $W_{\gamma N} = \sqrt{2k\sqrt{s_{NN}}} = 34.6$ GeV.

1 Minimum Required Photon-Nucleon CM Energy

In the lab frame the limiting case for the minimum photon-nucleon center-of-mass energy $W_{\gamma N}$ is forward scattering, where the 4-momentum of the photon $k^\mu = (E_\gamma, \vec{k})$ and that of the vector meson $p^\mu = (E_V, \vec{p})$ are approximately equal $k^\mu \approx p^\mu$:

$$(1) \quad \begin{aligned} W_{\gamma N}^2 &= (k^\mu + P^\mu)^2 \\ &\approx (p^\mu + P^\mu)^2 \\ &= m_N^2 + m_V^2 + 2(E_V E_N + p \cdot P) \end{aligned}$$

where $P^\mu = (E_N, \vec{P})$ is the 4-vector of the target nucleon. The energy E_N of the target nucleon is given by the center of mass energy $E_N = \sqrt{s_{NN}}/2$. Since $E_N \gg m_{N,V}$ we can neglect the squared mass terms in eq. 1 and can set $P \approx E_N$ so that

$$(2) \quad W_{\gamma N}^2 \approx \sqrt{s_{NN}} (E_V + p)$$

By introducing the transverse mass $E_T \equiv \sqrt{m_V^2 + p_T^2} = \sqrt{E_V^2 - p^2 + p_T^2} = \sqrt{E_V^2 - p_z^2}$ and by multiplying eq. 2 with $1 = E_T/E_T$ we get

$$(3) \quad W_{\gamma N}^2 = \sqrt{s_{NN}} \frac{E_T}{\sqrt{E_V^2 - p_z^2}} (E_V + p)$$

$W_{\gamma N}$ is minimal when the transverse momentum p_T of the vector meson is zero, so that $p = p_z$ and thus

$$(4) \quad \begin{aligned} W_{\gamma N, \text{min}}^2 &= \sqrt{s_{NN}} m_V \frac{E_V + p_z}{\sqrt{E_V^2 - p_z^2}} \\ &= \sqrt{s_{NN}} m_V \frac{\sqrt{E_V + p_z}}{\sqrt{E_V - p_z}} \\ &= \sqrt{s_{NN}} m_V e^y \\ W_{\gamma N, \text{min}} &= \sqrt{\sqrt{s_{NN}} m_V} e^{y/2} \end{aligned}$$

For $\sqrt{s_{NN}} = 200$ GeV this gives

$$(5) \quad \begin{aligned} W_{\gamma N, \text{min}}(y = -1) &= 7.55 \text{ GeV} \\ W_{\gamma N, \text{min}}(y = 0) &= 12.45 \text{ GeV} \\ W_{\gamma N, \text{min}}(y = +1) &= 20.53 \text{ GeV} \end{aligned}$$

2 Minimum Required Photon Energy

The minimum photon-nucleon center-of-mass energy can be related to a minimum photon energy in the lab frame:

$$(6) \quad \begin{aligned} W_{\gamma N}^2 &= (k^\mu + P^\mu)^2 \\ &= m_N^2 - Q^2 + 2(E_\gamma E_N + k \cdot P) \end{aligned}$$

With $Q \ll E_\gamma$ so that $k \approx E_\gamma$ and with $m_N \ll E_N = \sqrt{s_{NN}}/2$ so that $P \approx E_N$

$$(7) \quad W_{\gamma N} \approx \sqrt{2k\sqrt{s_{NN}}}$$

By setting the above equation equal to eq. 4 we get

$$(8) \quad W_{\gamma N, \min} = \sqrt{\sqrt{s_{NN}} m_V e^y} = \sqrt{2k\sqrt{s_{NN}}}$$

so that

$$(9) \quad k_{\min} = \frac{m_V}{2} e^y$$

For $m_V = 775.5$ MeV this gives (in the lab frame)

$$(10) \quad \begin{aligned} k_{\min}^{\text{lab}}(y = -1) &= 0.1426 \text{ GeV}/c \\ k_{\min}^{\text{lab}}(y = 0) &= 0.3878 \text{ GeV}/c \\ k_{\min}^{\text{lab}}(y = +1) &= 1.054 \text{ GeV}/c \end{aligned}$$

The momentum in the target rest frame is given by

$$(11) \quad k^{\text{target}} = \gamma_L \beta_L E_\gamma^{\text{lab}} + \gamma_L k^{\text{lab}}$$

Since γ_L is large, $\beta_L \approx 1$. The photons are quasi-real (small Q^2) so that $E_\gamma^{\text{lab}} \approx k^{\text{lab}}$ and thus

$$(12) \quad \begin{aligned} k_{\min}^{\text{target}} &\approx 2\gamma_L k_{\min}^{\text{lab}} \\ k_{\min}^{\text{target}}(y = -1) &= 30.81 \text{ GeV}/c \\ k_{\min}^{\text{target}}(y = 0) &= 83.75 \text{ GeV}/c \\ k_{\min}^{\text{target}}(y = +1) &= 227.7 \text{ GeV}/c \end{aligned}$$

In a similar way the minimum photon momentum in the source rest frame can be estimated using

$$(13) \quad k^{\text{source}} = -\gamma_L \beta_L E_\gamma^{\text{lab}} + \gamma_L k^{\text{lab}}$$

Again $E_\gamma^{\text{lab}} \approx k^{\text{lab}}$, but here $\beta_L = \sqrt{1 - 1/\gamma_L^2} \approx 1 - 1/(2\gamma_L^2)$ so that

$$(14) \quad \begin{aligned} k_{\min}^{\text{source}} &\approx \frac{k_{\min}^{\text{lab}}}{2\gamma_L} \\ k_{\min}^{\text{source}}(y = -1) &= 0.660 \text{ MeV}/c \\ k_{\min}^{\text{source}}(y = 0) &= 1.795 \text{ MeV}/c \\ k_{\min}^{\text{source}}(y = +1) &= 4.880 \text{ MeV}/c \end{aligned}$$

3 Maximum Photon Energy

Photons are emitted coherently by the nuclei, so that the uncertainty relation sets a lower limit for the photon wavelength and an upper limit for the photon momentum. For gold nuclei with a radius of $R_A = 7 \text{ fm}$ the photon momentum in the source rest frame is thus

$$(15) \quad k^{\text{source}} \lesssim \frac{\hbar}{R_A} \equiv k_{\max}^{\text{source}} = 28 \text{ MeV}/c$$

In the lab frame the nuclear radius is Lorentz-contracted $R_A^{\text{lab}} = R_A/\gamma_L$ so that

$$(16) \quad k_{\max}^{\text{lab}} = \frac{\hbar}{R_A/\gamma_L} = \gamma_L k_{\max}^{\text{source}} = 3.0 \text{ GeV}/c$$

In the target rest frame the effective Lorentz-contraction of the nuclear radius is determined by velocity addition theorems (using $\gamma_L = \cosh y_L$): $\gamma_{\text{eff}} = \cosh(2y_L) = 2 \cosh^2(y_L) - 1 = 2\gamma_L^2 - 1$

$$(17) \quad k_{\max}^{\text{target}} = \frac{\hbar}{R_A/\gamma_{\text{eff}}} = (2\gamma_L^2 - 1)k_{\max}^{\text{source}} = 653 \text{ GeV}/c$$

2.2 Layout of this note

Because of the volume of this note a complete reading would be a tedious task, instead, it is organized as a record of every step of the analysis and each section and its subsections should be enough to provide the relevant details for any question that may arise about the analysis. Section 3 describes that data collection with some emphasis on the UPC_Main trigger. Section 4 has a description and locations where the different data sets used in this analysis are to be found. Section 5 describes in detail the UPC micro DST maker StPeCMaker. Section 6 describes how the luminosity used to normalize the distributions obtained in this analysis was obtained. Section 7 goes into great detail to described the embedding of MC events in zerobias data events to extract corrections to losses introduced by geometrical acceptances, detector inefficiencies and background contaminations on the trigger. Section 12 is a brief description of an earlier embedding exercise mainly to get an idea of the efects of the TPC acceptance combined with its tracking efficiency. In Section 8 we describe the actual analysis of the data to generate distributions in rapidity and $-t$ followed by their normalization and correction using information extracted from embedding. Section 9 describes the estimate of the number of systematic uncertainties identified in this analysis. Section 10 describes the results obtained in this analysis. Some plots related to the f_2 and ρ' mesons is placed in Appendix A mainly as a repository.

3 Data collection and triggering

The data were collected with two triggers UPC_Main and UPC_Topo. The UPC_Main trigger relies on rapidity gaps defined by the small BBC tiles ($3 < \eta < 5$) on both sides of the collisions, low activity in the TPC detected with the TOF system ($1 < T_{of\,Hits} < 7$) supplemented with signal corresndong to 1 to ~ 6 beam momentum neutrons detected with the Zero degree calorimeters (ZDC). Figure 4 describes how the trigger is built and also provides some thresholds for the BBC small tile veto definition. (This information and much more can be obtained from STAR RunLog:

<http://online.star.bnl.gov/RunLogRun10/>

under the “trigger Details” section of a particular run.

The total number of events triggered by UPC_Main that were reconstructed in P10ik is 38.254 million events and the outputs are stored in 46942 files.

Information relevant to all STAR data productions is available at:

<http://www.star.bnl.gov/public/comp/prod/ProdList.html>

Details about the UPC streams are listed in:

http://www.star.bnl.gov/devcgi/RetriveTrigID.pl?rtrig=AuAu200_production;rprod=P10ik;rstream=upc

The page mentioned above does not list the UPC_Topo trigger, and as this analysis is focused on the UPC_Main trigger, the actual number of Topo triggers needs to be extracted from the data in a possible future analysis.

Trigger Definitions:

Detector bits (detector live / detector fired)									Condition 1	
	<i>FTPC</i>	<i>PP2PP</i>	<i>ETOW</i>	<i>BTOW</i>	<i>BSMD</i>	<i>TOF</i>	<i>ESMD</i>	<i>TPX</i>		
UPC_main	0/-	+/-	+/-	+/-	+/-	+/-	+/-	+/-	TOFmult1(5) TOFmult2(6) BBC-E(17) BBC-W(18) ZDC-TAC(22) ZDC-E(23) ZDC-W(24) ZDC-UPC(25) Laser_protection(96)	-
BBCsmall-WestADCsum-th (8)									-1	50
BBCsmall-WestTAC-select (8)									-1	0
BBC_QT_E_Sm_ADC_Th (9)									20	5

Figure 4: Definition of the UPC_Main trigger as it appears in the STAR RunLog page. Detector bits indicate the detectors read whenever the UPC_Main trigger tagged an event. The conditions listed on the right provide additional details on how the trigger is formed. Those conditions are described in the text. Bottom panel shows the thresholds on individual small BBC tiles as well as the sum of them.

4 Datasets

4.1 Raw data and MuDst

Data collected during the 2010 Au+Au at $\sqrt{s_{NN}} = 200$ GeV with the UPC triggers UPC_Main and UPC_Topo were written to disk through dedicated stream called st_upc. Production P2010ik of that data reconstructed tracks registered in the TPC gas volume, and transformed energy deposited in the complement of STAR detectors into physics related quantities. For the record, the arguments used to drive the complete reconstruction chain is listed below:

P10ik	rawData	SL10k	ry2010	DbV20101213 P2010a -VFMinit VFPPVnoCTB beamline pmdReco btof BEmcChkStat Corr4 OSpaceZ2 OGridLeak3D	auau 200GeV st_upc data, run 2010 production, DbV for fixed BSMD mapping, request for QM2011
-------	---------	-------	--------	---	--

Figure 5: Bfc arguments for UPC processing of 2010 data. Of particular interest for this analysis is the selection of the vertex finder algorithm “VFPPVnoCTB” and its reliance on beam line coordinates.

One of the outputs of the P10ik production, the so called data summary files (MuDst) are placed on disks to be read for further analysis within the STAR scheduler system. An example of a driver for the system is listed below:

```
<?xml version="1.0" encoding="utf-8" ?>
<job maxFilesPerProcess="60" minFilesPerProcess="5" filesPerHour="100"
      fileListSyntax="xrootd">
<command>
starpro
cd /star/u/ramdebbe/UPC/run10AuAu200/duplicateEvents/fromFileCatalogue
root4star -q -b /star/u/ramdebbe/UPC/run10AuAu200/duplicateEvents/
fromFileCatalogue/doMuEvent_muDstSteve.C
\(\"$FILELIST\", \"$SCRATCH/$JOBID.tree.root\"\  

</command>
<stdout URL="file:/star/data06/UPC/ramdebbeLog/$JOBID.out"/>
<stderr URL="file:/star/data06/UPC/ramdebbeLog/$JOBID.err"/>

<input URL="catalog:star.bnl.gov?production=P10ik,trgsetupname=AuAu200_production,
filetype=daq_reco_MuDst,
storage=local,filename~st_upc,runnumber[] 11061001-11077018" nFiles="all" />

<output fromScratch="*.root" toURL="file:/star/data06/UPC/run10AuAu200tree/
fromFileCatalogue/" />
</job>
```

4.2 Monte-Carlo sets

The Starlight dataset we use for all this project has been produced with STARlight version V1.1.1... extracted from Hepforge svn repository revision 166. We run it with the following slight.in file:

```
BEAM_1_Z      = 79
BEAM_1_A      = 197
BEAM_2_Z      = 79
BEAM_2_A      = 197
BEAM_1_GAMMA = 108.4 #Gamma of the colliding ion 1
BEAM_2_GAMMA = 108.4 #Gamma of the colliding ion 2
W_MAX         = 1.522
W_MIN         = 0.279
W_N_BINS     = 100
```

```

RAP_MAX      = 5.5
RAP_N_BINS   = 80
PROD_MODE    = 2
N_EVENTS     = 50
PROD_PID     = 113
RND_SEED     = 2560107
OUTPUT_FORMAT = 2
BREAKUP_MODE = 2
INTERFERENCE = 0
IF_STRENGTH  = 1.
COHERENT     = 1
INCO_FACTOR  = 0.6
BFORD        = 9.5
INT_PT_MAX   = 0.24
INT_PT_N_BINS= 120
CUT_ETA      = 0
ETA_MAX      = 1.0
ETA_MIN      = -1.0
CUT_PT       = 0
PT_MAX       = 0.1
PT_MIN       = 0.
XSEC_METHOD  = 1 # Set to 0 to use old method for calculating gamma-gamma luminosity
N_THREADS    = 1 # Number of threads used for calculating luminosity (when using the new method)
PYTHIA_FULL_EVENTRECORD = 0 # Write full pythia information to output (vertex, parents, daughter etc).

```

The ascii file is stored in:

/star/data01/pwg/ramdebbe/run10AuAu200tree/starlight/starlight_113_coherent_XnXn_5M.out
the root file with normalized distribution in rapidity, transverse momentum and t can be found in:
/star/data01/pwg/ramdebbe/run10AuAu200tree/starlight/starLightOutput_113_coherent_XnXn_1M_1MAY.root
We are using PROD_ID = 113 (pure ρ^0 because the data is corrected to subtract the contribution from the non-resonant pion continuum.

4.3 UPC output pico DST

The latest version of the output pico dst is placed in the data01 disk:

/star/data01/pwg/ramdebbe/run10AuAu200tree/latestVersion14_OCT/

```

20D26F19B0594F9815FF7B3213CE7D99_*.tree.root  2 files day11 run 35 to run 93
323C83D2C09E638B9DA922CF131B2F9C_*.tree.root  89 files day12 run  2 to day17 run 59
E7E889195BB8897DAF83775E6D0BF9D1_*.tree.root 168 files day19 run  2 to day31 run 89
1E182B931886673782B0B862377A01C2_*.tree.root 109 files day32 run 11 to day38 run 69
8C3E4A15E5359EDAF9CEA5FB2A3E3D82_*.tree.root 422 files day39 run  1 to day60 run 82
052604A8431B228277E3182A5672F287_*.tree.root 302 files day61 run  1 to day77 run 18
28D35F20D39D0FAC125BEF1D0933F5EB_*.tree.root recovered jobs from 1E182... set

```

5 Offline production of pico DST with StPeCMaker

Once all events resulting from the official STAR offline production are available, UPC events are selected with a root base analysis based on a single maker named StPeCMaker. All relevant source code files are in the stored in CVS and can be browsed in the following protected URL:

<http://www.star.bnl.gov/cgi-bin/protected/cvsweb.cgi/StRoot/StPeCMaker/>

The StPeCMaker opens the output files, determines the format of the output trees and sets several user choices about information to be included in the output trees. The maker makes instances of three objects; StPeCEvents which will do the actual selection of UPC candidate events, StPeCTrigger which collects trigger information and accepts the selection of events that fired different triggers. If simulated data is being precessed, StPeCGeant reads Monte-Carlo information and adds it to the output tree.

The StPeCMaker can be directed to read events that were written as StEvent objects. This format carries the complete STAR information on a fully reconstructed event. Events can also be read from files that store the reconstructed events as StMuDst objects, this is also a STAR standard, but it carry less details about the reconstruction and tends to focus on physics variables. The maker can also be instructed to read both formats. This last choice was added to work on the d+Au 2008 run which required a recalibration of the BEMC calorimeter energies, an operation only possible, at that time, from the StEvent section of the BEMC data. The maker can also be set to focus on a particular trigger. This analysis is done with the UPC_Main trigger but other subtasks required the selection of other triggers.

The StPeCEvent class performs the main task of the analysis; it identifies candidates for UPC events by selecting events with low activity at mid-rapidity. Starting with the data collected in 2010 Au+Au interactions, several reconstructed vertices may be present in an event. The StPeCEvent class has an overloaded “fill” method to work with data in StEvent or StMuDst format or both formats. These methods have been modified to loop over all vertices present in any event. These methods have the following common structure:

```
nPPairs = 0 ;
for (size_t verti = 0;verti<Nvert;++verti){

    StMuPrimaryVertex* V= muDst->primaryVertex(verti);

    if(useVertexLocal){
        new((*vertices)[verti]) StMuPrimaryVertex((const StMuPrimaryVertex &) *V);
    } //write vertex out

    // C++ magic: allows looping over tracks from a single vertex:
    StMuDst::setVertexIndex(verti);

    size_t Ntracks = muDst->primaryTracks()->GetEntries();

    nPrimaryTPC = 0;
    nPrimaryFTPC = 0;
    int countTOF = 0;
    for (int trackiter = 0;trackiter<Ntracks;trackiter++){
        tp = ( StMuTrack*)muDst->primaryTracks(trackiter);

        if (! (tp->flag()>0)) continue; // Quality check on the track

        if(fabs(tp->eta())<2.0) {
nPrimaryTPC++;
        } else {
nPrimaryFTPC++;
        }

        if(useTracksLocal){

new((*tracks)[nTracks++]) StMuTrack((const StMuTrack &) *tp); //write full track
        }
    }
}
```

```

if (( nPrimaryTPC > 0 || nPrimaryFTPC>0 ) && // at least one track in FTPC or TPC
   ( nPrimaryTPC < StPeCnMaxTracks && nPrimaryFTPC< StPeCnMaxTracks )&&
   (nPrimaryFTPC+nPrimaryTPC>=2)) { // [2,5] tracks in vertex
.
.
.
```

and count the number of tracks originating from them. If the event has at least one vertex with less than 7 tracks connected to it, pairs are formed with the class StPeCPair. Each track in the pair is stored as an StPeCTrack object, together with quantities calculated for the pair itself. Information from the trigger that fired the event is processed with the class StPeCTrigger and its method. All events are written to the output ntuple tree with a summary about the event, followed by the pairs and the trigger details. If the event has no UPC candidates the pairs and trigger section of the output will be empty.

What follows is a sample macro used to drive the analysis:

```

///////////////////////////////
//  

// macro: doMuEventWithCalo.C
// author: R. Debbe (2009)
//  

// This macro loops over events in muDST files, runs the
// BEMC cluster finder with proper gain calibration. It also prepares track pairs
// that satisfy the UPC criteria.
// Finally it outputs a root tree ntuple that includes a branch with cluster information
//  

//  

/////////////////////////////
#include "TH1.h"
#include "TH2.h"
#include "TChain.h"
#include "TSystem.h"
#include "TFile.h"
#include "iostream.h"
#include <exception>

class StMuDstMaker;
StMuDstMaker* reader;
class StChain;
class StGenericVertexMaker;

StChain          *chain = 0;
int              stat = 0;
int              n = 0;
int              count = 1;

/////////////////////////////
// This is the main method in the macro.
// It loads the libraries, creates the chain and
// instantiate the makers.
// This macro works only with MuDST events
//  

// the parameters are:
//     char* list = defines the list of data files
//     Int_t nFiles = defines how many files should be read from the list
void doMuEvent_mudstInput(char* list = "./file.lis",const char* outFile)
{
  gROOT->LoadMacro("$STAR/StRoot/StMuDSTMaker/COMMON/macros/loadSharedLibraries.C");

  loadSharedLibraries();
```

```

gSystem->Load("StDetectorDbMaker");
gSystem->Load("StDbBroker");
gSystem->Load("St_db_Maker");
gSystem->Load("StDaqLib");
gSystem->Load("StEmcRawMaker");
gSystem->Load("StEmcADCtoEMaker");
// libraries needed to extrapolate to TOF
gSystem->Load("libGeom");
gSystem->Load("St_g2t");
gSystem->Load("geometry");

gSystem->Load("St_geant_Maker");
gSystem->Load("StBTofUtil");

gSystem->Load("/star/u/ramdebbe/.sl64_gcc447/lib/StPeCMaker");
gStyle->SetOptStat(0);
// create chain
chain = new StChain("StChain");
maker = new StMuDstMaker(0,0,"",list,"",50000);

StMuDbReader* db = StMuDbReader::instance();
// make StEvent from StMuDst for BEMC re-calibrartion
StMuDst2StEventMaker *m = new StMuDst2StEventMaker();
m->Make();
St_db_Maker *dbMk = new St_db_Maker("StarDb","MySQL:StarDb");

StEmcADCtoEMaker *adc=new StEmcADCtoEMaker();
StPreEclMaker *ecl=new StPreEclMaker();

St_geant_Maker *geantMk = new St_geant_Maker("myGeant");
geantMk->LoadGeometry("detp geometry y2010");
geantMk->SetActive(kFALSE);

//instanciate StPeCMaker
StPeCMaker* UPCmaker = new StPeCMaker(outFile);
UPCmaker->treeFileName = outFile;

UPCmaker->setUseTracks(kTRUE); //write out tracks
UPCmaker->setUseBemc(kTRUE); //write out Calorimeter
UPCmaker->setUseTOF(kFALSE); //write out TOF tracks
UPCmaker->setUseVertex(kTRUE); //write vertex information
UPCmaker->setReadStMuDst(kFALSE);
UPCmaker->setReadStEvent(kFALSE);
UPCmaker->setReadBothInputs(kTRUE);
UPCmaker->setSuppressTreeOut(kTRUE); //suppress tree output
UPCmaker->setTriggerOfInterest("ZDC_Monitor");//select trigger
UPCmaker->SetDebug(10);

chain->Init();
while ( (stat==0 || stat==1))
{
    chain->Clear();
    StMuDst* mudst = maker->muDst();
    UPCmaker->setMuDst(mudst);
    stat = chain->Make();
    n++;
}
}

```

This analysis focused on events triggered by the UPC_Main trigger, the maker had the call:

```
UPCmaker->setTriggerOfInterest("UPC_Main");
```

5.1 Vertex selection with StPeCMaker

The UPC maker (StPeCMaker) has a new setter method to turn off the output of the UPC pico DST trees, this was done to save disk space and be able to investigate the algorithm that select vertices in each event as detailed in section 5. The figures that follow below are meant to show how some vertex related quantities changed throughout the 2010 run. The number of vertices found by the vertex finder is one of those quantities and the its behavior and the one of other quantities will be displayed as its average as function of the scheduler job index. The analysis of the MuDst was done with the STAR scheduler in groups of ten MuDst files provided by the FileCatalogue ordered in time. Each run may have several MuDst files and the index number of each file is a good substitute for the run number or actual time during data taking. The averages are extracted from histograms filled event by event and stored at the end of each job. Such averages are thus done over all events reads in 10 MuDst files.

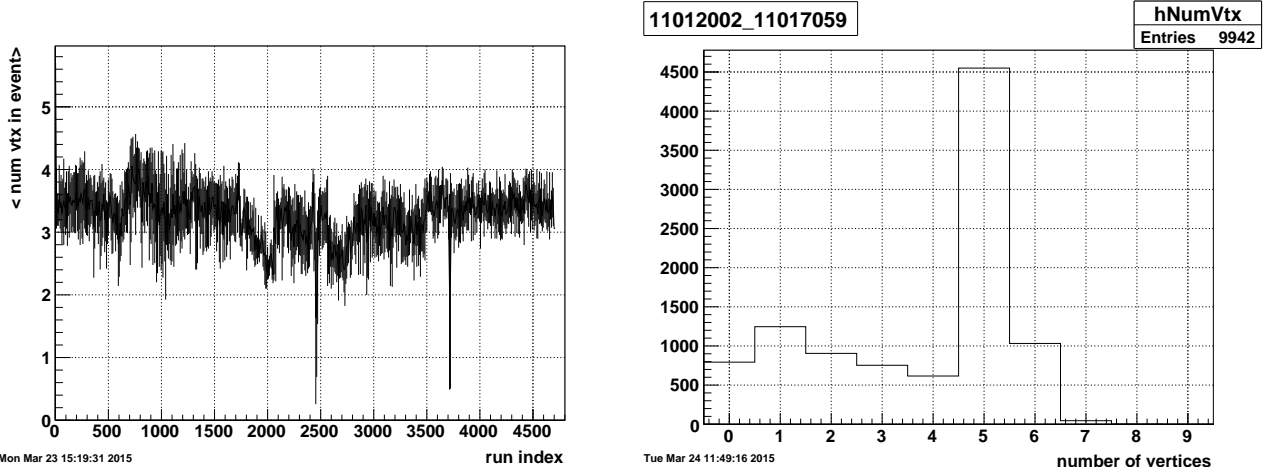


Figure 6: The left panel shows the average number of vertices found in an event as function of the run index. The histogram of the number of vertices per events shown on the right panel is for every event read from a set of 10 MuDst files . The histogram in this figure correspond to the files recorded between day 12 and 17.

Figure 6 displays the average number of vertices found throughout the 2010 run starting on run 35 of day 11 and ending on run 18 of day 77 in a total of 4800 files. The averages are extracted from histograms filled event by events. The right panel of the figure illustrate the number of vertices found by the vertex finder. Good vertex candidates appear at lower values of the vertex multiplicity. The peak at 5 vertices is an artifact of the finder as it stores vertex candidates that could be accepted in the Spin program but would be rejected in our analysis.

From actual data in order to characterize the vertex distributions, we used rho meson candidates from vertices that have at most 4 tracks and two TOF hit matches.

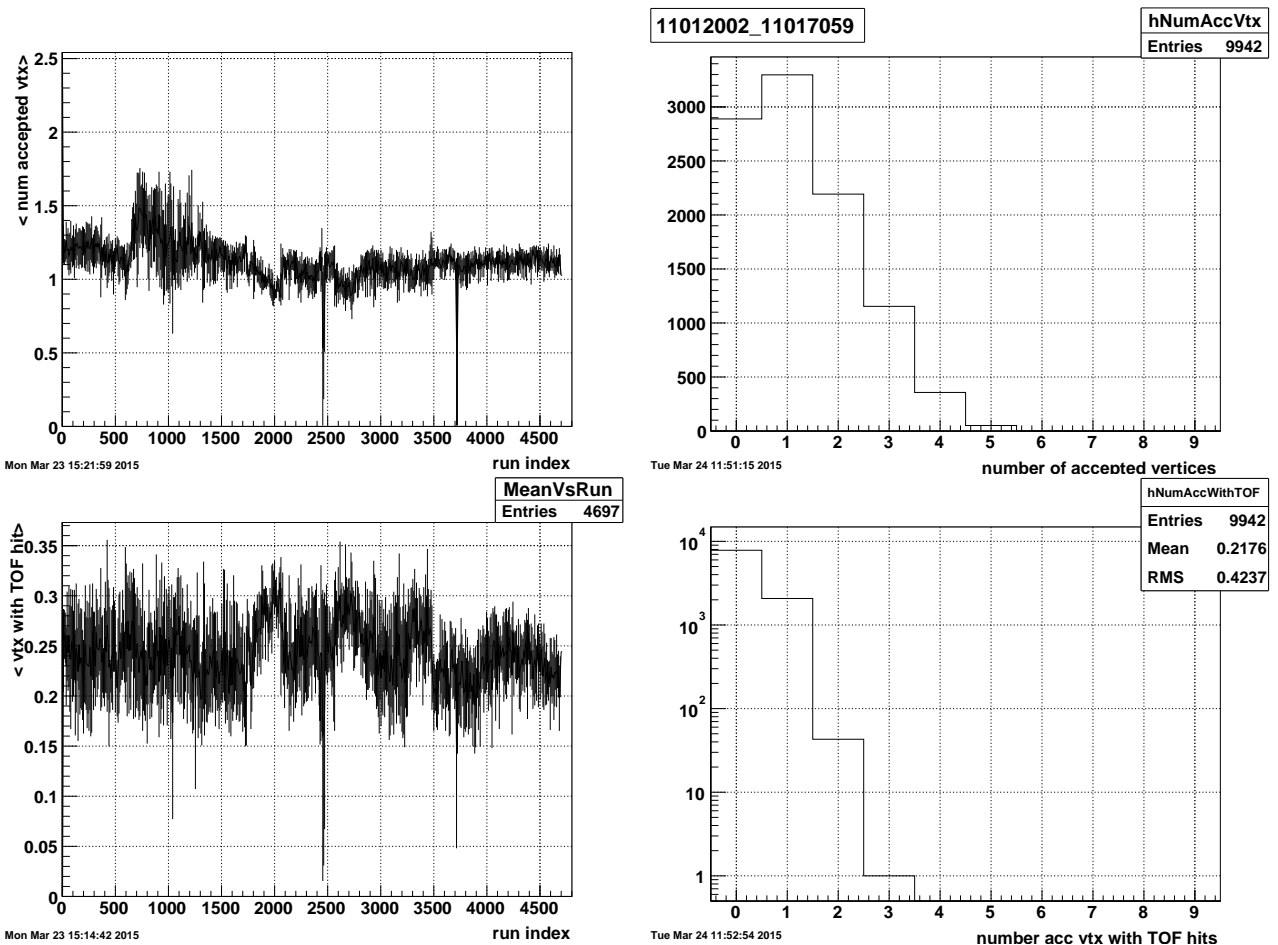


Figure 7: The top left panel shows the average number of accepted vertices. The top right panel shows the histogram of accepted vertices in the MuDst files. Histograms like this one are used to extract the average displayed on the left panel. The bottom left panel shows the average number of accepted vertices with at least one track connected to TOF signal. The bottom right panel shows the distribution of the number of such vertices for 10 MuDst files of day 12.

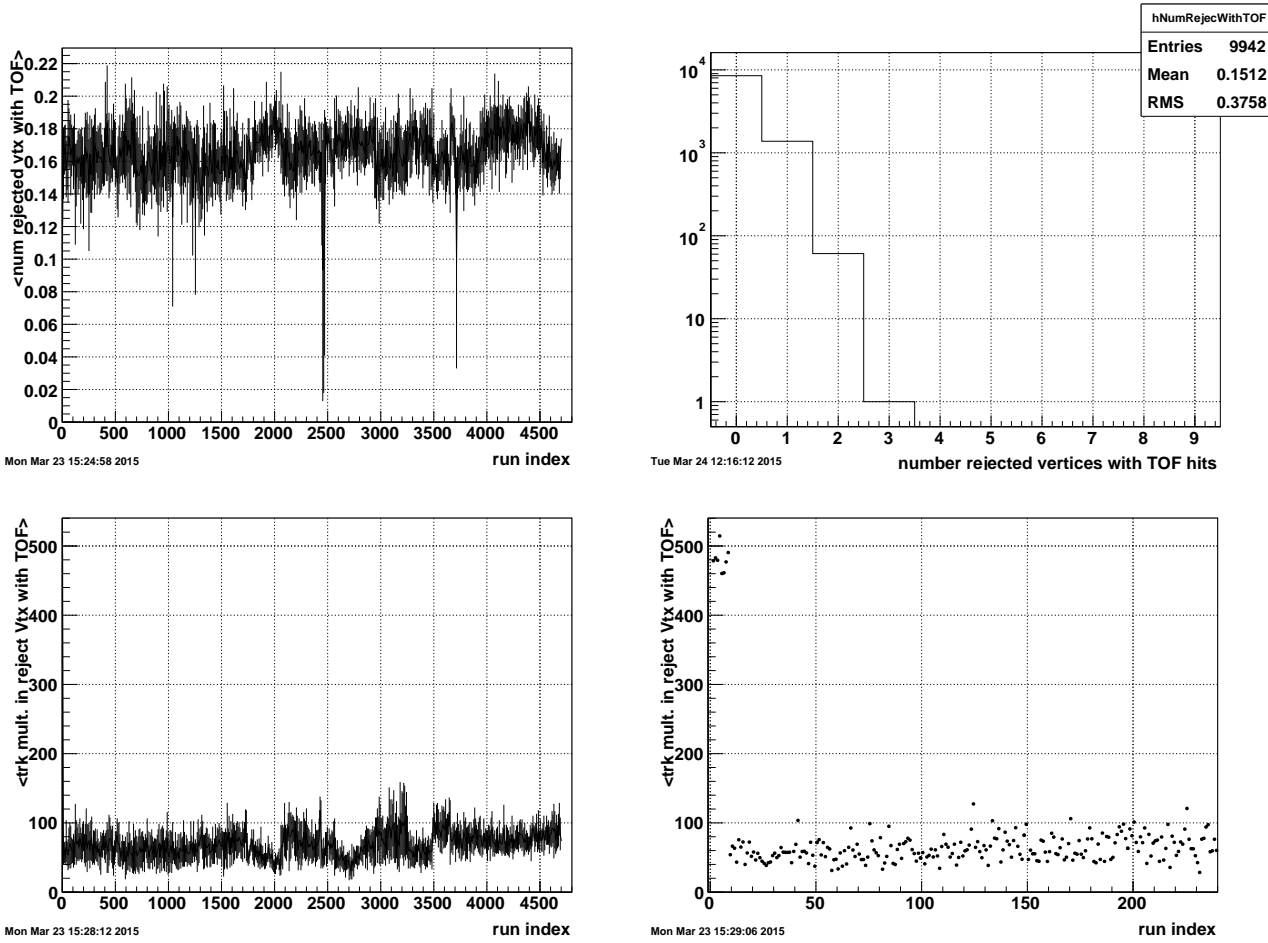


Figure 8: The top left panel shows the average number of vertices that have been rejected event though they do have one track reaching onto a valid TOF hit. The top right panel shows the distribution of the number of such vertices for 10 MuDst files. The bottom left panel shows the average track multiplicity for those rejected events as function of the run index, and the bottom right panel shows the same information bu zoomed on the first runs of 2010 to show that 8 of those files should not be included in the analysis because they show strong deviation from the rest of the runs.

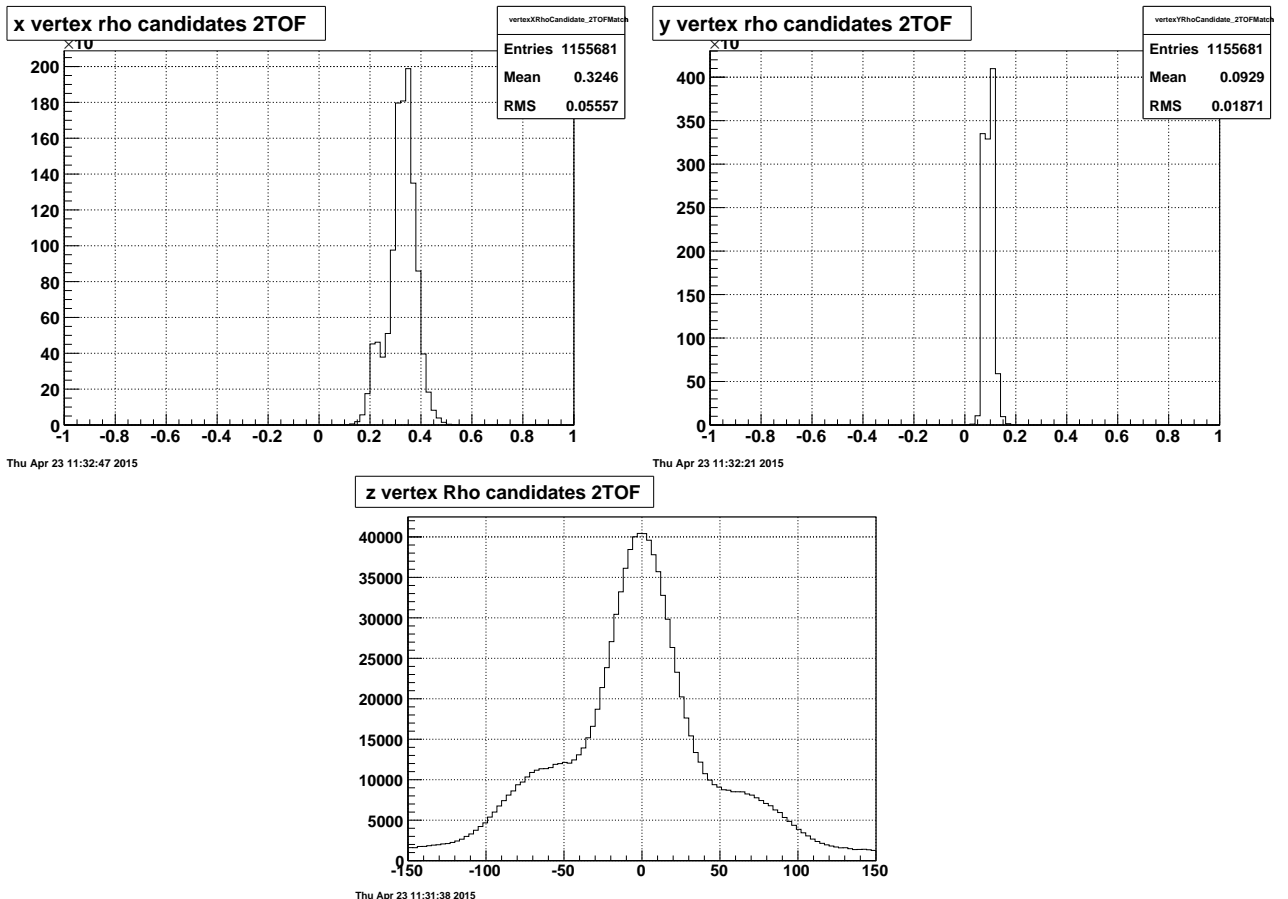


Figure 9: Top left panel shows the x coordinate of the vertex where a pair was found to be a good candidate for a ρ^0 meson. The top right panel shows the y vertex coordinate for the same vertex, the bottom panel shows the distribution of the z coordinate for vertices that have a pair which is a good ρ^0 candidate.

6 Luminosity

The luminosity is calculated from scaler counts obtained with detectors that have acceptance to most of the total cross section for Au + Au collisions. Such detectors include the ZDC, BBC and VPD. The ZDC detectors are the ones that can see the complete cross section, including the UPC events. The value of the total cross section for Au+Au collisions at $\sqrt{s_{NN}} = 200$ GeV is set to 10 ± 1 barns [11, 10]. Adding the presence of signal from the VPD detectors reduces the fraction of accessible total cross section to 6 ± 0.6 barns but it eliminates the false counts produced by ringing presents in the ZDC detectors. Adding VPDs to the triggers also introduces inefficiencies for vertices with absolute values of the z coordinates exceeding 50 cm.

The values of luminosity are calculated for each run with the Perl script getLumi_2010.pl. The script and its different outputs is available in the official STAR page:

<http://www.star.bnl.gov/protected/common/common2010/trigger2010/lumi200GeV/>

The file lum_perrun_UPC_Main.txt lists the run number, the start and end time (UNIX time), the RHIC fill number and the integrated luminosity in the run (in $(\mu b)^{-1}$) divided by the UPC_Main prescale for that particular run. The scaler contents used to produce this lists of luminosities were filled with signals from the VPD and ZDC detectors in a trigger labelled “minbias_monitor”. This list starts on day 39 of the 2010 run but the UPC_Main was operational starting on day 11.

In an earlier version of this analysis, an attempt was made to calculate the luminosity for all usable runs starting on day 11 and to switch to a so called base scaler sensitive to the complete Au+Au cross section.

<http://www.star.bnl.gov/protected/pcoll/ramdebbe/Luminosity100CT2012.pdf>

The new scaler records counts for the trigger named “ZDC_Monitor”. Figure 10 was used to argue that as the fraction of counts from the minbias_monitor and ZDC_Monitor remains flat from day 11 to 77, one can safely modify the perl script used to calculate luminosities by switching the base cross section from 6 to 10 barns and use the ZDC_Monitor scaler. In order to include non “elevated to physics” version of the UPC_Main trigger, the Perl script is run with the argument -t.

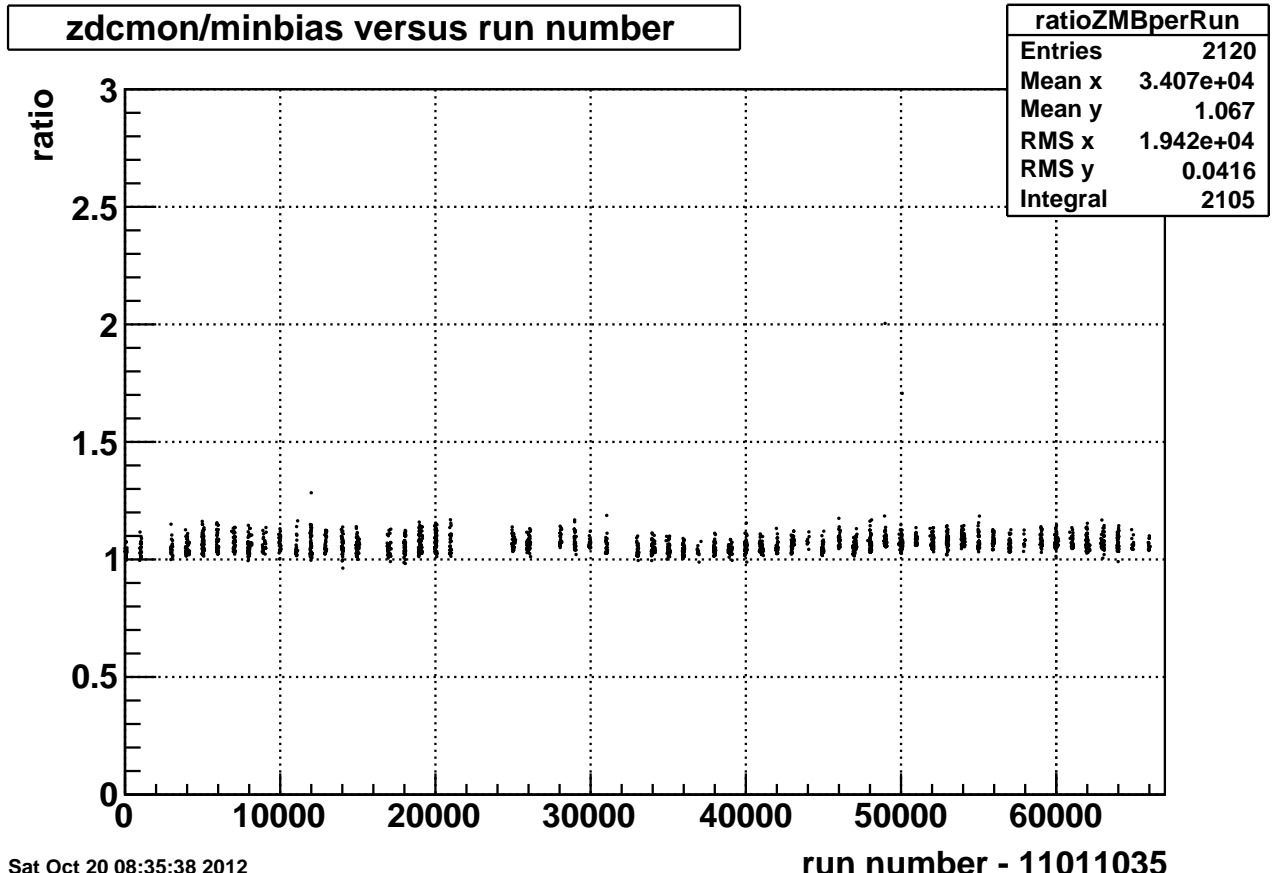


Figure 10: The ratio of scaler counts for the ZDC_Monitor trigger over the minbias_monitor trigger as function of (run number-11011035).

The total integrated luminosity based on the minbias_monitor trigger and spanning runs from day 39 to 77 (once the UPC_Main trigger was “elevated to physics” with Id= 260750 as it appears in the official page mentioned above) is equal to $679.2 \mu b^{-1}$. For the same period of run 10, the integrated luminosity based on the

ZDC_Monitor trigger has a value equal to $725.7\mu b^{-1}$.

An argument can be made using Fig. 10 again to extend the extraction of luminosities using the minbias_monitor scalers to the runs from day 11 to 39 based on the flatness of the displayed ratio. The luminosity per run has thus been calculated for all runs (day 11 to 77) using the ZDC_Monitor and minbias_monitor triggers. The total integrated luminosity for the ZDC_Monitor is equal to $1155\mu b^{-1}$. The one corresponding to the minbias_monitor is $1085.9\mu b^{-1}$, a difference of 6% comparable to the 7% difference from the day 39 to 77 period. With such differences in the same order as the systematic uncertainties allocated to the cross section values, it is then wise to migrate to the luminosity calculated with the minbias_monitor, such move eliminates the effects of ringing in the ZDC detectors but restricts the range of vertices along the beam line to $|vertex_z| < 50$ cm. For the rest of this note, the value of integrated luminosity use to normalize the cross sections will be $1085.9\mu b^{-1}$. In order to make sure that the integrated luminosity was obtained with the runs that were actually used in the analysis a shell script named loopOverLumiFile.sh was used to read the luminosity per run lum_perrun_UPC_main_vpdmib_allRuns.txt and then seach among all the log files produced by the STAR Scheduler at the time the UPC MuDst files were read for instances of that run number using the Unix tool grep. The luminosities per run are added up only if that search came back positive. The new value of integrated luminosity from all runs used in the analysis is $1074.6\mu b^{-1}$.

7 Full Chain correction with embedded events

Instead of attempting to extract acceptance corrections and other efficiencies independently be it with Monte-Carlo techniques or directly from data, we have decided to follow a safer path by making use of well developed STAR detector simulations and embedding techniques. By mixing generated events with unbiased events collected during run 2010 we have the means to simulate the detector response, the effects on the background on the reconstruction of the event.

In order to reproduce the state of all TPC anodes at the time of the 2010 Au+Au run the embedding of MC generated particles in zerobias events has to be done with the appropriate library ; SL10k_embed. Attempts at reproducing such state with most recent libraries failed for several reason. It was then decided to split the embedding exercise into two steps, the first one does the actual embedding using the SL10k_embed library with a small modification on the StBtofSimMaker code to allow for the writing of the BTofHitCollection on the output MuDst. The outputs of the first step are then read with code based on the most up to date library and a new MuDst is written with the latest version of the MC output.

The embedding of the first step is done with a STAR bfc chain:

http://www.star.bnl.gov/cgi-bin/protected/cvsweb.cgi/StRoot/macos/embedding/bfcMixer_Tpx.C

The actual call to run the bfc chain is shown below:

```
root4star -b <> EOF
.L bfcMixer_Tpx.C
bfcMixer_Tpx(500000,"$INPUTFILE0","test.tag.root", 0, 5, -1.8, 1.8, -200, 200, 100, 8, 1, 0,
               "P10ikAuAu200", "FlatPt", 1, "${fzd_file}.fzd","$SCRATCH/$JOBID.MuDst.root");
.q
EOF
```

The production name "P10ikAuAu200" sets the parameters that drive the reconstruction at end of the embedding. These parameters should be the same that were used to reconstruct the 2010 Au+Au data.

The starlight event generator is driven from kumac file, the following is a print out produced as the generator starts running:

```
>>> inputParameters::init(): info: successfully read input parameters from 'slight.in'
Rapidity beam 1: 5.37895, rapidity beam 2: -5.37895, rapidity CMS system: 0, beam gamma in CMS: 108.4
>>> inputParameters::init(): info: using the following starlight parameters:
config file name ..... 'slight.in'
beam 1 atomic number ..... 79
beam 1 atomic mass number ..... 197
beam 2 atomic number ..... 79
beam 2 atomic mass number ..... 197
Lorentz gamma of beams in CM frame ..... 108.4
mass W of produced hadronic system ..... 0.279 < W < 1.522 GeV/c^2
# of W bins ..... 100
maximum absolute value for rapidity ..... 5.5
# of rapidity bins ..... 80
cut in pT..... no
    minumum pT..... 0 GeV/c
    maximum pT..... 0.1 GeV/c
cut in eta..... no
    minumum eta..... -1
    maximum eta..... 1
meson production mode ..... 2
number of events to generate ..... 100
PDG ID of produced particle ..... 913
seed for random generator ..... 2560102
output format ..... 2
breakup mode for beam particles ..... 2
interference enabled ..... no
interference strength ..... 1
coherent scattering off nucleus ..... yes
scaling factor for incoh. VM prod. ..... 0.6
deuteron slope parameter ..... 9.5 (GeV/c)^{-2}
```

```

maximum p_T for interference calc. ..... 0.24 GeV/c
# of p_T bins for interference calc. ... 120
#####
initialising Starlight v1.1.1...
#####
>>> beamBeamSystem::generateBreakupProbabilities(): info: Requiring XnXn [Coulomb] breakup.
>>> starlight::luminosityTableIsValid(): info: using random seed = 2560102
>>> starlight::init(): info: creating luminosity table for coherent photon-Pomeron channel
Creating Luminosity Tables.
Calculating flux for photon energies from E= 0.001000000000000 to 20.116224964137931 GeV (CM frame)
bwnorm: 0.079184841441890
Luminosity Tables created.
Reading in luminosity tables. Gammaanarrowvm()
Creating and calculating crosssection. Gammaanarrowvm()
Using Narrow Resonance ...
gamma+nucleon Threshold: 0.004996523580870
Cross section (mb): 40.758031852186051
>>> starlightStandalone::run(): info: generating events:

```

The inputs for the first embedding step are raw data files from the st_zerobias stream ‘(with extension “.daq”) and the outputs of the event generator after their processing through the full STAR GEANT simulation, these second type of files have extension “.fzd” and contain as many events as the corresponding “daq” files.

An attempt was made to estimate how many ρ^0 mesons decaying into two pions would fire the UPC_Main trigger. The vector mesons were generated with the starlight event generator and embedded in zerobias events collected during the 2010 Au+Au run. Mixing of the MC and real data is done at the detector response level for all detectors except the ZDC calorimeters which will be considered fully efficient to detect the beam momentum neutrons which make the UPC_Main trigger the cleanest in the UPC program. The mixed events are then fully reconstructed with the complete STAR production chain, the analysis of the results is then done by processing the output MuDst’s.

7.1 Private embedding process summary

- Input files: fzd from a particular FSET generated at PDSF are copied to:
`/star/data01/pwg/ramdebbe/fzdFiles_secondEmbed/RhoPiPiFSET101/`
The zerobias data files are extracted from hpss onto:
`/star/data03/daq/2010/039/11039070zR/` (for run 70 of day 39)
- The first step of the embedding is done from:
`/star/u/ramdebbe/UPC/EmbeddingSL10k_fzd/`
with the xml script:
`submitBfcMixer_fzd.FSET101_SL10k_embedd.xml` (for FSET 101) with SL10k_embed library.
- Outputs (with MuDst, event and geant extensions) are written to:
`/star/data06/UPC/run10AuAu200tree/SL10k_embedOutput/`
- Second stage of the process is also done from:
`/star/u/ramdebbe/UPC/EmbeddingSL10k_fzd/`
with the xml script:
`submitWriteMuDst.xml` (this script set the STAR library to .DEV2)
the outputs (MuDst) are also written to:
`/star/data06/UPC/run10AuAu200tree/SL10k_embedOutput/`

7.2 Official embedding process at pdsf

Get request number Processed 1M events for ρ^0 meson embedding in zerobias events. Describe all steps.
Outputs in the for of UPC pico dst are now at:
`/star/data01/pwg/ramdebbe/run10AuAu200tree/mixedEmbeddingFSET*/`
for FSET starting at 107 and ending 115.

7.3 Reading the mixed embedding MuDst

The reading of MuDst is done based on code provided by Yury Fisyak and run with small modifications to suit particular needs of this analysis: First retrieve the necessary objects from the files:

```

TClonesArray *PrimaryVertices = mu->primaryVertices();
Int_t NoPrimaryVertices = PrimaryVertices->GetEntriesFast();
TClonesArray *PrimaryTracks = mu->array(muPrimary);
Int_t NoPrimaryTracks = PrimaryTracks->GetEntriesFast();
TClonesArray *GlobalTracks = mu->array(muGlobal);
Int_t NoGlobalTracks = GlobalTracks->GetEntriesFast();

TClonesArray *MuMcVertices = mu->mcArray(0);
Int_t NoMuMcVertices = MuMcVertices->GetEntriesFast();
TClonesArray *MuMcTracks = mu->mcArray(1);
Int_t NoMuMcTracks = MuMcTracks->GetEntriesFast();
TClonesArray *MuBTofHits = mu->btofArray(0);
Int_t NoMuBTofHits = MuBTofHits->GetEntriesFast();

StBbcTriggerDetector& bbc = mu->event()->bbcTriggerDetector();

```

The so called “truth information” is extracted from the MuMcTracks arrays and the vector meson is reconstructed from its decay products:

```

// ===== loop over MC tracks
//
Double_t massPion = 0.139;

StThreeVectorF momentum ;
int foundPiPlusMC = 0;
int foundPiMinusMC = 0;
float invariantMass = 0.;
float rapidity = 0.;

for (Int_t kg = 0; kg < NoMuMcTracks; kg++) {
    StMuMcTrack *mcTrack = (StMuMcTrack *) MuMcTracks->UncheckedAt(kg);

    allMCMomentum->Fill(mcTrack->Pt());
    if(mcTrack->GePid()==8 || mcTrack->GePid()==9) {

        momentum = mcTrack->Px();
        if(mcTrack->pT()>-10. && mcTrack->GePid()==8) {
            px_tr1 = mcTrack->pT()*TMath::Cos(momentum.phi());
            py_tr1 = mcTrack->pT()*TMath::Sin(momentum.phi());
            pz_tr1 = mcTrack->pT()*TMath::SinH(mcTrack->Eta());
            energy_tr1 = TMath::Sqrt(massPion*massPion + mcTrack->Pt()*mcTrack->Pt());
            foundPiPlusMC = 1;
        }
        if(mcTrack->pT()>-10. && mcTrack->GePid()==9) {
            px_tr2 = mcTrack->pT()*TMath::Cos(momentum.phi());
            py_tr2 = mcTrack->pT()*TMath::Sin(momentum.phi());
            pz_tr2 = mcTrack->pT()*TMath::SinH(mcTrack->Eta());
            energy_tr2 = TMath::Sqrt(massPion*massPion + mcTrack->Pt()*mcTrack->Pt());
            foundPiMinusMC = 1;
        }

        allPionMomentum->Fill(mcTrack->Pt());
        allMCRapidity->Fill(mcTrack->Px().pseudoRapidity());

        //
        //calculate inv. mass and y only if two pions are present
    }
}

```

```

//  

if(foundPiPlusMC>0 && foundPiMinusMC>0) {  

float sumEnergy = energy_tr1 + energy_tr2;  

float sumMomentumSquare = (px_tr1 +px_tr2)*(px_tr1 +px_tr2) +  

(py_tr1 +py_tr2)*(py_tr1 +py_tr2) +  

(pz_tr1 +pz_tr2)*(pz_tr1 +pz_tr2) ;  

invariantMass = TMath::Sqrt(sumEnergy*sumEnergy - sumMomentumSquare);  

rapidity = 0.5*TMath::Log((sumEnergy+(pz_tr1 +pz_tr2))/(sumEnergy-(pz_tr1 +pz_tr2)));  

}  

}  

}  

if(foundPiPlusMC>0 && foundPiMinusMC>0){  

MCinvariantMass->Fill(invariantMass);  

MCrhoRapidity->Fill(rapidity);  

MCrhoRapidityFullRange->Fill(rapidity);  

}

```

The histograms filled with information extracted from the MC arrays are shown below, first the pion information:

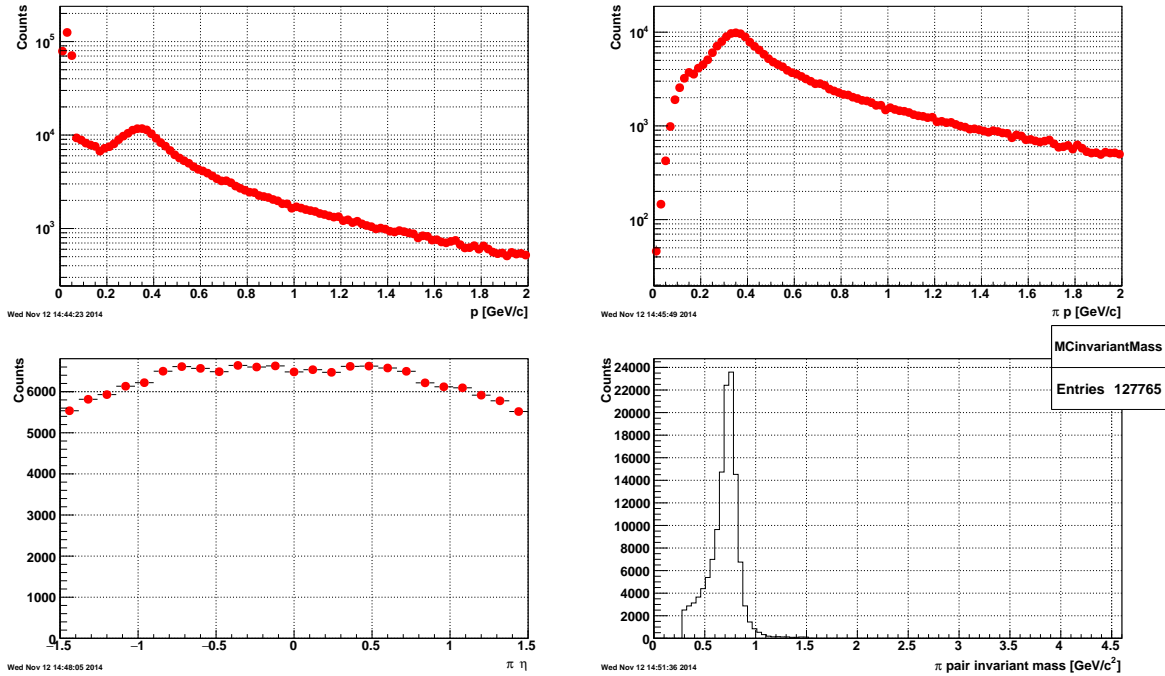


Figure 11: Top left panel shows the momentum distribution of all MC tracks, the top panel right shows the momentum of MC tracks matched with a GEANT Id of charged pions (8 or 9). The bottom left panel shows the rapidity distribution of the MC tracks with charged pion Id. The bottom right panel shows the invariant mass distribution of MC pion pairs as proof of the correct reconstruction of the MC vector meson (ρ^0).

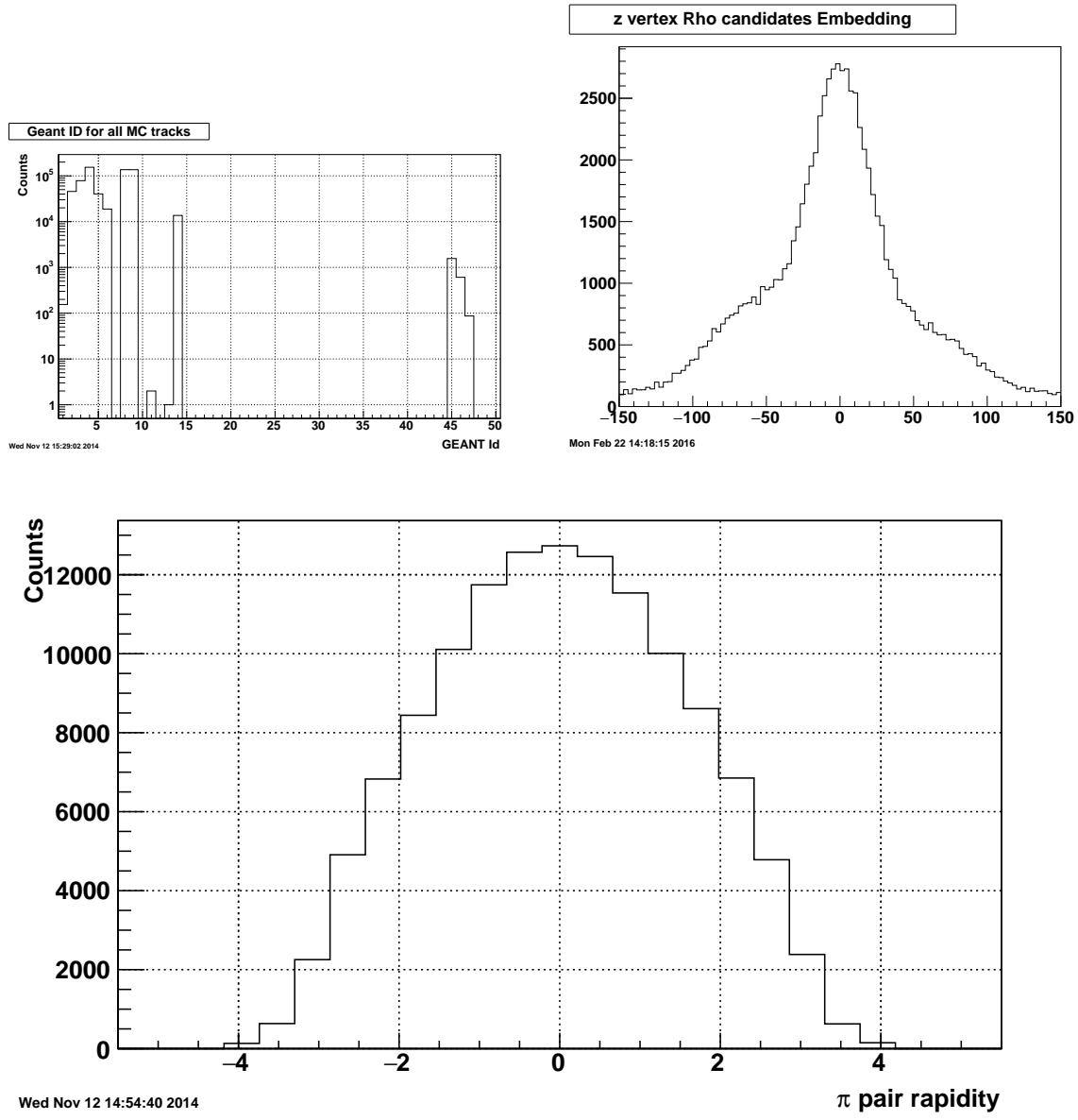


Figure 12: The top left panel shows the variety of MC particles generated by the event generator (pions: 8,9, and secondaries produced as GEANT transports the pions thru the STAR material (gamma 1, electrons 2,3, muons 5,6, protons 14, and heavier fragments 45 and up. The top right panel shows the distribution of the z coordinate of vertices in this embedding exercise. This is to demonstrate that we used an exact copy of the vertex distribution present in the real data as shown in the corresponding panel of Fig. 9. The bottom panel shows the full range rapidity distribution of the MC pion pairs (ρ^0).

The matching between reconstructed tracks and the generated pions (truth) is done in such a way as to mimic as much as possible the actual UPC_main trigger as it was run during the experiment. Low activity at mid-rapidity was identified with the TOF detector which tagged events with at least two and no more than 6 hits in TOF. The matching of reconstructed tracks to generated particles is based on the simulated signal in the TOF detector as the generated particles reach active areas of the TOF detector. The section of the program that deals with reconstructed tracks and how they are matched to MC particles starts by looping over all TOF hits as shown below. It is to worth emphasize how this algorithm connects the TOF hits first to generated particles in a STAR standard way: Each object has a method called idTruth; for a TOF hit, a value of idTruth() greater than -1 would be the id or key of an MC track that reached that element of TOF. This matching is done at the level of the TPC hits used to form a track.

```
// ===== Build map between BTofHit and Mc tracks      RD 27SEP

numberBTOfHits->Fill(NoMuBTofHits);
multimap<Int_t,Int_t> BTofHit2McTracks;
Int_t foundPiPlus = 0;
Int_t foundPiMinus = 0;
int MinNoMcTpcHits = 14;

for (Int_t kg = 0; kg < NoMuBTofHits; kg++) {
    StMuBTofHit *gHit = (StMuBTofHit *) MuBTofHits->UncheckedAt(kg);

    if (gHit->idTruth() <= 0 || gHit->idTruth() > NoMuMcTracks) {
        continue;
    }

    StMuMcTrack *mcTrack = (StMuMcTrack *) MuMcTracks->UncheckedAt(gHit->idTruth()-1);

    if (mcTrack->Id() != gHit->idTruth()) {
        continue;
    }
    if(gHit->index2Primary()>=0){
        StMuTrack *pTrack = (StMuTrack *) PrimaryTracks->UncheckedAt(gHit->index2Primary());
        if(pTrack){
            mcTrack->Print();
        if(mcTrack->pT()>-10. &&mcTrack->GePid()==8 && pTrack->nSigmaPion()<3 ){
            if (mcTrack->No_tpc_hit() < MinNoMcTpcHits) continue;
            foundPiPlus = 1;
            momentum = mcTrack->Pxzy();
            pionRapidity->Fill(mcTrack->Pxzy().pseudoRapidity());
            pionMomentum->Fill(mcTrack->Ptot());

            px_tr1 = mcTrack->pT()*TMath::Cos(momentum.phi());
            py_tr1 = mcTrack->pT()*TMath::Sin(momentum.phi());
            pz_tr1 = mcTrack->pT()*TMath::SinH(mcTrack->Eta());
            energy_tr1 = TMath::Sqrt(massPion*massPion + mcTrack->Ptot()*mcTrack->Ptot());
        }
        if(mcTrack->pT()>-10. && mcTrack->GePid()==9 && pTrack->nSigmaPion()<3 ) {
            if (mcTrack->No_tpc_hit() < MinNoMcTpcHits) continue;
            foundPiMinus = 1;
            momentum = mcTrack->Pxzy();
            pionRapidity->Fill(mcTrack->Pxzy().pseudoRapidity());
            pionMomentum->Fill(mcTrack->Ptot());

            px_tr2 = mcTrack->pT()*TMath::Cos(momentum.phi());
            py_tr2 = mcTrack->pT()*TMath::Sin(momentum.phi());
            pz_tr2 = mcTrack->pT()*TMath::SinH(mcTrack->Eta());
            energy_tr2 = TMath::Sqrt(massPion*massPion + mcTrack->Ptot()*mcTrack->Ptot());
        }
    }
}
}
```

```

}

if( (NoMuBTofHits>=2 && NoMuBTofHits<7) &&
    (foundPiPlus && foundPiMinus)           &&
    (sumEast<50 && sumWest<50) )           {
    float sumEnergyReco = energy_tr1 + energy_tr2;
    float sumMomentumSquareReco = (px_tr1 +px_tr2)*(px_tr1 +px_tr2) +
        (py_tr1 +py_tr2)*(py_tr1 +py_tr2) +
        (pz_tr1 +pz_tr2)*(pz_tr1 +pz_tr2) ;

    float invariantMassReco=TMath::Sqrt(sumEnergyReco*sumEnergyReco-sumMomentumSquareReco);
    float rapidityReco=0.5*TMath::Log((sumEnergyReco+(pz_tr1+pz_tr2))/(sumEnergyReco-(pz_tr1+pz_tr2)));

    RecoInvariantMass->Fill(invariantMassReco);
    if(acceptedRecoVertex==1 && abs(mcVertex->XYZV().z())<50. )RecorhoRapidity->Fill(rapidityReco);
    countGoodTriggers++;

}

// apply veto on small BBC tiles
if( NoMuBTofHits>=2 && foundPiPlus && foundPiMinus && (sumEast<50 && sumWest<50)){
    countNotVetoedTriggers++;
}

```

7.4 TOF geometry, alignment, detector response and veto use in trigger

The location of this sub-section may change as this is done with information extracted from UPC pico dst obtained by reading the MuDsts produced in the private embedding exercise. The aim here is to build arguments to convince people that TOF is well simulated and the acceptance extracted with a simulation that includes TOF is correct. So far I only have some figures to show the detector details, needs to find a way to check alignment. (The TOF people does alignment using data, need to get those details).

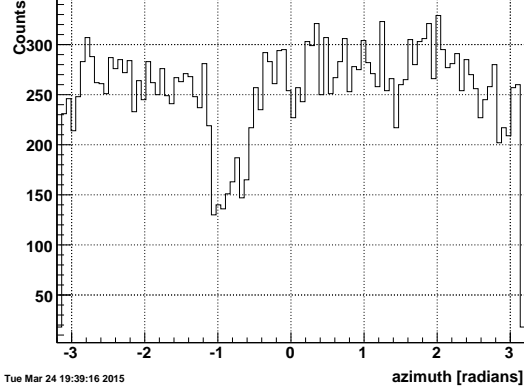


Figure 13: . Azimuthal distribution of reconstructed tracks (measured at DCA). The clear dip is due to inefficiencies on the sector 20 of the TPC.

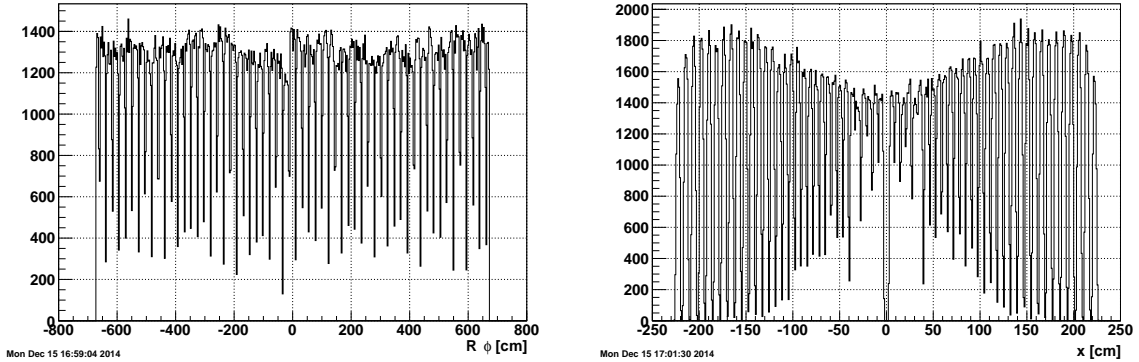


Figure 14: The left panel shows the projection of intercepts of tracks with the TOF detector to the $R\phi$ axis. The segmentation along $R\phi$ shows the 60 TOF trays. The right panel shows a similar projection but this time on the z axis. The binning is chosen to highlight the segmentation in modules along trays. Here one can see the 32 modules in each TOF tray.

In an attempt to check the alignment of the TOF detector I used the extrapolation of TOF tracks to TOF active cells. When I read data, I have access to two situations: if I use the coordinates of the extrapolation found in the so called TOFtracks, I get the combined effect of the GEANT geometry and alignments to TPC tracks done run by run. I can also use the TPC tracks from the MuDst and make the extrapolation myself. This second extrapolation makes use of the GEANT geometry and does not include the run-by-run offsets. The coordinates for the TOFtracks are displayed with black histograms and the ones produced with the GEANT geometry alone are shown with red histograms in Fig. 19. Both histograms are filled with data the black histogram is filled with all tracks the have `matchFlag==1`. The red histogram is filled with opposite charge pions (identified by TPC dE/dx) with good tracks ($nHit > 14$).

details of the extrapolation to TOF

```
StPeCPair::StPeCPair ( StMuTrack* trk1, StMuTrack* trk2,
                      Bool_t primaryFlag, StMuEvent* event, StBTofGeometry * pairTOFgeo ) {
    this->Clear();
```

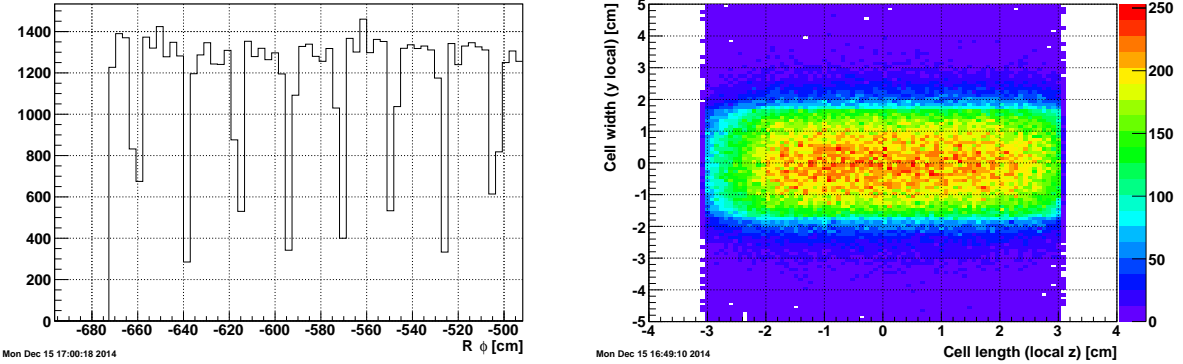


Figure 15: . Intercepts of tracks that match TOF hits in $R\phi$ and z plane projected on the Rphi axis, the binning is selected to highlight the fact that each module contains 6 cells. Right panel: Intercepts of tracks that match TOF hits to a TOF cell. The coordinates of the intercept are local.

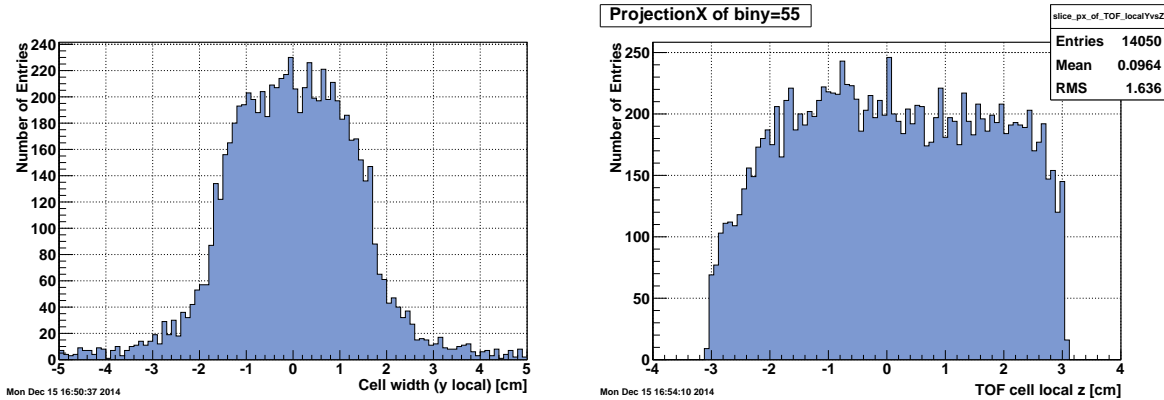


Figure 16: . The left panel shows the projection of intercepts of tracks with a TOF detector cell along the local y axis. The right panel shows a similar projection but this time along the local z axis.

```

pairTOFgeoLocal = pairTOFgeo;
.

.

hOuter1      = muTrack1->outerHelix() ;
hOuter2      = muTrack2->outerHelix() ;

.

// 
//extrapolate tracks to TOF
// 
vector<Int_t> idVec;
vector<Double_t> pathVec;
PointVec  crossVec;

if(pairTOFgeoLocal->HelixCrossCellIds(hOuter1,idVec,pathVec,crossVec))
{
    Int_t cellId    = -999;
    Int_t moduleId = -999;
}

```

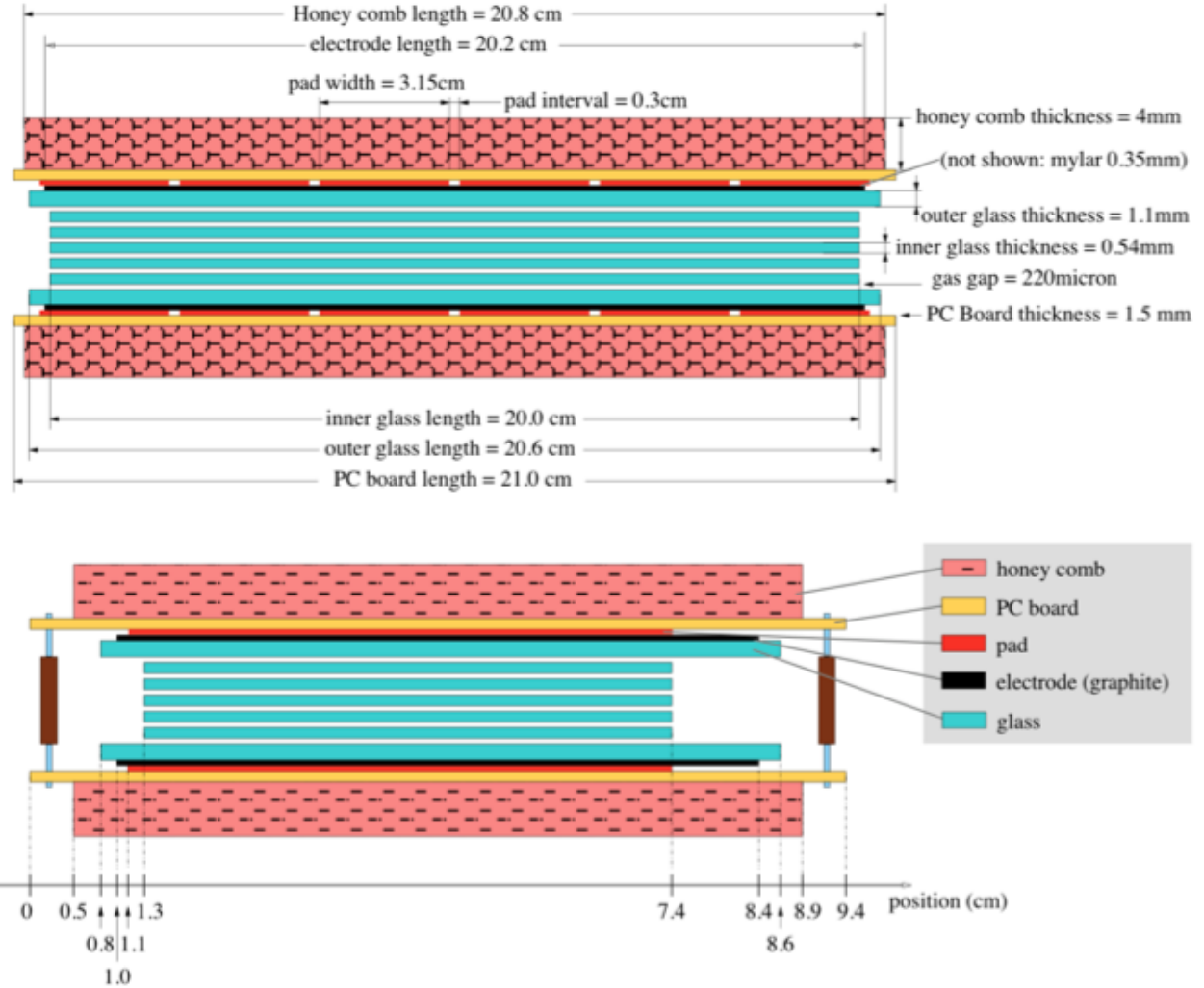


Figure 17: . .

```

Int_t trayId = -999;
pairTOFgeoLocal->DecodeCellId(idVec[0],cellId,moduleId,trayId);
tr1_extrapolatedTOF_mX = crossVec[0].x();
tr1_extrapolatedTOF_mY = crossVec[0].y();
tr1_extrapolatedTOF_mZ = crossVec[0].z();
}
if(pairTOFgeoLocal->HelixCrossCellIds(hOuter2,idVec,pathVec,crossVec))
{
    Int_t cellId = -999;
    Int_t moduleId = -999;
    Int_t trayId = -999;
    pairTOFgeoLocal->DecodeCellId(idVec[0],cellId,moduleId,trayId);
    tr2_extrapolatedTOF_mX = crossVec[0].x();
    tr2_extrapolatedTOF_mY = crossVec[0].y();
    tr2_extrapolatedTOF_mZ = crossVec[0].z();
}

```

The quality of the TOF hit is determined solely by demanding that the pointer to MC tracks be positive or zero and of no greater value than the number of MC tracks in the events. There is more information in the StMuBtofHit object that can be added at this level of the analysis but has not been done yet.

The StMuBtofHit has methods to obtain the indices of primary or global tracks that are connected to the hit. It also has a pointer to MC tracks obtained thru the method idTruth() which returns the index+1 in the StMuMcTrack. This is the heart of the matching between reconstructed tracks and MC particles. In an earlier incarnation of the code, the matching between reconstructed tracks and MC particles ended here because, once

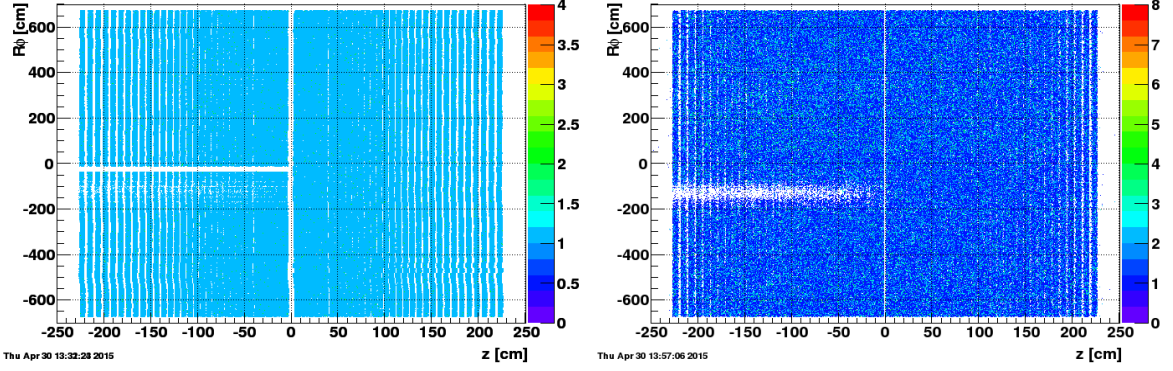


Figure 18: . The left panel shows the intercepts of extrapolated tracks for TOFtracks with a clean (flag==1) match to TOF, this extrapolation uses GEANT geometry suplemented with alignment based on data. The right panel shwos the intercept for track extrapolated to the TOF detector using GEANT geometry.

the TOF hit is connected to at StMuMcTrack, the GEANT id of the track was used to identify it as a pion and proceed to make pairs and look for ρ^0 candidates.

In order to mimic, as closely as possible, the track matching to the procedure used in the data analysis, we have added track quality conditions based on the number of TPC clusters (hits) used to build the tracks, and particle identification based on energy deposited in the TPC gas volume. The dE/dx based particle identification is done using a fitted function of the momentum of the particle and deviations to that fit expressed in number of standard deviations. Even though the MC tracks carry the information about the ionization in the TPC track, details like the number of standard deviations away from the calculated values are not available. To get that information we need to use the version of the MC track stored in the PrimaryTracks objects in StMuTrack. This operation provides an additional constraint on the matching operation as it demands the presence of a reconstructed vertex in the event.

Special interest is placed on the response of the TOF detector as it is the one that determines the value of the efficiency.

The distribution of TOF hits (a combination of hits produced by actual charged particles and recorded in the zerobias events, as well as the response to the MC generated particles) is shown in the top left panel of Fig. 21.

Events with more than 6 TOF hits would have been excluded by the UPC_Main which requires the event to have $2 \leq TOF_{hits} \leq 6$ the effect of this veto is also small ($\sim 1\%$).

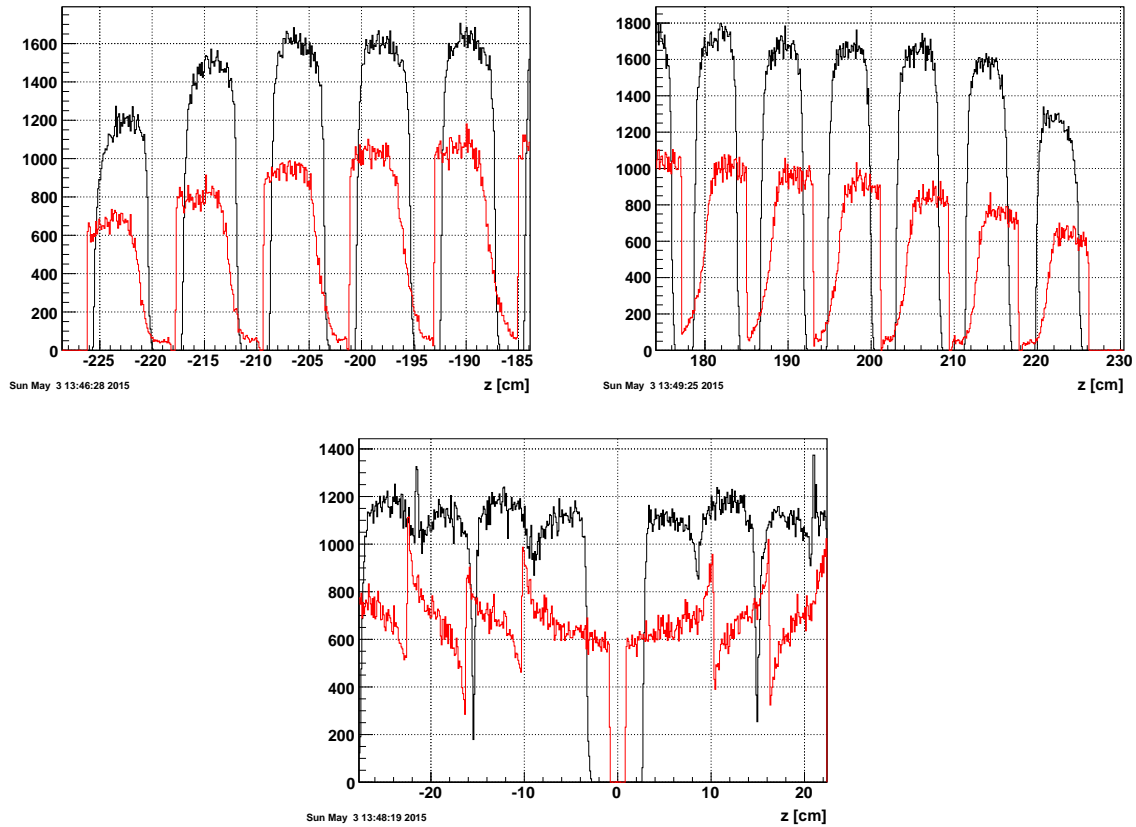


Figure 19: . The top left panel shows the intercepts of extrapolated tracks with TOF active elements that have hits with a black histogram. The same extrapolated that uses the GEANT geometry is shown with a red histograms The right panel shows a zoomed portion the left-most side of both histograms. The bottom left panel shows details of the righ-most side of the histograms, and the bottom right panel shows the center ($z \sim 0$). These projections are filled with tracks pointing to a single TOF tray.

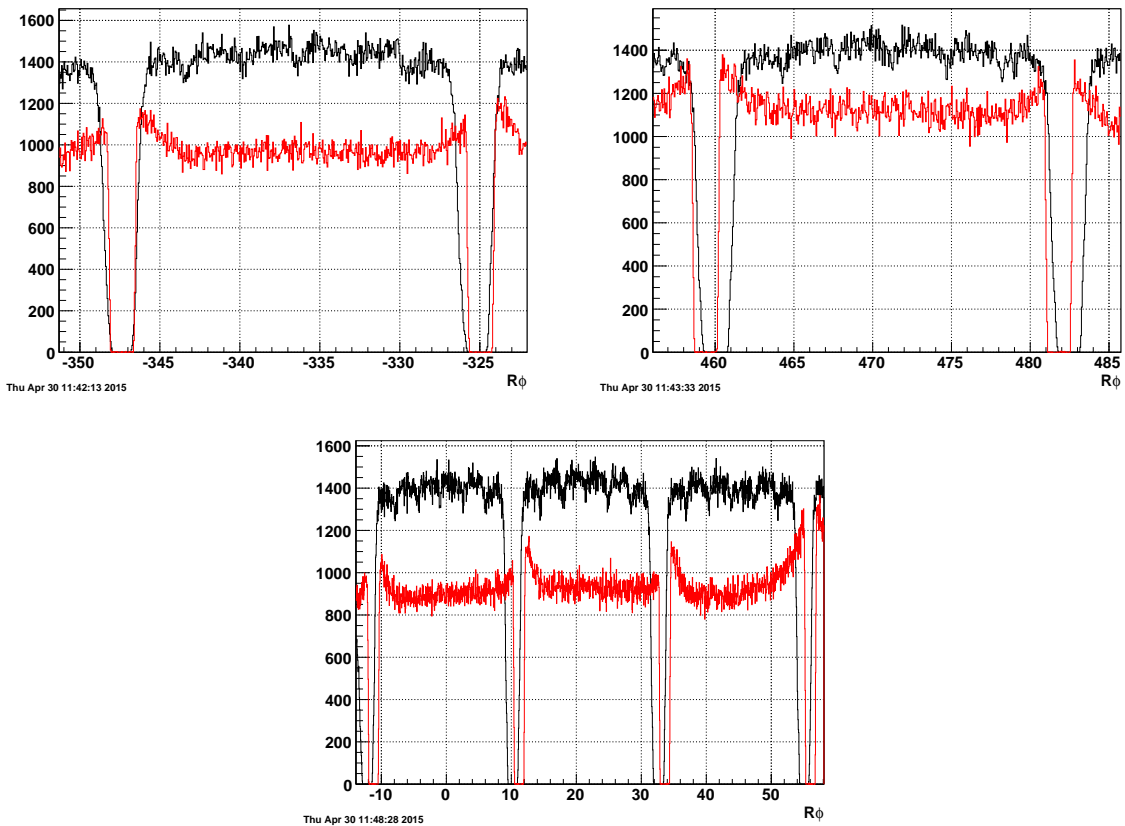


Figure 20: . The top left panel shows the projection of intercepts of tracks with a TOF detector cell along the local $R\phi$ coordinate on the cylindrical TOF surface. The top right panel shows a similar projection but zoomed on the region of negative values of z . Bottom panel shows similar detail of the projection but for positive values of z , and finally the bottom right panel shows the projection in the middle of the TPC.

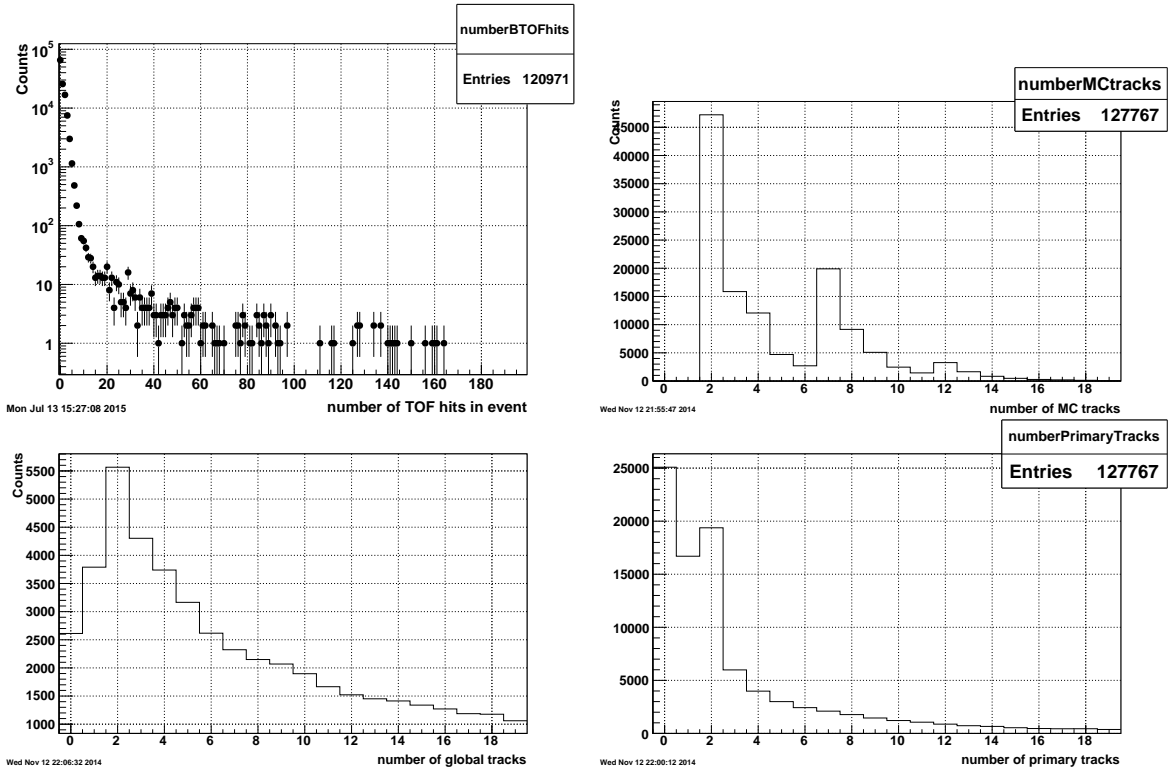


Figure 21: . The top left panel shows the number of TOF hits in the events. These hits include the MC generated particles extrapolated to the TOF active regions, as well as real data hits in the detector. The top right panel shows the number of GEANT and starlight generated particles. The bottom left panel shows the distribution of the number of global tracks found in the embedded events. Finally, the bottom right panel shows the distribution of reconstructed tracks associated to the primary vertex of the event.

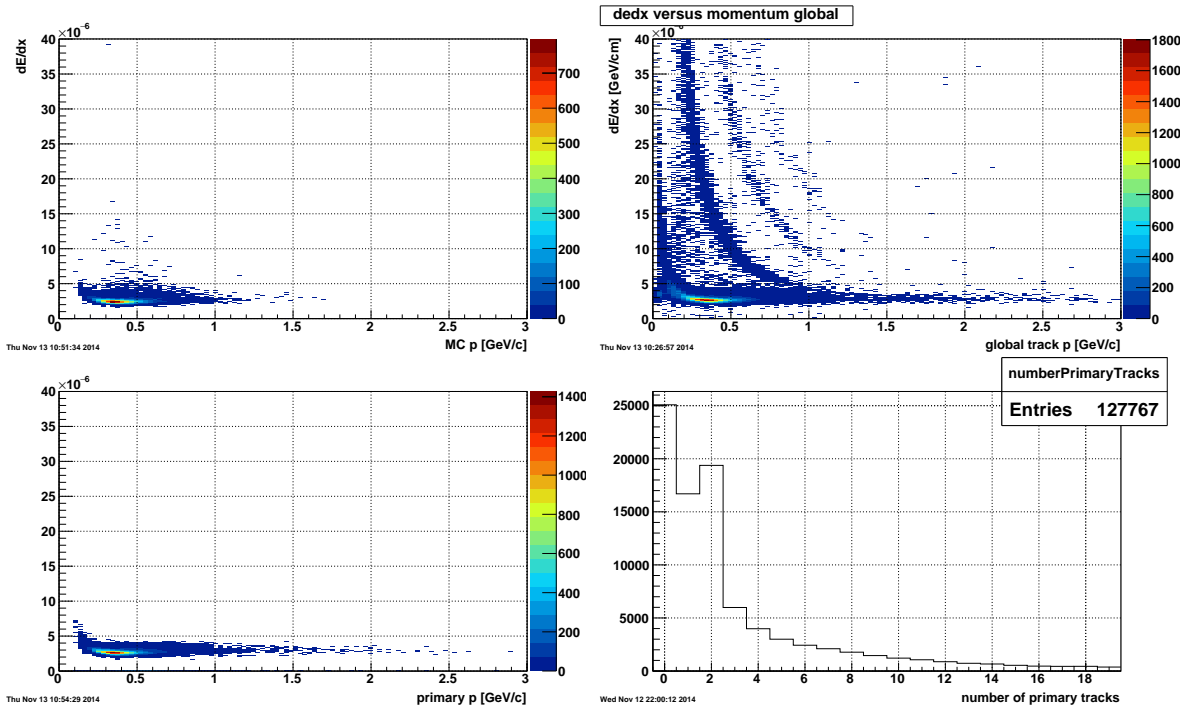


Figure 22: . The top left panel shows the GEANT simulated ionization losses for generated particles streaming through the TPC gas volume. The top right panel shows the ionization detected in the TPC for all tracks reconstructed in an event. The pion band dominates this figure together with some low momentum electrons. The next band is filled by protons followed by deuterons. The bottom left panel shows the ionization energy loss for primary tracks with the condition that it falls within 3 standard deviations from the calculated value.

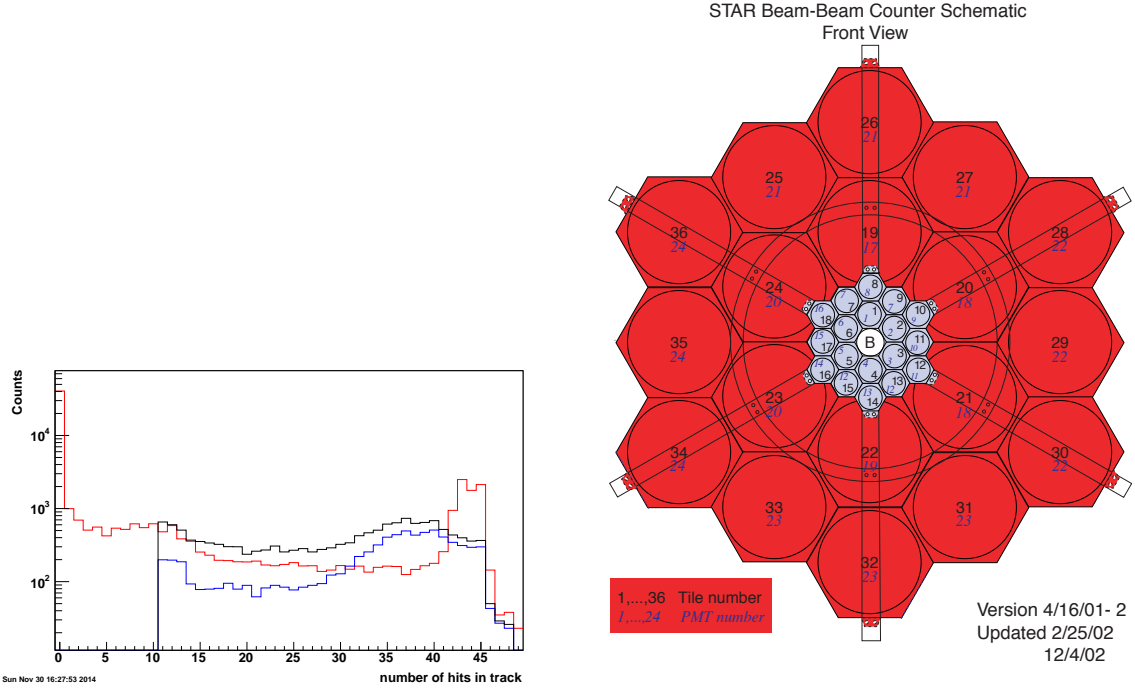


Figure 23: . Left panel shows the number of hits in three cases: MC tracks are shown as a red histogram, Blue for reconstructed primary tracks and black reconstructed global tracks. These tracks had already passed the condition of having more than 10 hits. Right panel: Arrangement of BBC tiles and PMTs connected to one or more tiles. The 18 small tiles cover the highest pseudo-rapidities ($3 < \eta < 5$) and are connected to 16 PMTs.

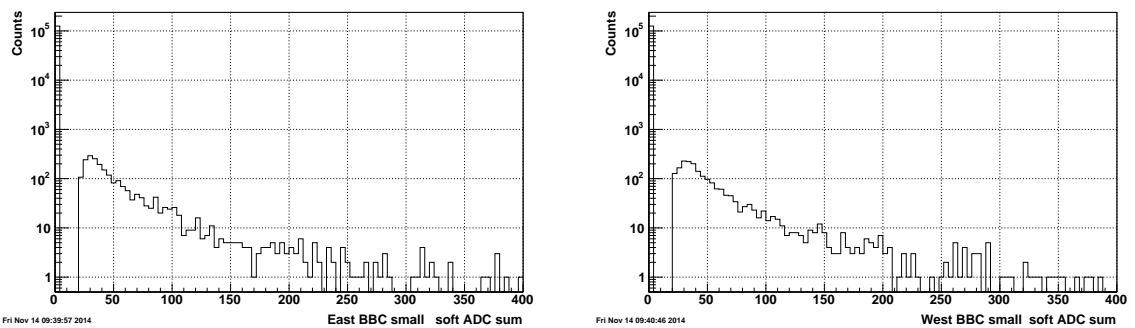


Figure 24: The left panel shows the sum of ADC from the East BBC small tiles. Each tile should have an ADC of more than 20 channels in order to be included in the sum. The right panel shows the corresponding sum for the small tiles of the West BBC detector. For both distributions, the threshold used for the UPC_Main rapidity gap vetoes is set at 50 channels.

7.5 BBC geometry, detector response and veto use in trigger

The Beam-Beam detectors BBC shown in the right panel of Fig. 23 are used in veto mode in the trigger, in this exercise, we estimate the fraction of events where the background in the zerobias events could eliminate good triggerable events. Sums of ADC values from all the small tiles are calculated for the East and West BBCs. A tile has to have an ADC with value greater than the same threshold as used for the defintion of the trigger; which for small tiles is set to 20 channels, Fig. 25 shows two distributions as a sample of individual tile distributions. The sum of small tiles in both BBCs detectors is shown in Fig. 24. The threshold used for these sums in the trigger definitions is set to 50 channels. (This information is available in the STAR RunLog under the “Trigger Details” section in every run. The effect from the small tiles veto on “UPC_Main triggers” has been estimated using the mixed embedding and only amounts to 4%

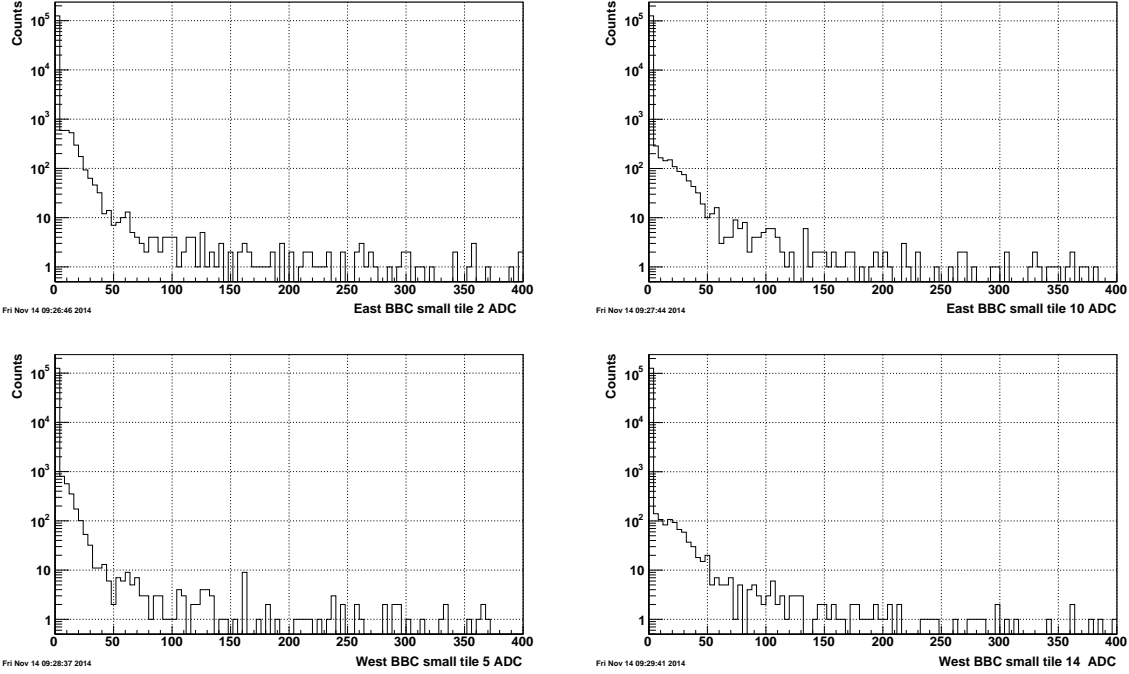


Figure 25: ADC distribution for four small BBC tiles shown as a representative sample in zerobias events. The signal shown in the figure came from tiles 2 and 10 on the East detector on the top panels, and signal from tiles 5 and 14 from the BBC West detector are shown in the bottom panels.

7.6 Track TOF matching extracted from embedding and from data

7.6.1 Introduction

This study is aiming at establishing a tool to compare data and embedding in order to quantify a systematic uncertainty related to the geometry of the TOF detector. This search is driven by the fact that, even after all corrections extracted from embedding are applied, the rapidity distributions show some clearly artificial drop at high rapidity and the distribution is not symmetric in rapidity. We are going to use the TOF-track matching as such tool and we expect to quantify any deviation between the detector geometry as registered in the data base and what may be the actual location of all active TOF elements.

This exercise was performed with the macro:

```
/star/u/ramdebbe/UPC/run10AuAu200/preparingPublication/extractTOFmatch_hit.C
```

which reads two data sets prepared for this exercise:

```
Data: "/star/data01/pwg/ramdebbe/run10AuAu200tree/productionRootFiles/UPCstudy200GeV_2010_2015
_DEC4_AllEvents_latestVersion_PID3sigma_vertexNumTrk2_hitsTrack14_LowMassCut250_5Ybins
_BkgPosNeg_TOFmatching.root";
Embedd: "/star/u/ramdebbe/UPC/run10AuAu200/readPrivateEmbeddingMuDst/fullChain_processed_2015
_PID3sigma_vertexNumTrk2_hitsTrack14_readyPDSFprod107_115_Production.readsAllEventsTestCentral_DEC.root";
```

The data has been collected with the UPC_Main trigger which includes the condition of 2 and no more than 6 TOF trigger hits (a TOF trigger hit is an OR of 8 adjacent TOF cells). Besides being an OR of several active elements the trigger TOF hits are feed to the trigger without further check. The TOF hits are subject to additional timing and signal checks, such difference explains why an event can have a smaller number of TOF hits compared to the trigger TOF hits. Figure 26 shows that for a particular number of trigger TOF hits a substantial number of events have higher number of TOF hits most likely noise hits in time with the trigger.

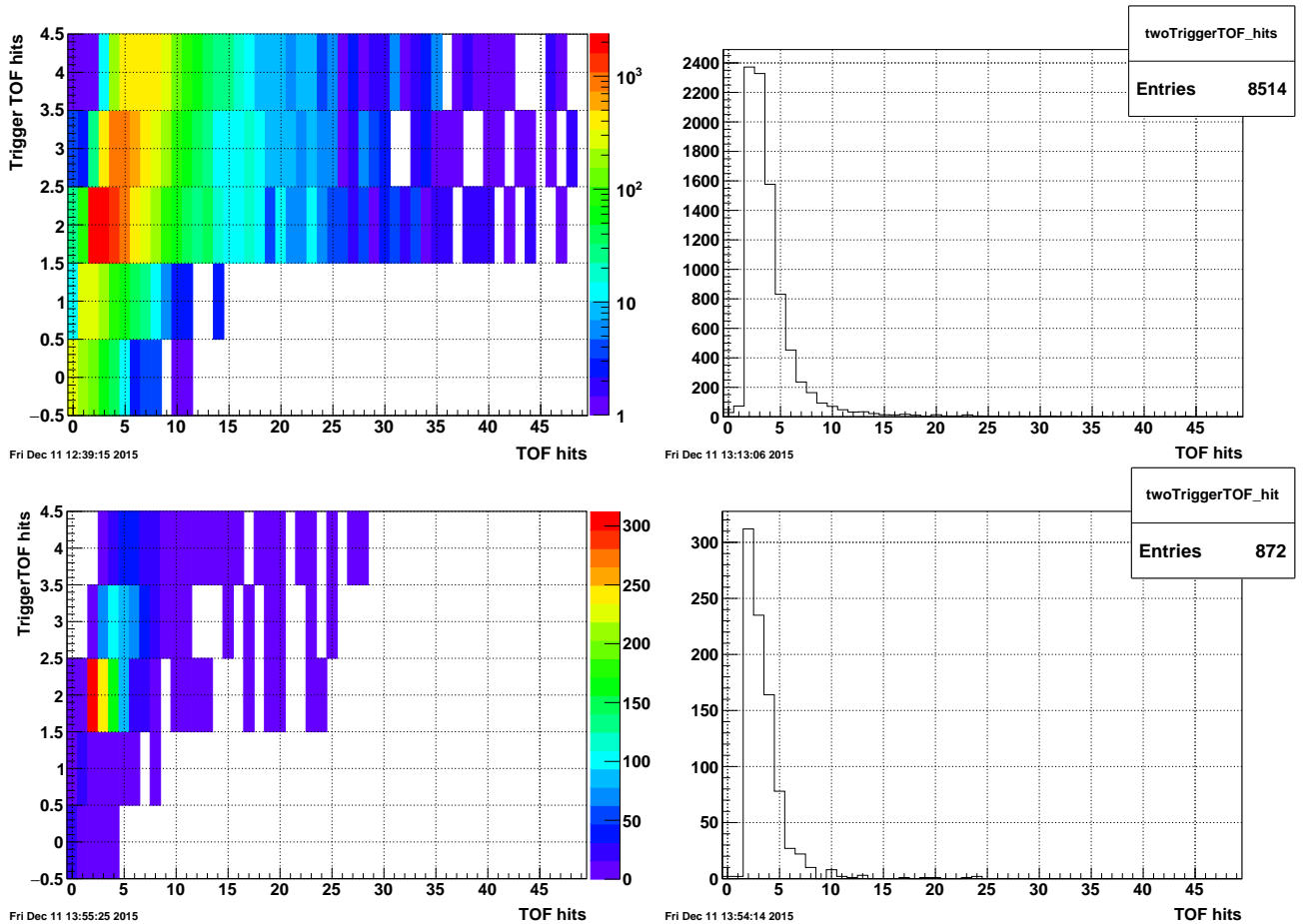


Figure 26: The left panel shows the correlation between the number of Trigger TOF hits versus the number of TOF hits for UPC_Main events. The right panel shows the number of TOF hits in events with 2 Trigger TOF hits. The fraction of events that had only one or more than 2 TOF hits is as high as 72%.

When working with data, the matching of tracks and TOF hits is done at the time the MuDst are produced and each TOF hit carries the index to the primary or global track that reached that active element of the TOF

detector. When we analyze the data written to the UPC pico Dsts, for each track we loop over the TOF hits and use the “index to primary track” to match that track to a particular TOF hit.

Whenever we work with data, the sample has been triggered with TOF and all events have TOF hits (some may not have tracks as we decided to write all events into the UPC pico dst for bookkeeping reasons). For that reason, whenever we study the matching of tracks to TOF hits in data we are only measuring the ability of the algorithm that performs the matching such result will be referred as TOFMatch efficiency.

The overall efficiency of the TOF system to detect a particle is the product of the actual detector response which is assumed to be the same for all cells or modules and labelled as TOFHit. The TOF efficiency also includes the TOF geometrical acceptance and the matching algorithm efficiency TOFMatch: $Epsilon_{TOF} = TOFHit \times TOFMatch$.

We use the geometrical acceptance of TOF (generated by Bill Llope) for $\sigma(Z_{vtx}) \sim 30\text{cm}$ and $|Z_{vtx}| < 50\text{ cm}$ with a value ranging from 84 to 88 %. In a recent e-mail Bill suggested that TOFHit would be high (90-95%). Figure 6 in [9] has that efficiency at 90% including absorption of low momentum particles.

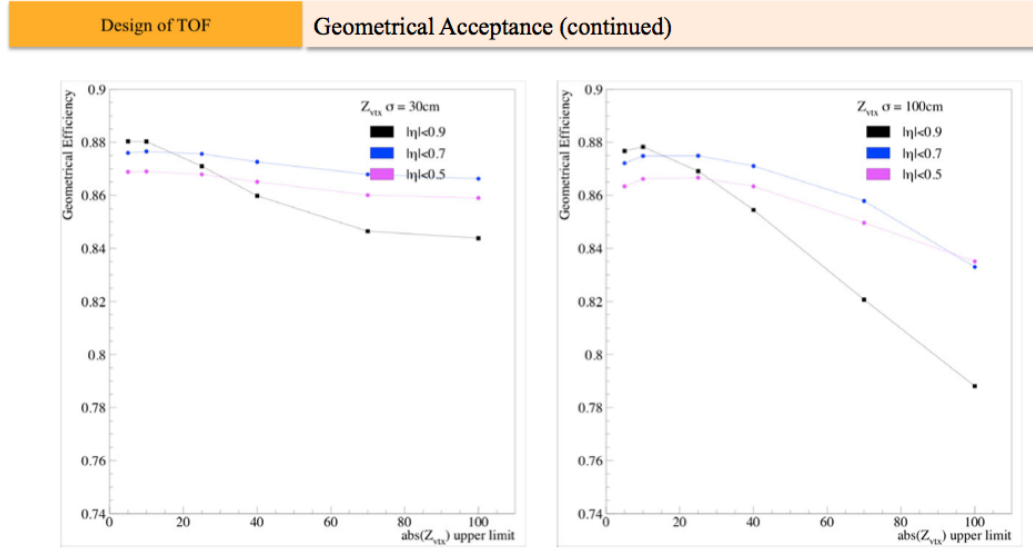


Figure 27: The geometrical acceptance of the full TOF detector (120 slats) for different vertex distribution and pseudo-rapidity windows.

The embedding logs indicate that the detector response was activated

7.6.2 Matching tracks to TOF hits

Starting with a sample of N_{tot} of two track events and both tracks in the TOF volume (the z coordinate of the track extrapolated to the TOF cylinder should satisfy: $|z| < 230. \text{ cm}$), the probability ϵ that a TPC track extrapolated to active section of the TOF detector satisfies the following relations:

$$N_0 = N_{tot} \times (1 - \epsilon)^2 \text{ where } N_0 \text{ counts the number of events where no tracks reached an active TOF cell.}$$

$$N_1 = N_{tot} \times 2\epsilon \times (1 - \epsilon) \text{ with } N_1 \text{ the number of events where only one track reaches an active TOF cell.}$$

$$N_2 = N_{tot} \times \epsilon^2 \text{ where } N_2 \text{ is the number of events where both tracks reach an active TOF cell.}$$

From 2D histograms recording pion pairs invariant mass versus rapidity for the three types of events we extract ϵ as function of rapidity for events with only two tracks. Figure 29

From the expressions presented above for N_1 and N_2 one can extract ϵ which is a combination of the geometrical TOF acceptance that includes the dead areas between TOF cells and the alignment of the TOF detector with respect to the TPC tracks. It also includes the efficiency of the match maker algorithm:

$$\epsilon = \frac{2N_2}{N_1 + 2N_2}$$

The macro /direct/star+u/ramdebbe/UPC/run10AuAu200/preparingPublication/extractTOFmatch.hit.C loops over the rapidity bins of the 2D histograms after the subtraction of the corresponding background histograms (same charge) is done. It then produces the result shown in Fig. 30 and 34.

The left panels of figures 30 and 34 show the TOFmatch quantity with black markers. That quantity has been extracted from data events with clean exclusive following the method described above with cuts in vertex ($|z| < 50 \text{ cm}$) and without vertex cuts respectively. The red markers display the ϵ_{TOF} efficiency as extracted from embedded ρ^0 in zerobias events. The right panels of those figures show the ratio of those quantities: ϵ_{TOF}

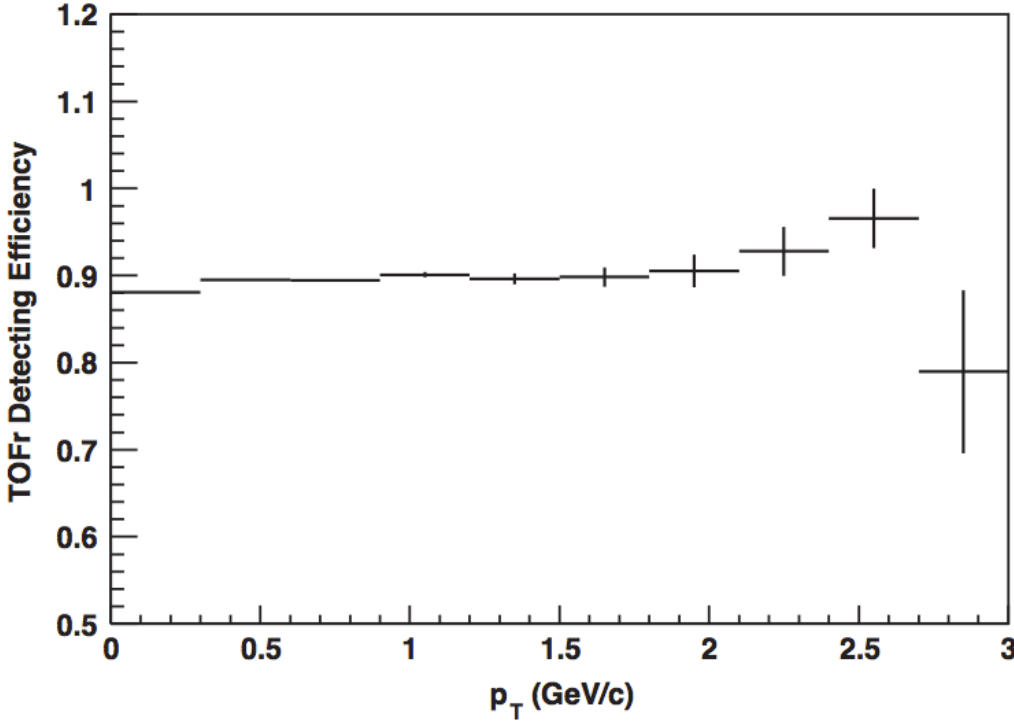


Figure 28: "TOFr detection efficiency as a function of particle transverse momentum" (Extracted from [9]).

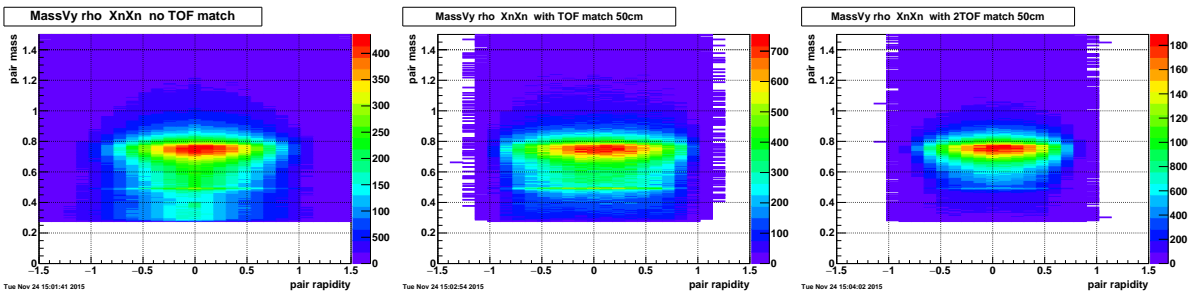


Figure 29: From left to right, each panel shows the correlation of invariant mass and the rapidity of the pion pair. All three histograms are filled with opposite charge pairs originating from vertices with only two tracks. The left most panel is filled with events that had no tracks reaching and active TOF cell, the middle panel is filled with pairs where only one track reaches TOF and the right panel was filled with events where both tracks reached active TOF cells.

from embedding divided by TOFmatch obtained from the ρ^0 data sample. As explained above the above the data sample has been triggered by the UPC_Main trigger which demand 2 or more TOF hits. In order to transform the TOFmatch extracted from data into a full TOF efficiency ϵ_{TOF} it needs to have a component which is only related to the detector response which we label as TOFHIT: $\epsilon_{TOF} = TOFmatch \times TOFHIT$. The best handle we have about that efficiency is a test performed with a TOF module prototype mounted in a CTB box during an early run at RHIC as described in [9]. We reproduce here Fig. 6 of that paper were the response of the detector appears constant as function of transverse momentum at a value of 90%.

Once we multiply TOFmatch by the detector efficiency obtained during the test of a prototype TOF module we can compare it to the one extracted from the embedded data sample. Such comparison shows a deficit at high rapidity for the efficiency extracted from the embedded sample. That deficit can be explained by a mismatch between the actual geometry of the TOF detector as it is installed in STAR and how it is described in the data base and used for Monte-Carlo simulations. The alignment of the TOF detector is done near mid-rapidity where the modules have no rotation. A systematic uncertainty related to this lack of full knowledge of the actual location of all TOF elements is then defined as: syst. uncert = $1.41 \times (\epsilon_{TOF}(data) - \epsilon_{TOF}(embed)) / \epsilon_{TOF}(data)$ where the 1.41 comes from the fact that we are working with two tracks with equal uncertainty added in quadrature.

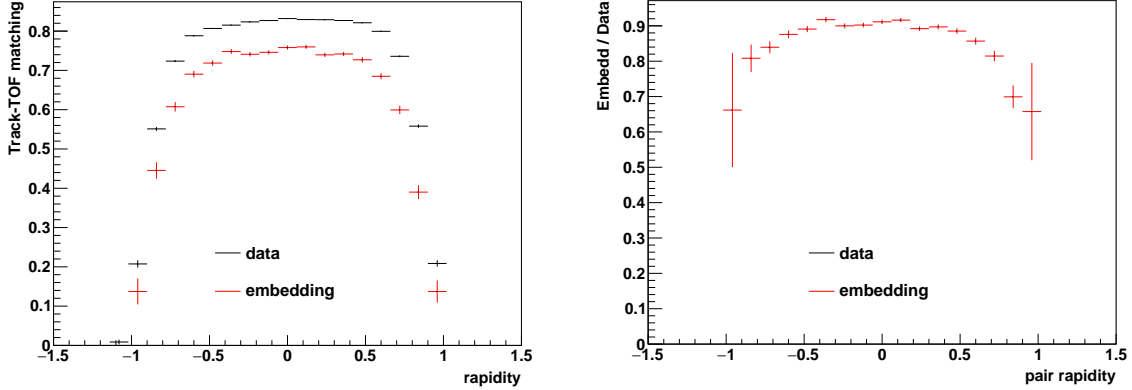


Figure 30: The black histogram shows the track TOF matching “efficiency” as described in the text. This quantity is extracted from data samples shown in Fig. 29. Eventhough this quantity relates to single tracks, for convenience, it is displayed as a function of the pair rapidity. The red histogram is the same quantity but extracted from embedding sets shown in Fig. 31. Both histograms were extracted with a $|Vtx_z| < 50$ cm

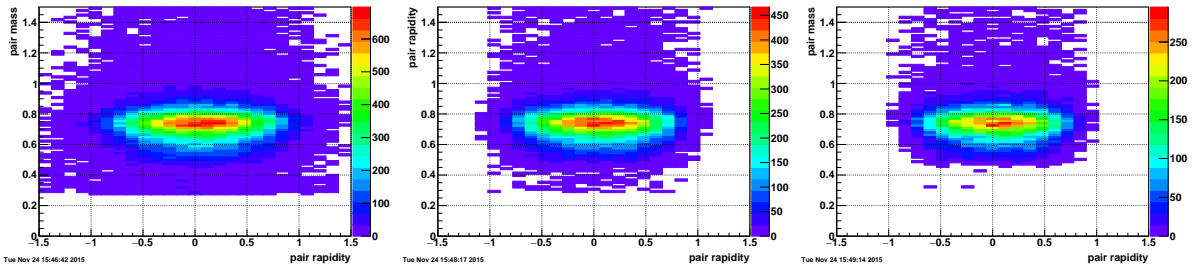


Figure 31: From left to right, each panel shows the correlation of invariant mass and the rapidity of the pion pair. All three histograms are filled with opposite charge pairs originating from vertices with only two tracks produced in the embedding project. The left most panel is filled with events that had no tracks reaching and active TOF cell, the middle panel is filled with pairs where only one track reaches TOF and the right panel was filled with events where both tracks reached active TOF cells.

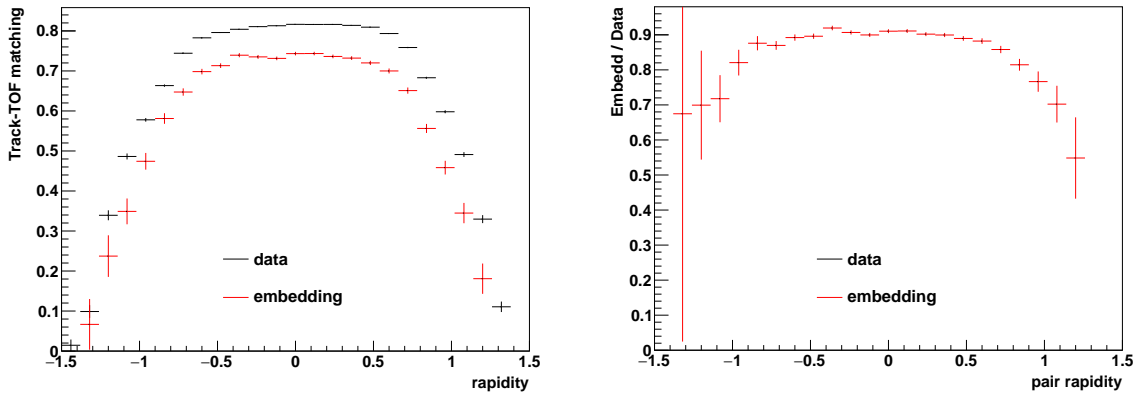


Figure 32: The black histogram shows the track TOF matching “efficiency” as described in the text. This quantity is extracted from data samples shown in Fig. 29. Eventhough this quantity relates to single tracks, for convenience, it is displayed as a function of the pair rapidity. The red histogram is the same quantity but extracted from embedding sets shown in Fig. 31. No vertex cuts were applied to extract these curves.

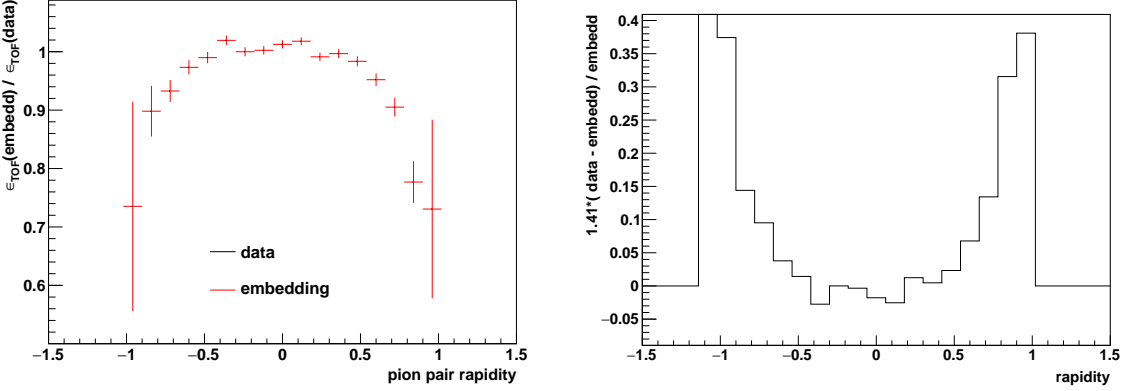


Figure 33: The left panel shows the ratio of ϵ_{TOF} extracted from the embedded events over the same quantity constructed from TOFmatch extracted from data and multiplied by the detector efficiency TOFHit. The right panel shows the corresponding systematic uncertainty extracted from the comparison of ϵ_{TOF} extracted from data and embedding (MC). The results shown in both panels were obtained with events with vertices that satisfy: $|z| < 50$ cm.

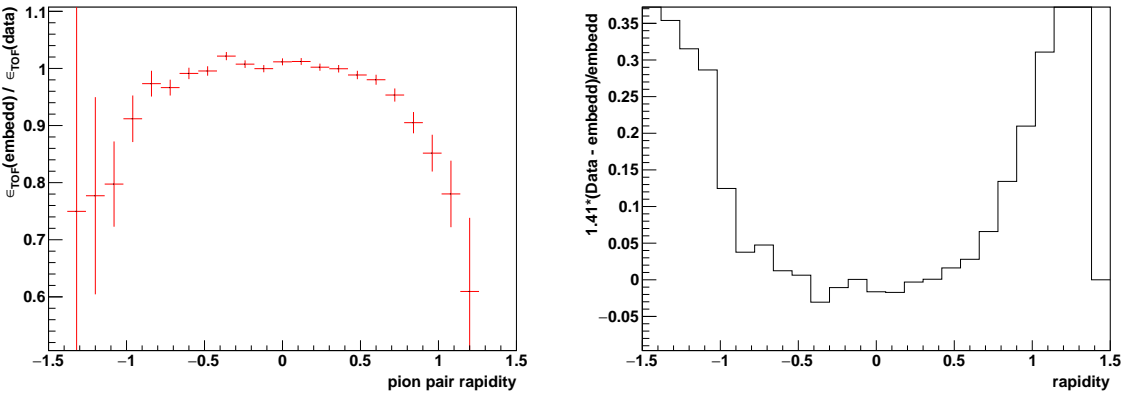


Figure 34: The left panel shows the ratio of ϵ_{TOF} extracted from the embedded events over the same quantity constructed from TOFmatch extracted from data and multiplied by the detector efficiency TOFHit. The right panel shows the corresponding systematic uncertainty extracted from the comparison of ϵ_{TOF} extracted from data and embedding (MC). The results shown in both panels were obtained with events with no conditions on the z coordinates of the vertices.

7.7 Extraction of efficiencies from the Mixed embedding

Figure 35 shows the distribution of pseudo-rapidity of the pions originating from the decay of the starlight ρ^0 meson with blue markers. The matching between reconstructed tracks and particles generated by starlight is done in the following way. The MuDst files produced during full reconstruction of the mixed events contains the information on TOF hits in the class StMuBTofHits which has a member named idTruth(), that member stores the id of the track that extrapolates to that particular TOF cell. A search for that track in the MC track container StMuMcTrack is done using the iD found in the TOF hit. If that MC track exists, its GEANT iD stored in its member GePid() set the final identification as a positive or negative pion.

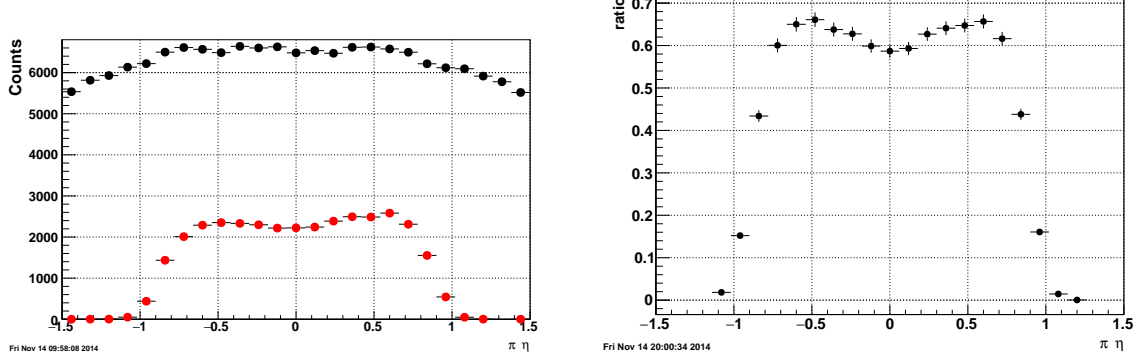


Figure 35: Left panel: Black markers show the pseudo-rapidity distribution of all primary tracks. The red markers show the corresponding distribution for primary tracks which hit an active TOF element. Right panel: The ratio of pseudo-rapidity distribution of primary reconstructed tracks that match a TOF hit and all primary tracks.

The ratio of the pseudo-rapidity distribution of reconstructed tracks matched to pions to the same distribution for all generated pions shown in Fig. 35 shows the effect of the TOF acceptance and the average TOF-track matching efficiency of 80%.

The momentum distribution of the MC particles produced by the event generator together with the momentum distribution of reconstructed tracks that extrapolate to active TOF cells are shown in Fig. 36. Most of the secondary particles generated by GEANT have low momentum and are not included in this figure. The right panel shows the combined effect of the detector acceptance, tracking reconstruction and TOF matching efficiency, averaged over all values of rapidity.

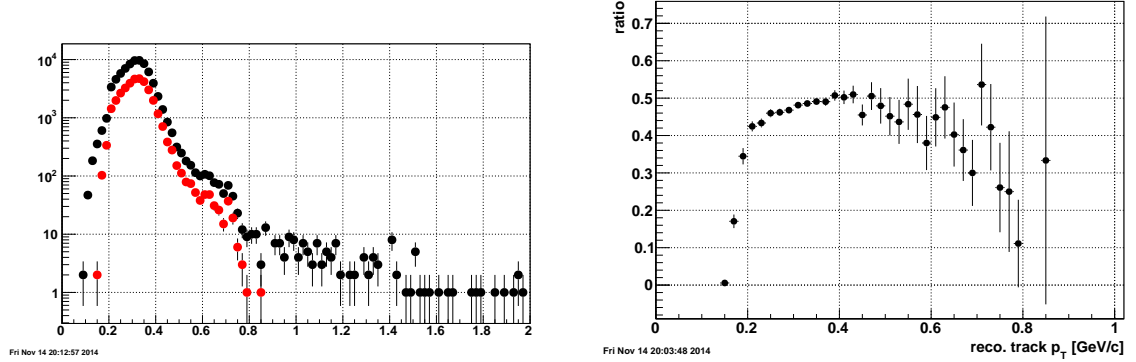


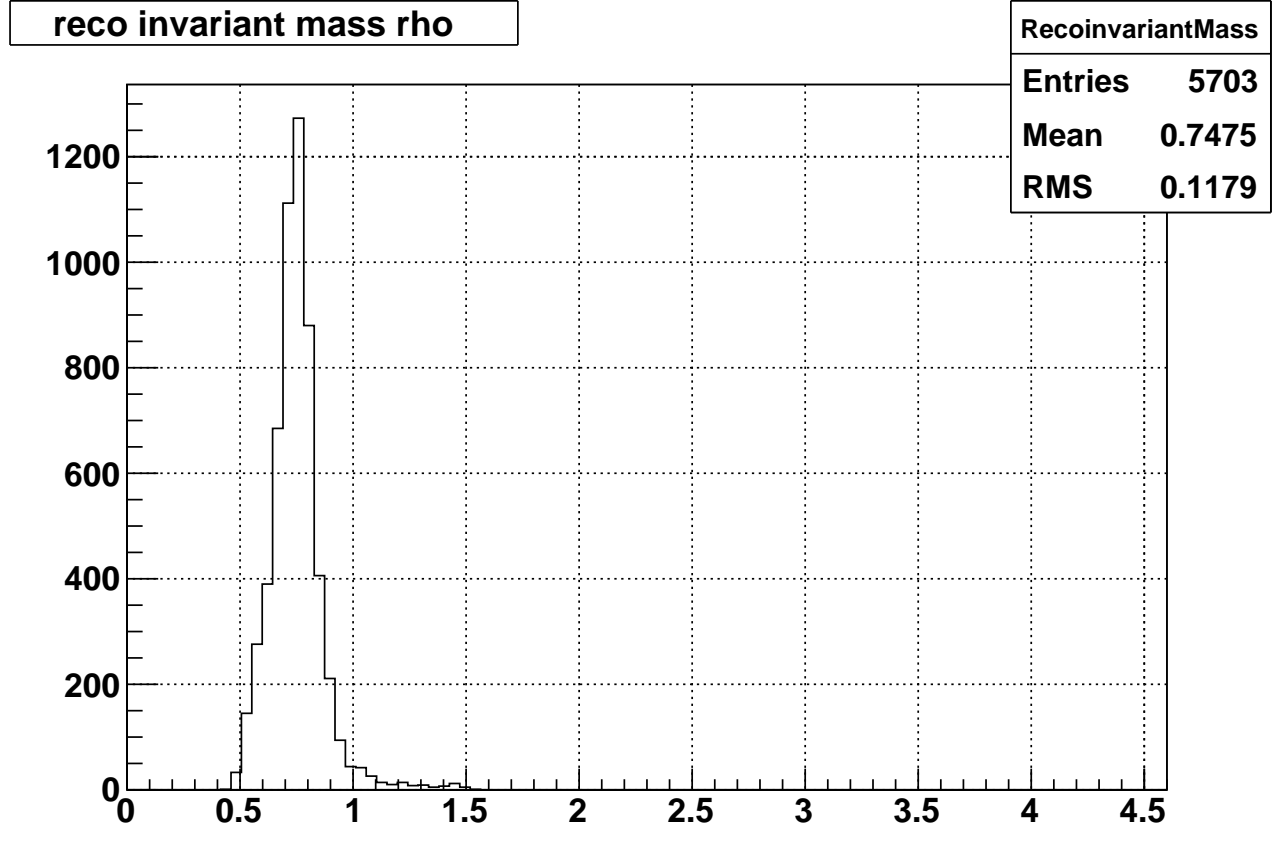
Figure 36: Left panel: Black markers show the momentum distribution of the pions generated by starlight. The red markers show the momentum of reconstructed tracks that have been matched to the original pions produced in the decay of the ρ^0 mesons. Right panel: The ratio of momentum distributions of reconstructed tracks matched to pions and all MC pions.

The ratio of momentum distributions of reconstructed tracks matched to generated pions to the one for all generated pions is shown in the right panel of Fig. 36. Its shape and magnitude matched the so called track-matching efficiency for the TOF detector.

Similar comparisons between generated and reconstructed objects can also be done at the level of the ρ^0 mesons. To begin that analysis, the invariant mass of generated pion pairs of opposite charge has been calculated

among the class of StMuMcTracks. The result is shown in Fig. 37 which shows the shape as the MC distribution shown in the bottom right panel of Fig. 11. The generated pions are identified by the GEANT Id of the MC tracks and all events have one pair of opposite charge. The rapidity distribution of the generated ρ^0 mesons is shown with black markers in the left panel of Fig. 38.

The reconstructed pions are identified by selecting TOF hits which matched MC tracks with GEANT Ids for charged pions (8 and 9). The matching is possible by the use of the member IdTruth in the StMuMcBtofHit class. Two such pions of opposite charge have to be present in the reconstructed events, the invariant mass of such pair is shown in Fig. 37 has the proper shape for a ρ^0 meson. The rapidity distribution for these reconstructed pion pairs is displayed with red markers in the left panel of Fig. 38. The rapidity range for these pairs is $-1 < y < 1$ consistent with the acceptance of the TOF detector. The ratio of reconstructed to generated ρ^0 mesons is shown in the right panel of Fig. 38 which in that particular case includes the losses for exclusive events originating from a gaussian vertex distribution along the nominal beam line.



Wed Nov 12 16:02:27 2014

Figure 37: The invariant mass distribution of the reconstructe pion pairs of opposite charge.

Whenever a result is to be displayed as function of transverse momentum or t , a similar “full chain correction” is needed as function of transverse momentum of the pion pair. Figure 39 shows such correction first as a two dimensional ratio of found ρ^0 candidates and generated mesons. The flat transverse momentum dependence was already extracted from the first embedding request as shown in Fig. 132. The difference in magnitude can be explained by the fact that the first embedding exercize did not include the vertex finder (60%) and TOF match (80%) contributions.

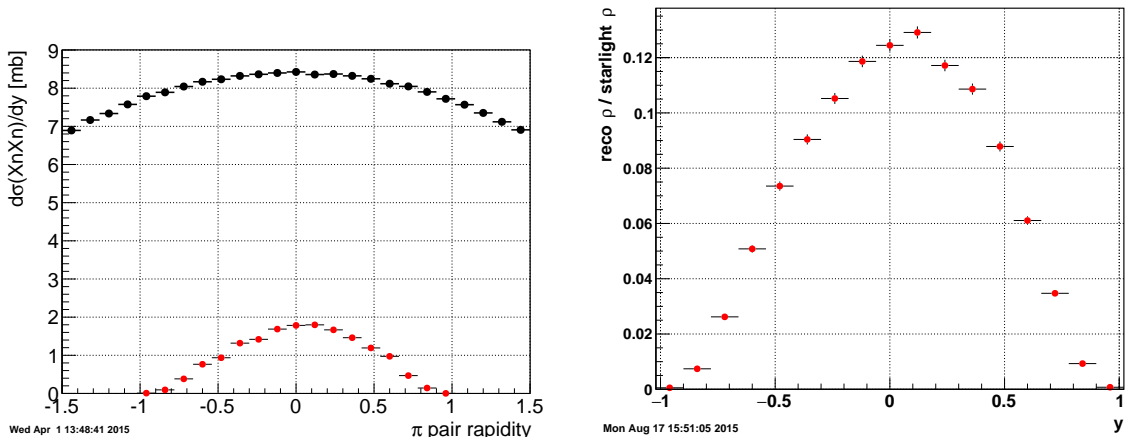


Figure 38: Left panel: The rapidity distribution of the generated pion pairs of opposite charge is shown with black markers. Similar distribution built with pion pairs identified as such with tracks that reached the active elements of TOF is shown with red markers. See details in text. Right panel: The ratio of the rapidity distribution of reconstructed pion pairs over the generated pairs. This ratio is used as a correction to be applied to the raw signal extracted from data as function of rapidity.

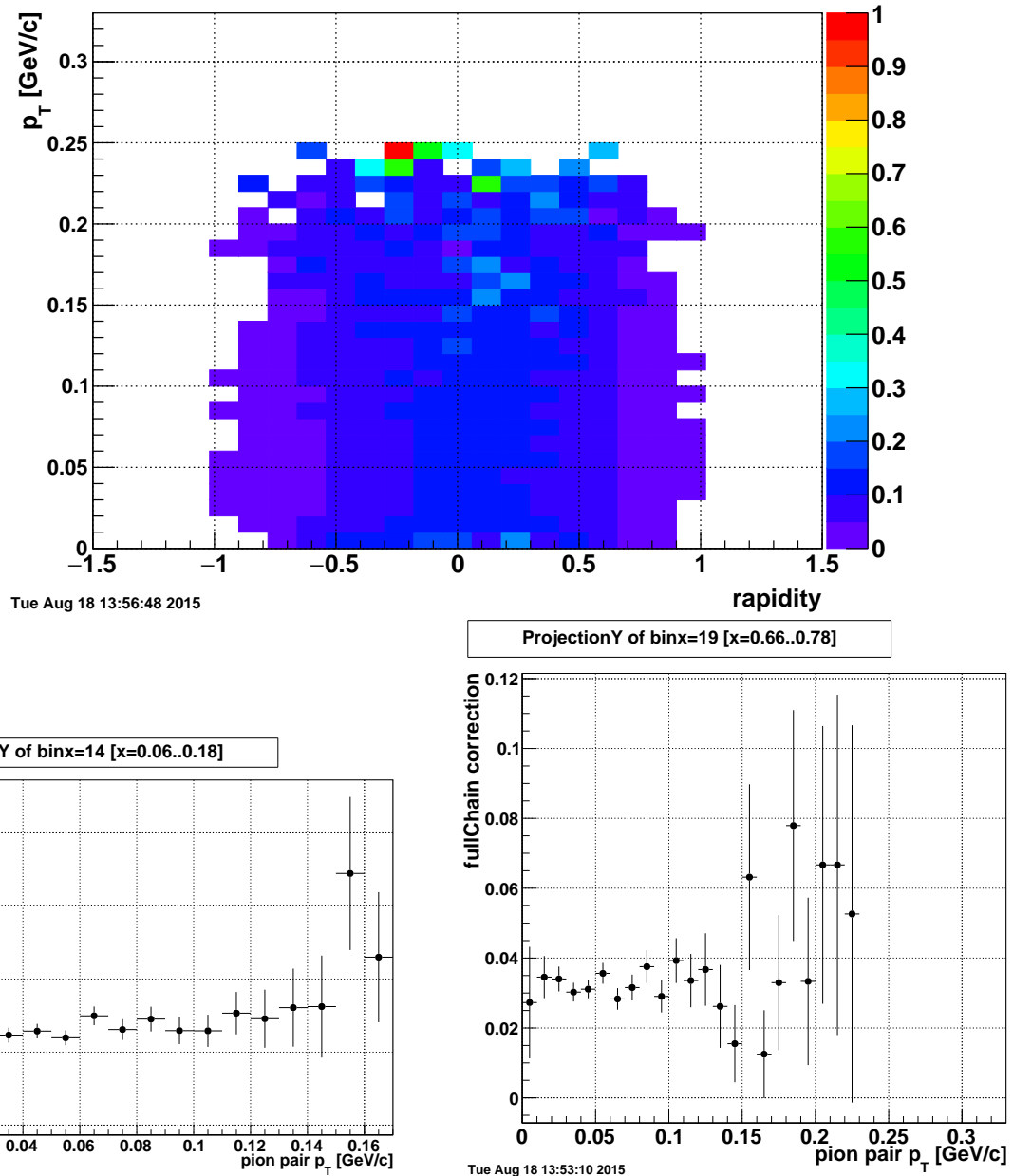


Figure 39: . The top panel shows the ratio of 2D histograms; the numerator is filled with p_T and rapidity values of reconstructed ρ^0 mesons, and the denominator is filled with same variables for the generated mesons. The bottom left panel shows the flat “fullChain” correction as function of the transverse momentum of the ρ^0 meson in a rapidity window close to $y=0$. The bottom right panel shows a similar correction but at a higher rapidity ($y \sim 0.75$).

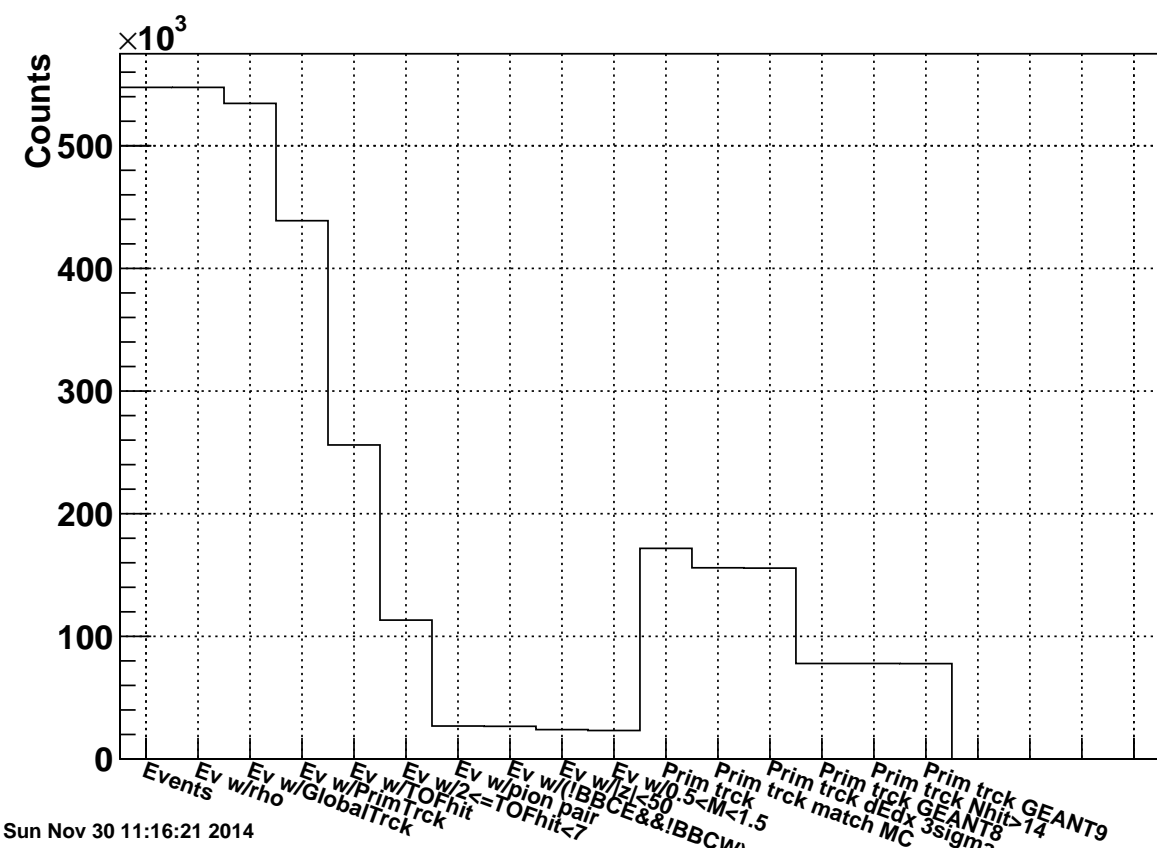


Figure 40: Histogram to visualize the effects of each of the cuts applied to the MuDsts produced by the embedding project.

Effect of different cuts (event wise)			
Cut description	Events that survive cut	Histogram bin number	Fraction survive
Total number of events	547596	1	
Events with MC ρ	547590	2	
Events with at least one global track	534534	3	
Events with at least one primary track	438892	4	
Events with at least one TOF hit	256046	5	
Events with $2 \leq \text{TOF hits} \leq 6$, a reco. vertex and at least a track pointing to a TOF hit	113254	6	
Events with one reco $\pi^+ \pi^-$ pair	26892	7	
Events with rap. gap (BBC)	26658	8	
Events with vertex $ z < 50\text{cm}$	23967	9	
Events with pair inv. mass $0.55 < M < 1.5$	23238	10	
Effect of different cuts on primary tracks			
Total number of prim. tracks	171737	11	
Total number of prim. tracks that match MC	155902	12	
Primary tracks with dE/dx 3σ cut	155643	13	
Primary tracks match GEANT id8	77872	14	
Primary tracks with $N_{\text{hits}} > 14$	77872	15	
Primary tracks match GEANT id9	77771	16	

Table 1: .

8 Analysis

The latest production of pico DST was done on 24-OCT-2014 from

/star/u/ramdebbe/UPC/run10AuAu200/cleanProcessing/fromFileCatalogue/
with scripts:

```
submitFromFileCatalogue011035_011093.xml  
submitFromFileCatalogue012002_017059.xml  
submitFromFileCatalogue018002_031089.xml  
submitFromFileCatalogue032011_038069.xml  
submitFromFileCatalogue039001_060082.xml  
submitFromFileCatalogue061001_077018.xml
```

The output of the StPeCMaker is written to disk as root ntuple trees. The analysis of the data at this final level has been done with the macro “processData” which was built upon an skeleton produced by the MakeClass method of root’s TTree class. The complete P10ik production produced 38502251 events written in 37504 MuDst files, At the time the data was aquired, a run may be written in up to 25 separate files. The offline production keeps that structure and the MuDst corresponding to a particular run are not read consecutively in the final pass of the analysis.

8.1 Data (2010) pico DST location

The files are located in the disk:

/star/data01/pwg/ramdebbe/run10AuAu200tree/latestVersion14_OCT/
and have names:

```
20D26F19B0594F9815FF7B3213CE7D99_*.tree.root 2 files  
323C83D2C09E638B9DA922CF131B2F9C_*.tree.root 89 files  
E7E889195BB8897DAF83775E6D0BF9D1_*.tree.root 168 files  
1E182B931886673782B0B862377A01C2_*.tree.root 108 files  
28D35F20D39D0FAC125BEF1D0933F5EB_*.tree.root 1 file  
8C3E4A15E5359EDAF9CEA5FB2A3E3D82_*.tree.root 422 files  
052604A8431B228277E3182A5672F287_*.tree.root 302 files
```

Refer to table 10 to match the file names and the range of run numbers.

8.2 Mixed Embedding (SL10k_embed + .DEV2) pico DST location

/star/data06/UPC/KFvertex/picoDst_PPV/3DCCFEC28BBDB300A8ABB8119DBFE252_*.tree.root
/star/data06/UPC/KFvertex/picoDst_PPV/C3B7C8FA9C1D01AE128B90BB56D00B58_*.tree.root

8.3 Performance monitoring throught the run

Figures 41, 42 and 43 show averages over each output file displayed as function of run number.

These figures indicate an overall stability of the data collection with the exception of the very first runs of day 11 where the ZDC averages deviate from the rest of the data.

As TOF is such integral part of the UPC_Main trigger, any background produced by noise in the detector or beam backgrounds would affect the purity of the trigger.

The Zero Degree Calorimeters (ZDC East and West) are also part of the trigger:

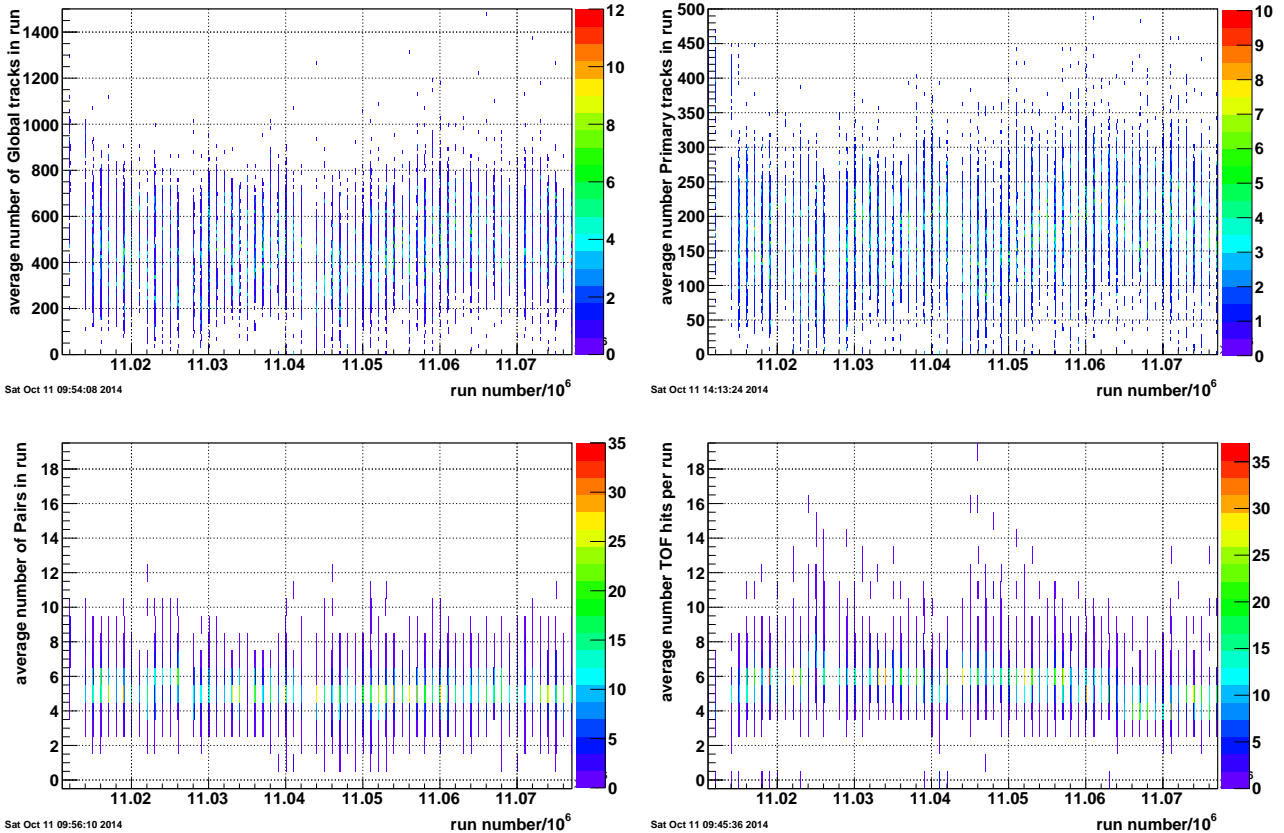


Figure 41: Top left panel shows the number of Global tracks in the event averaged over a run shown as function of the $(\text{run number})10^6$. Each run can have up to 25 separate files that are not read sequentially, such fact explains the spread in y. Top right panel shows the number of primary tracks in the events averaged over runs. Bottom left panel shows the number of pairs in an events averaged over runs. Bottom right panel shows the The number of actual TOF hits in the event averaged over a run.

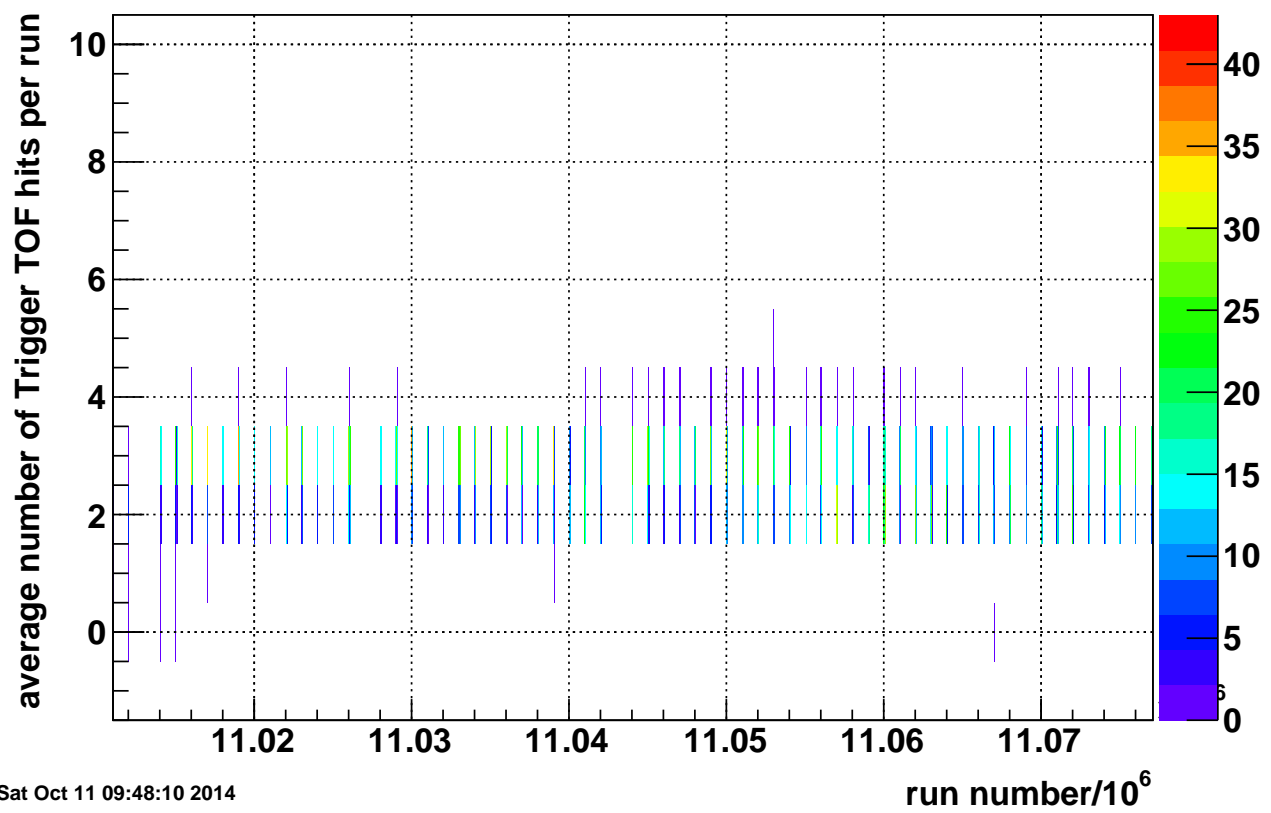


Figure 42: The number of Trigger TOF hits (Trigger TOF hit == ΣTOF) in the event averaged over a run.

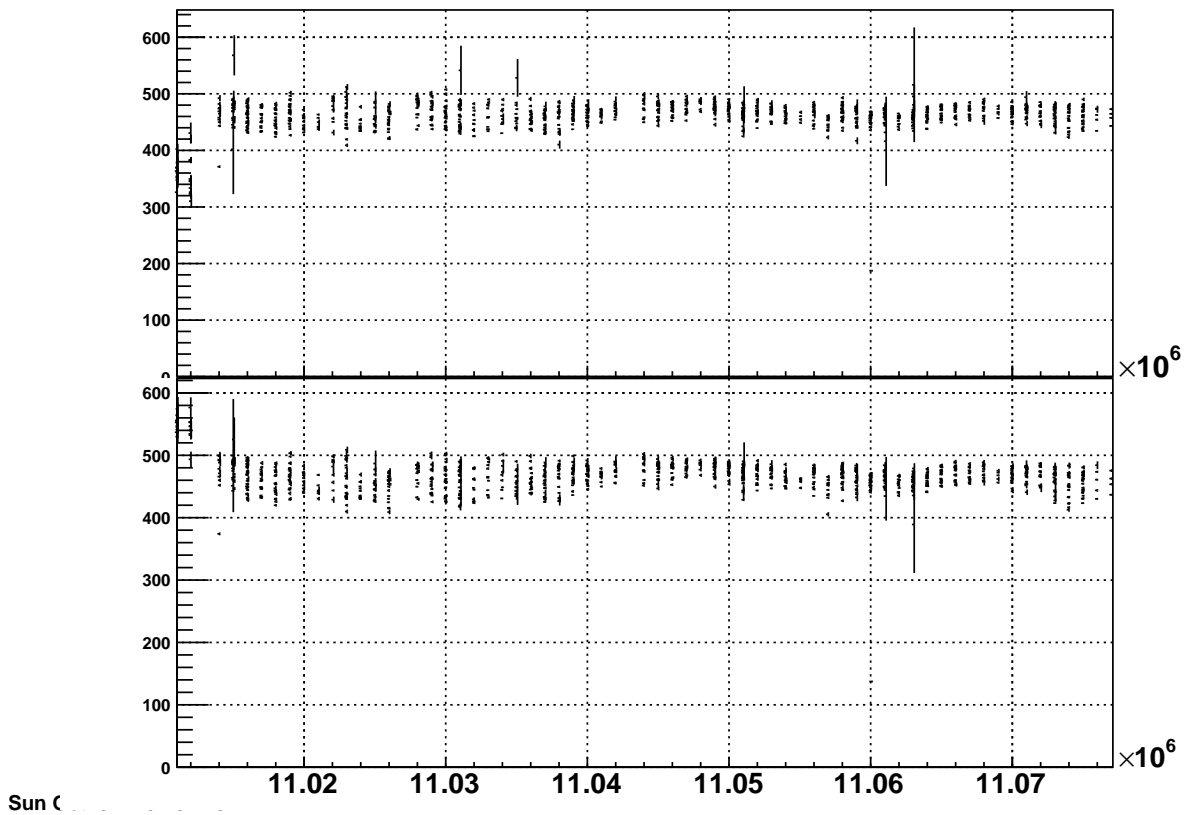


Figure 43: The top panel shows the average ADC for the un-attenuated signal of the ZDC East detector as function of the run number. The bottom panel shows the ADC average for the ZDC West detector. The displayed average corresponds to 2 neutrons.

8.4 UPC_Main definition and XnXn cross section

Here we estimate the fraction of the XnXn cross section that we do not “see” because of the ZDC ADC cuts 50, 1200 we use the “Mutual heavy ion dissociation in peripheral collisions at ultrarelativistic energies” [15]. We have also received a copy of the authors event generator RELDIS that we compiled and run at CERN.

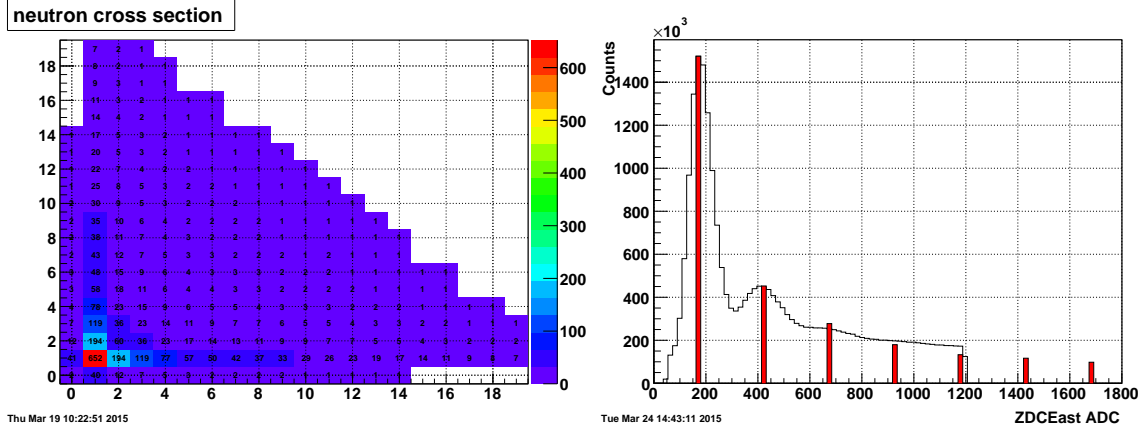


Figure 44: The left panel shows the results of the Mutual electromagnetic dissociation calculation by Pshenichnov et al. (RELDIS) as cross section values for all possible combinations of number of neutrons and other hadrons emitted towards the East and West ZDCs. The values of cross sections are displayed both with a color palette and the actual value of the cross section displayed on each bin. The right panel shows the agreement between the calculation and actual data from ZDC_West collected during run 2010. The calculated cross section value for the emission of a single neutron has been scaled to match the maximum of the one neutron peak. The cross section values are displayed with a red filled histogram. Caveat: this is only a rough comparison, more detailed comparisons follow at the end of this section.

Electromagnetic Mutual Dissociation			
Selection East	Ratio West	Data(%)	RELDIS(%)
1n	2n/1n	28.9	29.7
1n	3n/1n	15.3	18.2
2n	2n/1n	28.	30.9
2n	3n/1n	5.7	18.2
3n	2n/1n	29.	30.2
3n	3n/1n	6.9	19.
4n	2n/1n	29.8	29.5
4n	3n/1n	7.4	19.
	2n2n/1n1n	5.4	9.2
	3n3n/1n1n	0.8	3.5

Table 2: Comparison between ZDC data collected with the UPC_Main trigger and the RELDIS calculation. Histograms are filled with selections on the number of neutrons detectors in the East ZDC and fitted with 5 gaussian shapes as shown in Fig. 45. For each selection on the ZDC East, two ratios are presented both for data and the RELDIS calculation. The ratio 2n/1n is in remarkable agreement with the measured ratio. Such agreement is not present any more for the 3n/1n ratio in events with more than one neutron detected on the East ZDC. The last two rows are an attempt to compare the calculation to ratios extracted from data with one, two, and three events in both ZDCs. It should be noted that the third and further neutron peaks are weakly defined and a big systematic error should be assigned to any quantity extracted from them

The main result obtained from the use of the RELDIS event generator is a more accurate estimate of the fraction of the XnXn cross-section accessible with the UPC_Main trigger (1 and up to 5 neutrons on each ZDC within the 13.6 X 10 mm front face of each ZDC (see top right panel of Fig. 46); A fraction of 51.4% events satisfy the UPC_Main conditions. The correction to extract the full XnXn cross-section is then $1/(1-0.486) = 1.945$.

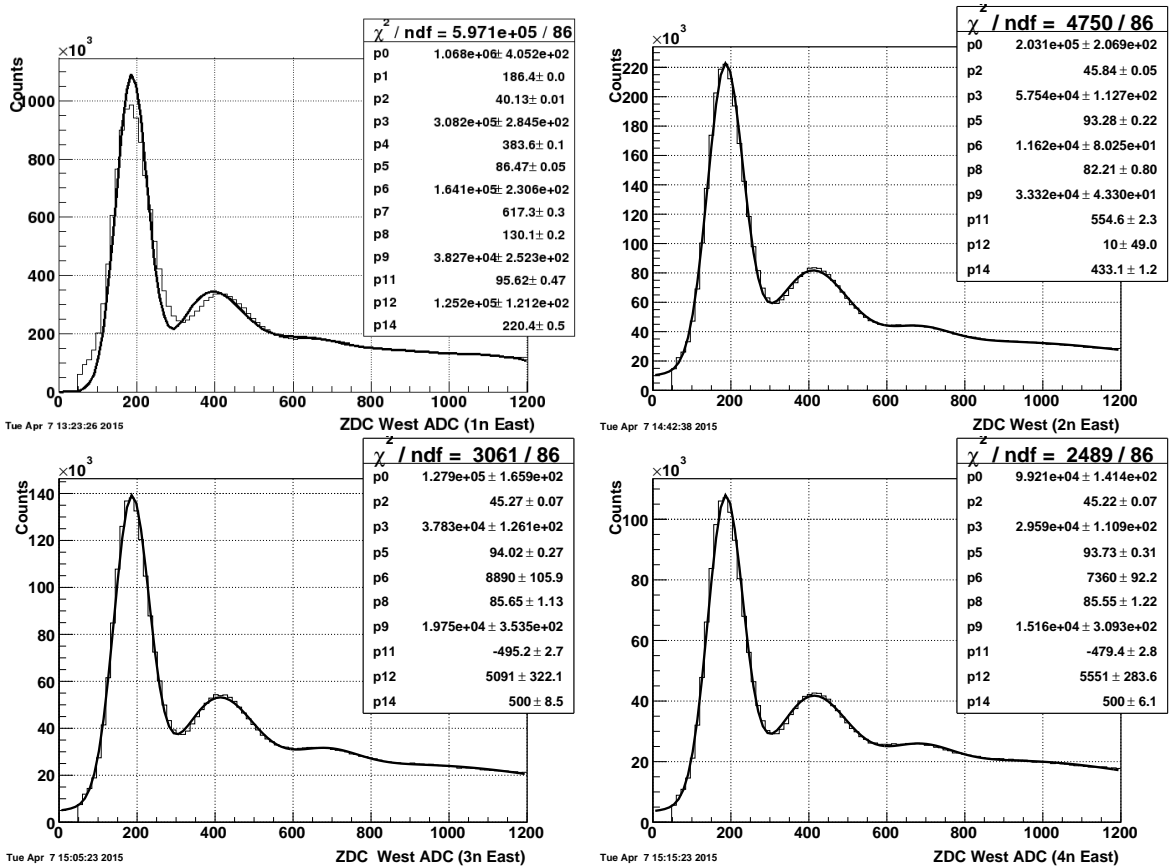


Figure 45: Fits to the ZDC West ADC distributions for events with four different number of neutrons detected in the East ZDC. Top left panel shows the fit to the ZDC distribution where the East ZDC detected one neutron. Top right panel is a fit to the distribution with 2 neutron in the East ZDC. Bottom left for 3 East neutrons and bottom right for 4 East neutrons. The distributions are fit with a sum of five gaussian shapes. The normalization and RMS of the gaussians is a free parameter of the fit. The centroids of the gaussians were obtained in incremental fits and held fixed when all five gaussians were used in the fit.

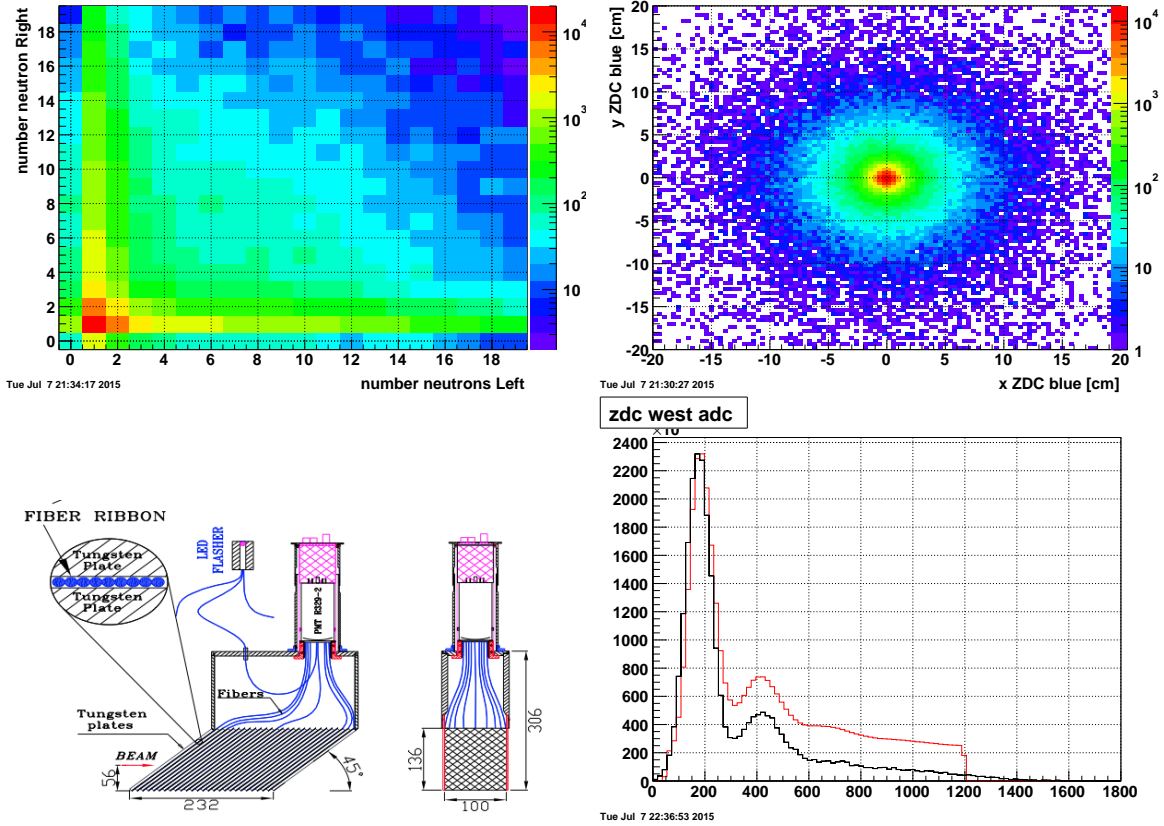


Figure 46: Top left panel shows the counts of events with neutrons streaming towards the East and West sides of the IR, the top right panel shows the entrance points of neutrons reaching the West ZDC. The bottom left panel shows a schematic of the ZDC detectors. The bottom right panel shows the ADC distribution as measured in the West ADC with a red histogram. The same figure displays the sum of gaussians with detector response for neutrons generated with the RELDIS event generator with a black histogram. The generated events are normalized to match the data's first neutron peak.

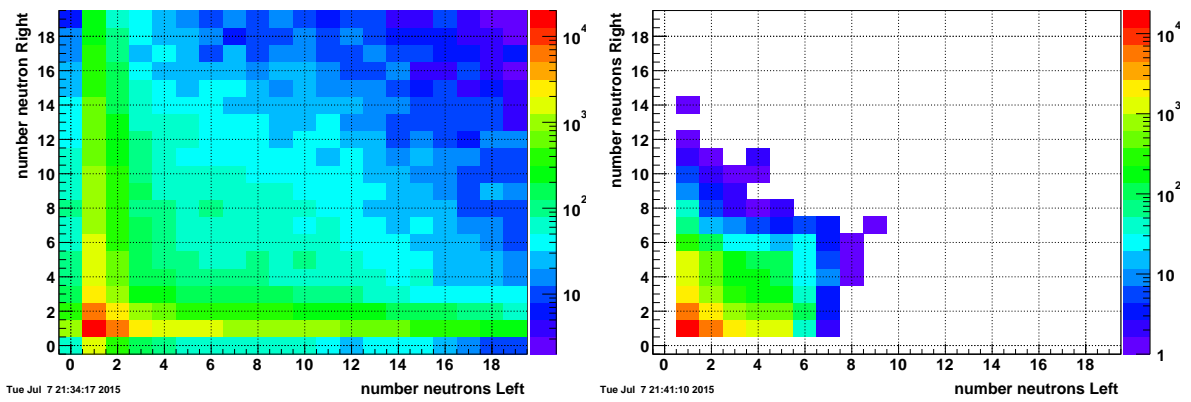


Figure 47: These two panels show the overall distribution of neutrons for the full cross-section (XnXn) (left panel) and the corresponding one for events that satisfy the UPC_Main trigger condition.

8.5 Comparison between data and the RELDIS event generator

This is an attempt to quantify how close can the RELDIS event generator describe the mutual dissociation events detected with the UPC_Main trigger. The size of the data sets is not comparable; we have 38M events collected during run10 and I have generated 2.5M RELDIS events. We are going to compare the calculation and the data at the level of ADC distributions. The RELDIS generator produces fluxes of neutrons pointing left and right. We select the energetic neutrons ($p > 60$ GeV/c) that project into the acceptance of both East and West ZDCs. (We add one Moliere radius to make sure the showers are fully contained). The energy of the neutrons is added and converted to ADC channels (charge) using information from test beam reported in a NIM publication and scaled to align the 1n peak with the corresponding peak in the data distributions. The left panel of Fig. 48 shows the full data collected in run 10 and the right panel shows 2.5 M RELDIS events with signal in both ZDCs.

In this 2D histograms one can see that the majority of events, both in data and Monte-Carlo, do no have a correlation between the number of neutrons in the ZDC with the exception of the so called 1n1n events which account for the biggest fraction of events. Both data and Monte-Carlo show clear peaks for 1n and 2n events in both ZDC. The 3n events are also visible in the data, but not so much in RELDIS events.

8.5.1 Comparison of all collected UPC_Main events and RELDIS generated events

Eight 1D ADC distributions were prepared with the complete set of UPC_Main events collected in run 10. No additional conditions are imposed on these events. The 1D histograms shown in Fig. 50 were filled with events that had from 1 to 4 neutrons in the East ZDC, and those shown in Fig. 51 were filled with information from the East ZDC for events with selected number of neutrons in the West ZDC. The cuts used to define each peak are a bit arbitrary: 1n [0-300], 2n [300-600], 3n [600-850], 4n [850-1200]. The same cuts are applied to East and West ZDC. Figure 49 shows that the gains of both ZDC detectors have been matched and their ADC distribution do overlap.

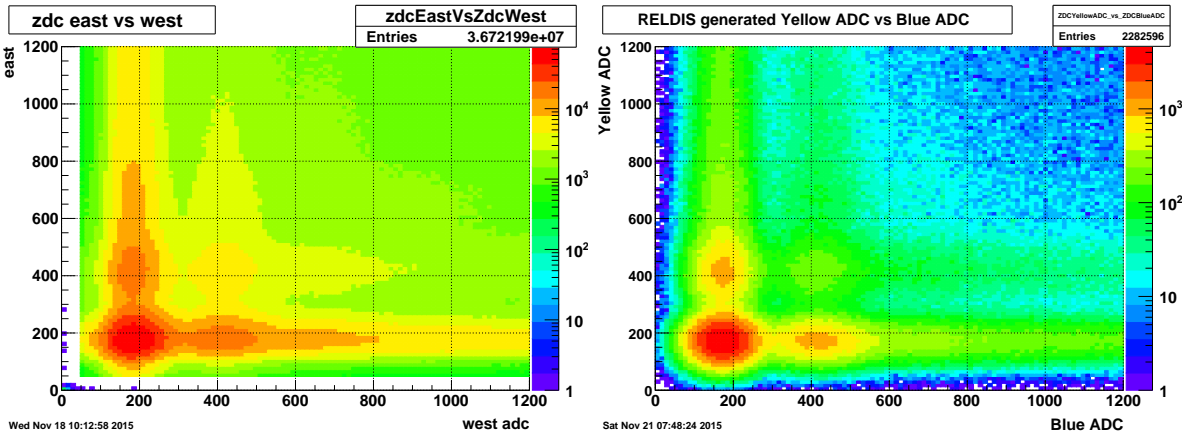


Figure 48: The left panel shows the ZDCs ADC distributions in events that fired the UPC_Main trigger. The right panel shows the same information but this time for RELDIS generated events that had at least one neutron with more than 60 GeV in momnetum reaching the acceptance of both ZDC calorimeters. Detector response has been obtained from test beam results NEED citation.

As can be seen in Fig. 50, the upper limit of the UPC_Main trigger (1200 ADC channels) is just above the centroid of the 4 neutron peak. Not the 5 neutrons we advertized originally. This new neutron counting has already been included in the in the XnXn correction.

The four histograms are fitted with the sum of four gaussian functions, all parameters are kept free with the exception of the sigma of the peaks with more than one neutron. For those peaks the sigma of the distribution should follow the relation: $\sigma_n = n \times \sigma_1$ where σ_1 is the width of the gaussian fitting the one neutron peak.

Figures 50 and 51 show the quality of the fits for both East and West ZDCs, the value of the χ^2 appears high as the error are solely statistical and small. As the distributions get wider they affect the fit at lower number of neutrons. That explains the fact that the gaussians fitting the two and three neutron peaks have centroids smaller than the peak values of the full distribution. The centroid of the fourth gaussian is not well defined because the fit cannot account for the effect of the 5 and higher number of neutrons and it will not be used in these work.

The top left panels of Figures 50 and 51 which are filled with events that have only one neutron in the opposite ZDC, are the one with the worst fit. This may be an indication of some additional background but the fit is failing because of the requirement that the widths of the peaks be multiples of the width of the 1n peak. Otherwise as the number of neutrons in the opposite ZDC increases, the fits do reproduce both East and West distribution very well.

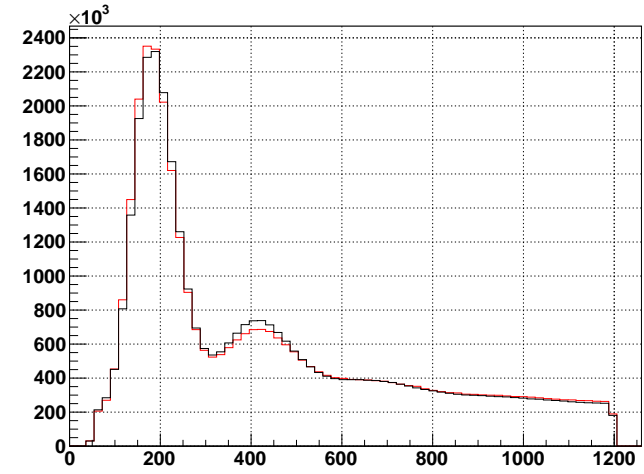


Figure 49: The read histogram shows the ADC distribution for the unattenuated sum of the East ZDC. The black histogram shows the corresponding distribution obtained with signal from the West ZDC for the same events in the complete UPC_Main data set. This figure is meant to show that both detector gains are well matched and the use of a single set of cuts to define the different peaks is well justified.

Figure 55 shows similar fits performed on ADC distributions for events generated with the RELDIS event generator. We have a data set of 100K events in root ntuple format. That file is read with the root macro processRELDIS.C. The macro only loops over neutrons in the events, it projects towards East and West ZDC and makes sure that they enter one Moliere radius inside the ZDC acceptance with momenta as high as 60 GeV/c. The response of the detector has been extracted from one of the first ZDC publication and is based on beam tests: $\sigma_E = 1.12 \times \sqrt{E} + 0.093 \times E$ where E is the sum of the energy of all neutrons that entered the ZDC acceptance.

We find a deviation from a linear response of the ZDC calorimeters as the centroids extracted from the fits do not lie on a straight line. Figure 52 shows the value of the centroids for all eight fits. The small deviations from fit to fits are only visible for the third and fourth peaks. The centroids of the first three peaks and the zero point are fitted with a second order polynomial. The fourth centroid is excluded because it requires the presence of higher number of neutrons above the trigger cut.

The comparison to numbers extracted from fits to RELDIS ZDC response are not indicating that the model does a good description of the data. The data shows a higher fraction of events with more than one neutron, such behavior could be related to background from peripheral hadronic interactions.

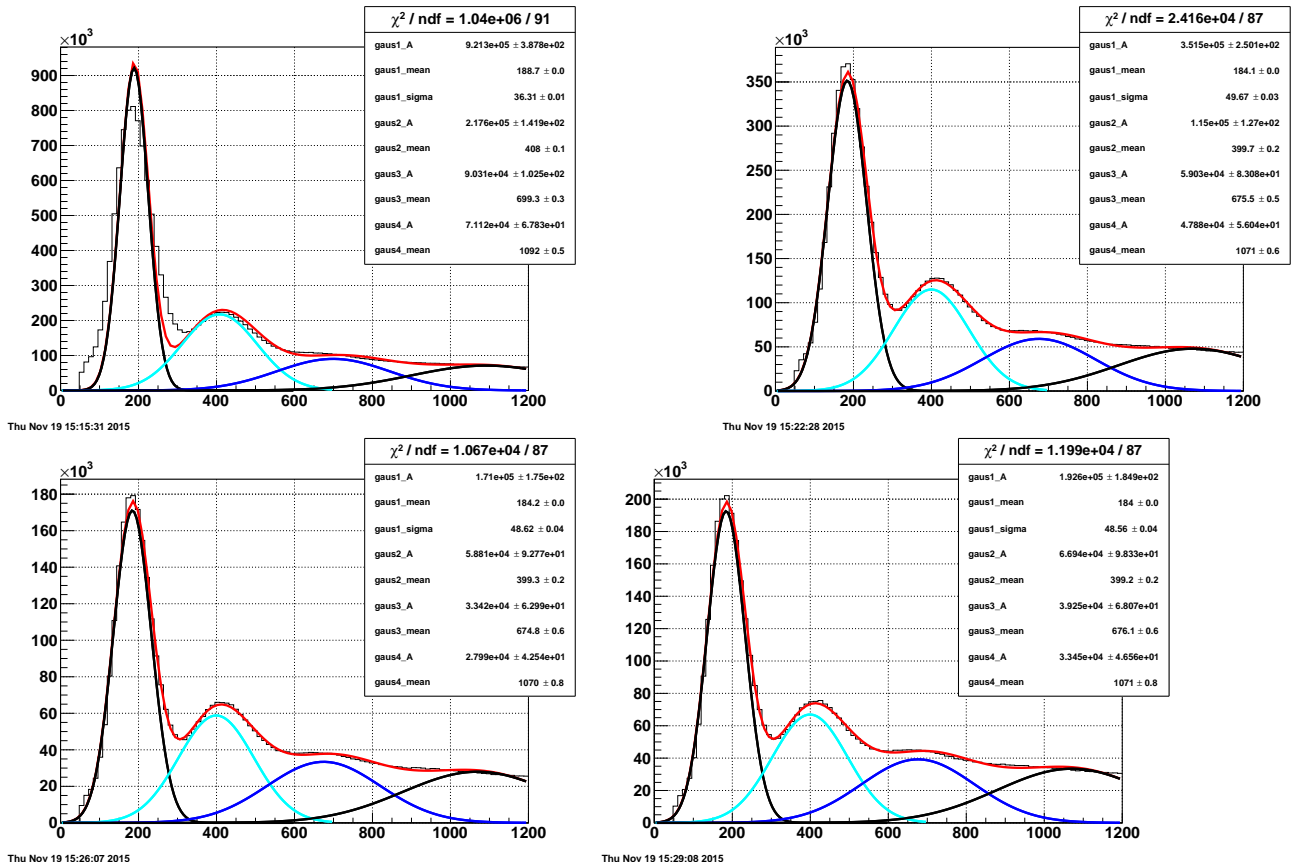


Figure 50: Fits to West ZDC ADC distributions filled with events that have 1 to 4 neutrons detected in the East ZDC. The top left panel shows the events with 1 neutron in East ZDC, the top right shows the 2n, the bottom left the 3n and finally the bottom right shows the 4n East ZDC events

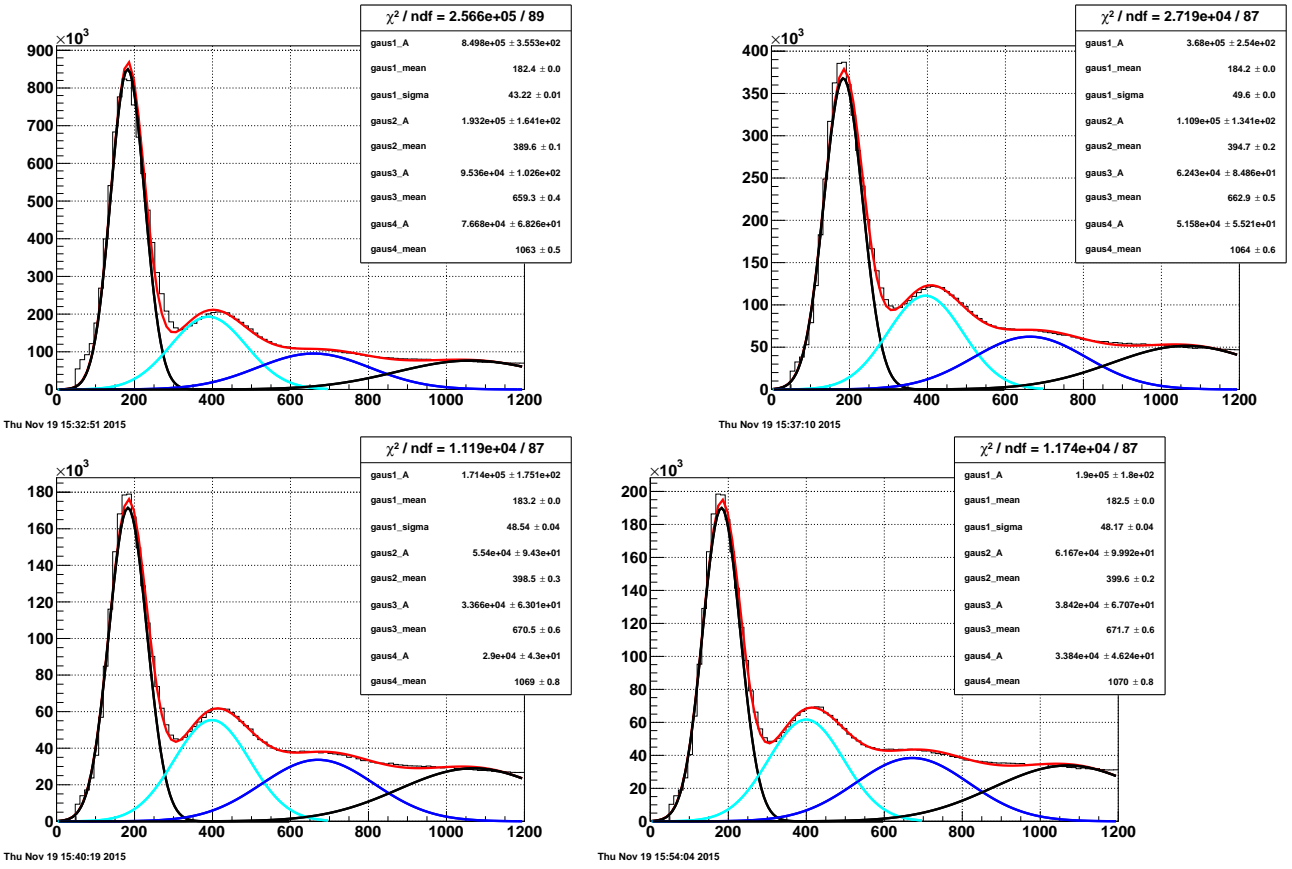


Figure 51: Fits to East ZDC ADC distributions filled with events that have 1 to 4 neutrons detected in the West ZDC. The top left panel shows the events with 1 neutron in West ZDC, the top right shows the 2n, the bottom left the 3n and finally the bottom right shows the 4n West ZDC events.

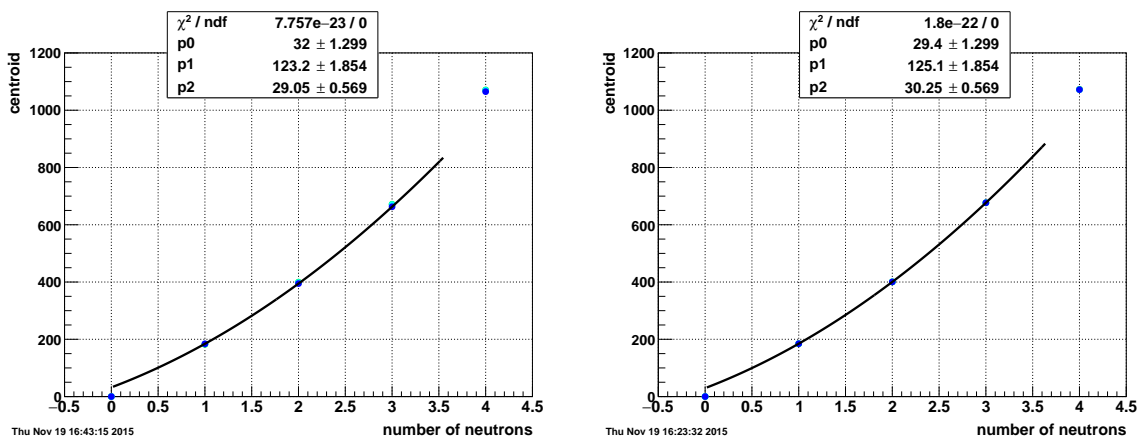


Figure 52: The left panel shows the centroids of the different peaks extracted from the fits as function of the number of neutrons for the West ZDC ADC distributions described above. The right panel shows similar information extracted from fits to the East ZDC distributions.

8.5.2 Reducing background with selected events with an exclusive ρ^0 meson

In an attempt to eliminate background events I have repeated the fits to the data but this time, I only use events with a clean pion pair of opposite charges accepted as a ρ^0 candidate. The fits are shown in figures 53 and 54 as well as table 3 which summarizes the fits as cross sections. This is table 1 from the paper:

	1n	2n	3n
1n	1.38 ± 0.24	0.57 ± 0.11	0.39 ± 0.07
2n	0.57 ± 0.11	0.23 ± 0.04	0.18 ± 0.03
3n	0.40 ± 0.07	0.19 ± 0.03	0.15 ± 0.03

Table 3: Mutual dissociation cross section (in mb) for events with exclusive coherent ρ^0 photoproduction. The row number shows the number of neutrons detected in the East ZDC and the column number lists the number of neutrons detected in the West ZDC. The cross sections listed in the table are an average of two measurements: one of them uses the West ZDC to set the number of neutrons on that beam with ADC channel cuts defined by the dip between the 1 and 2 neutron peaks, and the other measurement has the East ZDC selecting events in similar manner. These two measurements differ in the off diagonal term and the systematic uncertainty on the selection of the number of neutrons in either ZDC is set to be equal to the deviation from the average value. Statistical errors are small (< 1%) and are not listed. Systematic errors arising from the cuts used to select the events added were added in quadrature to the sum in quadrature of the relevant common uncertainties listed in table 3 of the paper (17%).

The ADC cuts have been changed from previous values, now we use the following:

- 1n: 0-300 channels which correspond to bins 0-26.
- 2n: 300-523 channels 27-44 bins
- 3n: 524-865 channels 45-73 bins

The fits are done with five gaussians but we only record the results from the first three gaussians. The fourth and fifth have proven difficult to handle. In all fits the fifth gaussian tends to overwhelm the fourth one.

The centroids of the first and second gaussians are free parameters, all other centroids are fixed to be n times the single neutron ADC channel gap. (calculated from the 1n and 2n gaussians and allowing for a small negative pedestal at -18 channels).

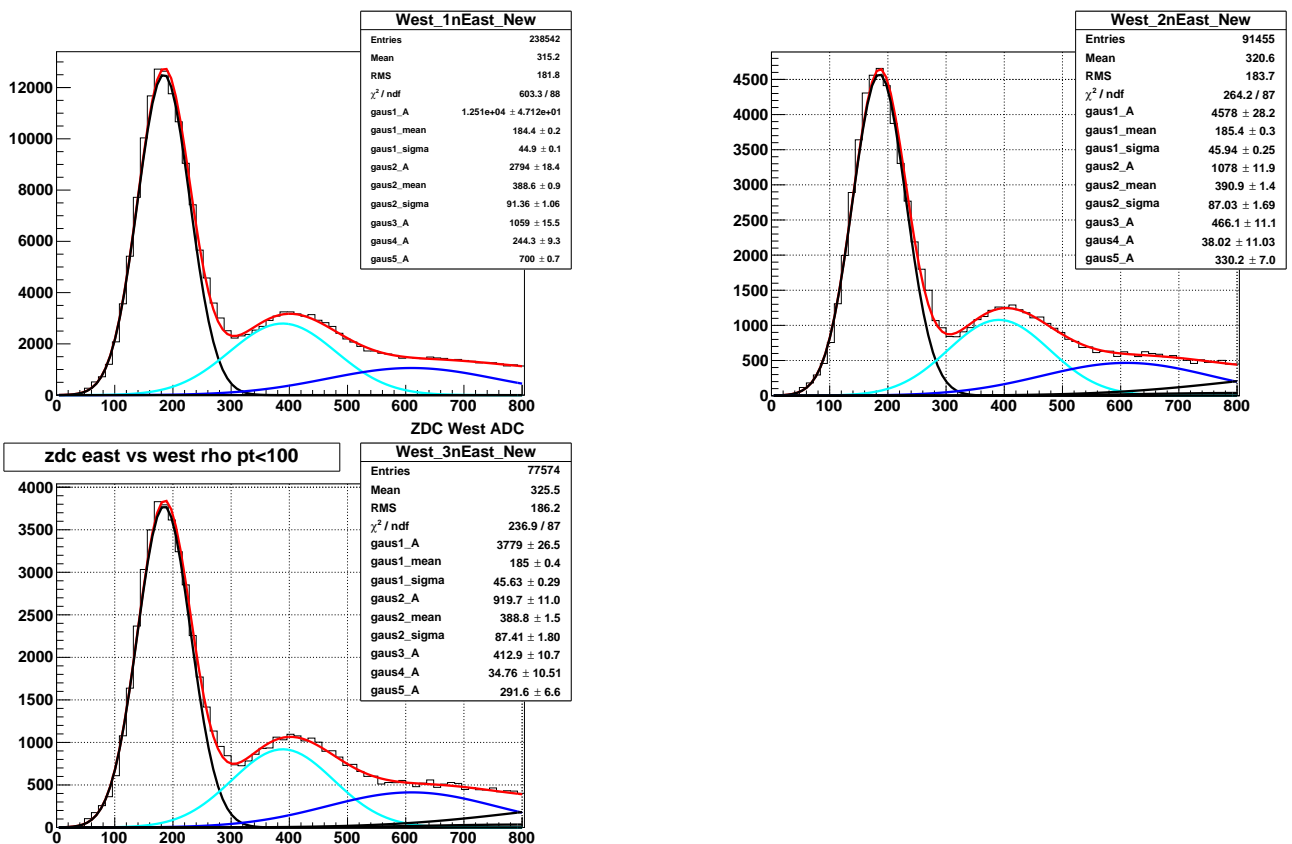


Figure 53: Fits to West ZDC ADC distributions filled with events that have a clean coherent ρ^0 meson (only two tracks out of vertex) and 1 to 4 neutrons detected in the East ZDC. The top left panel shows the events with 1 neutron in East ZDC, the top right shows the 2n, the bottom left the 3n and finally the bottom right shows the 4n East ZDC events

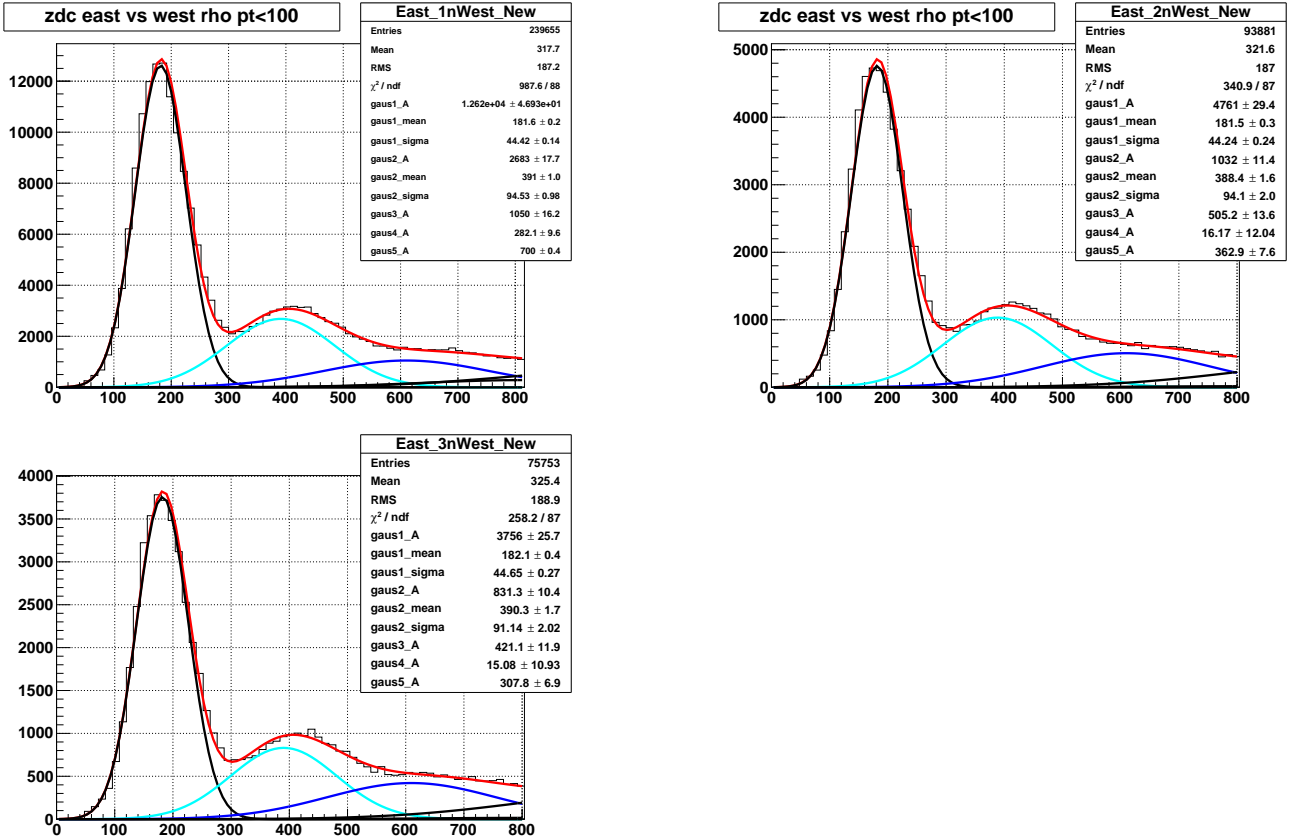


Figure 54: Fits to East ZDC ADC distributions filled with events that have a clean coherent ρ^0 meson (only two tracks out of vertex) and 1 to 4 neutrons detected in the West ZDC. The top left panel shows the events with 1 neutron in West ZDC, the top right shows the 2n, the bottom left the 3n and finally the bottom right shows the 4n West ZDC events

Table 4 summarizes the fits shown in Fig 50. The first column list the number of neutrons required to be detected in the East ZDC. The second, thid and fourth column list the integrals of the gaussians used to fit the 1, 2 and 3 neutron peaks. The fifth column has the ratio of integrals $2n/1n$ between the two neutron peak and the single neutron peak, similar ratio is shown in column six for the three neutron peak and the one neutron peak. Similar information but for the East ZDC (with cuts on the West ZDC) is summarized in Table 5

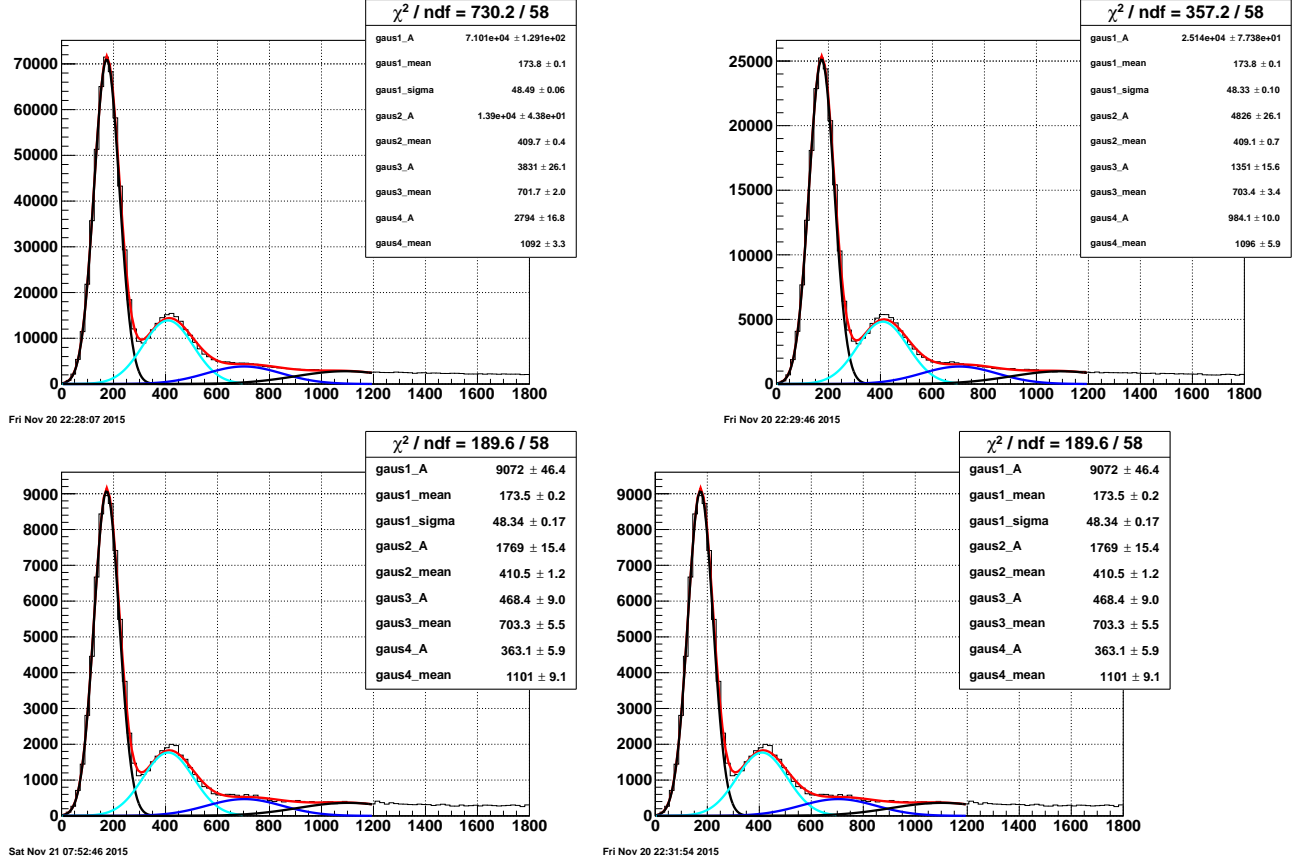


Figure 55: Fits to Blue ZDC distributions generated with the RELDIS event generator and detector response extracted from test beam data.

neutron East ZDC	Integral 1n West	2n West	3n West	2n/1n	3n/1n	1n1n/1nXn	2nXn/1nXn
1n	8.38e7	5.149e7	3.28e7	0.61	0.38	0.41	
2n	4.37e7	2.73e7	2.14e7	0.62	0.49		0.55
3n	2.08e7	1.4e7	1.21e7	0.67	0.58		
4n	2.34e7	1.59e7	1.43e7	0.68	0.61		

Table 4: Integrals of gaussians used to fit the ADC distribution of the West (Blue) ZDC in events that had from 1 to 4 neutrons detected in the East (Yellow) ZDC. The ratio of integrals for the 2 to 1 and 3 to 1 neutron peaks are listed in the last two columns.

neutron West ZDC	Integral 1n West	2n West	3n West	2n/1n	3n/1n
1n	9.206e7	4.61e7	3.4e7	0.50	0.37
2n	4.57e7	2.64e7	2.26e7	0.58	0.49
3n	2.086e7	1.31e7	1.22e7	0.63	0.58
4n	2.29e7	1.466e7	1.34e7	0.64	0.58

Table 5: Integrals of gaussian used to fit the ADC distribution of the East (Yellow) ZDC in events that had from 1 to 4 neutrons detected in the West (Blue) ZDC. The ratio of integrals for the 2 to 1 and 3 to 1 neutron peaks are listed in the last two columns.

neutron East ZDC	Integral 1n West	2n West	3n West	2n/1n	3n/1n	1n1n/1nXn	2nXn/1nXn
1n	1.399e6	700629	448106	0.50	0.32	0.49	
2n	642769	335938	221631	0.52	0.34		0.48
3n	279925	152356	106105	0.54	0.38		
4n	270503	148371	106074	0.55	0.39		

Table 6: Integrals of gaussians used to fit the ADC distribution of the West (Blue) ZDC in events with a clean coherent ρ^0 meson. Besides that, those events had from 1 to 4 neutrons detected in the East (Yellow) ZDC. The ratio of integrals for the 2 to 1 and 3 to 1 neutron peaks are listed in the last two columns.

neutron West ZDC	Integral 1n East	2n East	3n East	2n/1n	3n/1n	1n1n/1nXn	2nXn/1nXn
1n	1.4044e6	675207	463715	0.50	0.32	0.49	
2n	649462	325563	240203	0.52	0.34		0.48
3n	275052	140332	107313	0.54	0.38		
4n	262090	137102	101908	0.55	0.39		

Table 7: Integrals of gaussians used to fit the ADC distribution of the East (Yellow) ZDC in events with a clean coherent ρ^0 meson. Besides that, those events had from 1 to 4 neutrons detected in the West (Blue) ZDC. The ratio of integrals for the 2 to 1 and 3 to 1 neutron peaks are listed in the last two columns.

neutron East ZDC	Integral 1n West	2n West	3n West	2n/1n	3n/1n	1n1n/1nXn	2nXn/1nXn
1n	8.63e6	3.28e6	1.39e6	0.38	0.16	0.32	
2n	3.04e6	1.14e6	491095	0.38	0.16		0.33
3n	1.099e6	418076	170253	0.38	0.15		
4n	757943	288580	134164	0.38	0.18		

Table 8: Integrals of gaussian distributions used to fit RELDIS distribution of the West (Blue) ZDC in events that had from 1 to 4 neutrons detected in the East (Yellow) ZDC. The ratio of integrals for the 2 to 1 and 3 to 1 neutron peaks are listed in the last two columns.

From the tables 5 and 4 one can see that both ZDC detectors have a similar response, but compared to the simulated RELDIS events shown in table 8, the event generator produces a smaller number of 2, 3 neutron events. One could extrapolate that statement and say the RELDIS mutual dissociation has more GDRs with a single “evaporated” neutron.

Even for events with a clean exclusive ρ^0 meson the comparison between RELDIS and data continues to show a deficit on the number of events with multiple neutrons on both ZDCs. We may have reduced the background but the requirement of a vector meson at mid-rapidity biases the data towards higher photon fluxes (smaller impact parameter) and complicates this comparison. If we use the ratio labelled as “2nXn/1nXn” we can quantify such deficit as 15%.

ratio	West fits	East fits	RELDIS UPC_Main cond.	RELDIS published [15]	[16]	(GEMINI++)
1n1n/1nXn	0.49	0.49	0.32	0.329	0.448	
2nXn/1nXn	0.48	0.48	0.33	0.327	0.197	

Table 9: Comparison between data and two calculations. We compare the yields of events with only 1 neutron on both ZDCs and the yield of events with one neutron in East or West ZDCs (1n1n/1nXn) and the ratio 2nXn/1nX where events that have two neutrons in any ZDC are compared to events with a single neutron in any of the ZDC. The data ratios are extracted directly for the left 2D histogram shown in Fig. 48, and the ratios between generated events labelled as: "RELDIS UPC_Main cond." are produced with the known number of neutrons that reached the ZDC acceptance with more than 60 GeV/c in momentum.

8.5.3 Extrapolation of data from 1-4 neutrons to 1-14 neutrons

Using the fits already performed in the clean data sample with a clean ρ^0 meson we will attempt at extracting the trend for the "evaporation" of more than 4 neutrons due to Mutual Electromagnetic Dissociation. The choice of the function that will describe that trend should include the fact that the function should fall fast and reach zero at a reasonable number of neutrons. Here we are taking guidance from Fig. 12 upper left panel of ?? where the cross section for mutual dissociation drops down to 7 mb for 19 neutrons. The best function so far is the upper tail of a landau distribution which actually decays to values close to zero.

Figure 56 shows the fits to the amplitude of the gaussian distribution fitted to data where we required some number of neutrons in the East ZDC with cuts on ADC channels as shown in Fig. 53. Each amplitude value is associated with a number of neutrons detected in the ZDC's. Figure 57 shows the corresponding fits for fits done on the East ZDC signal with conditions on the West as displayed in Fig. 54.

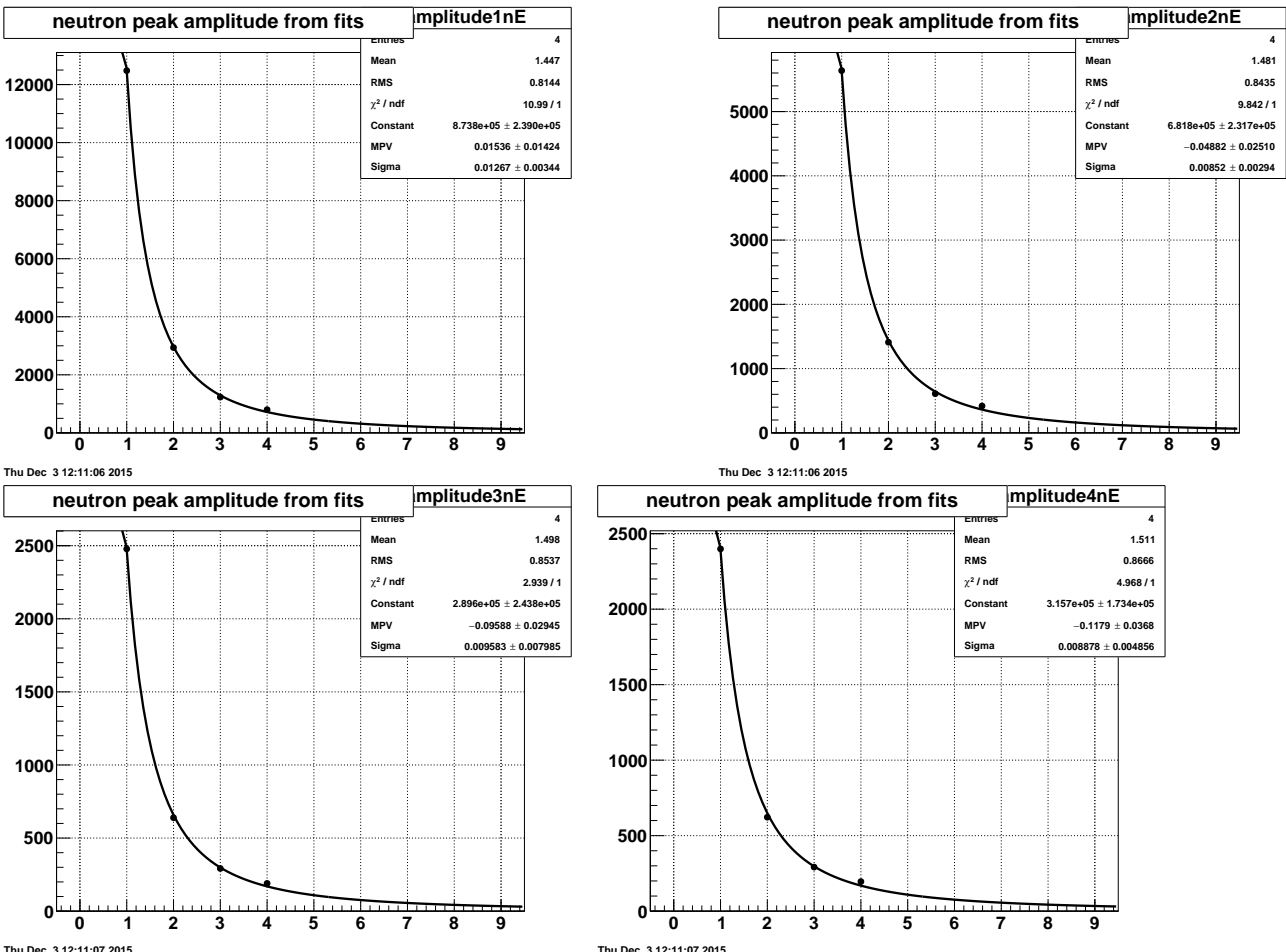


Figure 56: Fits to the amplitude of the gaussian distributions used to fit the different peaks seen in the West ZDC. Each amplitude is paired to an associated number of neutrons.

The extrapolation is done first with the fits to West ZDC peaks and cuts applied to the East ZDC signal. The extrapolation up to 14 neutrons in the West ZDC uses the fits shown in Fig. 56. The z axis of Fig. 58 shows the integral of the gaussian that fitted the first four peaks and then integrals of gaussians defined by the amplitude obtained from the landau fits, sigma values proportional to the number of neutrons and centroid fixed at 0. The

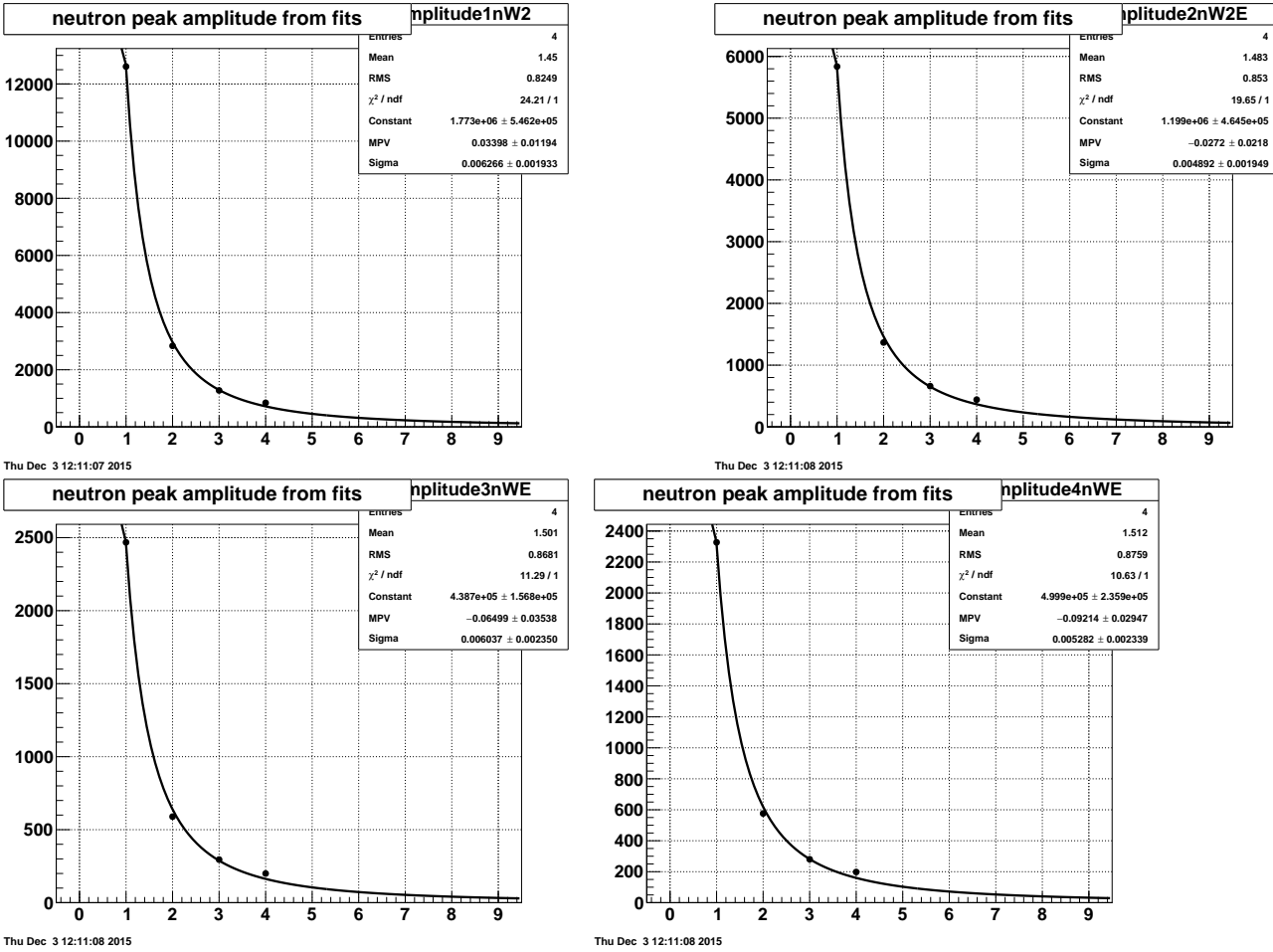


Figure 57: Fits to the amplitude of the gaussian distributions used to fit the different peaks seen in the East ZDC. Each amplitude is paired to an associated number of neutrons.

extrapolation beyond 4 neutrons in the East ZDC (along the vertical axis of Fig. 58 used the same amplitudes shown in Fig. 53 but in a different order; the landau fit to extrapolate along the 1 West neutron bins used the four amplitudes of the 1 neutron peaks in that figure. Same procedure applies to the 2-4 neutron bins. Along each extrapolation beyond four neutrons the gaussian integrals displayed in the z axis have the same value for their sigma value. The extrapolation along the vertical axis needs to be continued to have a continuos coverage but it is expected to have a small contribution because we will be extrapolating tails that are already attenuated.

To estimate the correction that transforms cross-sections measured with the UPC_Main trigger to full XnXn cross-sections we integrate from bins 1 to 4 on both axis and get $4.286e+06$ counts. The integral from 1 to 14 neutrons on both axis results in $9.815e+06$ counts. This translates into a correction value of 2.27 (we extracted a value of 2.11 from RELDIS). The same correction extracted from the fits to the East ZDC signal produced $4.281e+06$ counts with the UPC_Main conditions and $9.176e+06$ for all neutrons making it to the ZDCs. The new value of the corections is then: 2.14 a 6% difference that could be quoted as systematic uncertainty on the XnXn correction.

This correction can also be extracted using the fits to the signal in the East ZDC for events that satisfy conditions on the West ZDC. We can also fit only three peaks with the landau function because the fit to the 4 neutron peak is not well constrained. We should be able to quote a systematic uncertainty to the correction.

8.5.4 Correction from UPC_Main to XnXn cross sections using STARlight

The analysis of 1n1n events has produced a rapidity distribution that has good agreement with the corresponding cross section generated by STARlight as seen in Fig. 77. We use the ratio of STARlight rapidity cross section ($XnXn/1n1n$) to renormalize the data 1n1n to data XnXn as shown in the top panel of Fig.78. Both run10 (red markers) and the STAR 2007 publication show good agreement. To rescale the UPC_Main results as function of the t variable we followed a slightly different path. First we average over rapidity the ratio (1n1n/UPC_Main) (using the red markers in Fig. 76) then, we extract a rapidity average of the STARlight ratio ($XnXn/1n1n$) and multiply the two numbers, the result is equal to 2.685

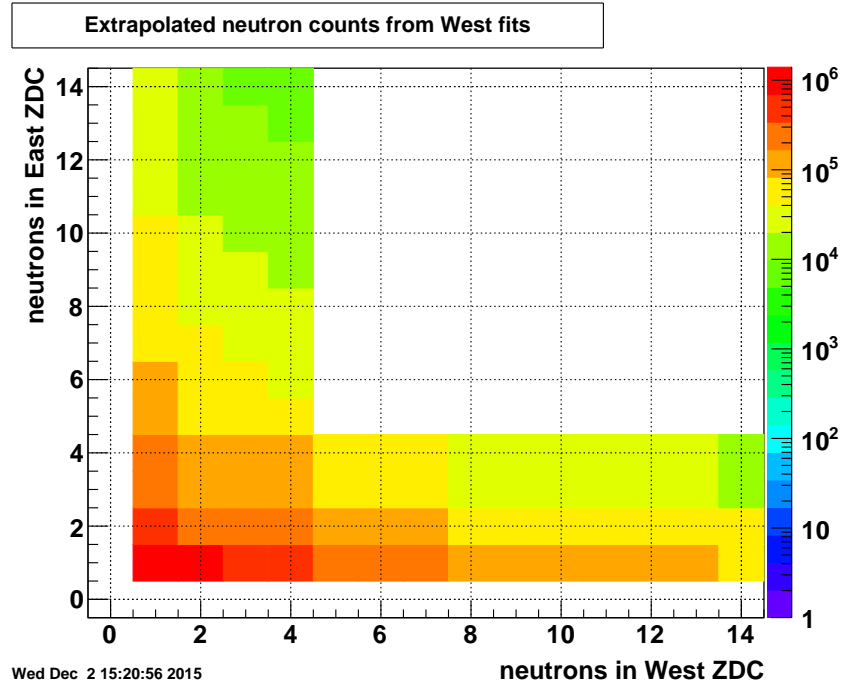


Figure 58: Integrals of gaussian distributions fitting West ZDC ADC histograms for events that have a number of neutrons ranging from 1 to 4 in the East ZDC. The z axis of this figure is the integral of the fitted gaussing. Beyond the 4 neutrons bins the extrapolation is done using the high end of Landau distributions as explained in the text.

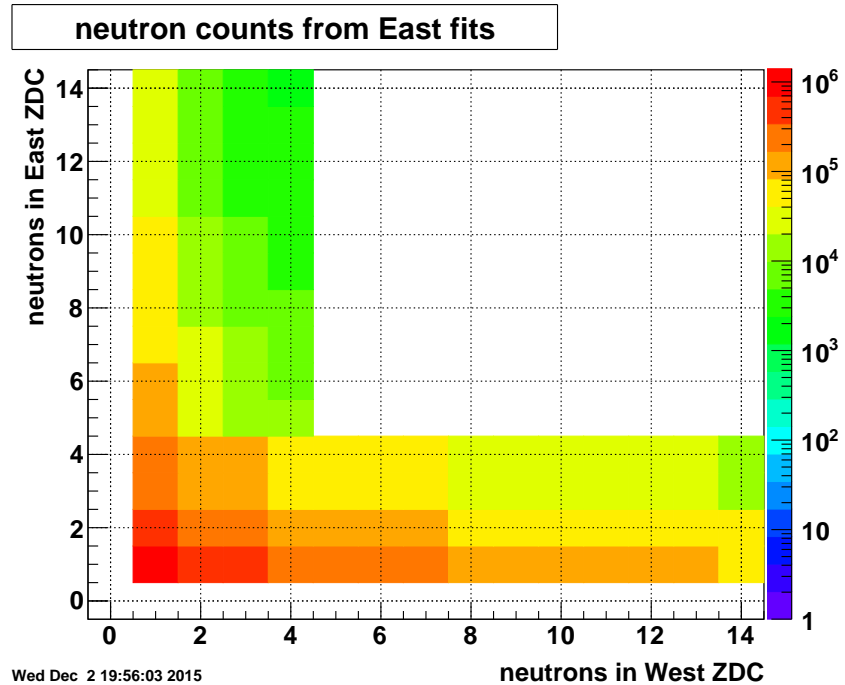


Figure 59: Integrals of gaussian distributions fitting East ZDC ADC histograms for events that have a number of neutrons ranging from 1 to 4 in the West ZDC. The z axis of this figure is the integral of the fitted gaussing. Beyond the 4 neutrons bins the extrapolation is done using the high end of Landau distributions as explained in the text.

8.6 Number of events analyzed

The processData macro reads all the UPC output trees and checks that all runs being processed are listed in the luminosity per run list. The complete pass over those files finds a total of 24458645 events.

The STAR production page:

http://www.star.bnl.gov/public/comp/prod/prodsum/AuAu200_production.P10ik.html

lists a total of 38502251 events triggered by UPC_Main. The difference in those counts could be attributed to the fact that the UPC output trees have not been written with the latest version of StPeCMaker and only record events with UPC candidates.

Several tests were performed to track the origin of the difference in number of events listed in the production page and what we find at the last stage of the analysis.

First we compared the number of events stored in the MuDst files placed in the local disks of rcas nodes with similar number obtained from information stored in the hpss tape storage system. The two sums differ by 1 count in 10000, a negligable difference.

For this particular analysis, the STAR Scheduler has set to use the framework XROOTD (<http://xrootd.org/>). This framework allows for the jobs to run in nodes that have the data on their local disks. Because some number or error flagged by xrootd were present in the logs of our jobs, an effort was made to evaluate the nature of whatever was producing the errors. Scripts were written to loop over the “report” files produced by the Scheduler to find log files and the number of events listed for them by the FileCatalogue. Those numbers are then compared with the number of events processed by StPeCMaker as they are logged in the log files. Instances of mismatch between those numbers were found for runs where the xrootd server was unable to open the requested file. What is the reason for such failure to open a file is not yet known, but the effect of this loss of events has been quantified and found to be smaller than 1% as shown in table 10.

Event count monitoring					
Day+run	job Id	Report file	StPeCMaker	processData (macro)	diff%
11035_11093	20D26F1..	4103	4103		0.
12002_17059	323C83D..	2278762	2264273		0.6
18002_31089	E7E8891..	7270638	7258676		0.2
32011_38069	1E182B9..	3931476	3930122		0.03
32011_38069 106	28D35F2..	130474	130474		0.
39001_60082	8C3E4A1..	13142727	13098228		0.3
61001_77018	052604A..	11487773	11452445		0.3
11035_77018 (all)		38245953	38138321	36712103	4.2

Table 10: Counting events in the jobs submitted for this analysis. The column “Day+run” indicate the portion of runs processed in a particular job 12002_17059 follow the standard STAR run labelling scheme and in this case list all runs from day 12 of the 2010 period starting at run number 2 and ending on run 59 of day 17. The second column has a truncated version of the job Id allocated by the condor batch system. The third column lists the sum of number of events for all runs processed in the job. These are counts of events that were reconstructed successfully on the production P10ik. The fourth column lists the corresponding sum of events that the UPC maker (StPeCMaker) read from the MuDsts found on local disks. The fifth column list all events found in the output files written by StPeCMaker and read with the macro “processData” generated by the root TTree MakeClass method. this macro is run over all output files in a single job. Finally, the last column lists the loss of events whenever the UPC maker reads the MuDst’s. The loss shown in the last row compares the number of events found in the maker outputs and the total listed in the third column (all UPC_main events reconstructed in production P10ik).

8.7 The processData analysis macro

The macro loops over the pairs stored in the output trees. Because the input events could have up to 5 vertices of varying quality, the output trees may also have pairs that originate from different vertices. It is thus necessary to identify the one vertex that is connected to the trigger. Such connection is done using the so called TOFtracks, tracks that have been matched to a valid TOF hit. If the pair has been formed with at least one of those TOFtracks, the vertex of the pair tracks is thus identified as the primary vertex. To study possible biases in this selection, the macro stores relevant information for all vertices present in the event.

Each track in a particular pair is identified using the energy deposited in the TPC gas. A band cut is applied in the ionization losses as function of particle momentum, the cut is 3σ above and below the calculated value. Once the pair has been identified as a pion pair, a track quality condition is imposed on the both tracks which requires that it was built with at least 14 clusters to avoid low momentum particles that spiral in the magnetic field and can produce fake tracks.

Once a pair has satisfied those two conditions 2 dimensional histograms are filled. Once all events in the tree have been processed, the histograms are written into a root file.

```
Loop over pairs { 1
| Both tracks in pair are pions {2
| Both tracks have >14 hits      {3
| Cut on number of trks off vtx {4
|   Cut on rho mass            {5
|     Tracks of opposite charge {6
|       | At least 1 trk matched to TOF {8
|       | | 1n1n cut on ZDCs          {9
|       |
|       |
|       |
|       |   cut in vertex |z|<50cm {11
|       |
|       |-----}11
|
|       |
|       |   Both tracks match TOF hit    {10
|       |
|       |     cut in vertex |z|<50cm {
|       |
|       |     |-----}
|       |
|       |-- }10
|
|   |-- }9
|   XnXn no cut in ZDC
|
|   cut in vertex |z|<50cm {14
|   |
|   |-----}14
|
|   Both tracks match TOF hit    {13
|   |
|   |     cut in vertex |z|<50cm {
|   |
|   |     |-----}
|   |
|   |-- }13
|
|   |-- }8
|   no TOF match
|
|   |
|   |-- }6
```

```

| Tracks of equal charge      {7
| | At least 1 trk matched to TOF {16
| | | 1n1n cut on ZDCs      {17
| | |
| | |
| | |   cut in vertex |z|<50cm {19
| | | |
| | | |-----}19
| | |
| | |
| | | Both tracks match TOF hit    {20
| | | |
| | | |   cut in vertex |z|<50cm {
| | | | |
| | | | |-----}
| | | |
| | | |-----}20
| | |
| | |
| | |----- }17
| |
| | XnXn (no cut in ZDC)
| |
| |   cut in vertex |z|<50cm {
| | |
| | |-----}
| |
| | Both tracks match TOF hit    {23
| | |
| | |   cut in vertex |z|<50cm {
| | | |
| | | |-----}
| |
| | |----- }23
| |
| |
| |
| |--}16
| no TOF match
|
|
|
|-----}7
|     }5
|     } 4
|     } 3
|     } 2
|--- } 1

```

The pairs considered as signal should have opposite charge, originate from a vertex that has only two tracks, has and invariant mass consistent with a ρ^0 meson, and is accompanied with the detection of one neutron on both ZDC detector (1n1n events), or up to 6 neutrons (XnXn events). The backgrounds for this type of measurement are well described by pair of same charge.

The information from selected signal and background pairs is the stored in the following histograms:

Signal (opposite charge):

Vertex identified with TOF:

One neutron in each ZDC (1n1n):

```

HrhoPtvsRapidity1n1n_withTOFmatch          //Pt vs y of $rho$
HrhoPtvsRapidity1n1n_withTOFmatch_PievtCorr //Pt vs y of $rho$ weight by eff. ($pi$ level)
HrhoInvMassvsRapidity1n1n_withTOFmatch
HrhoInvMassvsRapidity1n1n_withTOFmatch_PievtCorr

```

HrhoDndPt2dy_1n1n_withTOFMatch

Cut on vertex z 50 cm:

```
HrhoPtvsRapidity1n1n_withTOFmatch_50          //Pt vs y of $\\rho$  
HrhoPtvsRapidity1n1n_withTOFmatch_PievtCorr_50 //Pt vs y of $\\rho$ wheight by eff. ($\\pi$ level)  
HrhoInvMassvsRapidity1n1n_withTOFmatch_50  
HrhoDndPt2dy_1n1n_withTOFMatch_50
```

No conditions on ZDC (XnXn):

```
HrhoPtvsRapidityXnXn_withTOFmatch          //Pt vs y of $\\rho$  
HrhoPtvsRapidityXnXn_withTOFmatch_PievtCorr //Pt vs y of $\\rho$ wheight by eff. ($\\pi$ level)  
HrhoInvMassvsRapidityXnXn_withTOFmatch  
HrhoInvMassvsRapidityXnXn_withTOFmatch_PievtCorr  
HrhoDndPt2dy_XnXn_withTOFMatch
```

Cut on vertex z 50cm:

```
HrhoPtvsRapidityXnXn_withTOFmatch_50          //Pt vs y of $\\rho$  
HrhoPtvsRapidityXnXn_withTOFmatch_PievtCorr_50 //Pt vs y of $\\rho$ wheight by eff. ($\\pi$ level)  
HrhoInvMassvsRapidityXnXn_withTOFmatch_50  
HrhoDndPt2dy_XnXn_withTOFMatch_50
```

No connection vertex-TOF:

One neutron in each ZDC (1n1n):

```
HrhoPtvsRapidity1n1n_noTOFmatch  
HrhoInvMassvsRapidity1n1n_noTOFmatch  
HrhoDndPt2dy_1n1n_noTOFMatch
```

No conditions on ZDC (XnXn):

```
HrhoPtvsRapidityXnXn_noTOFmatch  
HrhoInvMassvsRapidityXnXn_noTOFmatch  
HrhoDndPt2dy_XnXn_noTOFMatch
```

Background (same charge):

Vertex identified with TOF:

One neutron in each ZDC (1n1nBkg):

```
HrhoPtvsRapidity1n1nBkg_withTOFmatch  
HrhoPtvsRapidity1n1nBkg_withTOFmatch_PievtCorr  
HrhoInvMassvsRapidity1n1nBkg_withTOFmatch  
HrhoInvMassvsRapidity1n1nBkg_withTOFmatch_PievtCorr  
HrhoDndPt2dy_1n1nBkg_withTOFMatch
```

Cut on vertex z 50 cm:

```
HrhoPtvsRapidity1n1nBkg_withTOFmatch_50  
HrhoPtvsRapidity1n1nBkg_withTOFmatch_PievtCorr_50  
HrhoInvMassvsRapidity1n1nBkg_withTOFmatch_50  
HrhoDndPt2dy_1n1nBkg_withTOFMatch_50
```

No conditions on ZDC (XnXn):

```
HrhoPtvsRapidityXnXnBkg_withTOFmatch  
HrhoPtvsRapidityXnXnBkg_withTOFmatch_PievtCorr  
HrhoInvMassvsRapidityXnXnBkg_withTOFmatch  
HrhoInvMassvsRapidityXnXnBkg_withTOFmatch_PievtCorr  
HrhoDndPt2dy_XnXnBkg_withTOFMatch
```

Cut on vertex z 50cm:

```
HrhoPtvsRapidityXnXnBkg_withTOFmatch_50  
HrhoPtvsRapidityXnXnBkg_withTOFmatch_PievtCorr_50  
HrhoInvMassvsRapidityXnXnBkg_withTOFmatch_50  
HrhoDndPt2dy_XnXnBkg_withTOFMatch_50
```

No connection vertex-TOF:

One neutron in each ZDC (1n1nBkg):

HrhoPtvsRapidity1n1nBkg_noTOFmatch
HrhoInvMassvsRapidity1n1nBkg_noTOFmatch
HrhoDndPt2dy_1n1nBkg_noTOFMatch

No conditions on ZDC (XnXn):

HrhoPtvsRapidityXnXnBkg_noTOFmatch
HrhoInvMassvsRapidityXnXnBkg_noTOFmatch
HrhoDndPt2dy_XnXnBkg_noTOFMatch

8.8 Information extracted from the Mixed embedding project

This chapter is an attempt at factorising all components that form what we call the “full chain correction” extracted as a result of comparisons between generated events and their transport through the full STAR detector simulation and the several stages of analysis. We expect these components to be: the vertex finding efficiency, tracking efficiency in the TPC, matching to active TOF elements. All of these steps get affected by the presence of background. Trigger efficiency must also be present which if one assumes fully efficient detectors (TOF, BBC and ZDCs) will end up being driven solely by acceptance and background effects on the BBC vetoes.

The so called vertex finder efficiency is shown in Fig. 61. Because vertices require tracks, this “efficiency” is a composite of the tracking efficiency, and the vertex finding algorithm. The figure in question is a ratio of z vertex distributions for vertices found after event reconstruction which matched the generated vertex in the event. The matching is done using the number of shared track hits between MC and reconstructed tracks.

The extraction of the different versions of the so called “full chain correction” is done using an adapted version of the `processData.C` macro that sits in the folder:

```
UPC/run10AuAu200/readPrivateEmbeddingMuDst/processData.C
```

the macro reads the pico dst produced by the mixed embedding followed by processing with the StPeCMaker code. The output of this macro is a root file called “fullChainProcessed_exclusive2Tracks.root” and the different “full chain correction” are produced with the macro “`makeFullChainCorr.C`” or versions of it.

Some part of the analysis has been done putting the number of tracks found in the triggered vertex as high as four. This was done to accomodate the fact that the PPV vertex finder appears to have a tendency to associate additional tracks to the vertex. Such tendency can be seen with information from the Mixed Embedding project where we know that the original vertex has two tracks and then we can see how many tracks are found in the reconstructed vertex. Figure 60 shows such behavior.

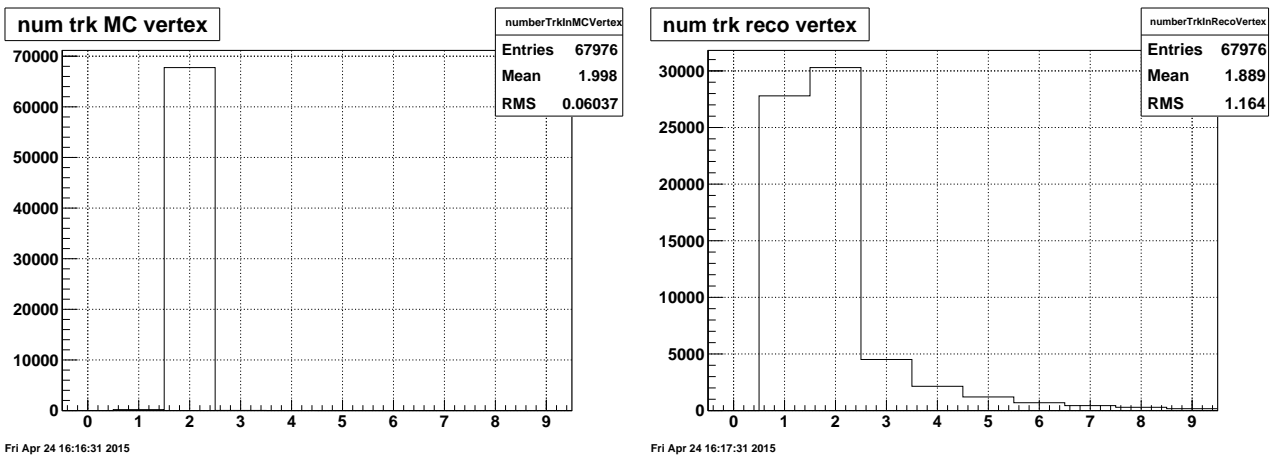


Figure 60: Left panel shows the number of tracks in the generated vertex. Out of the total number of events, ~0.3% of the events have 1 track or more than 2 tracks. More than two tracks can be understood with some prompt delta ray, but a single track is a bit harder. The figure on the right shows the distribution of the number of tracks in the reconstructed vertices, this shows that the fraction of vertices with number of tracks different from 2 is as high as 55

At later stages of the analysis it was decided to select events where the activity in the TPC (out of the selected vertex) is exactly of two tracks (an exclusive photo-production of a vector meson which then decays into two particles). The vertex finder efficiency extracted from the embedding project will then provide the necessary correction for events lost because one of the tracks was not reconstructed or because the finder added a spurious track to a good two track event. Figure 61 shows the “efficiency” of the vertex finder for eclusive production events where the vertex reconstructed is to have only two tracks.

For reference, it is also possible to extract efficiencies for individual tracks. Figures 62 and 63 show some typical results.

These figures were produced directly from the MuDst produced at the first stage of the mixed embedding; when the pions from rho decay are transported to the STAR setup using the SL10k_embed library. To produce these figures the `/UPV/VertexFinderEvaluation/MuMcYuri.C` loops over TOF hits, a TOF hit may have a match with a primary track, which in turn, may have a match to a MC pion. The 2D plot of Fig. 62 is the ratio of the p_T vs rapidity plot of the reconstructed positive tracks that pass quality cuts and are identified as pions with TPC dE/dx , over a similar plot filled with positive MC pions. The lower panels are projections along the p_T axis for two windows in rapidity.

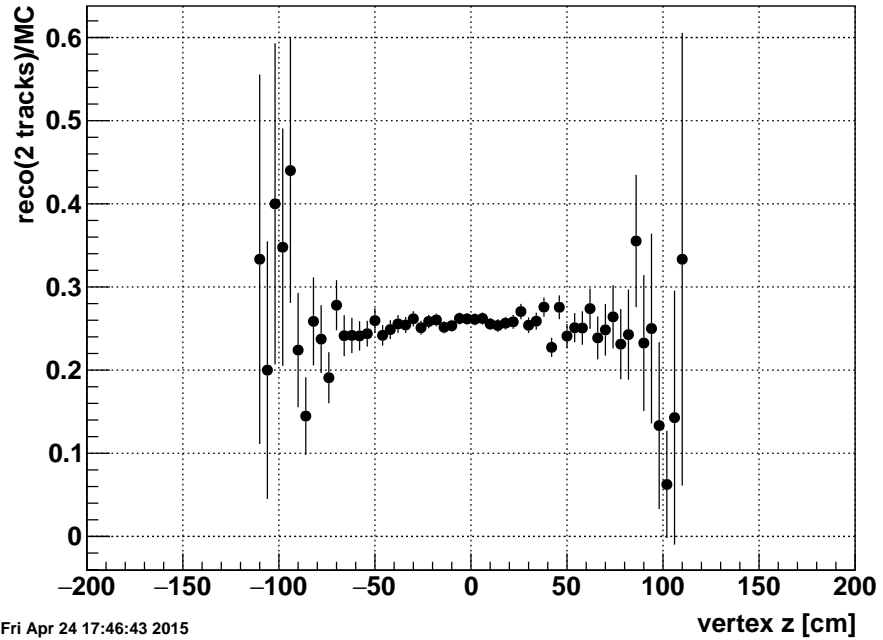
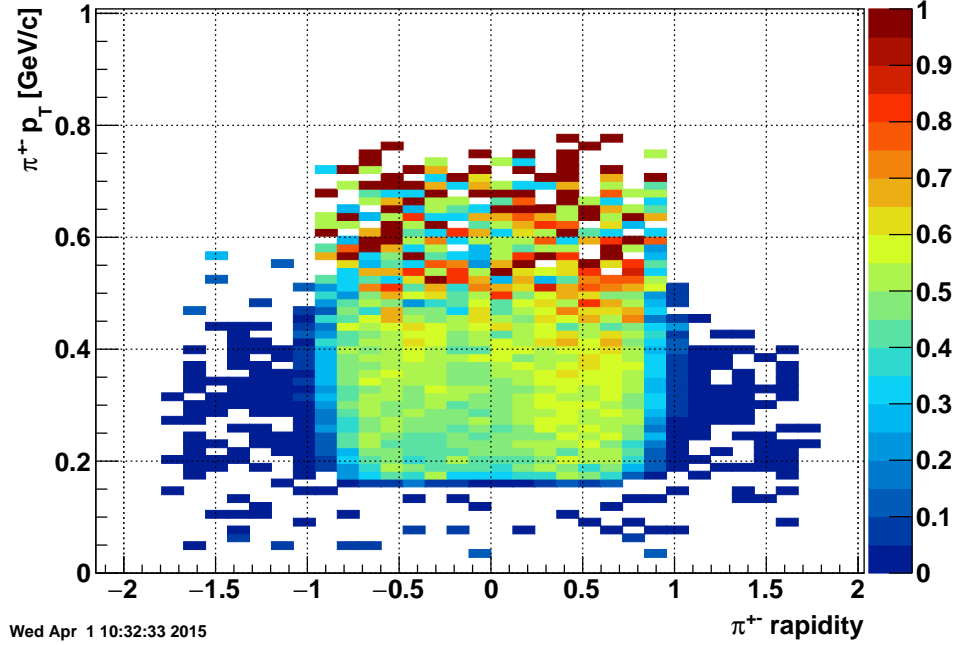


Figure 61: . Ratio of the z coordinate of reconstructed vertices over the corresponding distribution for MC vertices. The reconstructed vertices are matched to the MC ones through the method `IdTruth()` of the `StMuM-cVertex` class.

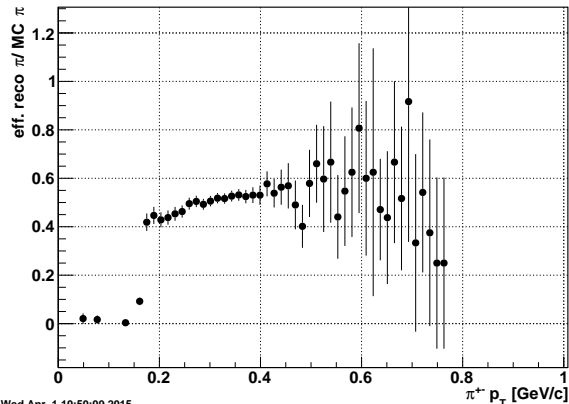
8.9 Relative t resolution

The reconstructed value of t is correlated with the corresponding generated value. Figure 65 shows the correlation. Using root's TProfile class with option "s" (which displays the RMS of the entries in each bin) the correlation is stored in the macro `/star/u/ramdebbe/UPC/run10AuAu200/readPrivateEmbeddingMuDst/MC_t_versus_reco_t_ProfileX.RM`. Another macro is used to display the RMS values as function of the generated values of t, the result is shown in Fig. 66.



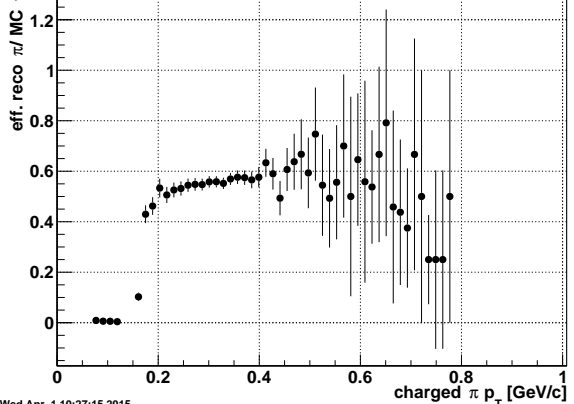
Wed Apr 1 10:32:33 2015

pion $y: [-0.7, -0.4]$



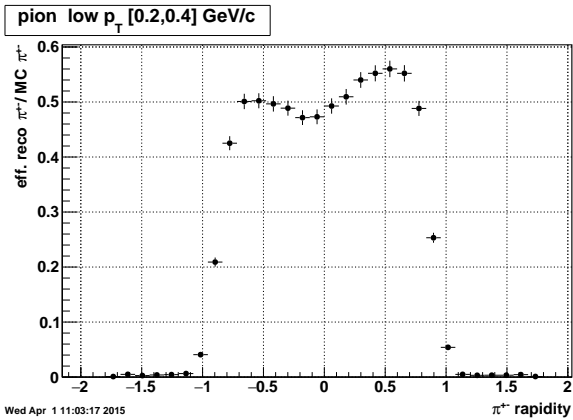
Wed Apr 1 10:50:09 2015

pion $y: [0.4, 0.7]$

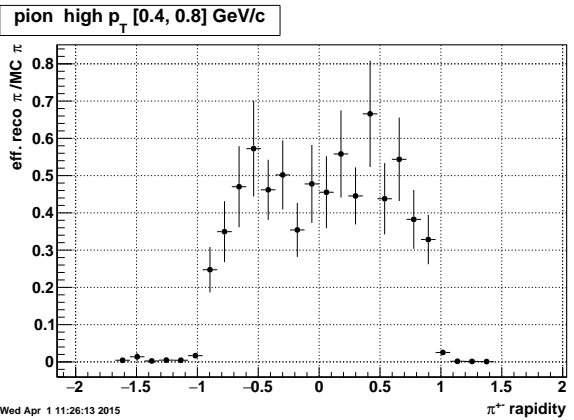


Wed Apr 1 10:27:15 2015

Figure 62: Top: ratio of reconstructed positive tracks tha match a TOF hit, satisfy tracking cuts, are identified as pions with the TPC dE/dx PID and have a match to one of the MC pions, over a similar plot filled with positive MC pions. Bottom left: (tracking efficiency)*(TOF matching) for a negative rapidity window $y: [-0.7, -0.4]$. Bottom right: same quantity for the simmetric window on positive rapidities.



Wed Apr 1 11:03:17 2015



Wed Apr 1 11:26:13 2015

Figure 63: Left: (tracking efficiency)*(TOF matching) as function of rapidity at low transverse momentum. Right: same efficiency but for the high end of the pion transverse momentum. The edges of the TOF detector are clearly visible at $|y| < 1$.

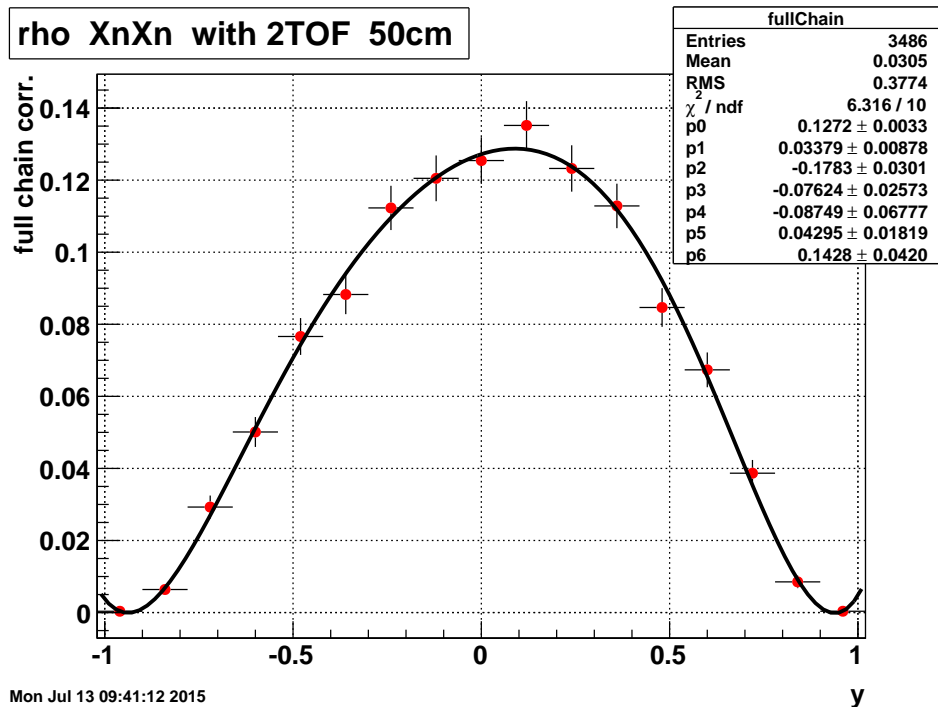


Figure 64: Fullchain correction for ρ^0 extracted from the complete set of FSETs (107-115) of the mixed embedding. Wide distribution of vertex z coordinates mimics the data distribution. PID of pions is defined with a 3 sigma cut and both pions reach active elements of TOF. Vertex z satisfies: $|z| < 50$ cm and the vertex had only two tracks.

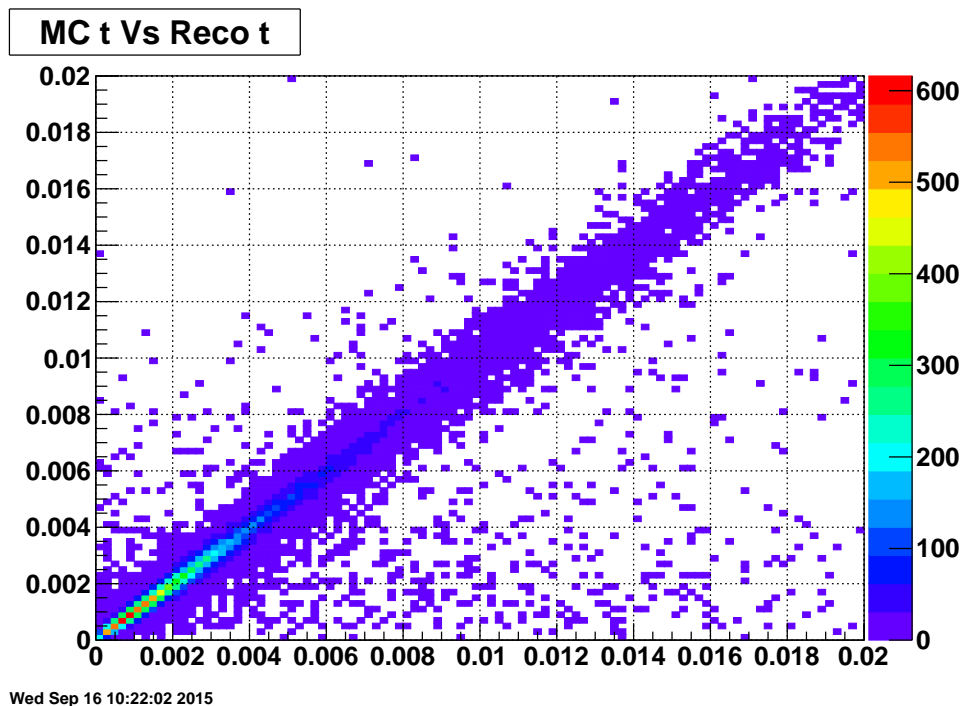


Figure 65: Correlation between generated (MC_t) “momentum transfer” of ρ^0 mesons plotted in the vertical axis versus the value measured in the reconstructed ρ^0 (Reco_t).

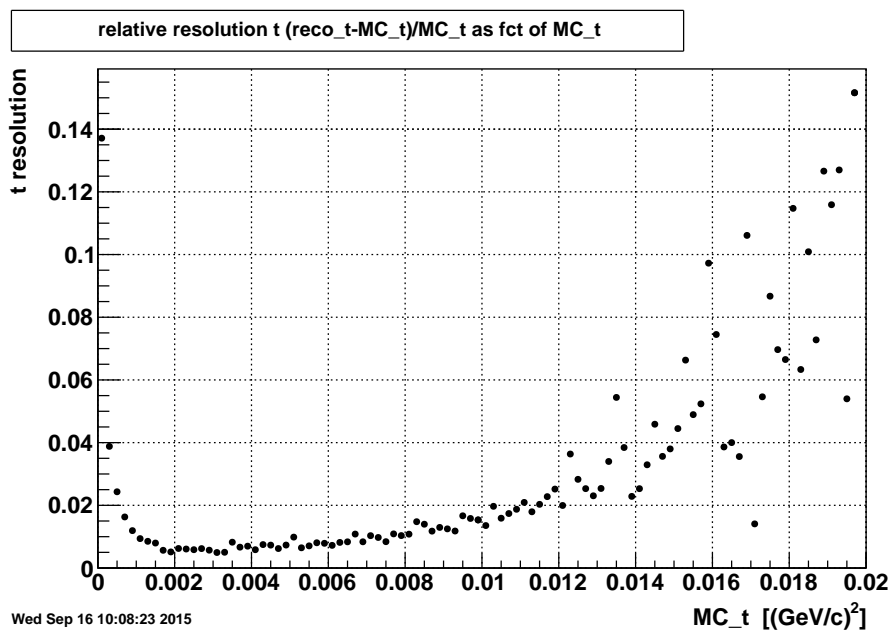


Figure 66: The RMS of the distribution at each bin of the previous figure divided by the generated momentum transfert. The value os such ratio is plotted as a function of MC_t

9 Results

9.1 Cross-section $d\sigma/dM$ as function of pion pair mass

Figure 67 shows the background subtracted invariant-mass of the selected pion pairs under the coherent peak mentioned above. This cross section is built in the following way:

$$\frac{d\sigma}{dM} = \frac{N_{counts}(M)}{\text{binWidth}(M) \times \text{rapidityRange} \times \text{fullChain}(m) \times \text{Luminosity}}, \quad (1)$$

This distribution is fitted with a modified Söding parametrization [?], which includes the presence of a constant distribution in mass of non-resonant pion pairs as well as the presence of the ω meson decaying into two charged pions as indicated in eqn. 2. The cross-section components corresponding to the ρ^0 and ω mesons are described with relativistic p-wave Breit-Wigner functions, both with real amplitudes A and C. The presence of non-resonant pion pairs is accounted with a real constant B:

$$\frac{d\sigma}{dM_{\pi^+\pi^-}} = \left| A_\rho \frac{\sqrt{M_{\pi\pi} M_\rho \Gamma_\rho}}{M_{\pi\pi}^2 - M_\rho^2 + i M_\rho \Gamma_\rho} + B_{\pi\pi} + C_\omega e^{i\phi_\omega} \frac{\sqrt{M_{\pi\pi} M_\omega \Gamma_\omega}}{M_{\pi\pi}^2 - M_\omega^2 + i M_\omega \Gamma_\omega} \right|^2 + f_p \quad (2)$$

where the momentum-dependent widths (expressed at $q^2 = M_{\pi\pi}$) Γ_ρ and Γ_ω are written as:

$$\Gamma_\rho = \Gamma_0 \frac{M_\rho}{M_{\pi\pi}} \left(\frac{M_{\pi\pi}^2 - 4m_\pi^2}{M_\rho^2 - 4m_\pi^2} \right)^{3/2}$$

and $\Gamma_\omega = \Gamma_0 \frac{M_\omega}{M_{\pi\pi}} \left(\frac{M_{\pi\pi}^2 - 9m_\pi^2}{M_\omega^2 - 9m_\pi^2} \right)^{3/2}$. With Γ_0 being the corresponding width for each meson. And f_p is a first order polynomial that could be needed to describe a remnant background.

The non-resonant component is shown with a dashed black line, the effect of the interference is shown with a blue dashed line, and finally the pure ρ^0 yield extracted from the fit is shown with the red dotted line.

To exploit the benefit of the full size of the ρ^0 dataset with approximately 390K candidates, a first fit to the invariant mass distribution for all values of rapidity has been performed. All parameters of the fitting functions are left to vary within some sets of limits. The result of the fit is shown in Fig. 67. The mass and width extracted from this integrated fit is then fixed for subsequent fits in five rapidity intervals.

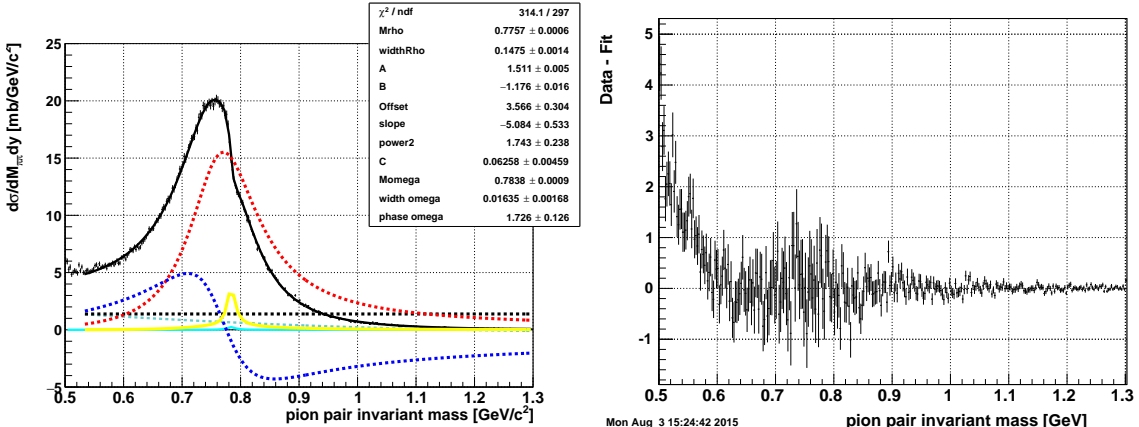


Figure 67: . Fits to the fully corrected invariant mass distribution of pion pairs with transverse momentum smaller than 100 MeV (coherent scattering off the Au nuclei). The fit function has three components: Breit-Wigner functions for the ρ^0 and ω mesons as well as a constant non resonant pion pair component. These three components do interfere. An additional polynomial is added to handle the presence of remnant backgrounds.

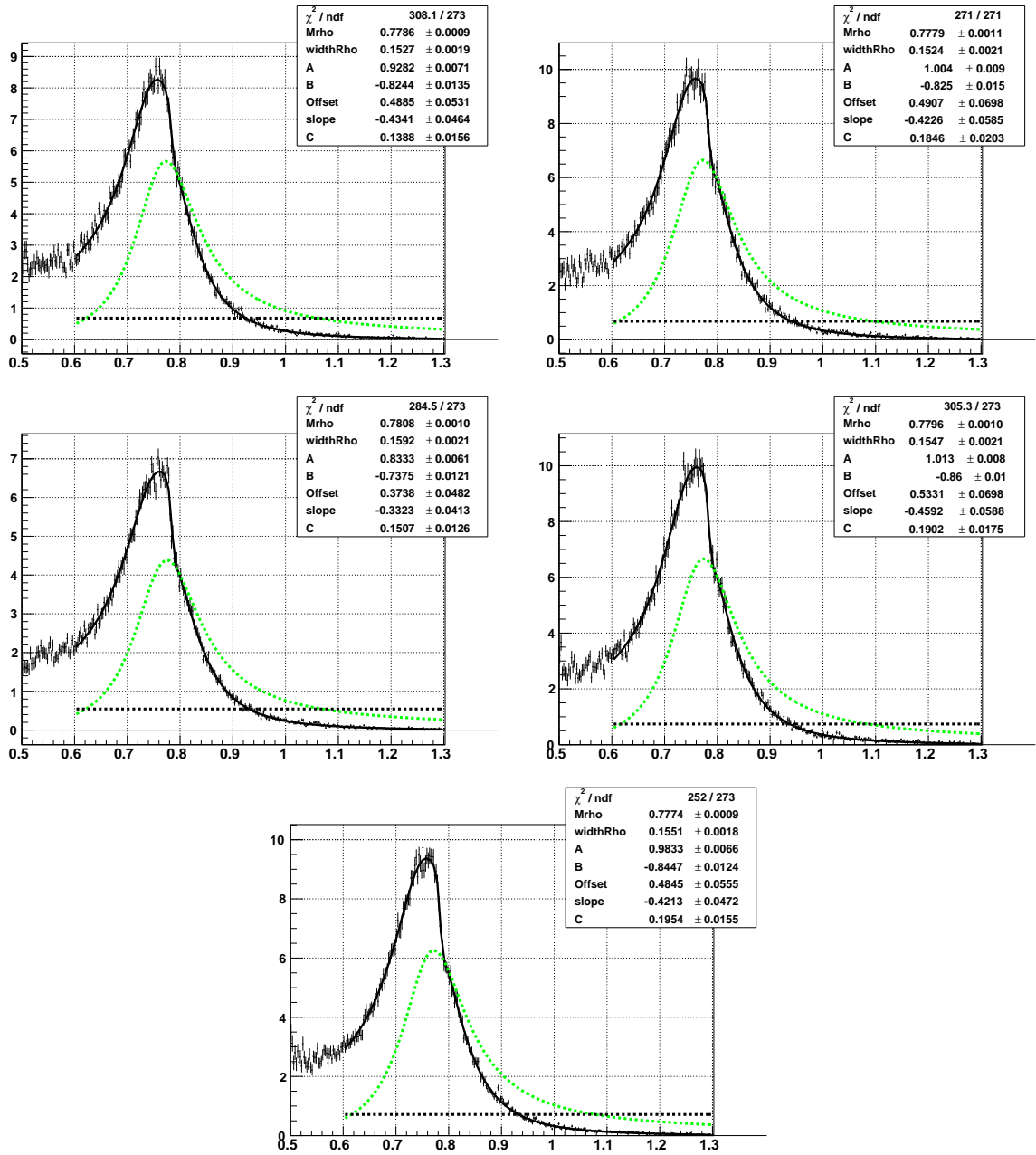


Figure 68: . Fits to fully corrected invariant mass distribution of pion pairs with transverse momentum smaller than 100 MeV (coherent scattering off the Au nuclei) in five rapidity bins. The rapidity bins were select to be equally populated. The fit function is the same used for the rapidity integrated fit, but the mass and width of the ω meson are fixed to the value found in the integrated fit.

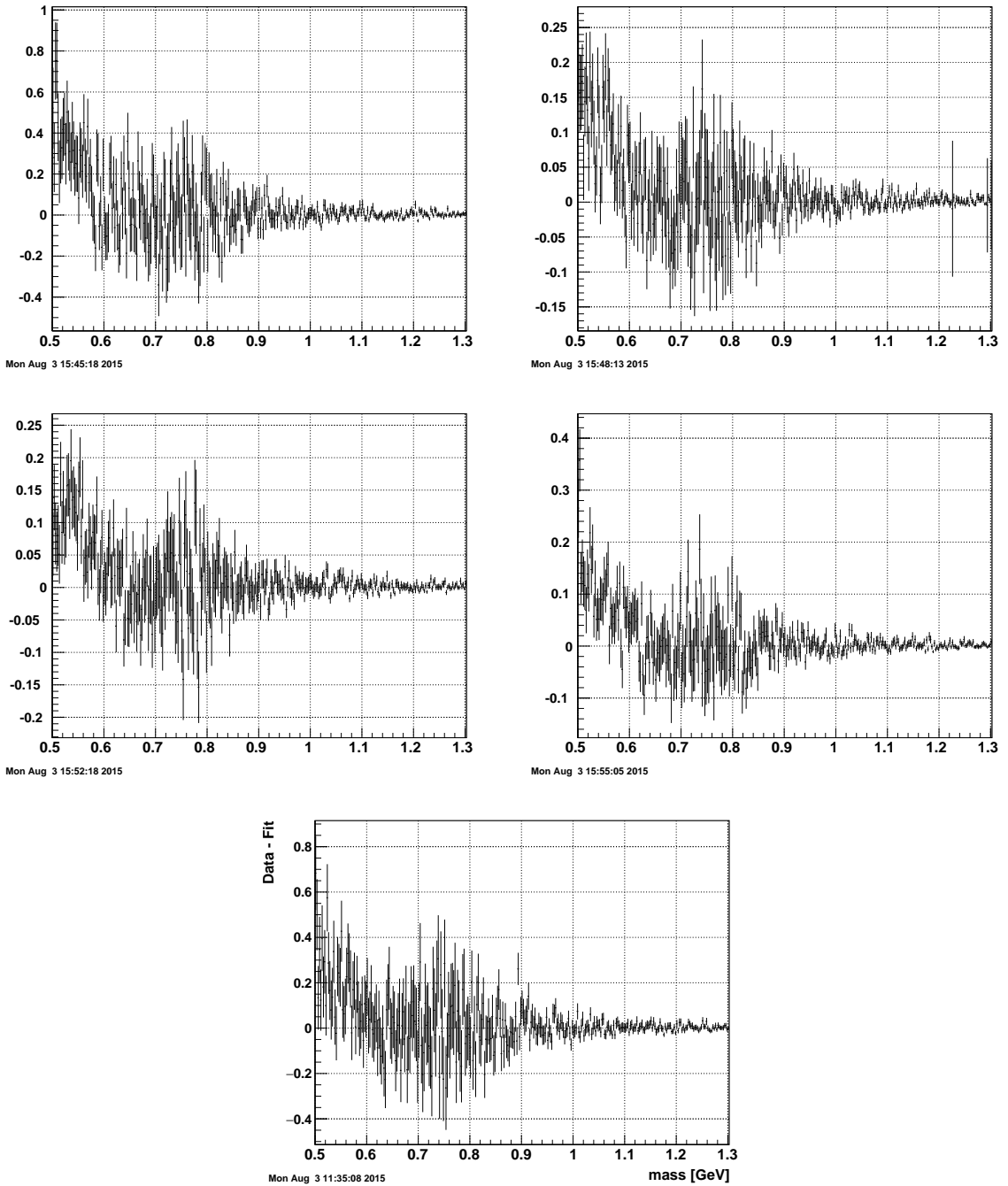


Figure 69: . Residual from fits to fully corrected invariant mass distribution of pion pairs. The background below 600 MeV is present in all five rapidity bins.

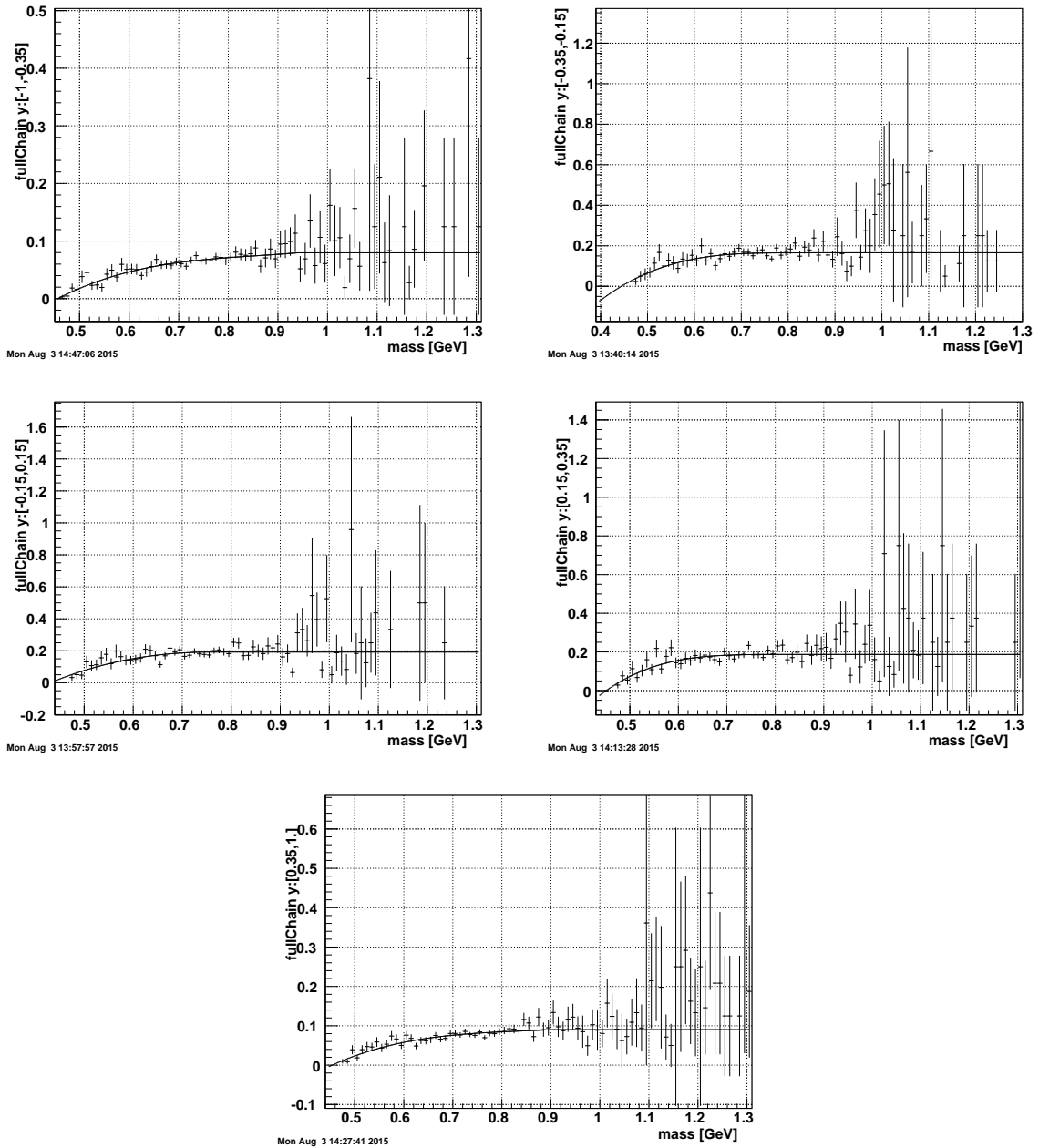


Figure 70: The so called “fullChain” correction extracted from embedding in the five rapidity bins. See text for details.

A detailed description of the fit to the rapidity integrated pion pair invariant mass distribution is shown in the left panel of Fig. 67. That distribution is fitted with function 2 shown with a full black curve in the figure. To describe each one of the other curves, it is necessary to expand that function once the absolute value $|..|^2$ is calculated, but before doing that it helps to make the following definitions:

$$\frac{d\sigma}{dM_{\pi^+\pi^-}} = |A_\rho f_1 + B_{\pi\pi} + C_\omega f_2|^2 \quad (3)$$

where $f_1 = D_\rho/J_\rho$ and $f_2 = D_\omega/J_\omega$ with:

$$J_\rho = M_{\pi\pi}^2 - M_\rho^2 + iM_\rho\Gamma_\rho \quad (4)$$

$$J_\omega = M_{\pi\pi}^2 - M_\omega^2 + iM_\omega\Gamma_\omega \quad (5)$$

$$D_\rho = \sqrt{M_{\pi\pi}M_\rho\Gamma_\rho} \quad (6)$$

$$D_\omega = \sqrt{M_{\pi\pi}M_\omega\Gamma_\omega} \quad (7)$$

$$\frac{d\sigma}{dM_{\pi^+\pi^-}} = A_\rho^2 f_1 f_1^* + A_\rho B_{\pi\pi} (f_1 + f_1^*) + A_\rho C_\omega^* f_1 f_2^* + A_\rho C_\omega f_1^* f_2 + B_{\pi\pi}^2 + B_{\pi\pi} C_\omega^* f_2^* + B_{\pi\pi} C_\omega f_2 + C_\omega^2 f_2 f_2^* \quad (8)$$

The red-dashed curve is the magnitude of the pure ρ production (Breit-Wigner) corresponding to the term: $A_\rho^2 f_1 f_1^*$. The full cyan curve corresponds to the magnitude of pure ω production (another Breit-Wigner): $C_\omega^2 f_2 f_2^*$. The blue-dashed curve labelled $\rho\pi\pi$ interf. in the figure, corresponds to the cross terms containing A_ρ and $B_{\pi\pi}$ in equation 8 ($A_\rho B_{\pi\pi} (f_1 + f_1^*)$). The ρ^0 and ω interference is shown with the full yellow curve and corresponds to the cross terms containing A_ρ and C_ω : $A_\rho C_\omega^* f_1 f_2^* + A_\rho C_\omega f_1^* f_2$.

The main result extracted from the fits is the relation between the non-resonant pion amplitude and the ρ^0 amplitude and a similar comparison of amplitudes for the ρ^0 and omega mesons. Those results are shown in Fig. 71. The right panel shows the extracted value of C/A in the present work with black markers together with a red band that displays the systematic uncertainties related to these quantities, the same ratio obtained by [8] is displayed with a black thick line because the rapidity of that measurement does not overlap with STAR acceptance. Their best result $\xi = 0.0106 \pm 0.0012$ is scaled by $\sqrt{\Gamma_\rho/\Gamma_\omega}$.

9.1.1 The phase of the ω meson production amplitude

The fit to the pion pair invariant mass performed in Fig. 67 assumed all three production amplitudes A_ρ , $B_{\pi\pi}$ and C_ω as real numbers. We explore here a possible non-zero phase in the ω amplitude: $C_\omega e^{i\phi}$. The fitting function allows for the inclusion of phases in the ρ^0 and ω production amplitudes:

```
// pasting Spencer code 17-JULY-2015
//
Double_t fitf_Spencer(Double_t *v, Double_t *par);
Double_t fitf_Spencer(Double_t *v, Double_t *par){
/* This reads histograms from Bill's TTree and fits for a rho, direct pipi and eventually an omega sign
April 9, 2015*/

// This is the fit function for the rho
// v[0] is the dipion mass
// par is the array containing the parameters being fitted
// par[0] is the rho mass
// par[1] is the rho width
// par[2] is 'A' the rho amplitude;
// par[3] is 'B' - the direct pion amplitude;
// par[4] is the constant background
// par[5] is the linear (in mass)background
// par[6] power 2
// par[7] power 3
// par[8] is the omega amplitude
// par[9] is the omega mass (can be fixed in main program)
// par[10] is the omega width (including detector effects)
// par[11] is the omega phase angle
// par[12] is the rho phase angle
```

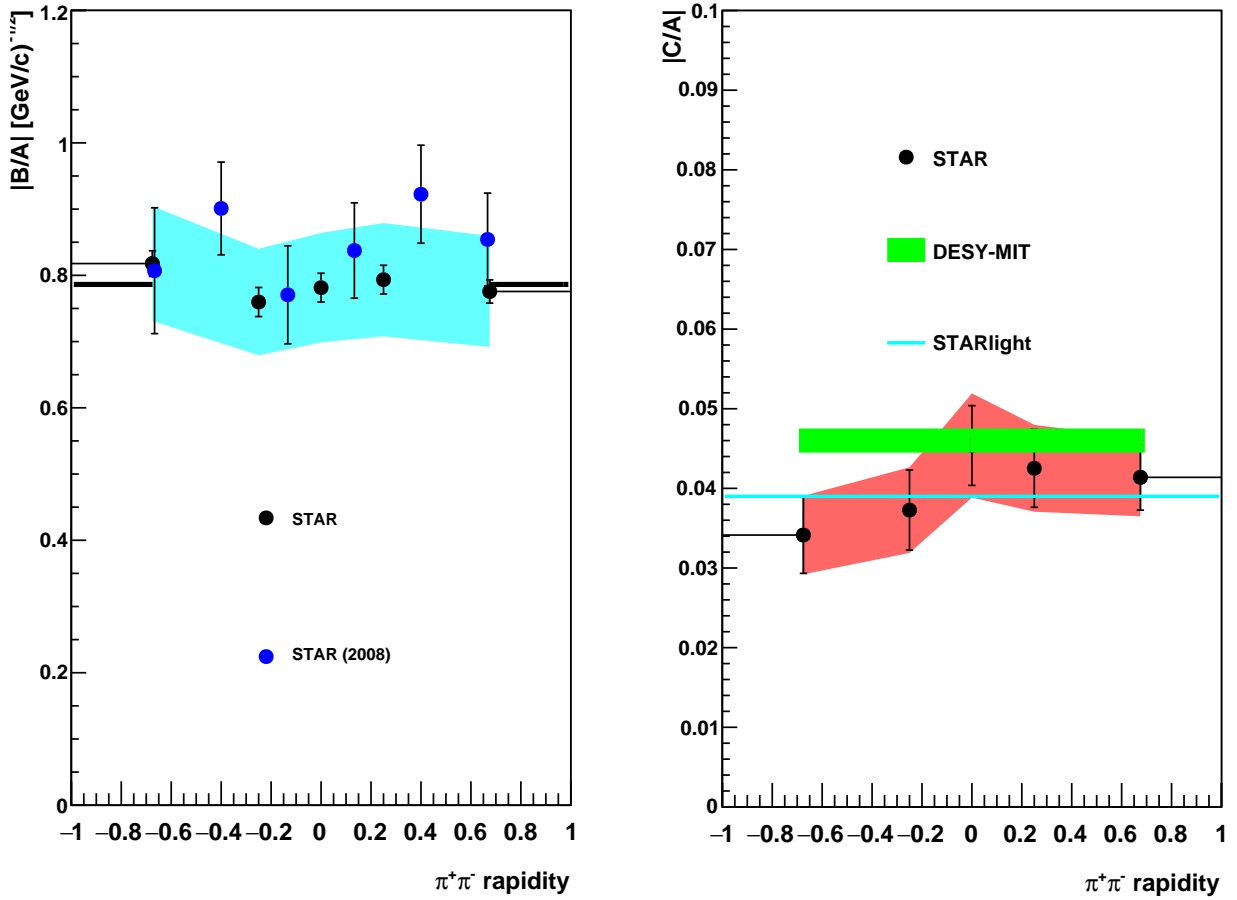


Figure 71: The left panel shows the ratio $|B/A|$ of amplitudes of non-resonant pion pair and ρ^0 mesons. The previous STAR results are shown with blue-filled circles. The right panel shows the ratio $|C/A|$ of the ω and ρ^0 amplitudes. The data is shown with red markers, while the red band includes the relevant systematic errors. The DESY-MIT $|C/A|$ measurement is shown with a green band. This measurement was at considerably lower photon energies; if converted to rapidity, these measurements would appear at large $|y|$, outside the current plot. The thin cyan line shows $|C/A|$ calculated using STARlight and the most recent branching ratio for $\omega \rightarrow \pi^+\pi^-$ decay [17].

```

// Now rotate by phase angle

double cosp=cos(par[11]);
double sinp=sin(par[11]);
double realrotomega=cosp*realomeganumer - sinp*imomeganumer;
double imrotomega=sinp*realomeganumer + cosp*imomeganumer;

// Sum real and complex parts

double realamp=realrhonumer+bterm+realrotomega;
double imamp=imrhonumer+imrotomega;
double fitval=realamp*realamp+imamp*imamp+polybg;

return fitval;

```

The fit shown in Fig. 67 had 11 free parameters and with a fit range from 0.53 to 1.3 GeV produced a good fit with $\chi^2/NDF = 1.06$. We proceed to explore χ^2 space to see more details around the phase we found in the fit shown on Fig. 67. After each fit the parameters are not reset to their default values, at a new step they start from the value found in the previous fit.

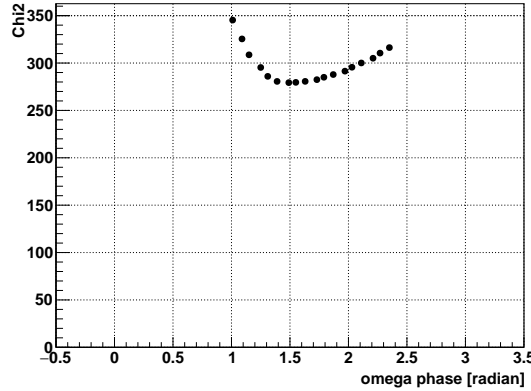


Figure 72: . The value of the χ^2 of fits were the value of the omega phase is changed from 1. to 2.4 radians in 18 steps of 0.08 radians. The minimum value of χ^2 ($\phi_\omega = 1.56$) is not exactly equal to the one found in Fig. 67 and appears to depend on the phase value at the beginning of the scan.

9.2 Cross-section $d\sigma/dy$ in rapidity

The final version of the paper will emphasize the diffraction pattern figure. The rapidity distribution discussed in this section may be included in the paper but it will not have much emphasis mainly because this is an already published STAR result [14]. This figure was used to establish the normalization of the diffractive pattern.

Two dimensional histograms in Invariant mass versus rapidity of selected pion pairs were filled for signal as well as background. The candidate rho mesons are found with a single subtraction of those two histograms, the projection of those raw counts constitute the signal found in this analysis. The signal yield is divided by the so called “full chain correction” shown in Fig. 38 extracted from the Mixed embedding project described in section 7.

The actual signal has a approximate 20% contribution from non-resonant pion pairs. That contribution has to be extracted before a final set of figures is generated. The extraction is done by fitting the invariant mass distributions in rapidity, transverse momentum or t bins. Such correction has been extracted using the fits shown in Fig. 68 in five rapidity bins. The ρ^0 Breit-Wigner function is integrated from twice the mass of the pion to $M_\rho + 5\Gamma_\rho$ and is compared to the normalized number of pion pair candidates found in that particular rapidity bin. The resulting ratio is constant in rapidity as shown in Fig. 73.

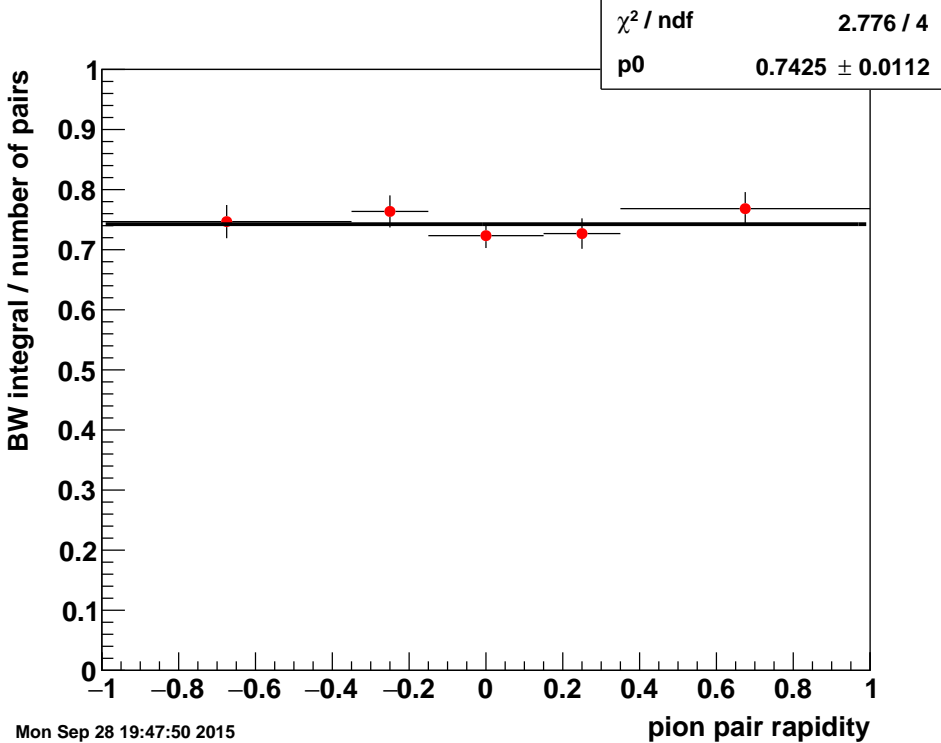


Figure 73: The red markers show the ratio of the ρ^0 Breit-Wigner integral from twice the mass of the pion to $M_\rho + 5\Gamma_\rho$ divided by the fully corrected number of pion pairs in each of the five rapidity bins. An average for what is then then correction to be applied to obtain yields or cross-section for pure ρ^0 mesons is obtained with a fit to a constant ($corr = 0.74 \pm 0.01$).

9.3 Correction to event loss due to vertex finder track assignment to vertices

The vertex finder has a tendency to associate spurious tracks to a vertex. Such behavior is best seen in Fig. 60 where the generated vertex has only two tracks and the additional tracks found in the reconstructed vertex can only come from the zero bias data background. This feature of the vertex finder translates into a loss in the selection of exclusive events. The correction for that loss can be extracted from the data by counting the number of ρ^0 mesons found while requiring up to 5 tracks connected to the selected vertex with the number extracted from the original analysis where we demand 2 tracks out of the vertex. The counting of ρ^0 mesons is done in the standard way in 5 bins in rapidity with fits to acceptance corrected pion pair mass distribution with equation 2. Once the fits done, we integrate the ρ^0 Breit-Wigner from $2M_\pi$ to $M_\rho + 5\Gamma_\rho$.

Figure 74 shows that all five fits are as good as the ones obtained for exactly two tracks out of the vertex as shown in Fig. 68. The average across the five rapidity bins has the value of $21 \pm 1\%$.

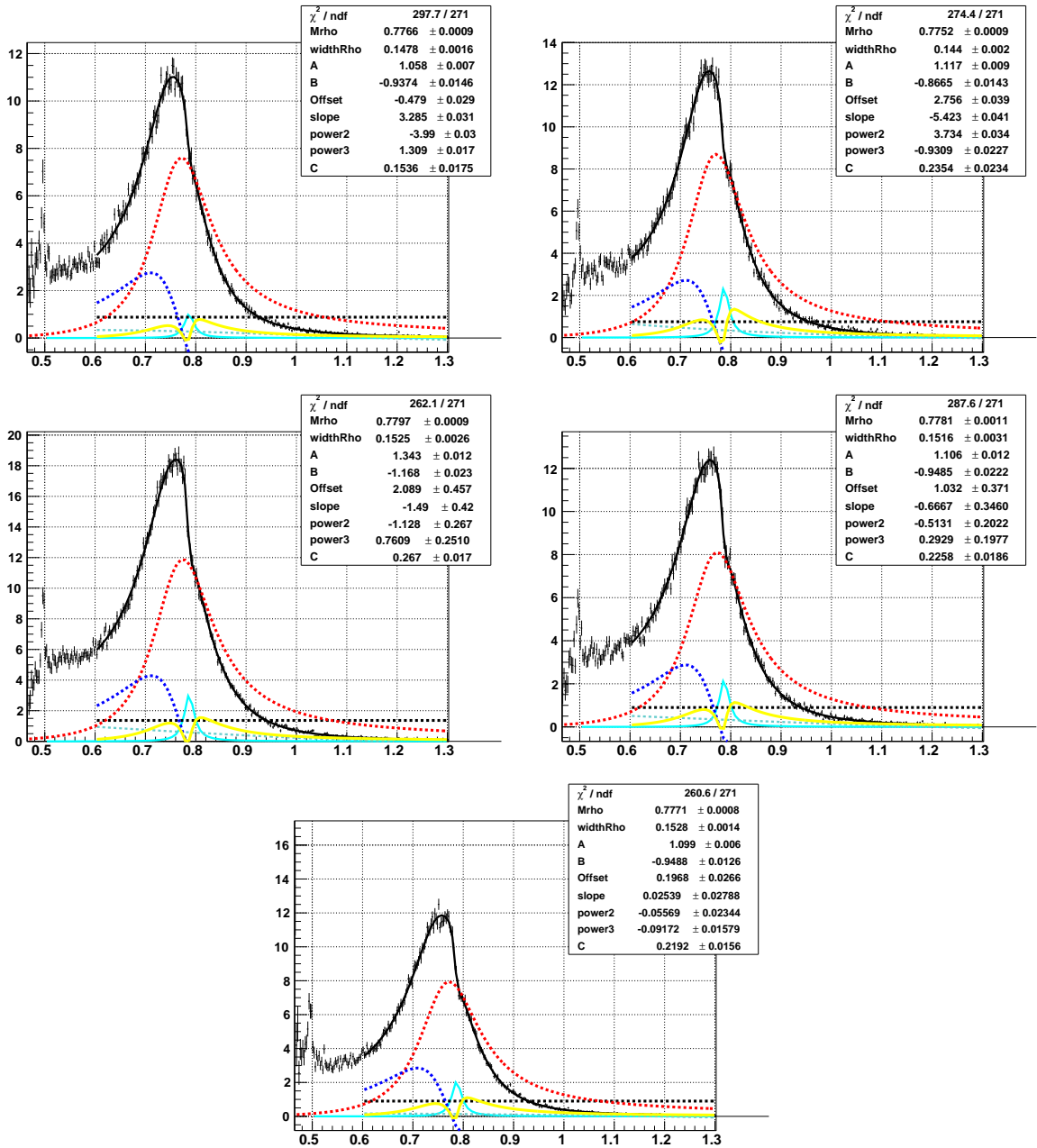


Figure 74: . Fits to fully corrected invariant mass distribution of pion pairs with transverse momentum smaller than 100 MeV (coherent scattering off the Au nuclei) in five rapidity bins the number of tracks from the vertex has been relaxed to 5 tracks instead of just two. As was the case for the fits for exclusive ρ^0 production, the mass and widths of the ω meson are fixed to the value found in the integrated fit.

A similar excersize has been performed with the data sets produced with the mixed embedding. The number of tracks on the selected vertices has been set to 2 and 5 and the number of selected pion pairs and the integrals of ρ^0 Breit-Wigner functions extracted from their fits are compared to estimate the losses introduced by the vertex finder tendency to add spurious tracks. Figure 75 shows the fits to the mass distribution of selected pion pairs. The left panel shows the fits and distributions extracted from the standard exclusive data set (only two tracks in the selected vertex)

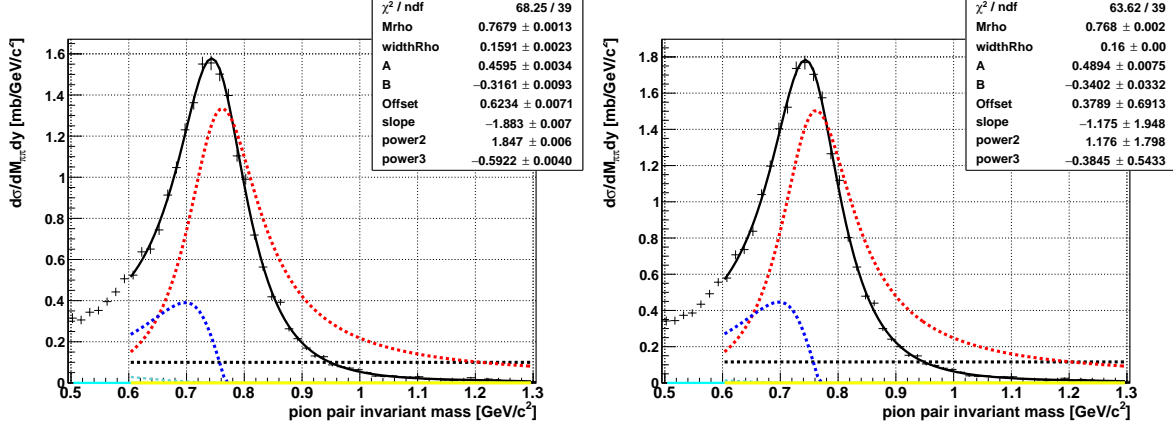


Figure 75: . Fits to fully corrected invariant mass distribution of pion pairs generated by StarLight (coherent with PID:913). The left panel shows the fit to the mass distribution extracted from the exclusive sample (two tracks out of vertex) and the right one the one for a data set extracted with up to 5 tracks out of the vertex.

Using the raw counts of reconstructed pion pairs or the integrals of the ρ^0 Breit-Wigner from $2M_\pi$ to $M_\rho + 5\Gamma_{rho}$ the increase introduced by the vertex finder is 13% in both cases. This excess is not equal to the one extracted from data (21%). It appears thus that the results presented in this work need to have an upward correction of 8%.

The following equation summarises the way the cross section is calculated:

$$\frac{d\sigma}{dy} = \frac{N_{counts}(y) \times f_{vtxLoss} \times f_{pureRho} \times f_{XnXn}}{\text{binWidth}(y) \times \text{fullChain}(y) \times \text{Luminosity}}, \quad (9)$$

where $N_{counts}(y)$ is the count of pion pairs that satisfy all condition required in this analysis in a particular rapidity bin (centered at y). The correction $\text{fullChain}(y)$ is shown in Fig. 64. The factor $f_{vtxLoss} = 1.08$ compensates for the fact that the vertex finder algorithm tends to add spurious tracks to the vertex producing a loss as vertices are rejected one we impose the so called “exclusive production” where only two track vertices are selected. The extraction of its value from data and embedded sets is described in the previous subsection 9.3. The factor $f_{pureRho}=0.75$ has been extracted from fits to invariant mass distribution as described above and summarized in Fig. 73. The factor $f_{XnXn} = 2.11$ is obtained with the RELDIS event generator and is only used to scale the cross-section measured with the UPC_Main trigger up to XnXn values. Luminosity is the integrated luminosity for all 2010 Au+Au runs used in this analysis which has the value of $1074.6 \mu b^{-1}$, see section ??.

Once all corrections and normalizations are applied the resulting cross section in rapidity are shown below. Figure 76 shows the rapidity distribution extracted from UPC_Main events with red markers, the same distribution is scaled with an overall correction obtained with the RELDIS event generator to the magnitude of an XnXn correction. The same figure also display the STAR published XnXn cross section from 2004 data and the cross section obtained with the StarLight event generator. Figure 77 show the 1n1n rapidity distribution, this time the direct comparison to StarLight is possible and there is no need to invoke the RELDIS correction.

The final version of the rapidity cross section shown in Fig. 78. We have drifted away from using the RELDIS event generator to scale the UPC_Main cross section up to a XnXn cross-section because its detailed comparison to data presented in section 8.5 was not optimal, while STARlight handles mutual dissociation with parametrization of actual mesurements.

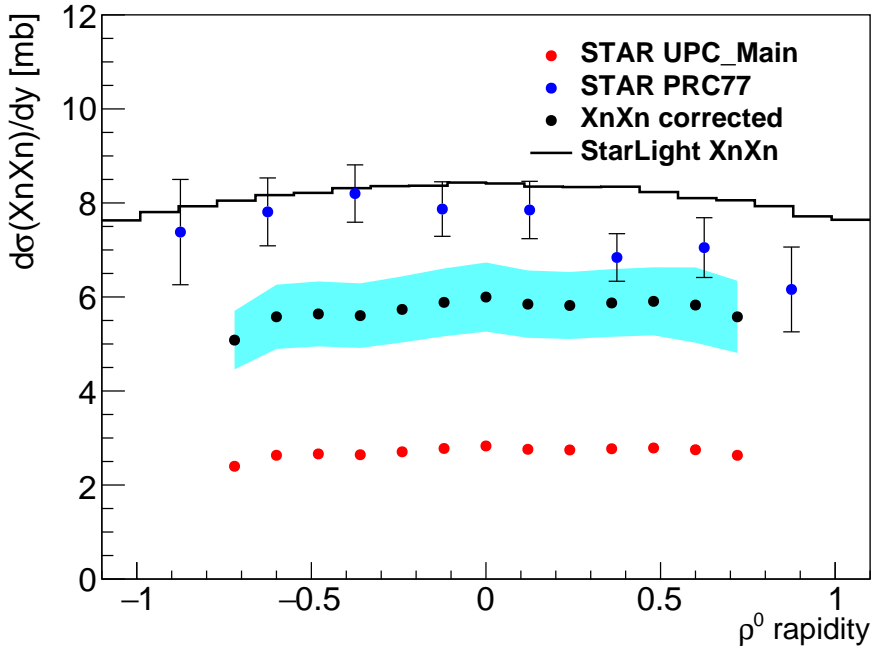


Figure 76: Red markers show the fully corrected rapidity distribution for pion pairs with invariant mass with values between 0.5 and 1.5 GeV detected in events with any neutron emmission by the Au ions (XnXn). The events used for this analysis have vertices with the z coordinate limited to $|Vtx_z| < 50$ cm. The black histogram shows the ρ^0 meson produced by StarLight together with a contribution from a pion pair continuum for events with XnXn mutual dissociation.

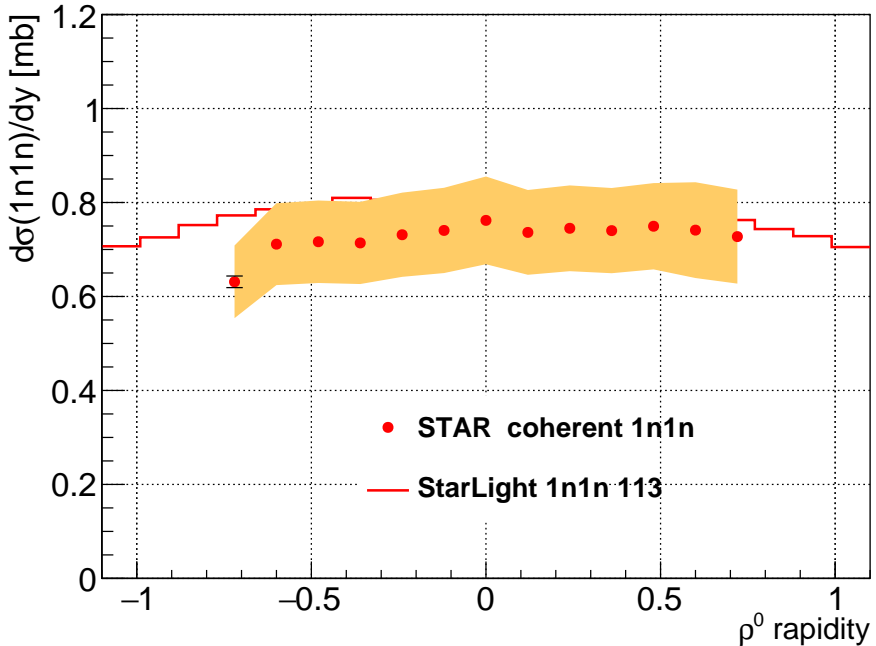


Figure 77: Red markers show the fully corrected rapidity distribution for pion pairs with invariant mass with values between 0.5 and 1.5 GeV detected in events with 1 neutron emmission by the Au ions (1n1n). The events used for this analysis have vertices with the z coordinate limited to $|Vtx_z| < 50$ cm. The black histogram shows the pure ρ^0 meson produced by StarLight (PID: 113).

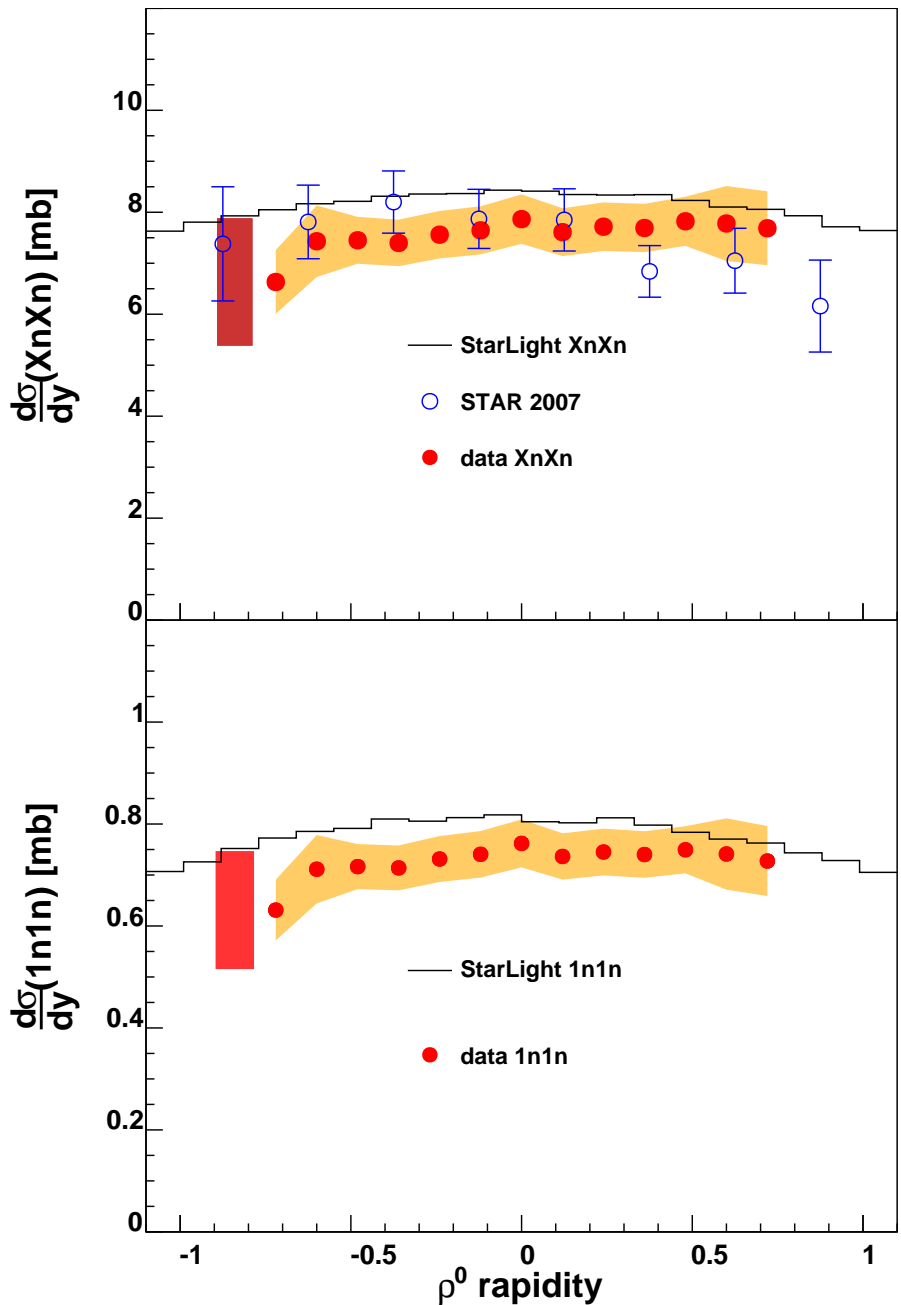


Figure 78: The red markers of the bottom panel show the fully corrected rapidity distribution for pion pairs with invariant mass with values between $2M_\pi$ and $5 \times \Gamma_\rho$ GeV detected in events with 1 neutron emission from both Au ions (1n1n). The events used for this analysis have vertices with the z coordinate limited to $|Vtx_z| < 50$ cm. Point-to-point systematic uncertainties added in quadrature are shown with the orange band. Statistical errors are smaller than the markers. The common systematic uncertainty, added in quadrature, is shown with the red box at the most negative value of rapidity. The red histogram shows the pure ρ^0 meson produced by StarLight (PID: 113). The top panel shows the cross-section displayed in the bottom panel after it was scaled by the ratio 1n1n/XnXn produced by the STARlight. The resulting XnXn distribution is then compared to the 2007 rapidity distribution shown with open blue markers. The black histogram has is the cross-section of coherent ρ^0 mesons calculated with STARlight.

9.4 Diffraction pattern $d\sigma/dt$

Includes Fourier transformation with some unfolding for bin migration in t and systematic errors. It also has comparisons to StarLight and sartre.

The following equation summarises the way the cross section as function of the momentum transfer -t is calculated:

$$\frac{d\sigma}{dt} = \frac{N_{counts}(-t) \times f_{vtxLoss} \times f_{pureRho} \times f_{XnXn}}{binWidth(-t) \times rapidityRange \times \langle fullChain \rangle \times Luminosity}, \quad (10)$$

where $N_{counts}(-t)$ is the count of pion pairs that satisfy all condition required in this analysis in a particular t bin. The overall correction obtained from embedding is constant in -t as can be seen in section 7 Fig. 39. We use an average over rapidity labeled as $\langle fullChain \rangle$. The rapidity dependence of that distribution is shown in Fig. 64, the value of the average is $\langle fullChain \rangle = 0.064$. The factor $f_{vtxLoss} = 1.08$ compensates for the fact that the vertex finder algorithm tends to add spurious tracks to the vertex producing a loss as vertices are rejected one we impose the so called “exclusive production” where only two track vertices are selected. The factor $f_{pureRho} = 0.75$ has been extracted from fits to invariant mass distribution as described below. The factor f_{XnXn} is obtained with two procedures, the first one is based on the RELDIS event generator and is only used to scale the cross-section measured with the UPC_Main trigger up to XnXn values, the value is then equal to 2.11. The second method, which appears more reliable, uses the Mutual dissociation that is used in the StarLight generator. For this second method the scaling is done in two steps: first the UPC_Main distribution is scaled down to match the 1n1n data. From that distribution we then scale up to XnXn using the StarLight ratio 1n1n/XnXn. The resulting value with the STARlight based procedure is equal to 2.685 Luminosity is the integrated luminosity for all 2010 Au+Au runs used in this analysis which has the value of $1074.6 \mu b^{-1}$, see section 6.

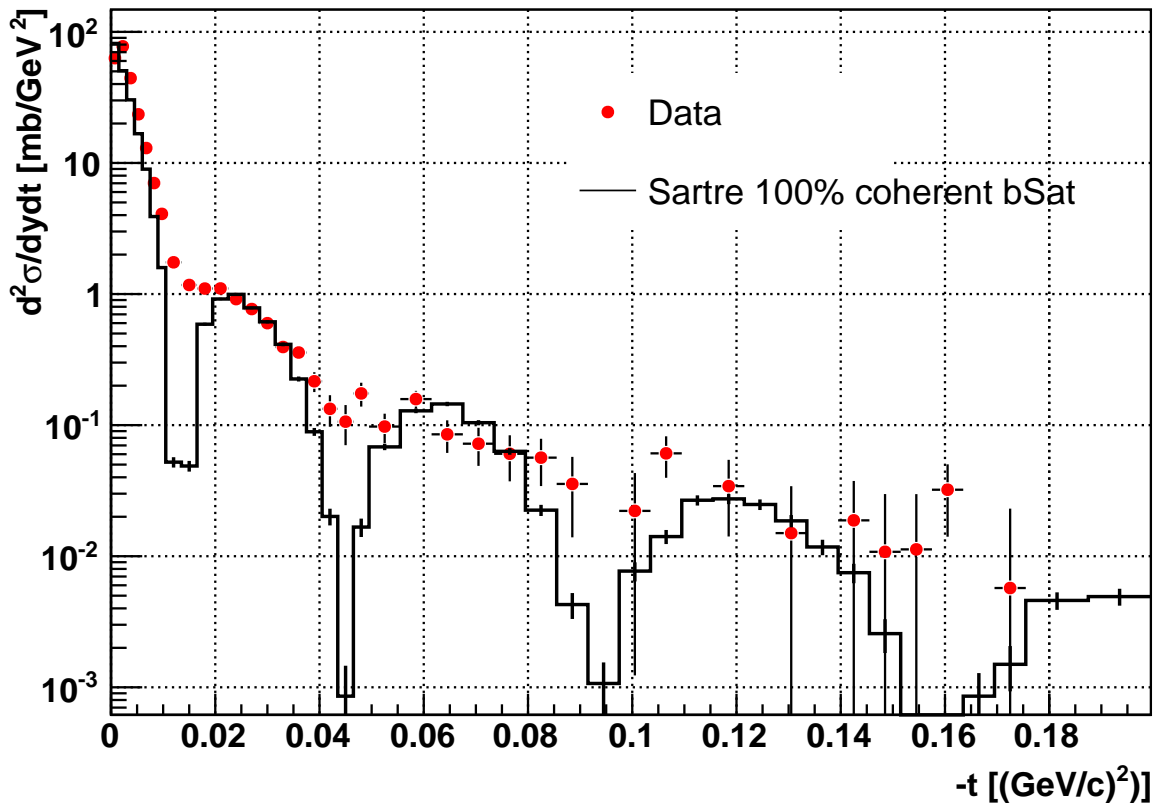


Figure 79: Un-normalized diffraction pattern as it was shown at WWND and EDSBLOIS.

The paper quotes the result of the fit to the first diffraction peak: $386.6 \pm 59.8 (GeV/c)^{-2}$ to be compared to an expected value of $10.8 A^{2/3} (GeV/c)^{-2}$ or 365.6 (got this relation from a paper on n+A to p+pi+A looks like $4\pi R^2$) Then I list the dip locations at 0.018 ± 0.005 and 0.043 ± 0.01 With these two points I can make a statement about the size of the scattering target using the dip location as function of the Bessel function J_0 zeroes as shown in Fig. ??

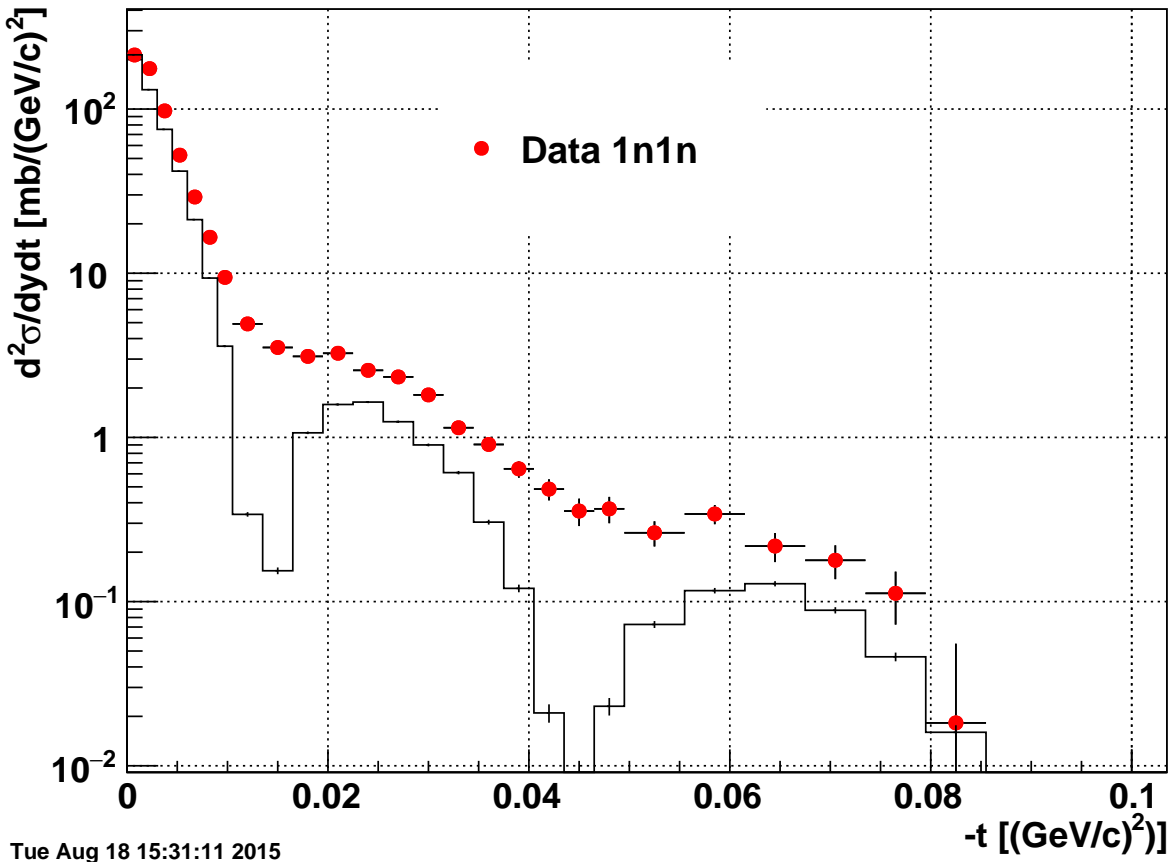


Figure 80: Diffraction pattern from 1n1n events with both tracks matched to TOF and $|v_z| < 50$ cm. Includes full chain correction as function of p_T from the completed mixed embedding project and normalization with the run luminosity. The black histogram shows the $-t$ of the recoil Au ion as generated with the sartre event generator. This comparison is only displayed to highlight the matching of the dips in the data and the event generator

Figure 86 shows the fits to fully corrected invariant mass distributions for the first bins in the t variable ($p_T < 100$ MeV/c).

A summary of these six fits in t bins is shown in Fig. 87 where the left panel shows the fraction of non-resonant pion pairs compared to the yield of ρ^0 mesons. The right panel shows how the fraction of ω to ρ^0 mesons change with the square of the transverse momentum of the pion pair. At higher values of $-t$, the presence of backgrounds and the drop in actual number of detected pion pairs conspire to make these measurements with some accuracy.

A similar exercise is done for the incoherent diffraction tail. First we fit the complete range from 0.2 to 1. GeV/c^2 with all parameters free. The results of that fit are shown in Fig. 88. The number of entries for that pion pair mass distribution is 151K for signal and 50K for same charge background.

Then we proceed to fit the mass distributions in smaller t bins (0.2 GeV/c^2 wide), the results of the first are shown in Fig. 89. The mass of the ρ^0 meson has been fixed to the value found in the previous fit from t 0.2 to 1.

The integral of the ρ^0 Breit-Wigner is calculated from $2M_\pi$ to $M_\rho + 5\Gamma_\rho$ and compared to the counts of $\pi\pi$ pairs with mass ranging from 600 MeV to 1.3 GeV. The result of that comparison is 0.76, 0.78, 0.46, 0.72 for each of the bins in $-t$. I call this a constant very close to what we extracted from similar fits at the coherent side of the distribution; 0.75.

9.5 Fits to coherent and incoherent portions of the cross section

Table 11 summarizes the extraction of the systematic error on the incoherent and coherent cross sections as extracted from the change of upper and lower limits of the fits to the dipole form factor for the distributions extracted from XnXn events.

The integral of the fit to the incoherent component in the XnXn events results in a value of cross section $\sigma_{incoh} = 2.89 \pm 0.02$ (stat.) ± 0.03 (syst.) mb in the measured rapidity range $|y| < 1$. The integral of the coherent component discussed below amounts to 6.49 ± 0.01 (stat.) ± 0.01 (syst.) mb.

$[(GeV/c)^2]$	A	Q_0^2	χ^2/NDF	Int. incoh.	Int.coh.
0.450	3.460 ± 0.024	0.099	19/10	$2.880 \pm 0.02 (stat) \pm 0.03 (syst.)$	$6.498 \pm 0.012(stat.) \pm 0.01 (syst.)$
0.400	3.481 ± 0.026	0.099	13/8	$2.906 \pm 0.021 (stat) \pm 0.03 (syst.)$	$6.486 \pm 0.012(stat.) \pm 0.01 (syst.)$
0.550	3.457 ± 0.022	0.099	20/15	$2.886 \pm 0.041 (stat) \pm 0.03 (syst.)$	$6.499 \pm 0.013(stat.) \pm 0.01 (syst.)$
0.600	3.452 ± 0.022	"	25/17	$2.881 \pm 0.02 (stat) \pm 0.03 (syst.)$	$6.502 \pm 0.013(stat.) \pm 0.01 (syst.)$
0.350	3.498 ± 0.028	"	10/6	$2.920 \pm 0.02 (stat) \pm 0.03 (syst.)$	$6.477 \pm 0.013(stat.) \pm 0.01 (syst.)$
0.150	3.453 ± 0.020	"	24/16	$2.881 \pm 0.02 (stat) \pm 0.03 (syst.)$	$6.502 \pm 0.013(stat.) \pm 0.01 (syst.)$

Table 11: Fits to the incoherent part of the XnXn cross-section as function of t. In all cases the fits start at $-t=0.2$ $[(GeV/c)^2]$ except the last entry at 0.150 above the location of the nominal boundary for coherent ρ^0 photoproduction ($p_T < 100$ MeV/c). The fits stop at different values of t listed in the first column, and they are used to study the contamination from hadronic interactions and to extract a systematic uncertainty related to the definition of such boundary between UPC events and very peripheral hadronic interactions. The parameters of the dipole form factor function are listed together with their related errors. The incoherent component of the cross section is calculated as the integral from $t=0$ and up to $t=0.5$ $[(GeV/c)^2]$ the quoted error on that cross section is statistical, read directly from the fit following the definition of the dipole form factor normalization (see text). The integral of the coherent component of the cross section is calculated by adding the first 32 bins of the histogram resulting from the subtraction of the fitted function from the full cross section. The error quoted for the integrated coherent component is Poissonian and calculated from the number of events in all those bins.

$[(GeV/c)^2]$	A	Q_0^2	χ^2/NDF	Int. incoh.	Int. coh.
0.800	0.181 ± 0.003	0.0847	50/25	$0.154 \pm 0.002 (stat) \pm 0.004 (syst.)$	$0.702 \pm 0.004 \pm 0.003 (syst.)$
0.700	0.183 ± 0.003	"	39/21	$0.156 \pm 0.002 (stat) \pm 0.004 (syst.)$	$0.701 \pm 0.004 \pm 0.003 (syst.)$
0.900	0.179 ± 0.003	"	70/29	$0.152 \pm 0.002 (stat) \pm 0.004 (syst.)$	$0.703 \pm 0.004 \pm 0.003 (syst.)$
0.600	0.184 ± 0.003	"	32/17	$0.157 \pm 0.002 (stat) \pm 0.004 (syst.)$	$0.700 \pm 0.004 \pm 0.003 (syst.)$
0.500	0.188 ± 0.003	"	19/13	$0.160 \pm 0.003 (stat) \pm 0.004 (syst.)$	$0.703 \pm 0.004 \pm 0.003 (syst.)$

Table 12: Fits to the incoherent part of the 1n1n cross-section as function of t. In all cases the fits start at $-t=0.2$ $[(GeV/c)^2]$ well above the location the nominal boundary for coherent ρ^0 photoproduction ($p_T < 100$ MeV/c). The fit stops at different values of t labelled "High -t" in order to study the contamination from hadronic interactions and to extract a systematic uncertainty related to the definition of such boundary between UPC events and very peripheral hadronic interactions. The 1n1n events have higher values for the upper limit of the fits as the contamination appears to be weak. All three parameters of the power law function are listed together with their related errors (diagonals of the covariant matrix of the fit). The incoherent component of the cross section is calculated by integrating the fit function from $t=0$ to $t=0.5$ $[(GeV/c)^2]$. The quoted error on that cross section is statistical; read directly from the fit following the definition of the power law normalization (see text). The integral of the coherent component of the cross section is calculated by adding the first 32 bins of the histogram resulting from the subtraction of the fitted function from the full cross section. The error quoted for the integrated coherent component is Poissonian and calculated from the number of events in all those bins.

The corresponding ratios are:

$$\sigma_{incoherent}^{XnXn}/\sigma_{coherent}^{XnXn} = 0.445 \pm 0.003(stat.) \pm 0.005(syst.)$$

Table 12 summarizes the extraction of the systematic error on the incoherent and coherent cross sections as extracted from the change of upper and lower limits of the fits to the dipole form factor for the distributions extracted from 1n1n events.

The integral of the fit to the incoherent component in the 1n1n events results in a value of cross section $\sigma_{incoh} = 0.15 \pm 0.01 (stat.) \pm 0.004 (syst.)$ mb in the same measured rapidity range. The integral of the 1n1n coherent component amounts to $0.702 \pm 0.004 (stat.) \pm 0.003 (syst.)$ mb.

$$\sigma_{incoherent}^{1n1n}/\sigma_{coherent}^{1n1n} = 0.214 \pm 0.015(stat.) \pm 0.006(syst.).$$

9.6 Comparison of integrated cross sections

We have extracted three differential cross sections: $d\sigma/dM$, $d\sigma/dy$ and $d\sigma/dt$. When integrated over the corresponding variable the results should show an agreement with the overall systematic uncertainty of the measurement. Before we proceed with such integration we review all steps followed for each differential cross section extraction including the corection applied in every case.

The processing of the data written in the UPC pico dst's is done with the same macro "processData.C" described in section 8.7. The macro writes a root file with 2D histograms that correlate several variables of the

selected ρ^0 candidates. For completeness, we list one more time the conditions satisfied by the selected pion pairs as they fill each histogram. All three histograms are filled with:

- Events that have a vertex with only two tracks that match two TOF hits.
- Both tracks have more than 14 hits.
- Both tracks are identified as pions with the TPC dE/dx method. Opposite and same charge pairs are used to fill separate histograms.
- The z coordinate of the selected vertex satisfies: $|z| < 50$ cm.
- The event was triggered by the UPC_Main trigger (1-4 neutrons in both East and West ZDCs)

The following table adds details about each differential cross section:

cross section	input histogram	p_T^{pair} conditions	M_{pair} conditions
$d\sigma/dM$	HrhoInvMassvsRapidityXnXn_withTOFmatch_50_cohNewBin	$p_T^{pair} < 100 MeV/c$	$0.6-1.2 GeV/c^2$
$d\sigma/dy$	HrhoInvMassvsRapidityXnXn_withTOFmatch_50_cohNewBin	$p_T^{pair} < 100 MeV/c$	$0.25-1.5 GeV/c^2$
$d\sigma/dt$	HrhoInvMassVstXnXn_withTOFmatch_50	none	$0.6-1.2 GeV/c^2$

Table 13: The second column of the table lists the input histograms (for opposite charge pairs) used to generate the differential cross section listed in column one. Additional conditions applied to selected pair before the histograms are filled are listed in the third column.

As can be seen in equation 1, the resulting $d\sigma/dM$ is extracted from events triggered by UPC_Main and does not have the f_{XnXn} correction. It does not include the small f_{vertex} correction. This cross section is a mixture of non-resonant pion pairs ρ^0 and ω mesons. The other two differential cross sections have the correction $f_{pureRho}$ which eliminates the non-resonant pion pair contributions (the ω meson is considered negligible). The fit to the function 2 will provide the contribution from the ρ^0 mesons.

The comparison between integrals of the three differential cross section produces the following results:

$$d\sigma/dy(|y| < 1) = \int \frac{d\sigma}{dM dy} dM = \int_{0.6}^{1.2} Breit - Wigner_\rho dM = 3.16 mb \times f_{XnXn} \times f_{vertex} = 9.2 mb$$

where $Breit - Wigner_\rho$ is the ρ^0 component extracted from the fit to function 2 to be integrated from 0.6 to $1.2 GeV/c^2$, $f_{XnXn} = 2.685$ and $f_{vertex} = 1.08$.

$$\begin{aligned} d\sigma/dy(|y| < 1) &= \int \frac{d\sigma}{dt dy} dt = \sum d\sigma/dt(t_i) dy \times binWidth(t_i) = 7.3 mb \\ d\sigma/dy(|y| < 0.7) &= \int \frac{d\sigma}{dy} dy = \sum d\sigma/dy(y_i) \times binWidth(y_i) = 11.6/1.4 = 8.3 mb \end{aligned}$$

The difference between these results and the average (8.3 mb) is at most equal to 12%, a value smaller to the total systematic uncertainty of the measurement. It is possible that a better description of the incoherent component of the $d\sigma/dt$ differential cross section would produce a higher value of the integrated coherent component.

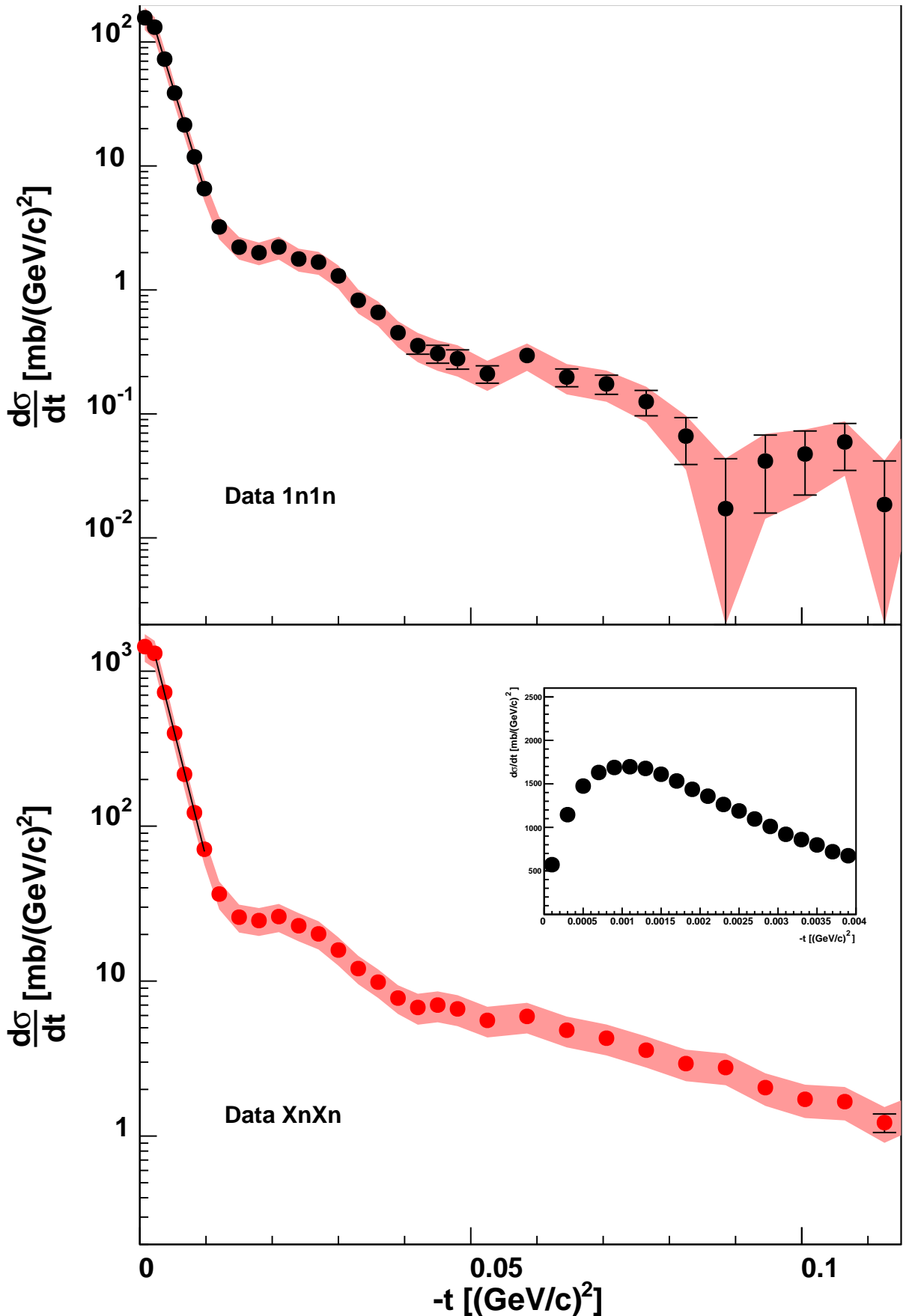


Figure 81: Diffraction pattern from XnXn events (bottom panel) and 1n1n (top panel) as it appears in Figure 7 of the paper. These distributions are constructed with two track vertices (both tracks matched to TOF hits) and $|v_z| < 50$ cm. The normalization includes the “fullChain” correction as function of t obtained from the embedding project, luminosity and XnXn cross section loss related to UPC_Main trigger (bottom panel).

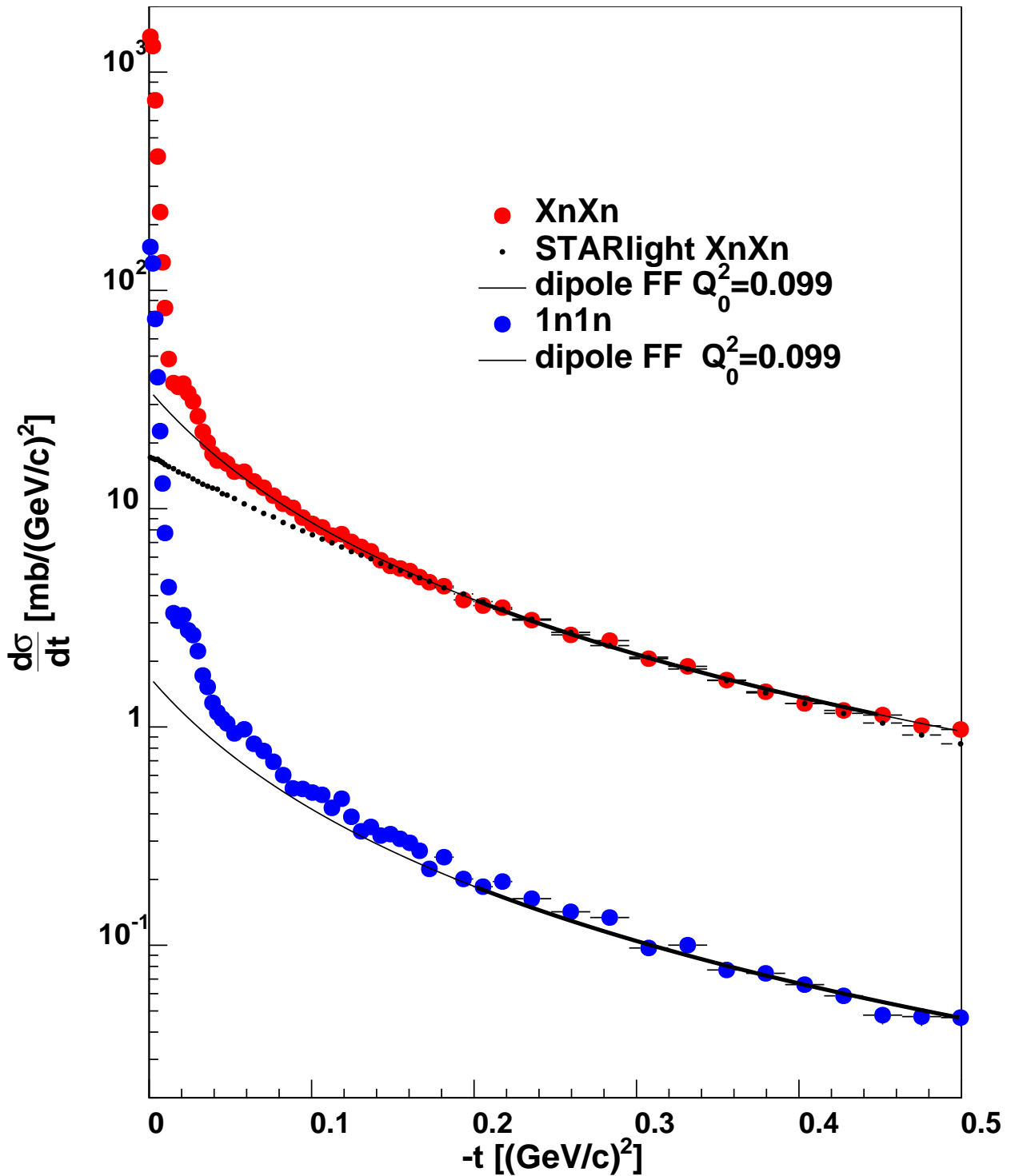


Figure 82: Diffraction pattern from XnXn and 1n1n events as it appears in Figure 6 of the paper. These distributions are constructed with two track vertices (both tracks matched to TOF hits) and $|v_z| < 50$ cm. The normalization includes the “fullChain” correction as function of t obtained from the embedding project, luminosity and XnXn cross section loss related to UPC_Main trigger using STARlight ratios 1n1n/XnXn.

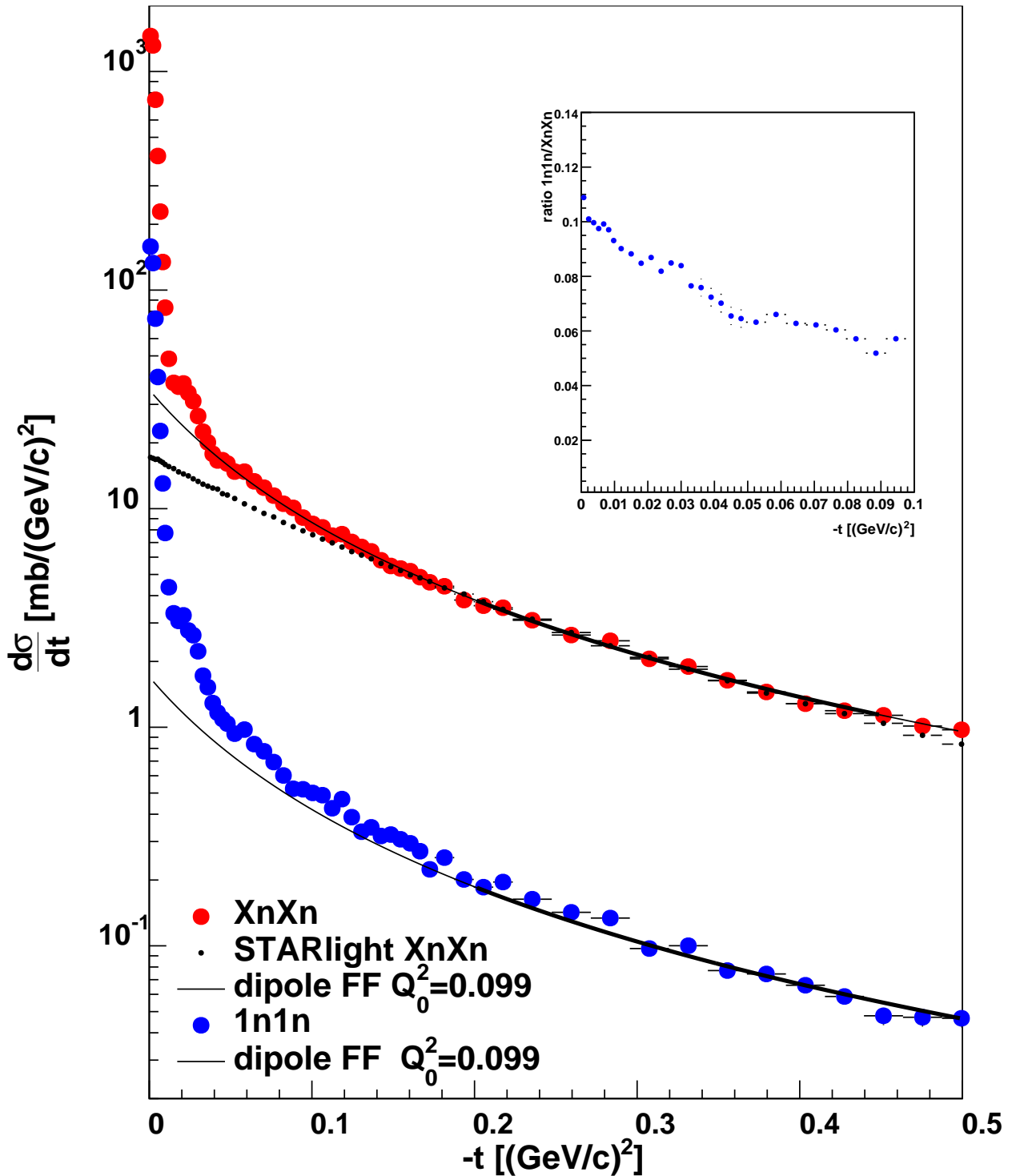


Figure 83: Diffraction pattern from XnXn and 1n1n events as it appears in Figure 6 of the paper. The insert shows the ratio $1n1n/XnXn$ and can be seen as an indication that the effects of the electromagnetic dissociations do not factorize from the ρ^0 elastic scattering. These distributions are constructed with two track vertices (both tracks matched to TOF hits) and $|v_z| < 50$ cm. The normalization includes the “fullChain” correction as function of t obtained from the embedding project, luminosity and XnXn cross section loss related to UPC_Main trigger using STARlight ratios $1n1n/XnXn$.

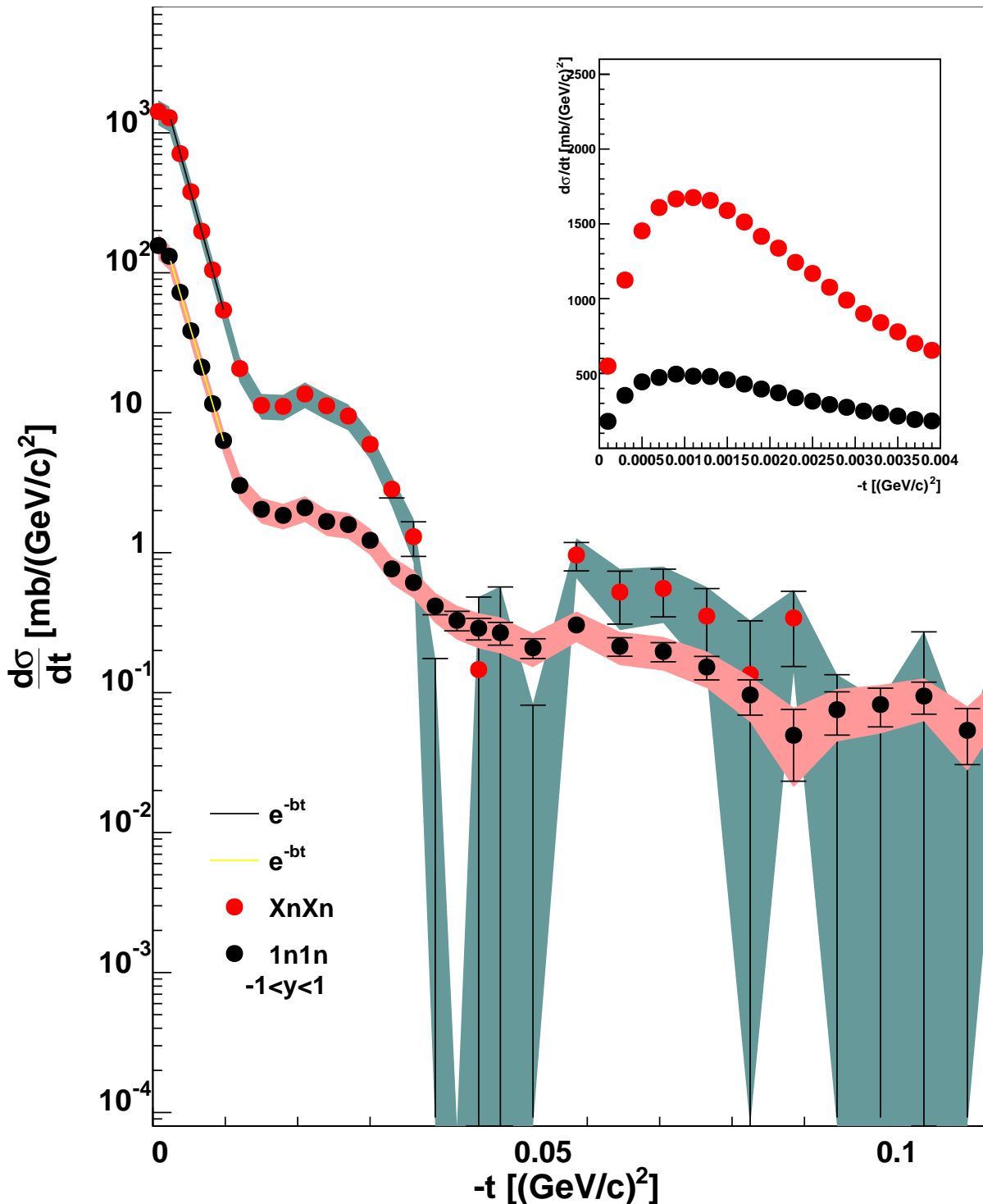


Figure 84: Diffraction pattern for coherent ρ^0 scattering of the Au target for both $XnXn$ (red markers) and $1n1n$ events black markers. This distribution is the result of the subtraction of the incoherent component using a fit to the so called dipole form factor. This is the final version of Figure 7 of the paper. The insert shows the interference region for $1n1n$ and $XnXn$ events. The destructive interference appears to extend to higher values of t for the $XnXn$ events, as another indication that photon exchange may not be factorizable.

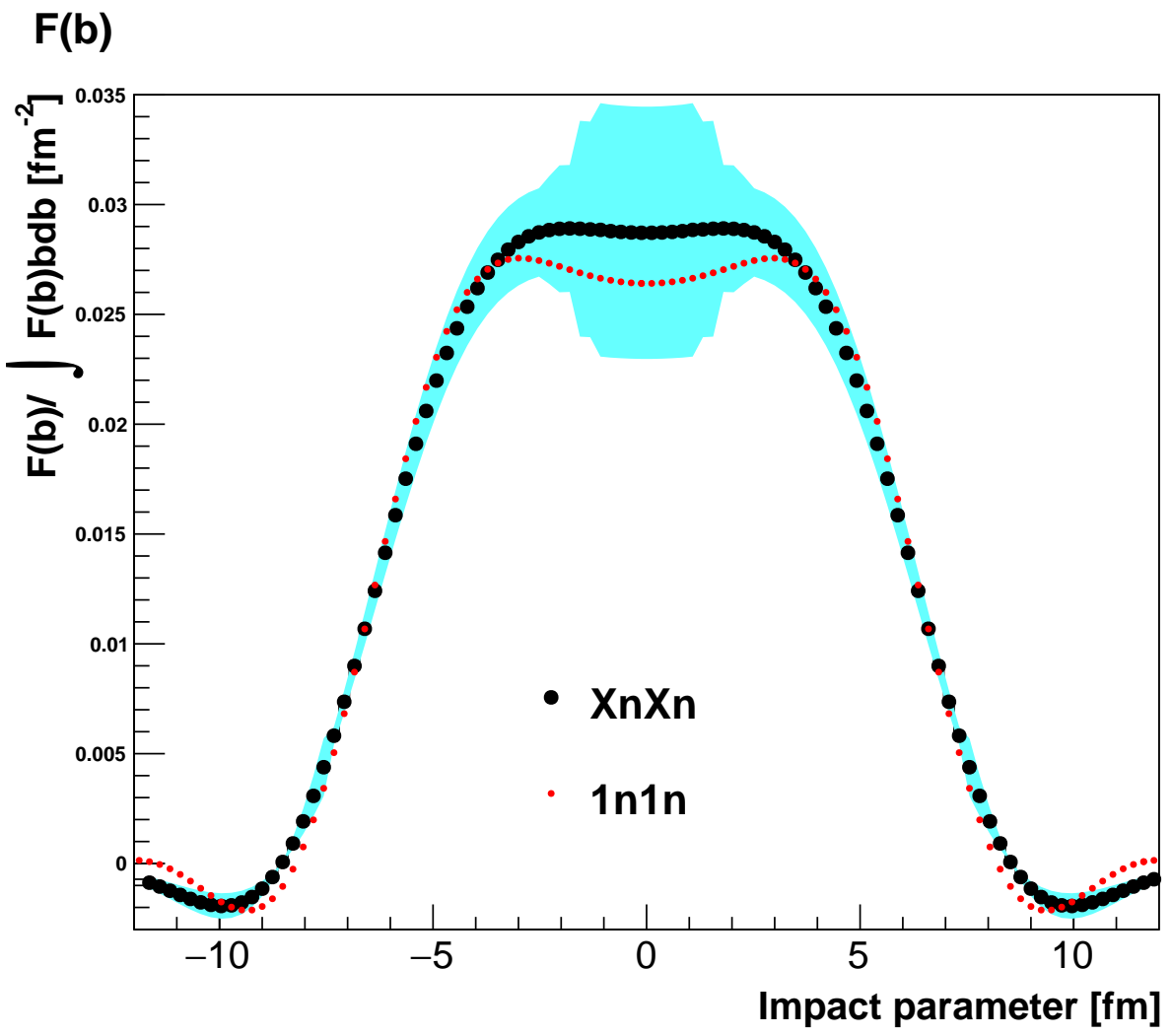


Figure 85: Fourier-Bessel transform of the diffraction pattern for coherent ρ^0 scattering of the Au target for both XnXn (black markers) and 1n1n events (small red markers). This is the final version of Figure 8 of the paper. .

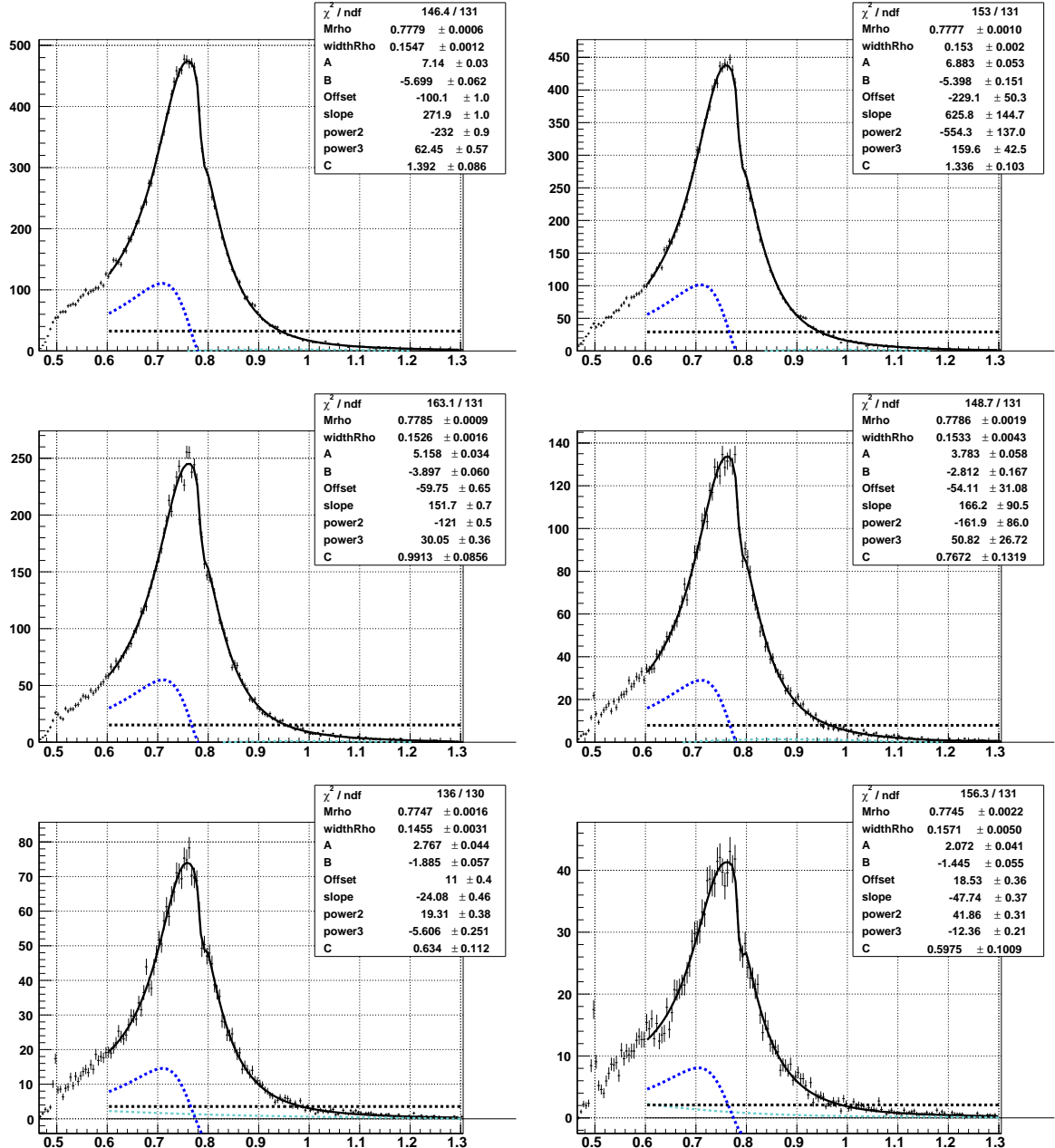


Figure 86: Fits to fully corrected invariant mass distributions in 6 bins in $-t$. The bins in t are $0.0015 \text{ GeV}/c^2$ wide.

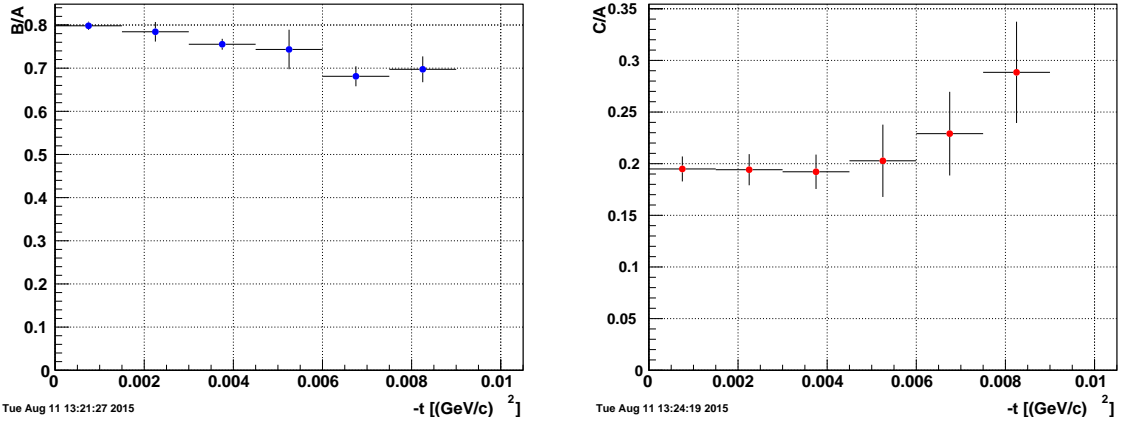


Figure 87: Left panel: The B/A ratio as function of the first 6 t bins. This ratio is a measure of the mixture between non-resonant and resonant pion pairs. Right panel: The C/A ratio as function of -t showing the fraction of ω mesons decaying into opposite charge pion pairs, compared to similar decays of the ρ^0 meson. The presence of backgrounds and the drop in statistics make the extraction of these ratios much harder at higher values of transverse momentum.

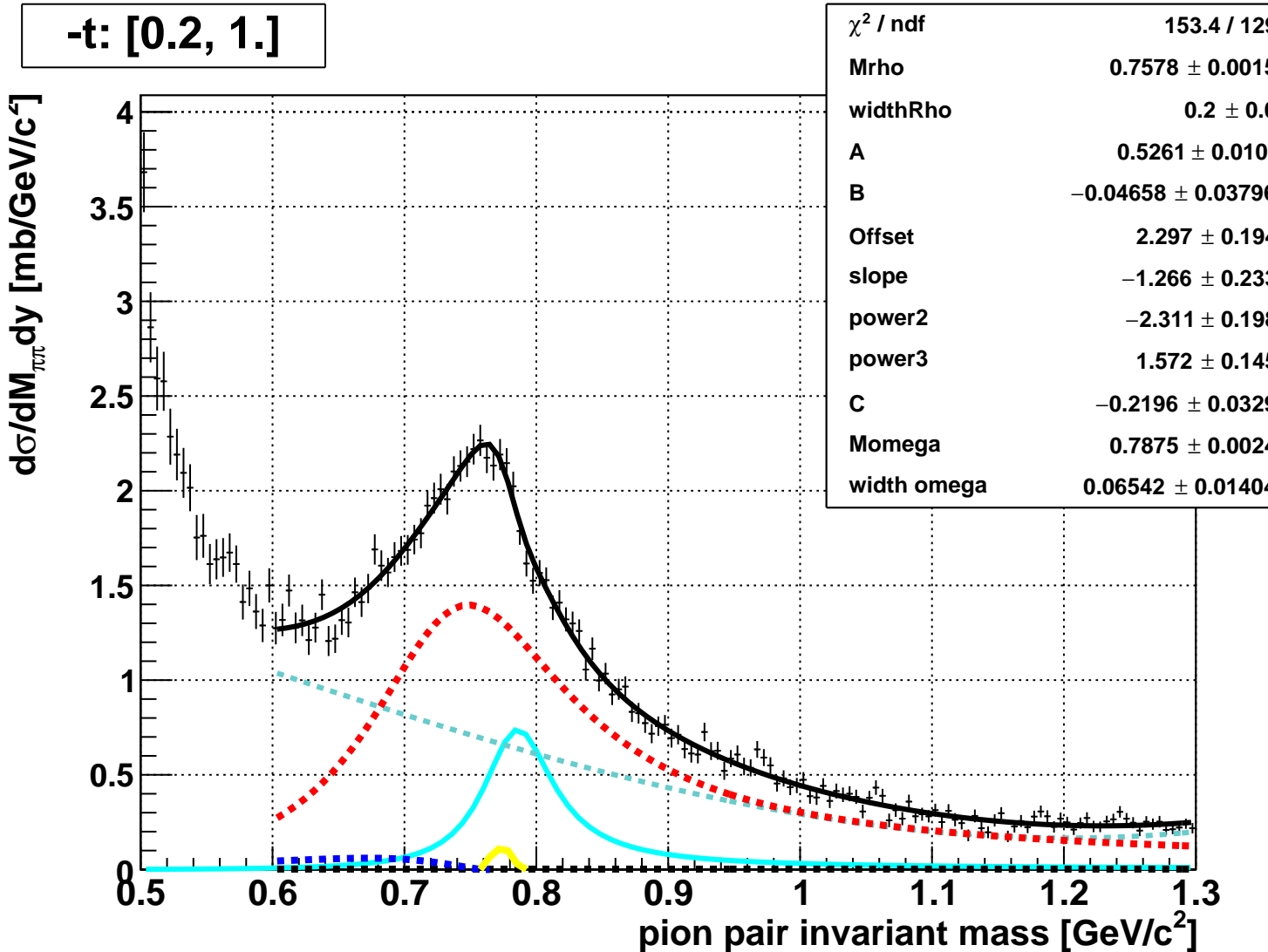


Figure 88: Fits to fully corrected invariant mass distributions for -t integrated from 0.2 to 1 $(\text{GeV}/c)^2$ with all parameters free.

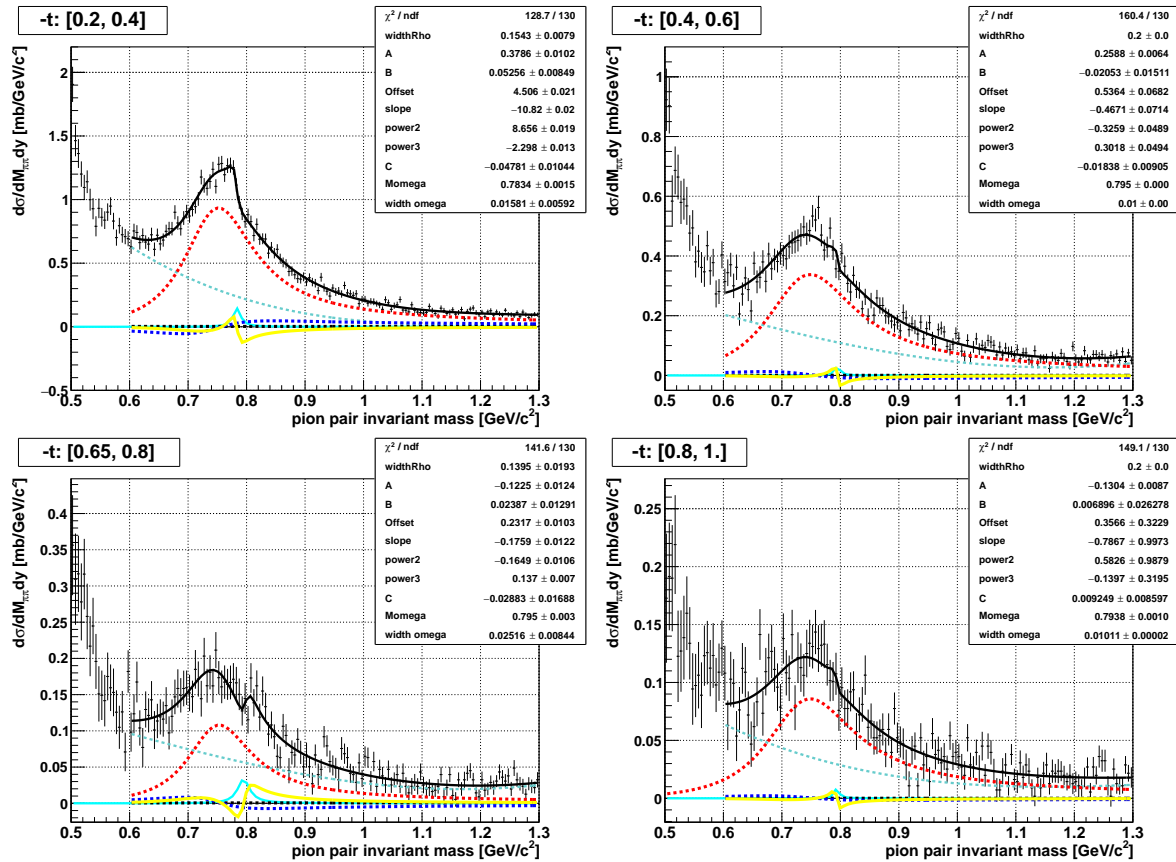


Figure 89: Fits to fully corrected invariant mass distributions in 4 t bins 0.2 GeV/c^2 wide.

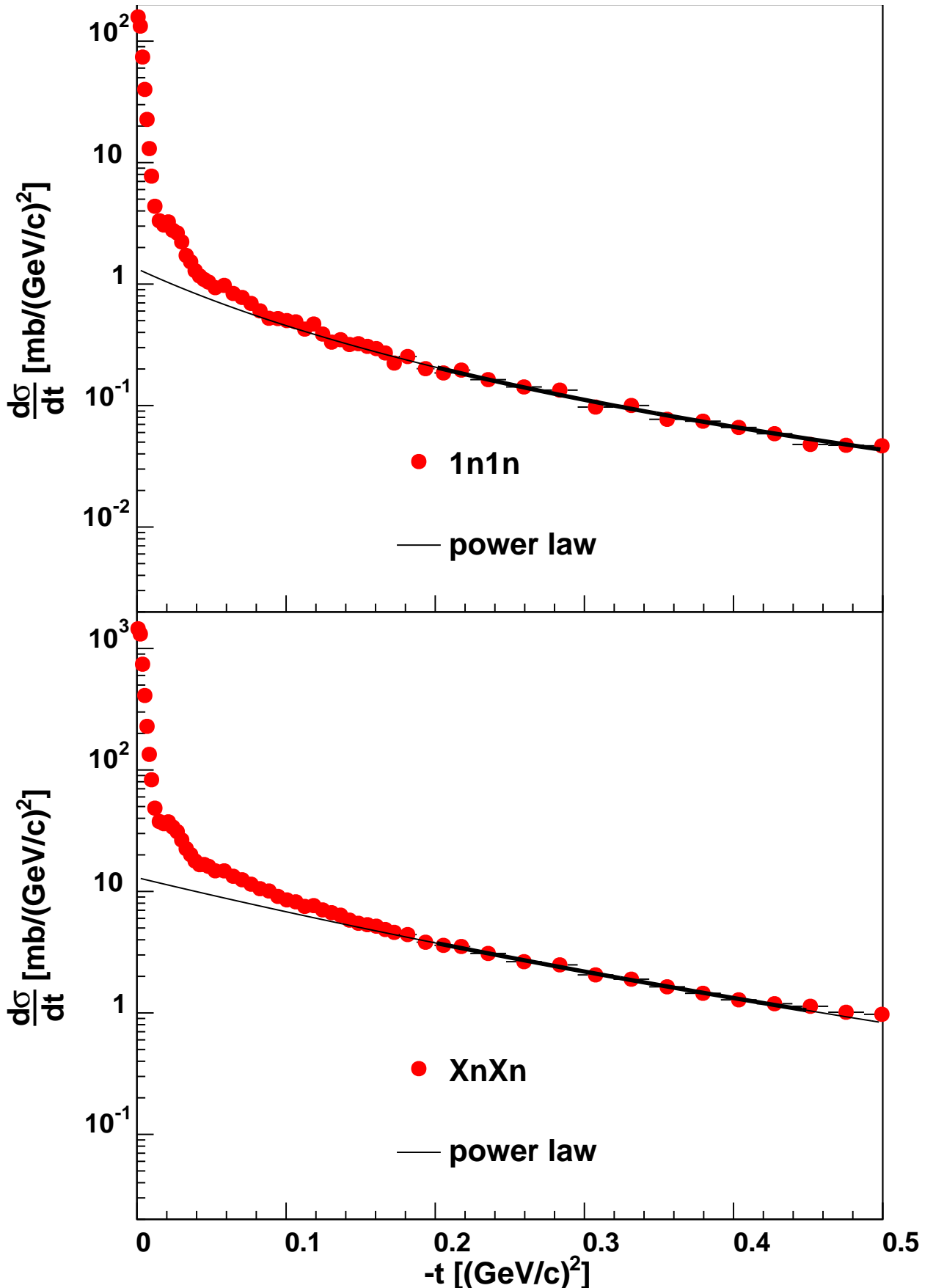


Figure 90: The fully normalized $-t$ distribution for exclusive ρ^0 mesons detected in events with mutual dissociation into a single neutron (1n1n) is shown in the top panel. The same distribution constructed from events with mutual dissociation into any number of neutrons (XnXn) is shown in the bottom panel. The high t part of those distributions, which is dominated by the contribution from incoherent interactions is fit to a power law shape described in detail in the text. The upper limit of the fit was selected to avoid contamination from hadronic interactions, which tends to be more pronounced in the XnXn events. The fitted function is shown with a full line for the fit range and with a dotted line below it.

10 Systematic Uncertainties discussion

10.1 Procedure

In most of the cases where a parameter is set, one can allocate an estimated uncertainty by changing that value and reanalyzing the data as well as regenerating the embedding full chain correction. The data is analyzed in /UPC/run10AuAu200/cleanProcessing/ with the macro processData.C which has the variables

```
//  
//  
int cutNumTrackVtx = 2; // exclusivity cut on vertex multiplicity -----  
//  
//  
//  
//  
int numSigmaPion = 3; // PID  
//  
//  
//  
//  
int numHitsTrack = 14; // track quality  
//  
//
```

which appear with their default values.

The fullChain correction is produced in /UPC/run10AuAu200/readPrivateEmbeddingMuDst/ with the macro processData.C where the same variables listed above can be set to the appropriate values. The output file name carries the values of the variables:

```
Char_t *name=Form("fullChain_processed_%d_PID%d_sigma_vertexNumTrk%d_hitsTrack%d_wideVertex103104.root",  
int(version), numSigmaPion, cutNumTrackVtx, numHitsTrack );
```

The output files are stored in:

```
/star/data01/pwg/ramdebbe/run10AuAu200tree/SystematicUncert/fullChainFiles/
```

10.2 Systematic uncertainties in invariant mass distributions

The results extracted from fitting the pion pair invariant mass distributions have uncertainties related to two factors. The lower limit of the fit is not well defined and can vary from 530 MeV, (just beyond the prominent peak at 495 MeV due to the K_s^0 decaying into two pions of opposite charge) and a higher value above 600 MeV where the fits are not affected by remnant backgrounds. Another source of uncertainty has been identified in the so called fullChain efficiency correction extracted from pion pairs embedded in actual data sets. Almost a million embedded events are used in this study but the statistical fluctuations are of a magnitude such that fits are performed to get smooth functions to be used to do the actual correction of the data without introducing such fluctuations.

An estimate of the magnitude of the systematic uncertainty related to the lower limit in the fits to mass distributions has been extracted by fitting the rapidity dependent distribution in five bins while changing the lower limit in mass in four values of M ; 530, 600, 650 MeV/c^2 . These fits are performed on fully corrected mass distributions which used the fullChain efficiency labelled “Rebin4Pol5” extracted from embedded mass distribution with bin size equal to 10 MeV fitted with a fifth order polynomial. Figures 111 to 115 show the four fits for each of the five rapidity bins.

Figure 116 shows the values of B/A and C/A ratios as function of rapidity for the four values of the lower limit in mass. The relative deviation from the average value is also listed in table 18

The fullChain efficiencies extracted from the embedding project are fitted to polynomial functions. The choice of that function introduces an uncertainty in the resulting fits. We estimate such uncertainty by changing the order of the polynomial function from three to five, while the fits continue to be close representation of the distributions extracted from embedding. Figures 118 and ?? show the fits where the fullChain efficiency is fitted with a fourth and fifth order polynomial respectively. The information for the case of a third order polynomial is obtained from the previous fits where the lower limit of the mass fits is set at 600 MeV.

Figure 99 summarizes the changes in the ratios B/A and C/A when the fullChain efficiency is fitted with polynomials of order ranging from three to five.

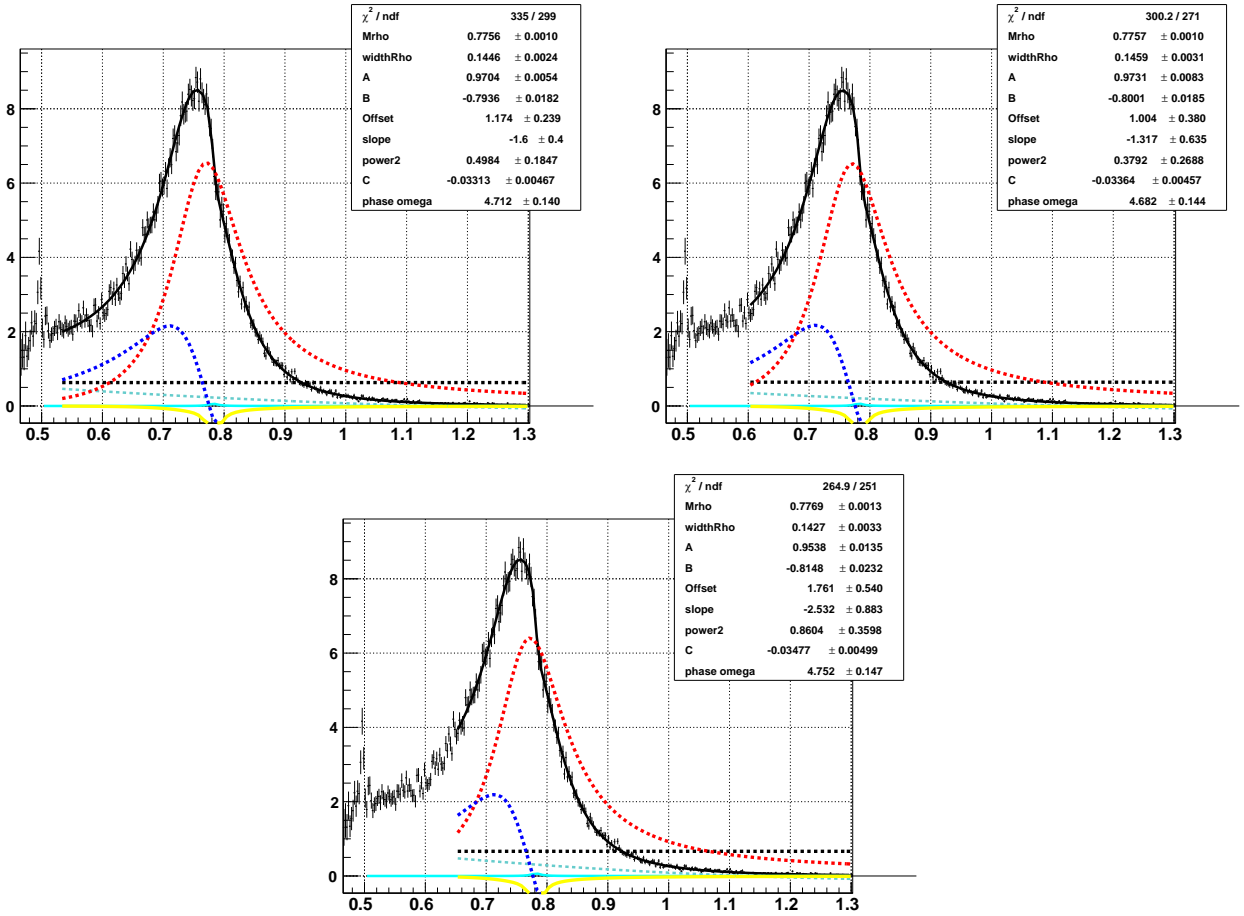


Figure 91: Fits to the fully corrected invariant mass of selected data pion pairs in the rapidity interval $y:[-1, -0.35]$. The lower limit in mass for these fits changes from 530 MeV on the top left panel and grows clock-wise to 600 and 650 MeV respectively. As is the case in all rapidity dependent fits in this work, the mass and widths of the ω meson have been fixed to the value obtained in the rapidity integrated fit.

rapidity	B/A Lower limit of fit	C/A Lower limit of fit	B/A fullChain fit	C/A fullChain fit
-1., -0.35	2.7 %	4.%	2.0%	7.4%
-0.35 -0.15	0.96%	1.1%	0.6%	5.1%
-0.15, 0.15	0.66%	1.0%	1.9 %	3.4%
0.15, 0.35	1.66%	1.1%	1.9%	1.4%
0.35, 1.	0.97%	1.3%	2.3%	3.7%

Table 14: Systematic uncertainties allocated to the B/A and C/A ratios. The fits to the pion pairs invariant mass are normally done from 600 MeV up to 1.3 GeV. Changing the lower limit does produce different values of the B/A, such changes ranged from 500, 550, 600 and 650 MeV. The mass fullChain corrections are used as smooth functions obtained from fits to embedding data. The choice of functions sets another systematic uncertainty and polynomials of third, fourth and fifth order were used to extract a systematic error.

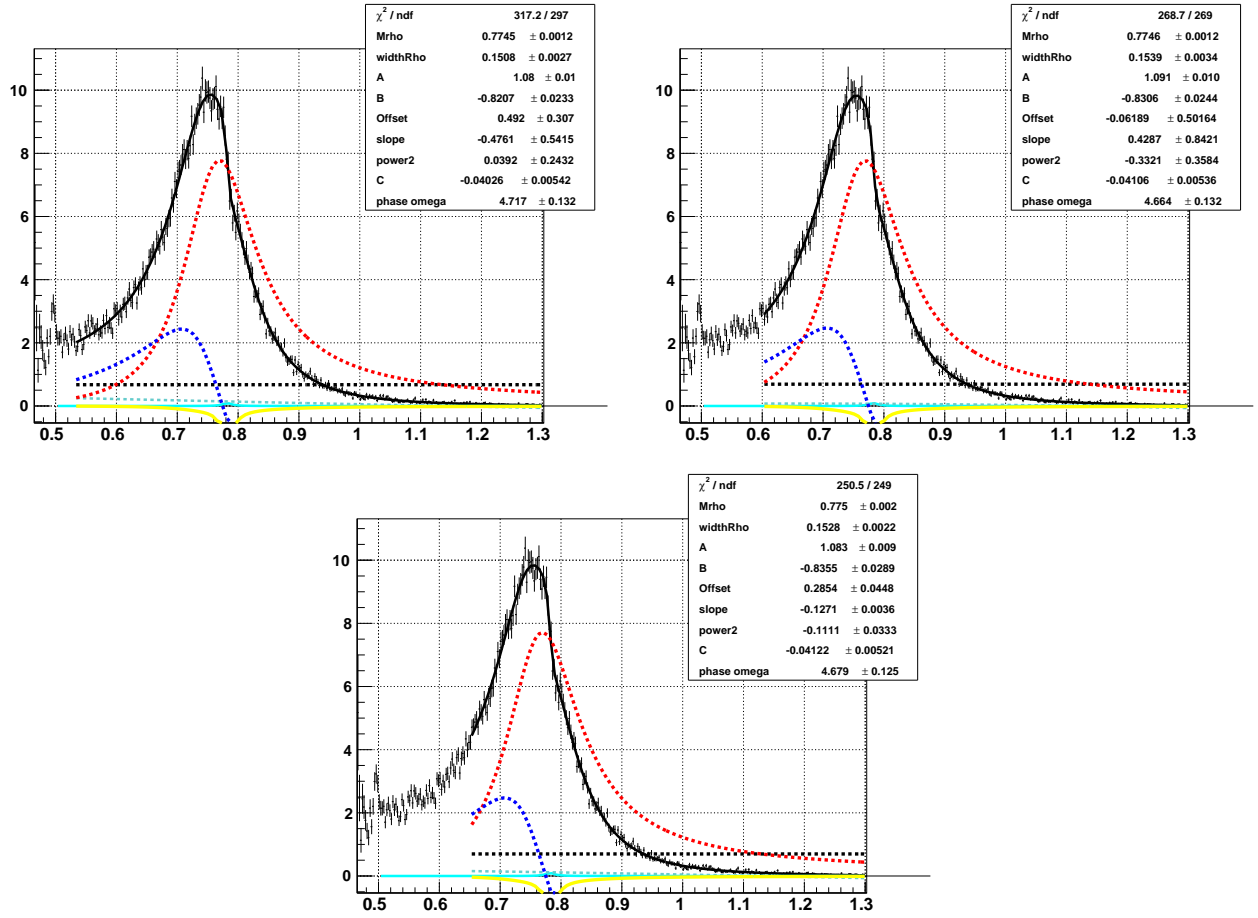


Figure 92: Fits to the fully corrected invariant mass of selected data pion pairs in the rapidity interval $y: [-0.35, -0.15]$. The lower limit in mass for these fits changes from 530 MeV on the top left panel and grows clock-wise to 600 and 650 MeV respectively. As is the case in all rapidity dependent fits in this work, the mass and widths of the ω meson have been fixed to the value obtained in the rapidity integrated fit.

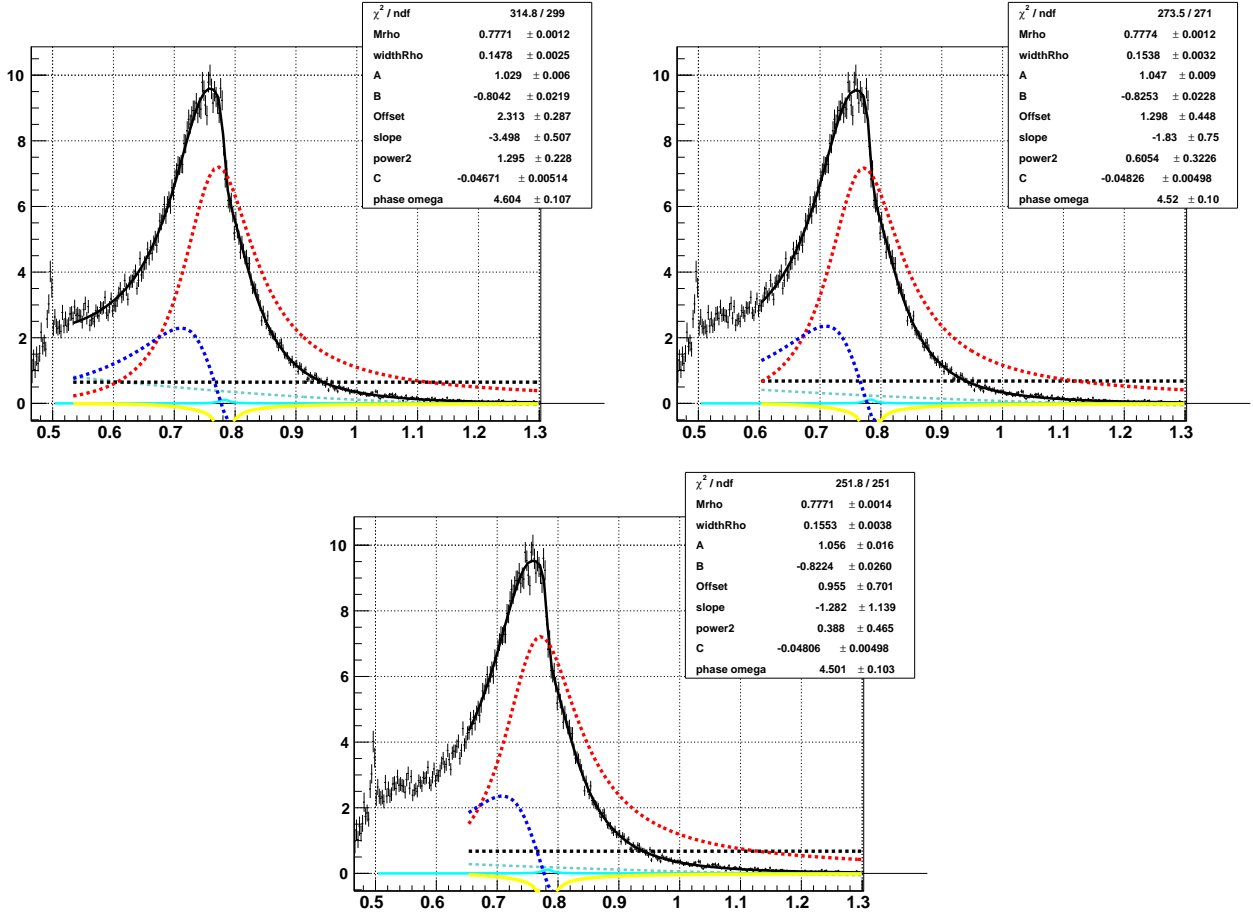


Figure 93: Fits to the fully corrected invariant mass of selected data pion pairs in the rapidity interval $y:[-0.15, 0.15]$. The lower limit in mass for these fits changes from 530 MeV on the top left panel and grows clock-wise to 600 and 650 MeV respectively. As is the case in all rapidity dependent fits in this work, the mass and widths of the ω meson have been fixed to the value obtained in the rapidity integrated fit.

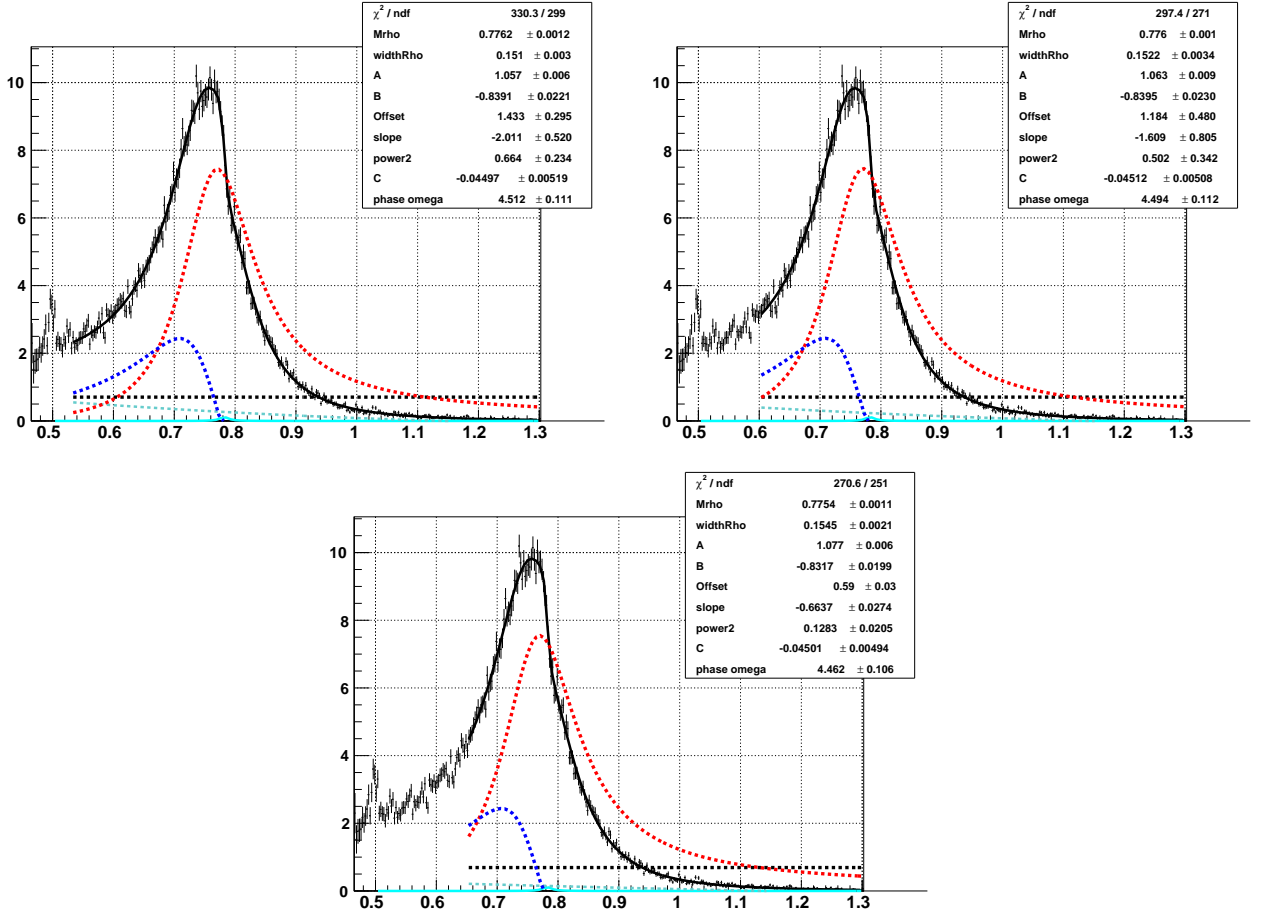


Figure 94: Fits to the fully corrected invariant mass of selected data pion pairs in the rapidity interval $y:[0.15, 0.35]$. The lower limit in mass for these fits changes from 530 MeV on the top left panel and grows clock-wise to 600 and 650 MeV respectively. As is the case in all rapidity dependent fits in this work, the mass and widths of the ω meson have been fixed to the value obtained in the rapidity integrated fit.

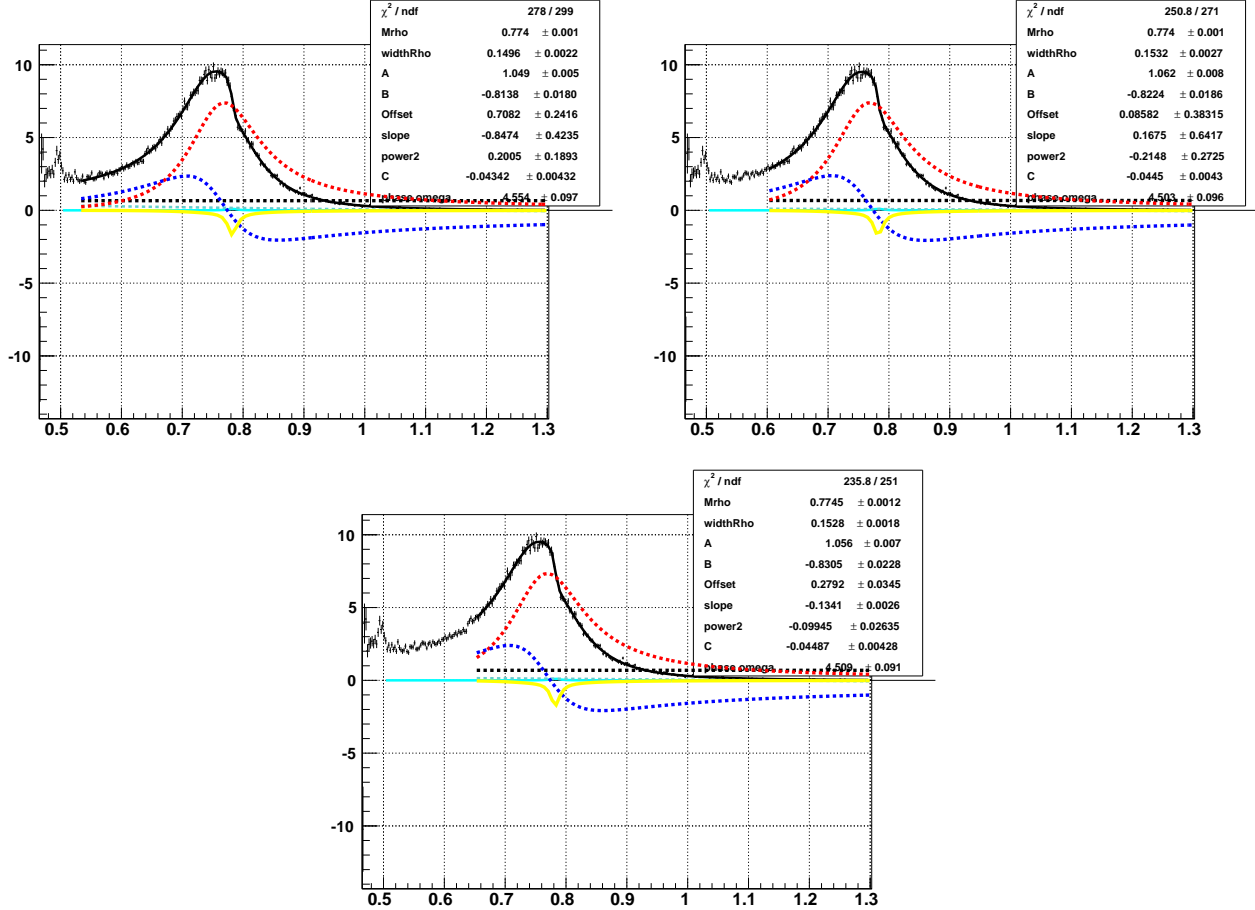


Figure 95: Fits to the fully corrected invariant mass of selected data pion pairs in the rapidity interval $y:[0.35, 1.]$. The lower limit in mass for these fits changes from 530 MeV on the top left panel and grows clock-wise to 600 and 650 MeV respectively. As is the case in all rapidity dependent fits in this work, the mass and widths of the ω meson have been fixed to the value obtained in the rapidity integrated fit.

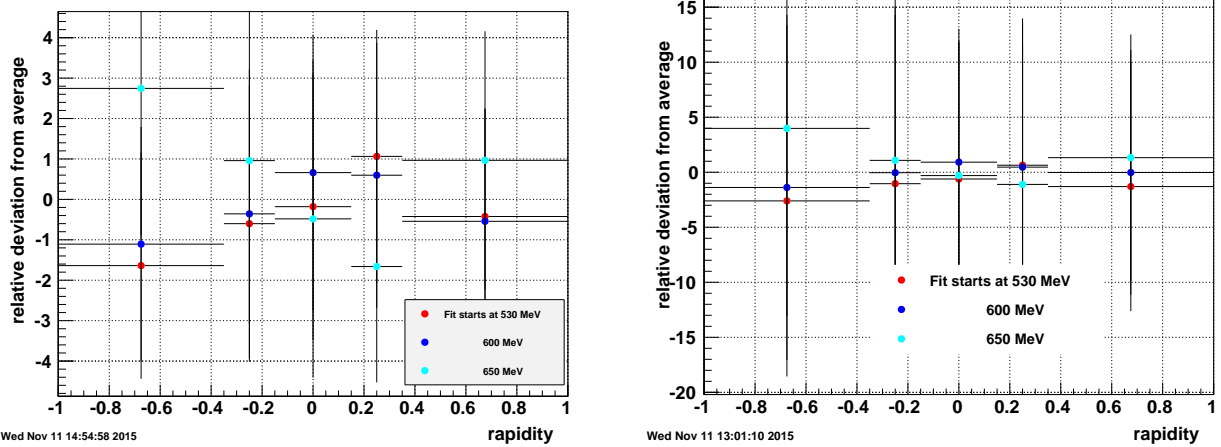


Figure 96: The left panel shows the relative deviations of B/A values extracted for fits that have three lower limits 530, 600 and 650 MeV/c^2 . The deviations are calculated with respect to the average value for the three measurements. the systematic error assigned to the selection of this fit boundary is assigned as being the maximum relative deviation for each rapidity bin. Similar information is shown in the right panel but this time for the C/A ratio.

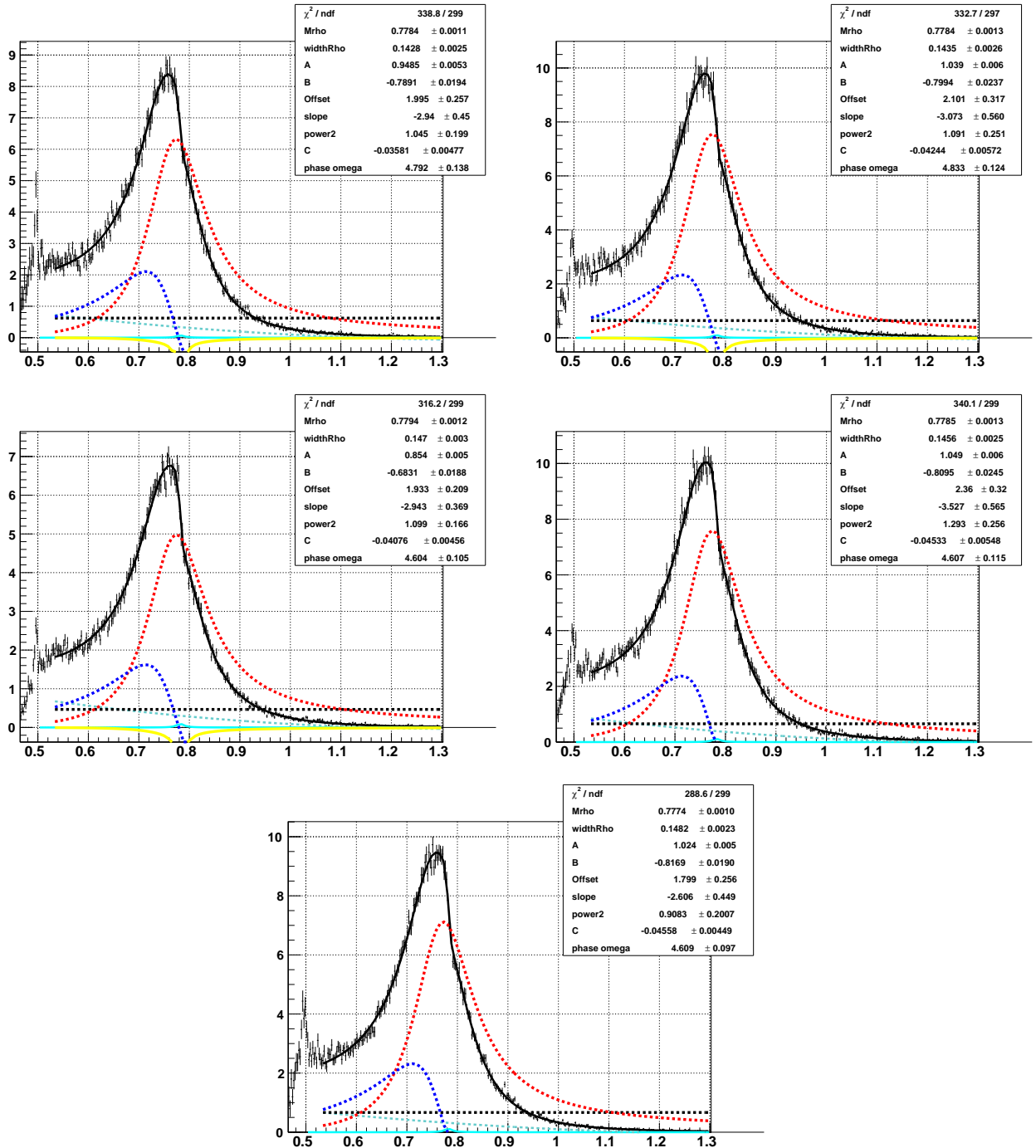


Figure 97: Fits to the fully corrected invariant mass of selected data pion pairs in each rapidity interval. The shape of the mass correction extracted from embedding is fitted with a third order polynomial. As is the case in all rapidity dependent fits in this work, the mass and widths of the ω meson have been fixed to the value obtained in the rapidity integrated fit.

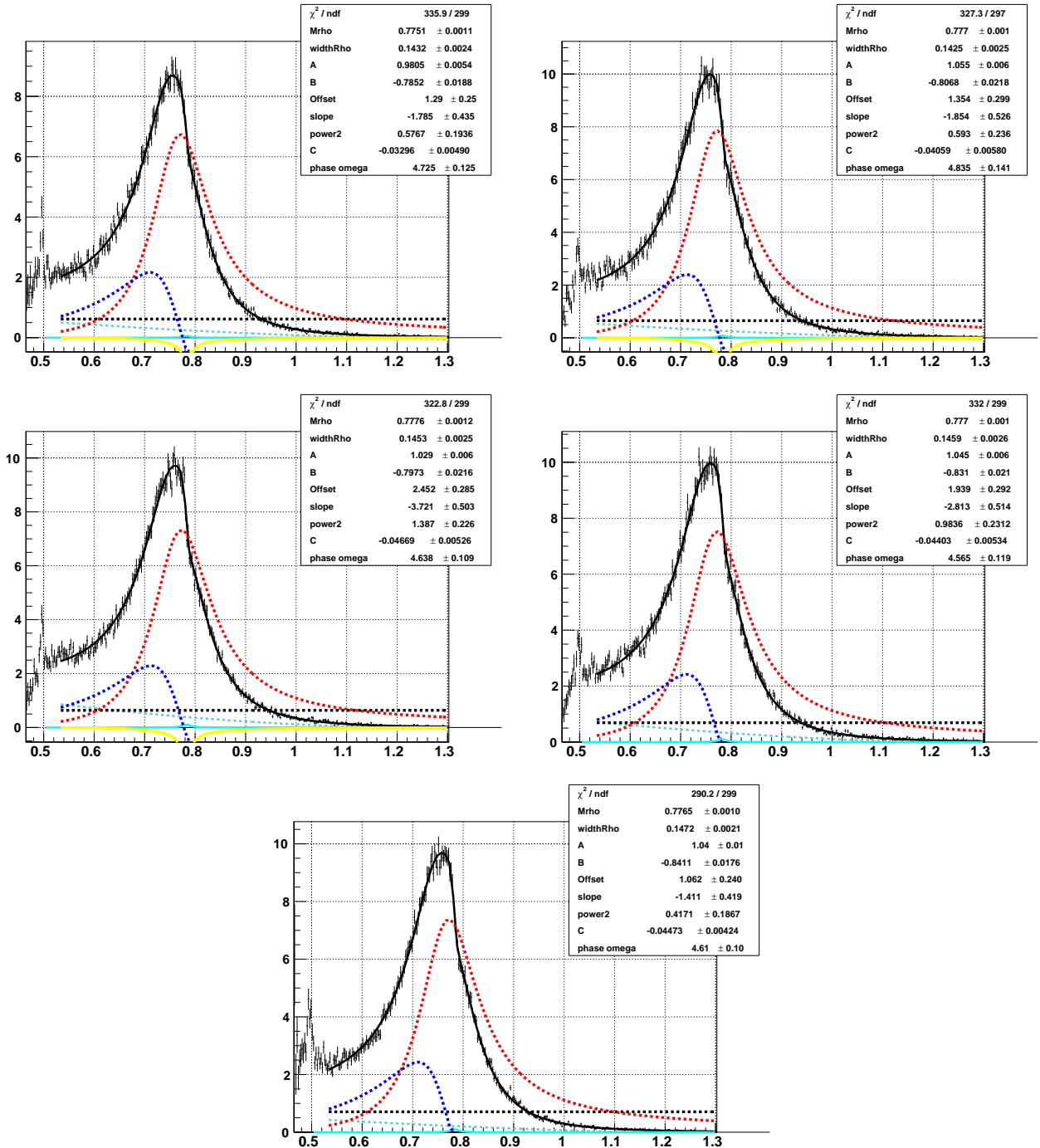


Figure 98: Fits to the fully corrected invariant mass of selected data pion pairs in each rapidity interval. The shape of the mass correction extracted from the embedding project is fitted with a fourth order polynomial. As is the case in all rapidity dependent fits in this work, the mass and widths of the ω meson have been fixed to the value obtained in the rapidity integrated fit.

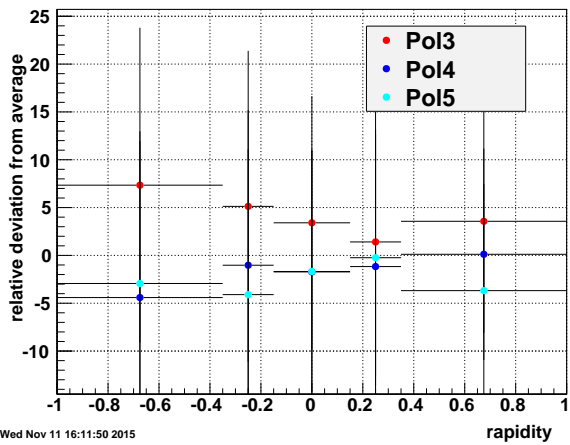
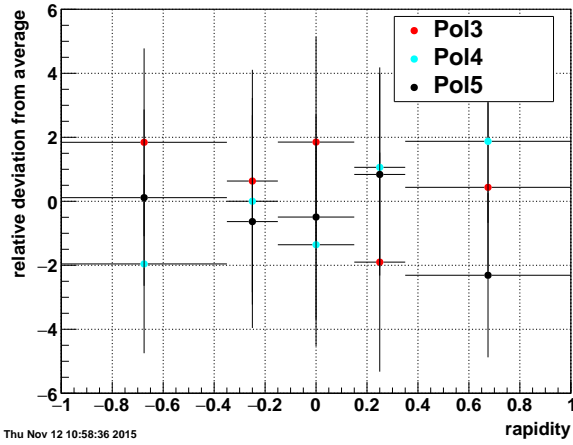


Figure 99: Left panel shows the B/A ratio (non-resonant pion pair to ρ^0) for three fits to the fullChain efficiency as function of pion pair mass. The right panel shows the C/A ratio (ω to ρ^0) for the same three fits to the mass efficiency.

10.3 Systematic uncertainties in the ω meson phase

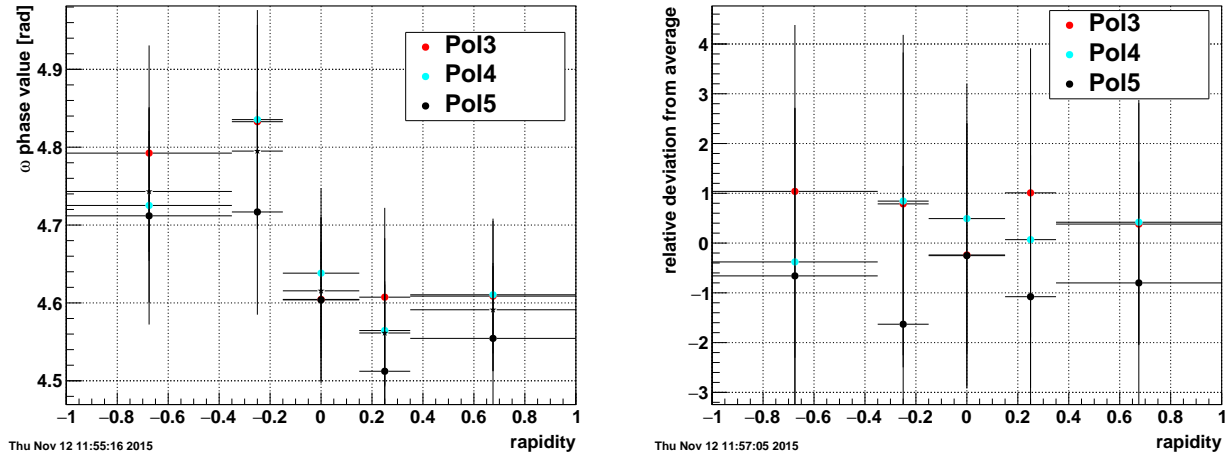


Figure 100: Left panel shows the phase of the ω mesons as extracted from mass fits in five rapidity bins. The black star markers correspond to the average in each bin. The other markers show the result of the fits for three descriptions of the fullChain correction as function of pion pair mass. The right panel shows the relative deviation from the average value in each rapidity bin. The biggest deviation is then considered as the systematic uncertainty for the ω phase related to the description of the mass corrections with polynomials.

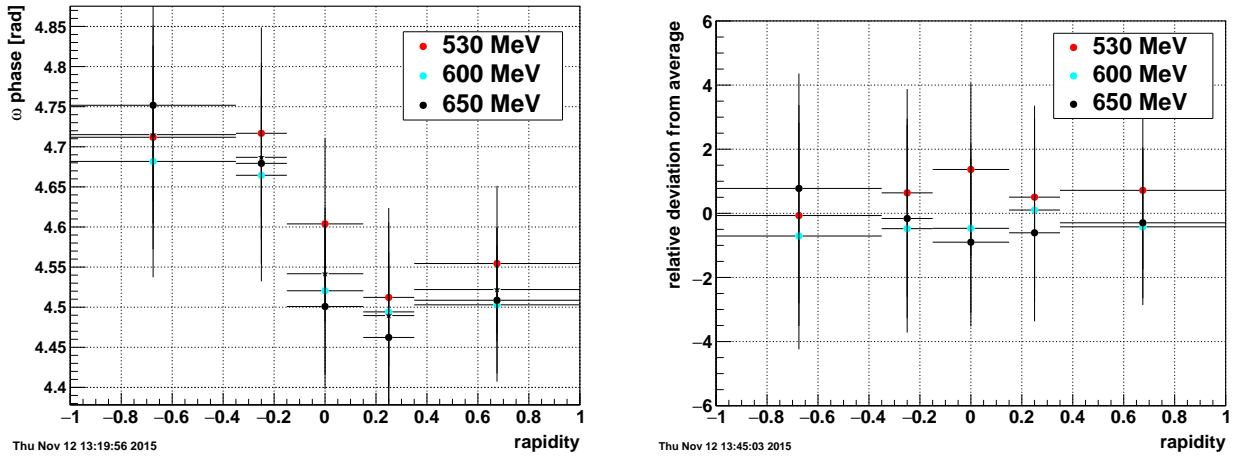


Figure 101: The left panel shows the phase of the ω mesons as extracted from mass fits in five rapidity bins. The black star markers correspond to the average in each bin. The other markers show the result of the fits for three values of the lower bound in the fits to the pion pair mass distribution. The right panel shows the relative deviation from the average value in each rapidity bin. The biggest deviation is then considered as the systematic uncertainty for the ω phase related to the setting of lower bound in the fits.

<i>rapidity</i>	ω phase Lower limit of fit	ω phase fullChain fit
-1., -0.35	0.75 %	1.0%
-0.35 -0.15	0.64%	1.6%
-0.15, 0.15	1.37%	0.5 %
0.15, 0.35	0.61%	1.1%
0.35, 1.	0.72%	0.8%

Table 15: Systematic uncertainties allocated to the B/A and C/A ratios. The fits to the pion pairs invariant mass are normally done from 600 MeV up to 1.3 GeV. Changing the lower limit does produce different values of the B/A, such changes ranged from 500, 550, 600 and 650 MeV. The mass fullChain corrections are used as smooth functions obtained from fits to embedding data. The choice of functions sets another systematic uncertainty and polynomials of third, fourth and fifth order were used to extract a systematic error.

10.4 Systematic uncertainties in rapidity distributions

The macro makeFullChainCorr_rapidity.C will generate the fullChain correction as function of rapidity by comparing the distribution of ρ^0 candidates found in the embedding (properly normalized with 40.7 mb cross section and the number of events found after all embedding steps) and the original cross-section produced by starlight XnXn. The resolution distribution is also stored in the above directory of data01 with names:

fullChainCorrec_withPol6Fit_PID3_Hits14_vertex2.root

fullChainCorrec_withPol6Fit_PID2_Hits14_vertex2.root

The fits to those corrections to 6 order polynomials are shown in Fig. 102:

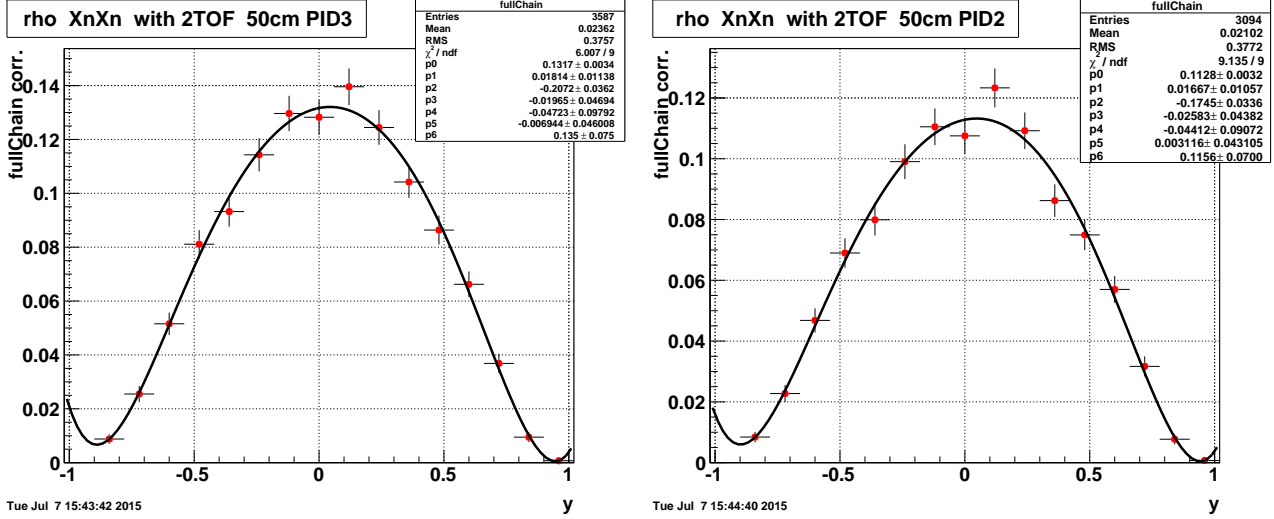


Figure 102: Systematic uncertainty due to PID of pions by changing from 3 to 2 sigmas expressed as function of rapidity.

And the systematic uncertainty of the number of sigma cuts used to identify pions is shown in Fig. 103.

We have also investigated the uncertainty introduced at the time of the fitting of the fullChain correction obtained from the embedding exercise. We have produced three version of the fullChain correction in rapidity by fitting the same histogram comparing cross-sections calculated from reconstructed ρ^0 mesons in the embedded data set and a XnXn rapidity cross-section produced by starlight. The three fits are shown in Fig. 104.

We also investigated the uncertainty connected to our cut on the number of hits used to define a track. The minimum number of hits is set at 14 mainly to reject tracks produced by low momentum particles that spiral in the drift volume. The systematic uncertainty is extracted by comparing rapidity distributions produced with the same selection in the minimum number of track hits both in the data processing and in the extraction of the fullChain efficiency from the embedded samples. Such comparison is shown in Fig. 106 and it appears small.

A more drastic change in the minimum number of hits required to build a track can be made by requiring a minimum of 25 hits. Such tracks have a much higher quality but such condition is not normally used. We produce an estimate of the systematic uncertainty by changing the NHit minimum from 14 to 25 in Fig. 107 mainly to get a feeling of how fast such uncertainty grows by changing the quality of the tracks drastically. This supposedly high change produced an uncertainty that barely reaches 3%.

rapidity	PID cut	Fit to efficiency	number of track hits	normalization	RELDIS (XnXn only)
-1., -0.5	8.%	0.25%	0.2%	10%	15%
-0.5 0.	5.%	0.25%	0.05%	10%	15%
0., 0.5	5.%	0.25%	0.05%	10%	15%
0.5, 1.	8.%	0.25%	0.2%	10%	15%

Table 16: Systematic uncertainties allocated to the pion particle identification with DE/dx in the TPC, the extraction of the fullChain efficiency in the embedding project, the selection of good quality tracks and the normalization of all extracted distributions. The different values of the uncertainties are listed in four wide rapidity bins.

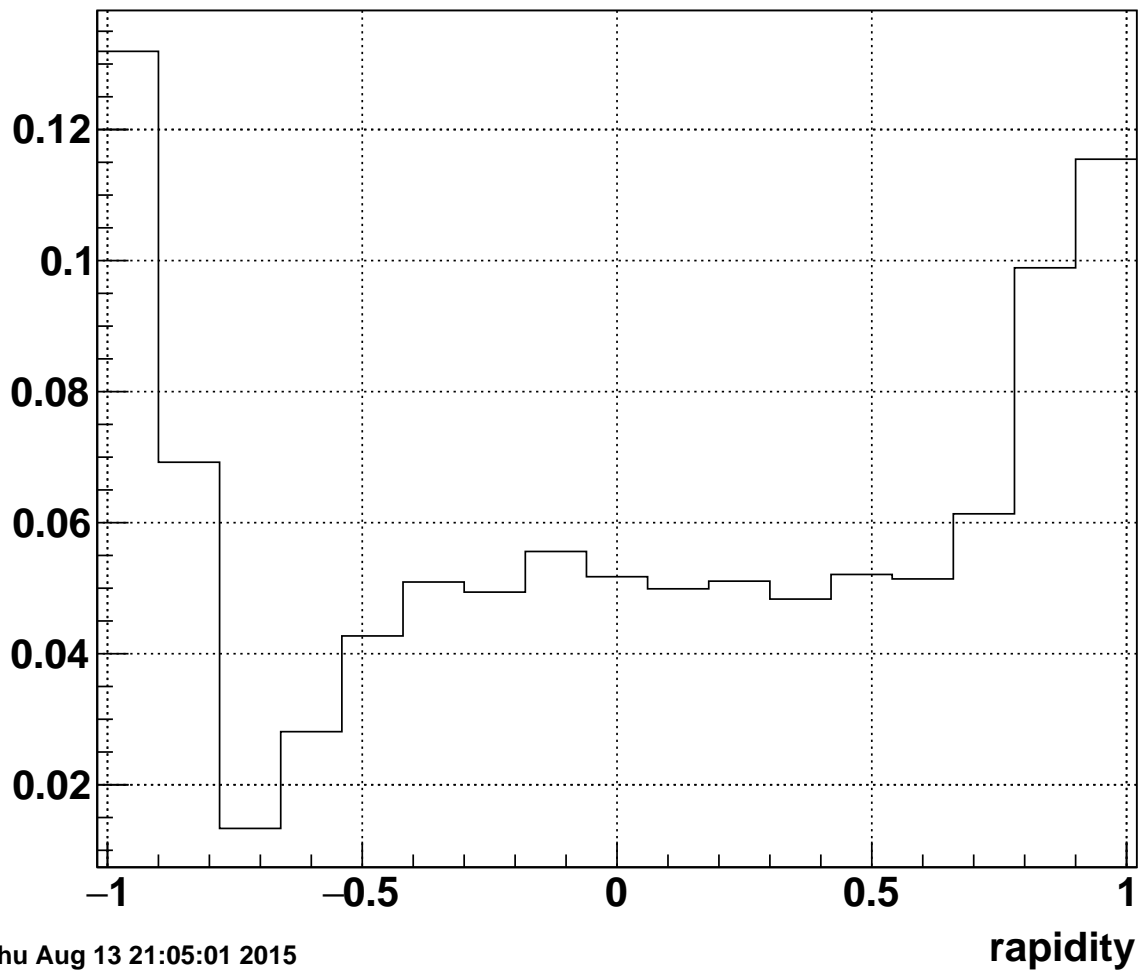


Figure 103: Systematic uncertainty allocated to the particle identification using dE/dx in the TPC.

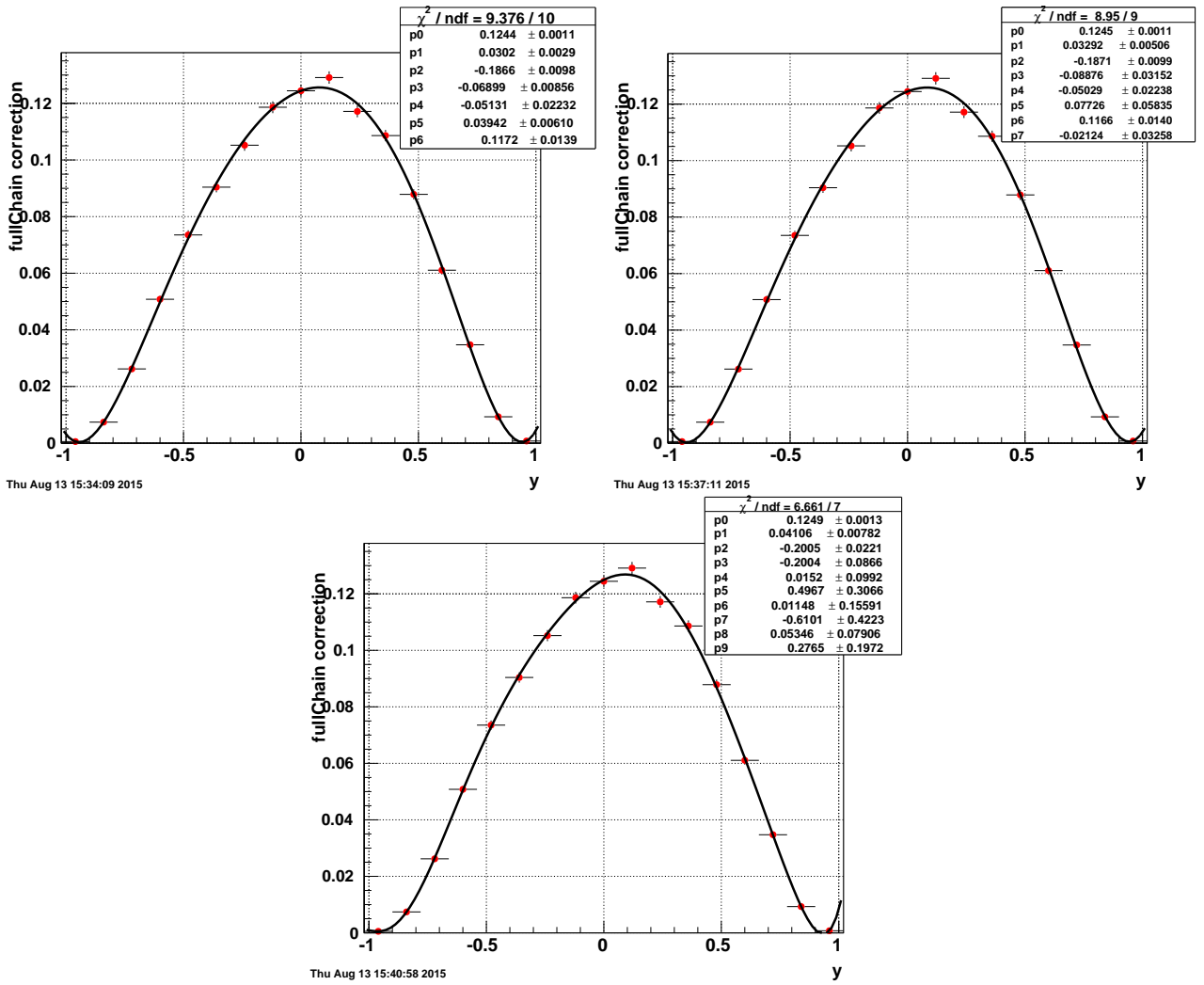
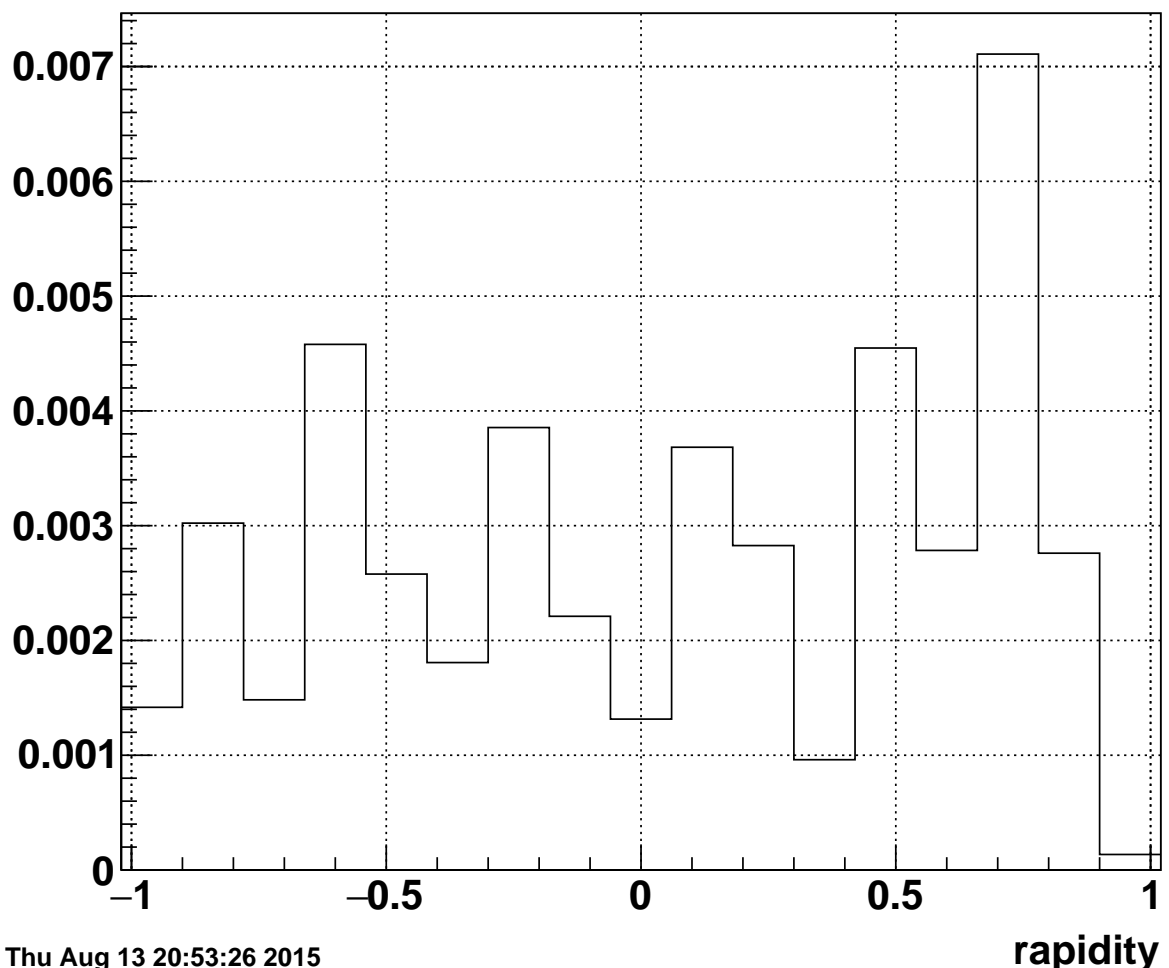


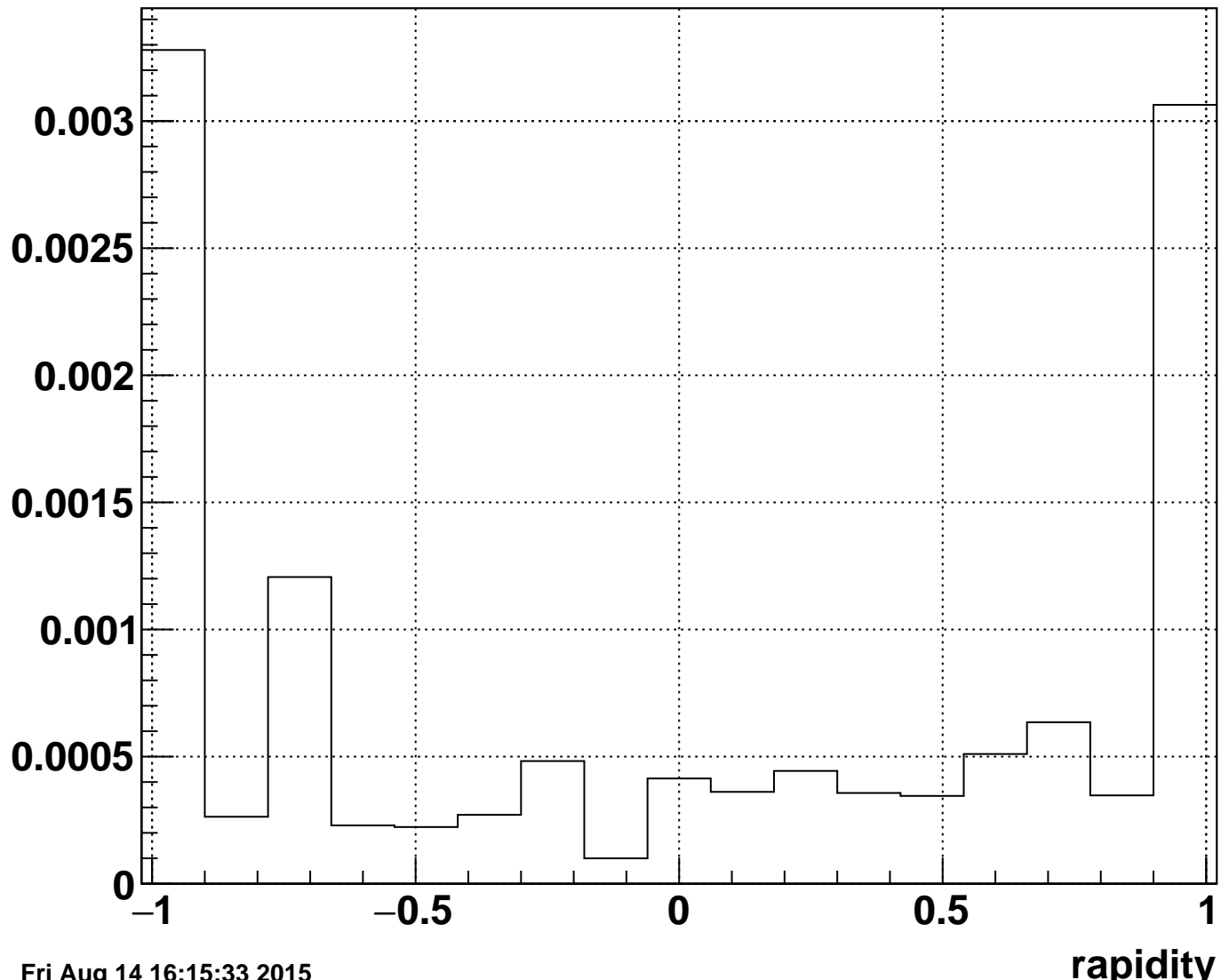
Figure 104: Fits to the fullChain correction extracted from the embedded data set. The ρ^0 mesons selected have been exclusively produced, the pions are identified with 3 sigma cuts in DeDx, both tracks have at least 14 hits and the vertices have the cut $|V_z| < 50$ cm. The top left panel shows the histogram fitted with a sixth order polynomial, the left panel shows similar fit to a seventh order polynomial, and finally, the bottom panel shows the fit to a ninth order polynomial.



Thu Aug 13 20:53:26 2015

rapidity

Figure 105: Systematic uncertainty allocated to the fits performed to the fullChain efficiency correction.



Fri Aug 14 16:15:33 2015

Figure 106: Systematic uncertainty associated with a change of the minimum number of hits required in the selected tracks from 14 to 15.

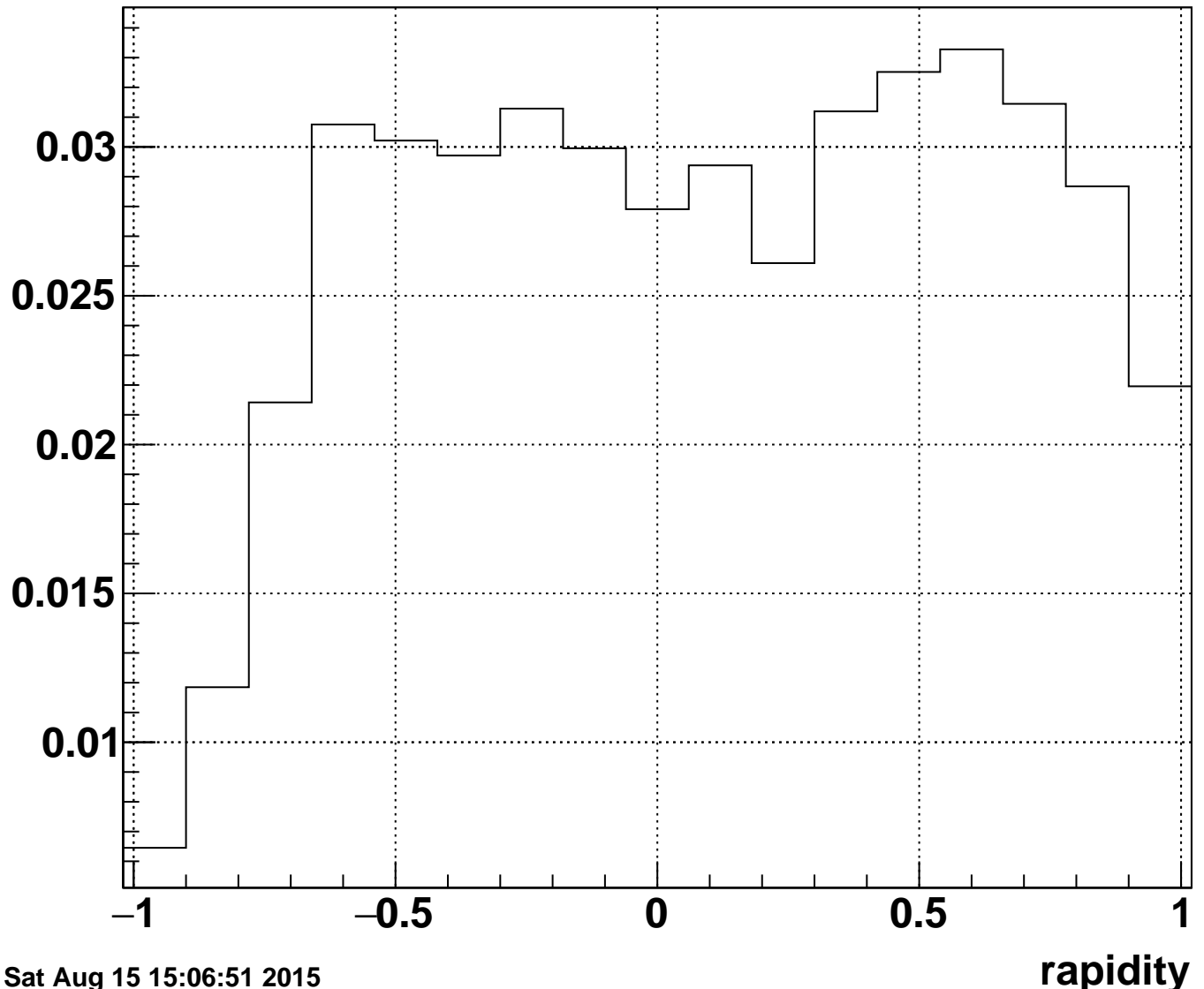


Figure 107: Systematic uncertainty associated with a drastic change of the minimum number of hits required in the selected tracks from 14 to 25. This estimate of the related uncertainty is not included in the final value, it is presented here as an upper limit because requiring 25 hits in a track is a restrictive condition.

$-trange[(GeV/c)^2]$	track sel.	pion PID	Bkg sub.	Incoherent comp. sub.	Integrated luminosity	RELDIS
0 - 0.02	0.2%	8%	1.5	0.5%	10%	15%
0.02 - 0.04	0.2%	8%	1.5	3.0%	10%	15%
0.04 - 0.1	0.2%	8%	1.5	8.5%	10%	15%

10.5 Systematic uncertainties in $-t$ distribution

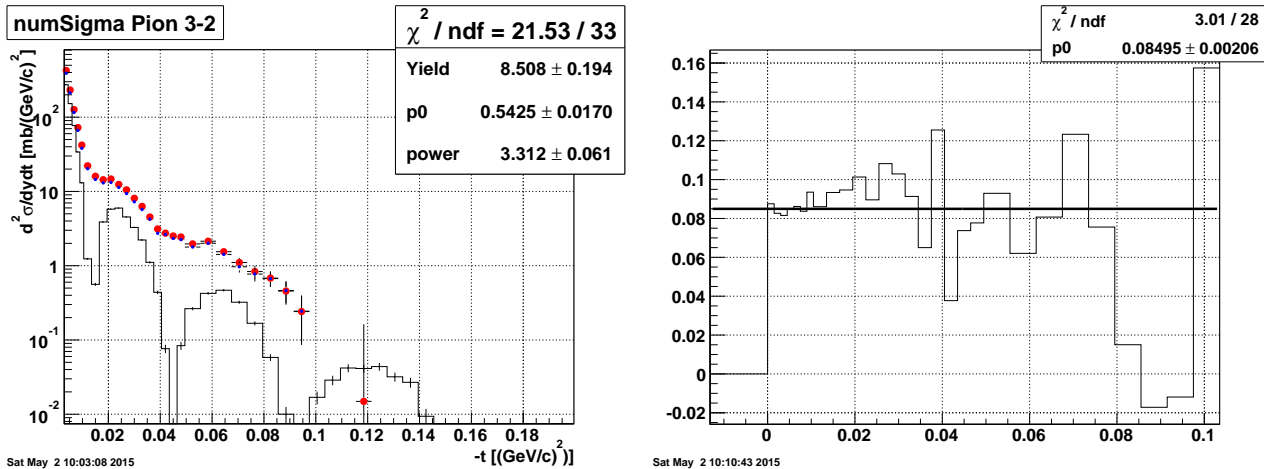
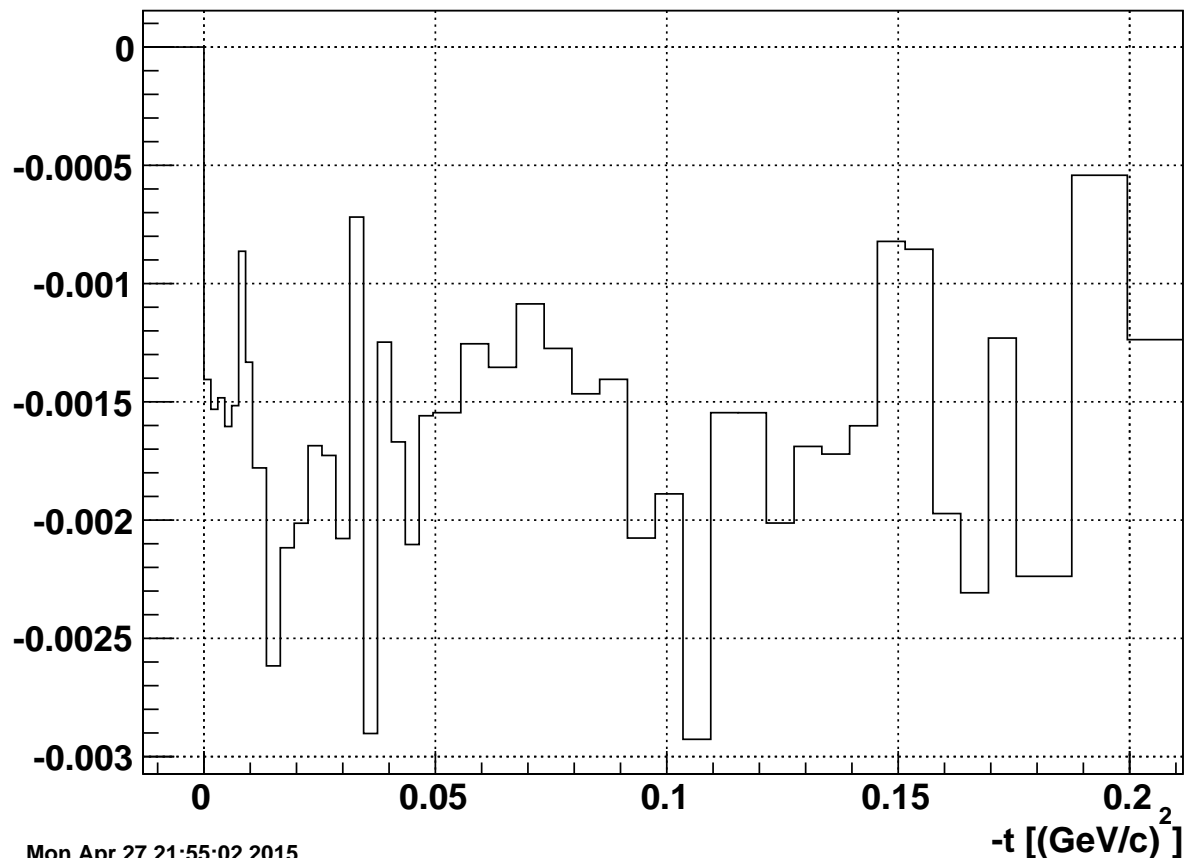


Figure 108: Systematic uncertainty due to PID of pions by changing from 3 to 2 sigmas.

systematic uncert num Hits in tracks 15-12



Mon Apr 27 21:55:02 2015

Figure 109: Systematic uncertainty due track quality selection based on the minimum number of hits included in the construction of a track. The uncertainty is constructed from the spectra built with tracks having at least 15 hits and the one obtained with a minimum of 12 hits.

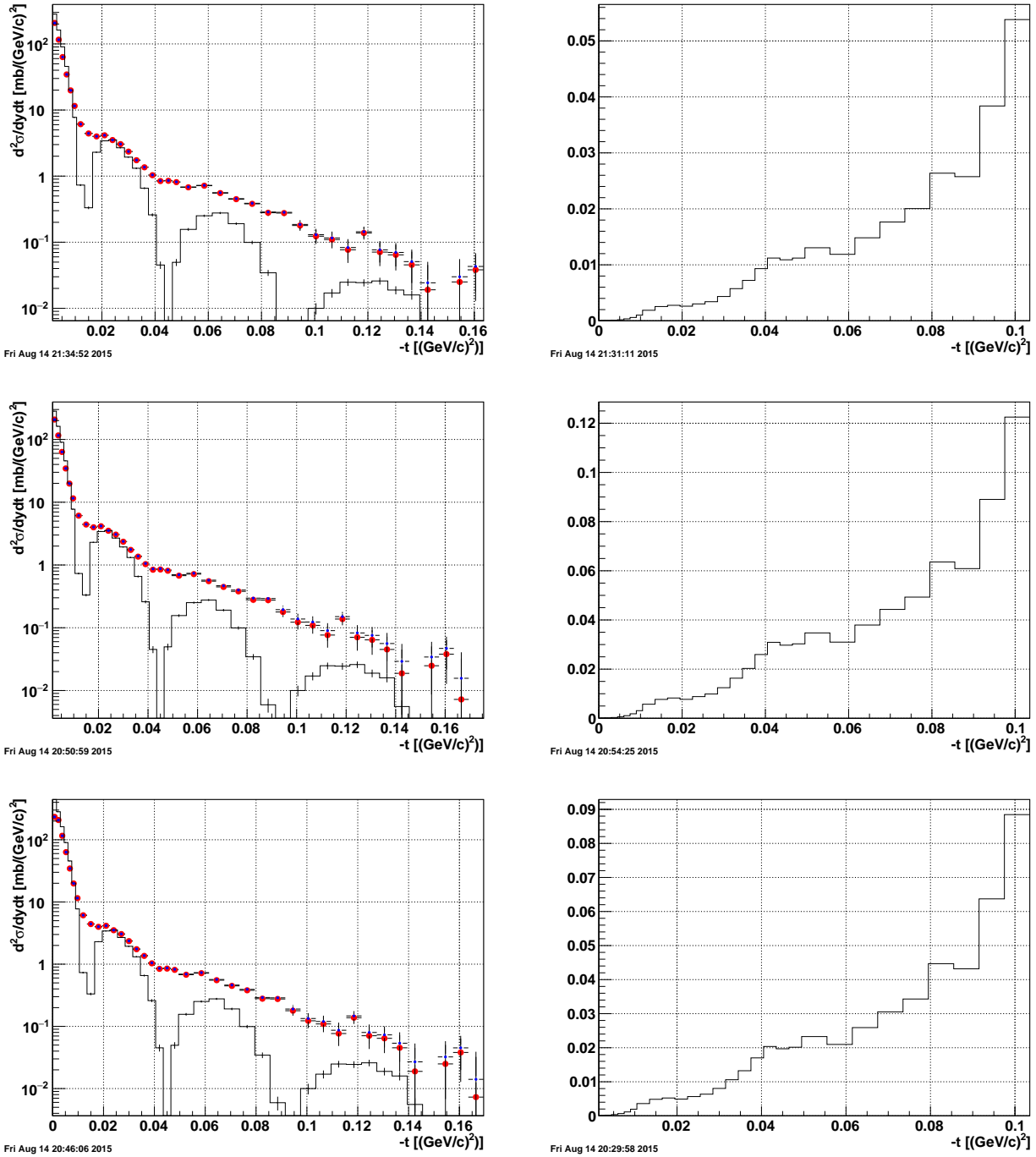


Figure 110: Systematic uncertainty to be allocated to the incoherent component subtraction. These uncertainties are extracted by changing each one of the fit parameters by one sigma value.

10.6 Summary of all systematic uncertainties identified for the ρ^0 diffraction paper

This section summarizes all systematic uncertainties identified for the different measurements presented in the ρ^0 diffraction paper. All uncertainties described here are presented as relative to the value of the measurement. They are always present as “per-cent” of the data points. We have separated the uncertainties into two categories: common errors which are listed as a single number affecting all data points as an overall factor. Other systematic uncertainties have a clear dependence on variables like rapidity or transverse momentum. These so called “point-to-point” systematic uncertainties, are presented in separate tables relevant to each one of the figure where these uncertainties are displayed. For simplicity, the dependence on each relevant variable is given in a coarse binning.

Besides the listing of Common and Point-to-point uncertainties we also display tables in a format close to the one used in the Durhma archives where one can read all the details presented in a figure.

The common uncertainties apply to figures 4 and 6. Figure 3 is a ratio of quantities extracted from fit to invariant mass distributions and most of these common uncertainties are expected to cancel out. For that particular figure we only include the common uncertainty associated to the TOF geometry modeling.

10.6.1 Common uncertainties

Uncertainty on:	Estimated value (%)	Description or comments
Luminosity	10.%	
ZDC response	5.%	Actual locat. loose shower. ADC to neutron number
TOF	7.%	Modeling of the TOF detector
Vertex	5.%	Only one sample of Bkg
BBC veto	2.%	Bkg related. Driven by our knowledge of Bkg
Cross-section Luminosity	10.%	Standard within STAR
STARlight	6.%	Applies to XnXn results only%
TPC tracking efficiency	6.%	STAR standard (NIMA 499 (2003) 659-678)
fullChain efficiency	7.%	fullChain Ev. gen. Material budget
Background subtraction	1.5%	
Sum in quadrature	18.1%	Only common uncertainties were added

Table 17: An estimate for the common systematic uncertainties identified in the generation of the rapidity and $-t$ distributions shown in Figures 4 and 6 expressed as a per-cent of the measured cross-section.

The “ZDC response” systematic uncertainty is related to our incomplete knowledge of the detector response and its capabilities to fully contain the showers. The uncertainty about the beam orientation for all collider stores used in this study and non linearities in the summed signal read out from the ZDC detectors.

The “BBC veto” systematic uncertainty comes from our uncertainty on how often the BBC veto rejects otherwise good events. This occurs mostly due to overlapping events (including beam-gas interactions). The probability depends on the instantaneous luminosity. Based on the studies of embedded zero-bias events, the BBC veto rejects 4% of reconstructable ρ^0 (i.e. those with both tracks in the TPC). We assign a $\pm 50\%$ uncertainty to account for luminosity variations, etc., and arrive at a total uncertainty of 2% for this component of the trigger.

10.6.2 Point-to-point uncertainties for Figure 3

The two ratios shown in Fig. 3 B/A and C/A are extracted from fits to the invariant mass distributions in five rapidity bins and the point-to-point uncertainties identified were related to those fits. The first is related to the fact that we fixed the lower limit in mass. That limit is changed to values above and below the selected default and the maximum relative deviation is taken to be a good estimator of that uncertainty. The fits are done after the mass distributions are corrected with the so called fullChain corrections as functions of pair invariant mass extracted from embedding. Those fullChain corrections are fitted to polynomials. The order of the polynomial has been varied and the highest relative deviation in each of the five rapidity bins is used as our best estimator of the uncertainty related to the mass fullchain correction. As mention in the section about Common uncertainties, the common systematic uncertainty allocated to the TOF detector geometry modeling is included in both ratios because both ratios are expected to be symmetric about $y=0$. As can be seen in Fig. 3, such symmetry is not present in the fit results and the inclusion of this TOF geometry uncertainty is necessary.

An estimate of the magnitude of the systematic uncertainty related to the lower limit in the fits to mass distributions has been extracted by fitting the rapidity dependent distribution in five bins while changing the lower limit in mass in four values of M ; 530, 600, 650 MeV/c². These fits are performed on fully corrected mass distributions which used the fullChain efficiency labelled “Rebin4Pol5” extracted from embedded mass distribution with bin size equal to 10 MeV fitted with a fifth order polynomial. Figures 111 to 115 show the four fits for each of the five rapidity bins.

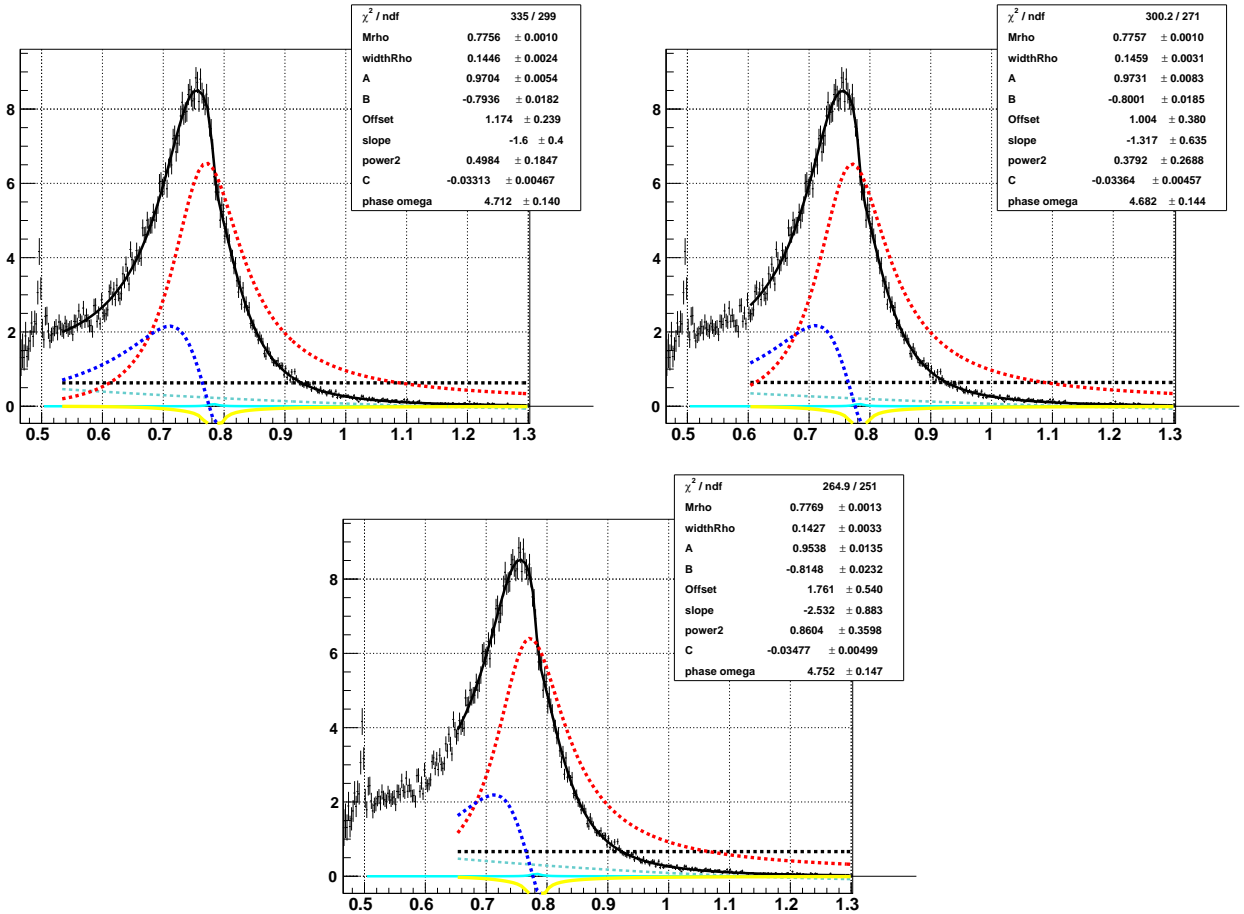


Figure 111: Fits to the fully corrected invariant mass of selected data pion pairs in the rapidity interval $y: [-1., -0.35]$. The lower limit in mass for these fits changes from 530 MeV on the top left panel and grows clockwise to 600 and 650 MeV respectively. As is the case in all rapidity dependent fits in this work, the mass and widths of the ω meson have been fixed to the value obtained in the rapidity integrated fit.

Figure 116 shows the values of B/A and C/A ratios as function of rapidity for the four values of the lower limit in mass. The relative deviation from the average value is also listed in table 18

The fullChain efficiencies extracted from the embedding project are fitted to polynomial functions. The choice of that function introduces an uncertainty in the resulting fits. We estimate such uncertainty by changing the order of the polynomial function from three to five, while the fits continue to be close representation of the distributions extracted from embedding. Figures 118 and ?? show the fits where the fullChain efficiency is fitted

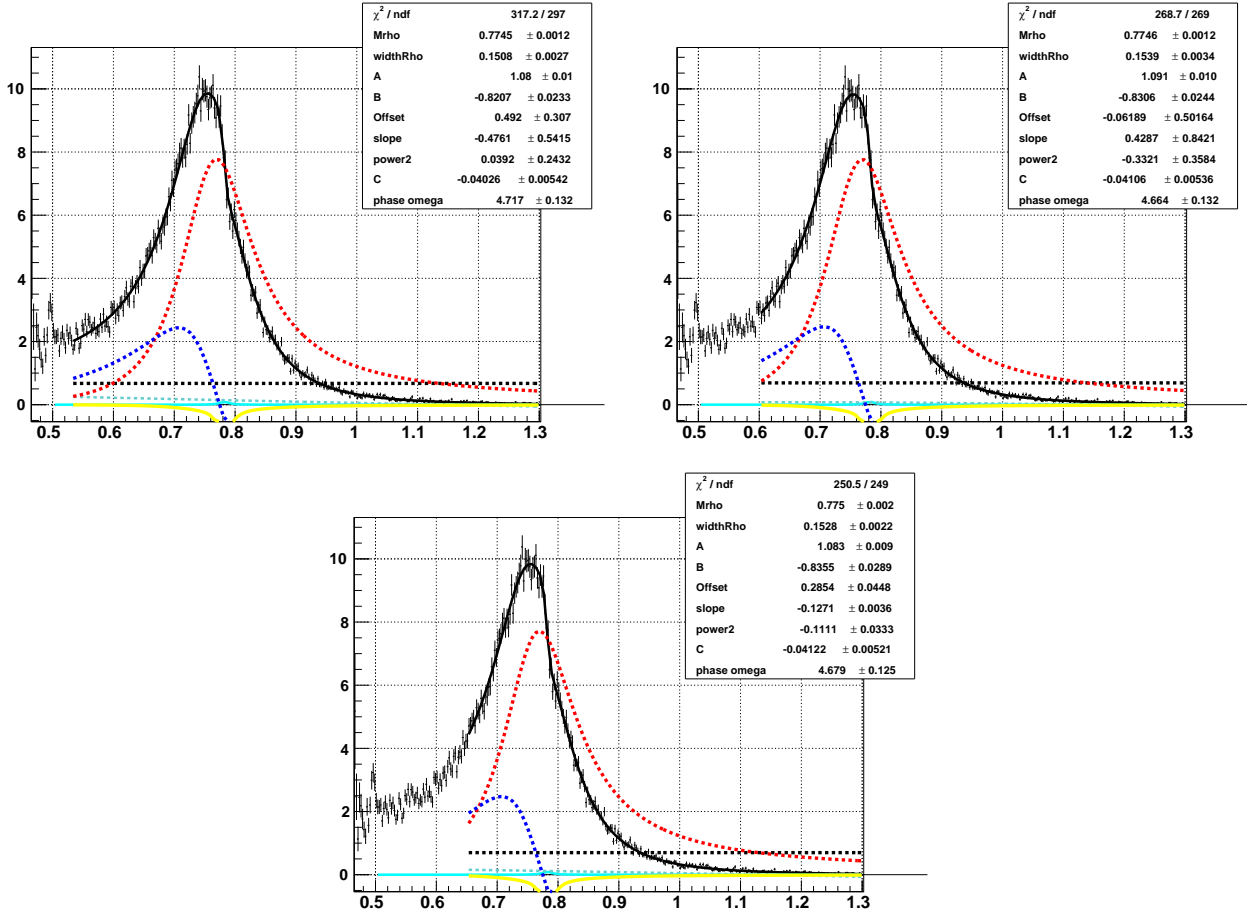


Figure 112: Fits to the fully corrected invariant mass of selected data pion pairs in the rapidity interval $y: [-0.35, -0.15]$. The lower limit in mass for these fits changes from 530 MeV on the top left panel and grows clock-wise to 600 and 650 MeV respectively. As is the case in all rapidity dependent fits in this work, the mass and widths of the ω meson have been fixed to the value obtained in the rapidity integrated fit.

with a fourth and fifth order polynomial respectively. The information for the case of a third order polynomial is obtained from the previous fits where the lower limit of the mass fits is set at 600 MeV.

rapidity	B/A Lower limit of fit	C/A Lower limit of fit	B/A fullChain fit	C/A fullChain fit
-1., -0.35	2.7 %	4 %	2.0%	7.4%
-0.35 -0.15	0.96%	1.1%	0.6%	5.1%
-0.15, 0.15	0.66%	1.0%	1.9 %	3.4%
0.15, 0.35	1.66%	1.1%	1.9%	1.4%
0.35, 1.	0.97%	1.3%	2.3%	3.7%

Table 18: Systematic uncertainties allocated to the B/A and C/A ratios. The fits to the pion pairs invariant mass are normally done from 600 MeV up to 1.3 GeV. Changing the lower limit does produce different values of the B/A, such changes ranged from 500, 550, 600 and 650 MeV. The mass fullChain corrections are used as smooth functions obtained from fits to embedding data. The choice of functions sets another systematic uncertainty and polynomials of third, fourth and fifth order were used to extract a systematic error.

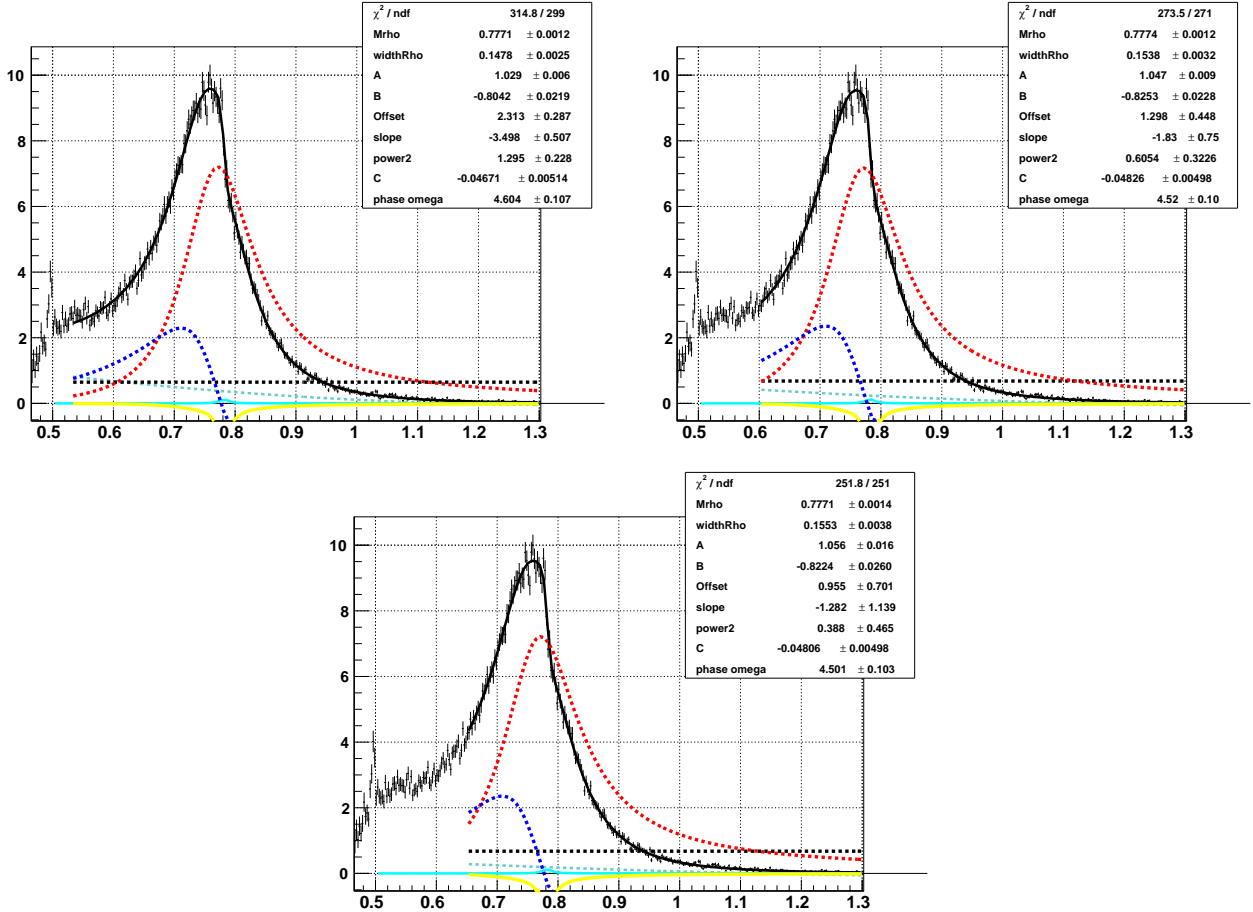


Figure 113: Fits to the fully corrected invariant mass of selected data pion pairs in the rapidity interval $y:[-0.15, 0.15]$. The lower limit in mass for these fits changes from 530 MeV on the top left panel and grows clock-wise to 600 and 650 MeV respectively. As is the case in all rapidity dependent fits in this work, the mass and widths of the ω meson have been fixed to the value obtained in the rapidity integrated fit.

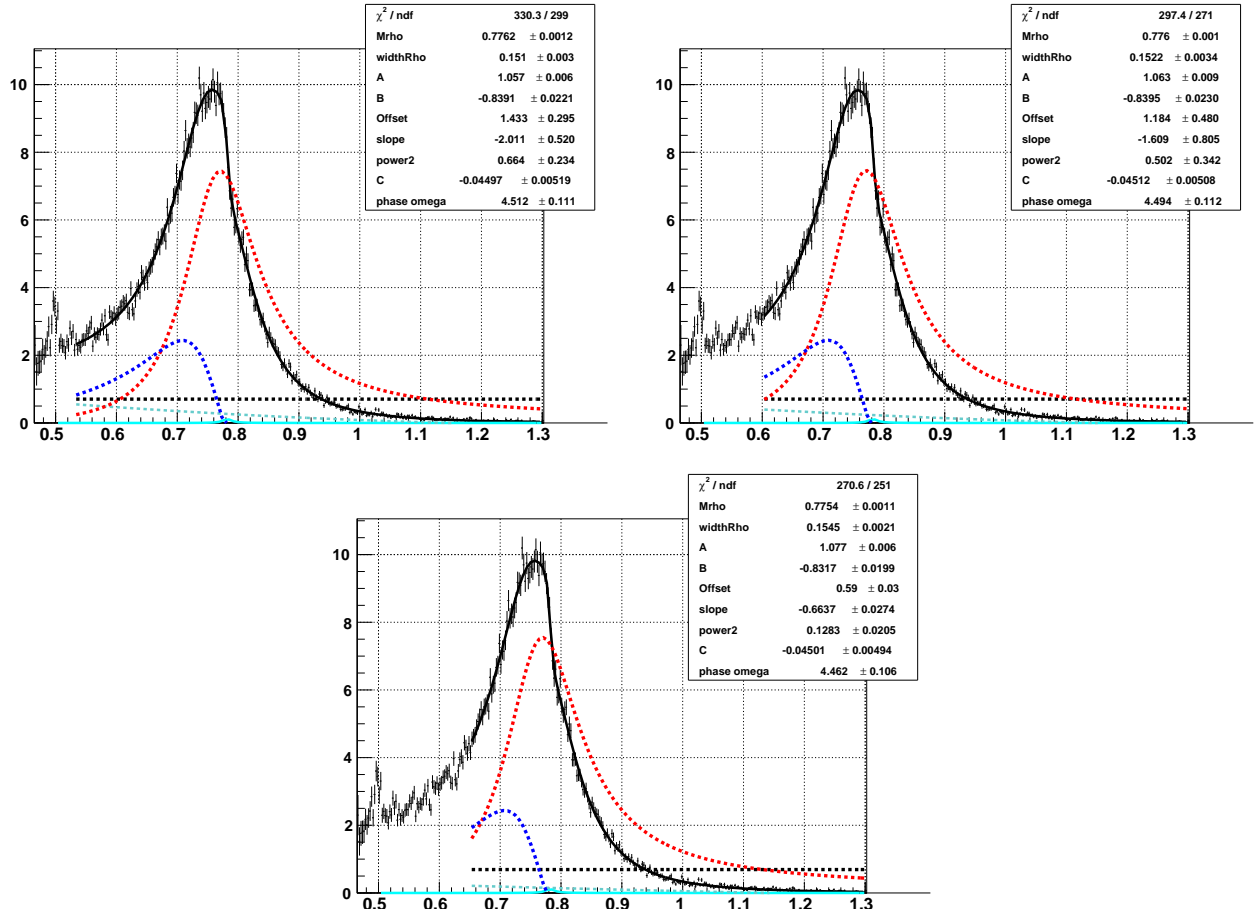


Figure 114: Fits to the fully corrected invariant mass of selected data pion pairs in the rapidity interval $y:[0.15, 0.35]$. The lower limit in mass for these fits changes from 530 MeV on the top left panel and grows clock-wise to 600 and 650 MeV respectively. As is the case in all rapidity dependent fits in this work, the mass and widths of the ω meson have been fixed to the value obtained in the rapidity integrated fit.

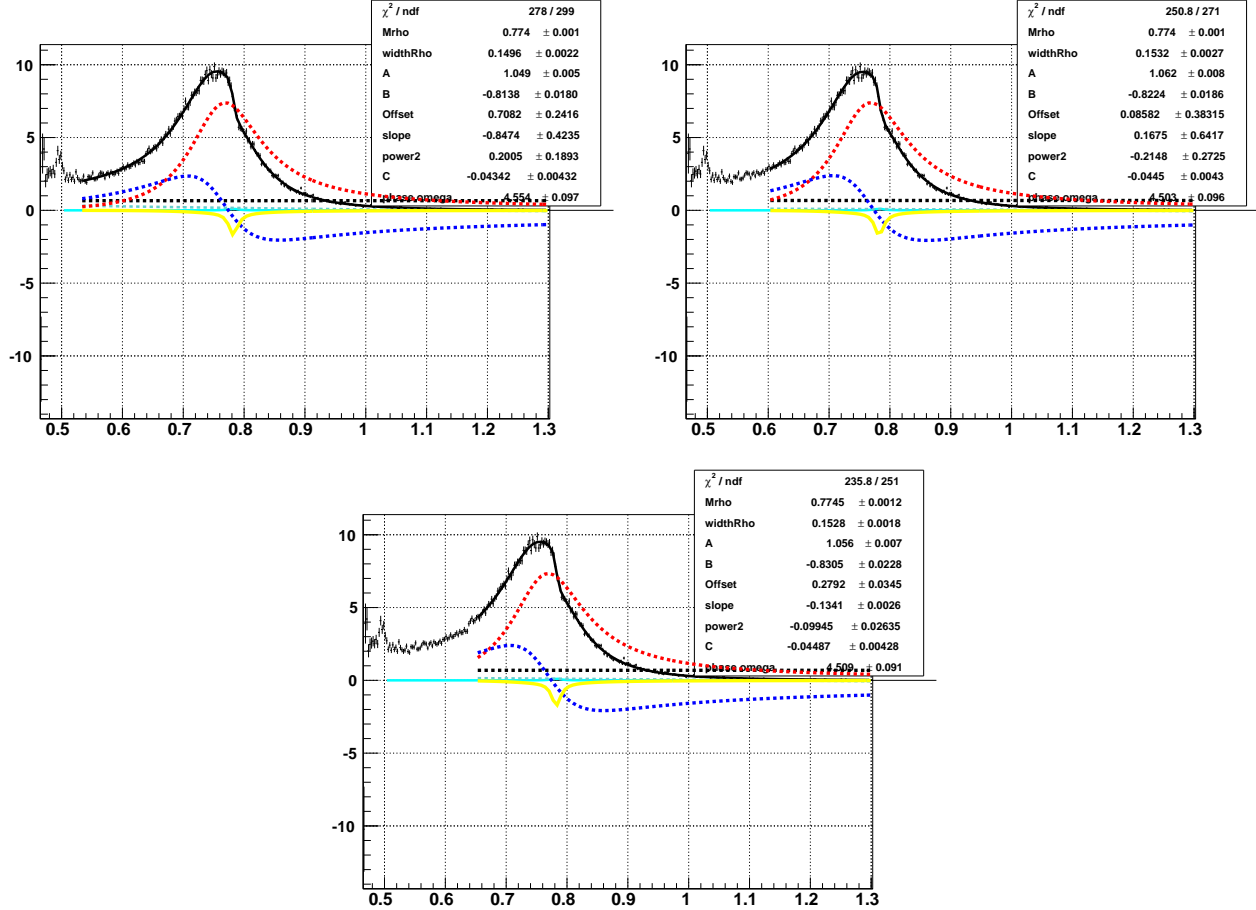


Figure 115: Fits to the fully corrected invariant mass of selected data pion pairs in the rapidity interval $y:[0.35, 1.]$. The lower limit in mass for these fits changes from 530 MeV on the top left panel and grows clock-wise to 600 and 650 MeV respectively. As is the case in all rapidity dependent fits in this work, the mass and widths of the ω meson have been fixed to the value obtained in the rapidity integrated fit.

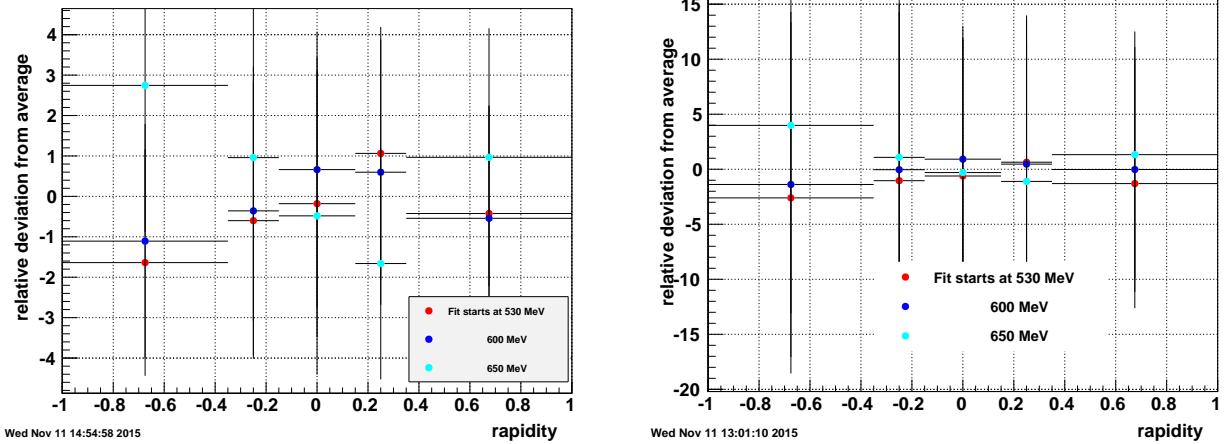


Figure 116: The left panel shows the relative deviations of B/A values extracted for fits that have three lower limits 530, 600 and 650 MeV/c^2 . The deviations are calculated with respect to the average value for the three measurements. the systematic error assigned to the selection of this fit boundary is assigned as being the maximum relative deviation for each rapidity bin. Similar information is shown in the right panel but this time for the C/A ratio.

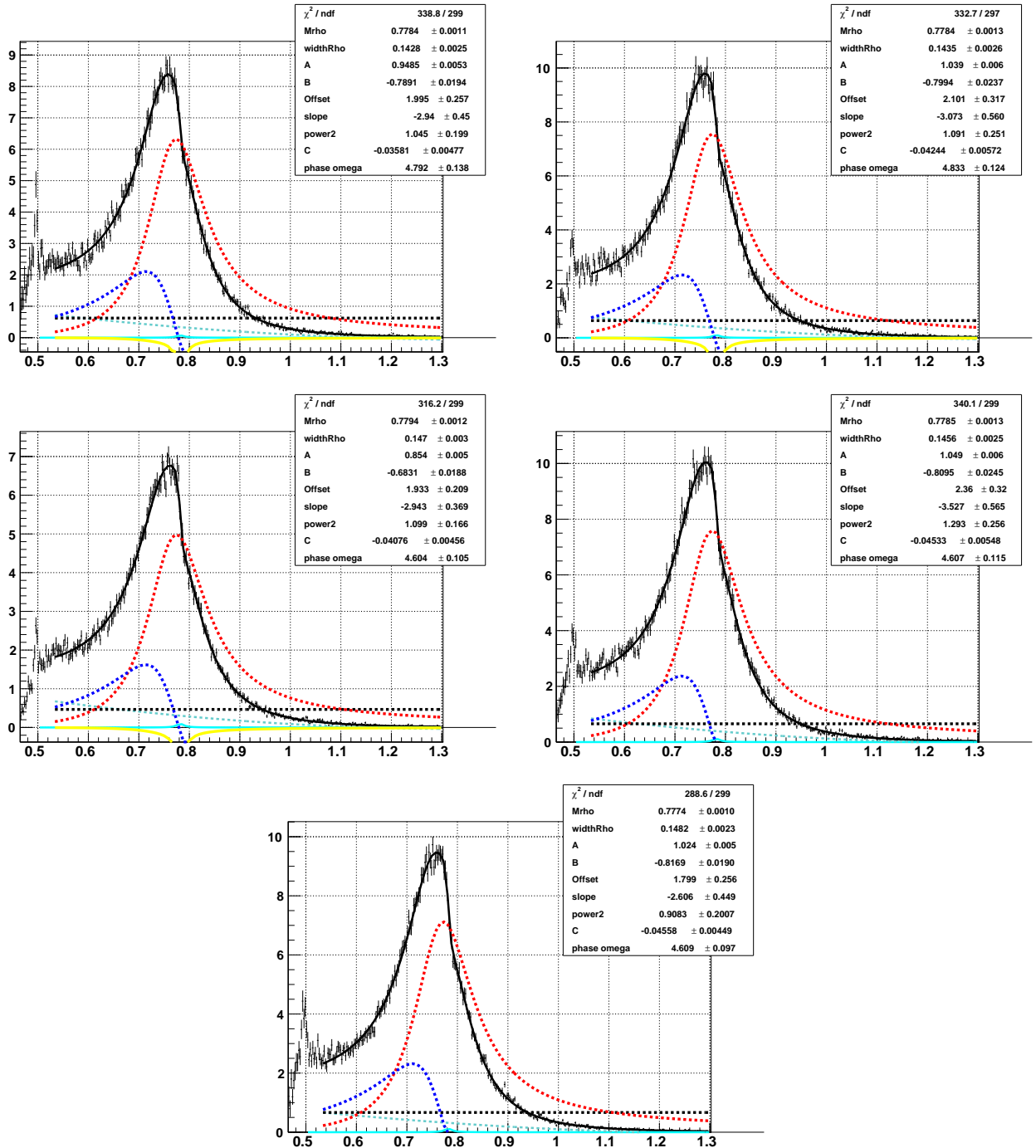


Figure 117: Fits to the fully corrected invariant mass of selected data pion pairs in each rapidity interval. The shape of the mass correction extracted from embedding is fitted with a third order polynomial. As is the case in all rapidity dependent fits in this work, the mass and widths of the ω meson have been fixed to the value obtained in the rapidity integrated fit.

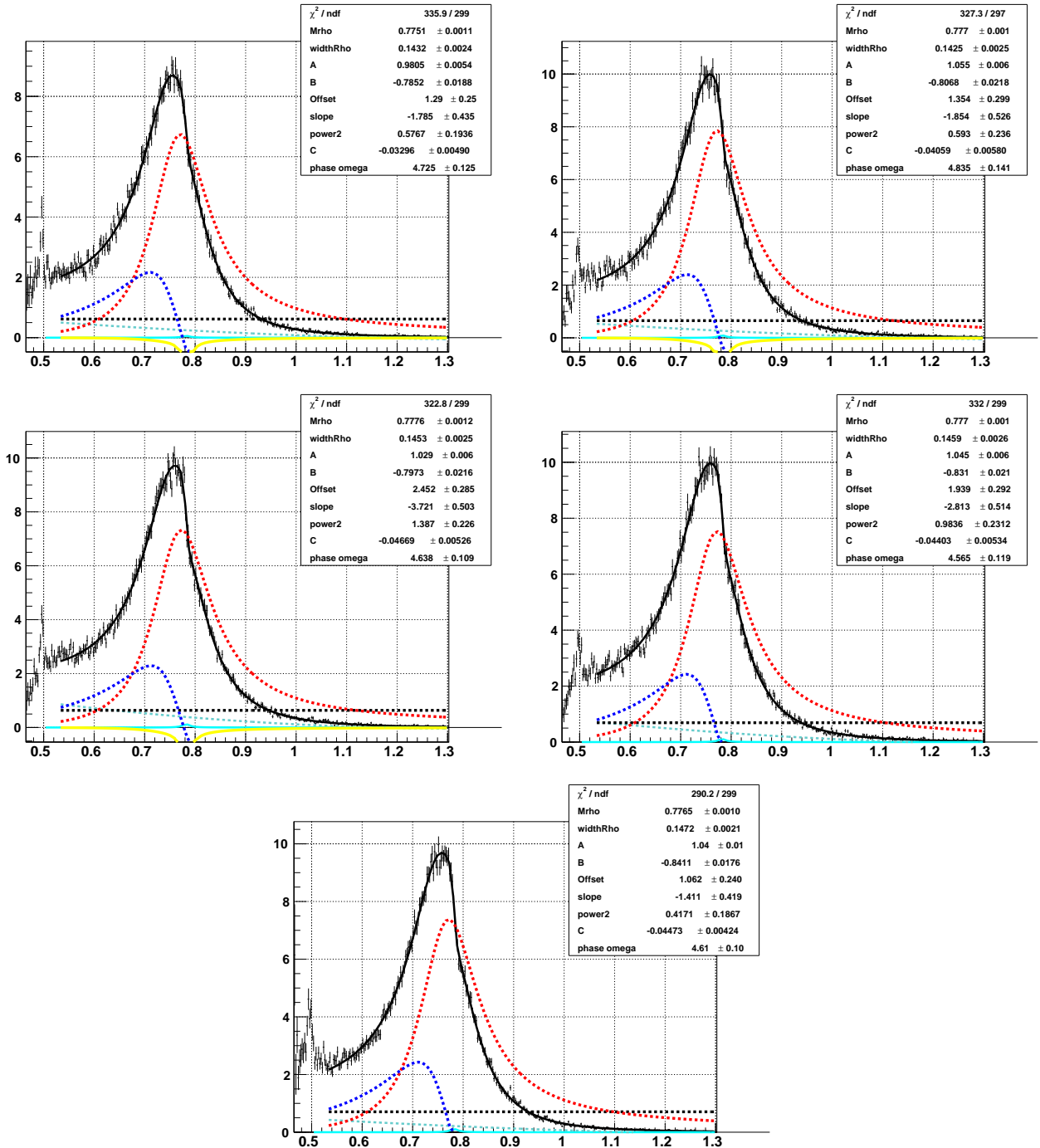


Figure 118: Fits to the fully corrected invariant mass of selected data pion pairs in each rapidity interval. The shape of the mass correction extracted from the embedding project is fitted with a fourth order polynomial. As is the case in all rapidity dependent fits in this work, the mass and widths of the ω meson have been fixed to the value obtained in the rapidity integrated fit.

10.6.3 Systematic uncertainties in the ω meson phase

From the sets of fits performed on the pion pair invariant mass distribution we also extract information about how the ω meson phase changes with the different fit conditions. That information is presented in figures 119 where the changes to the fits were done on the description of the mass correction extracted from embedding, and 120 where we varied the lower bound of the fits. The left panels of each figure shows how the phase changes in the five rapidity bins and the right one displays the relative deviation from an average of the phase in each rapidity bin. From the right panels we select the highest deviation as the systematic uncertainty for the ω phase.

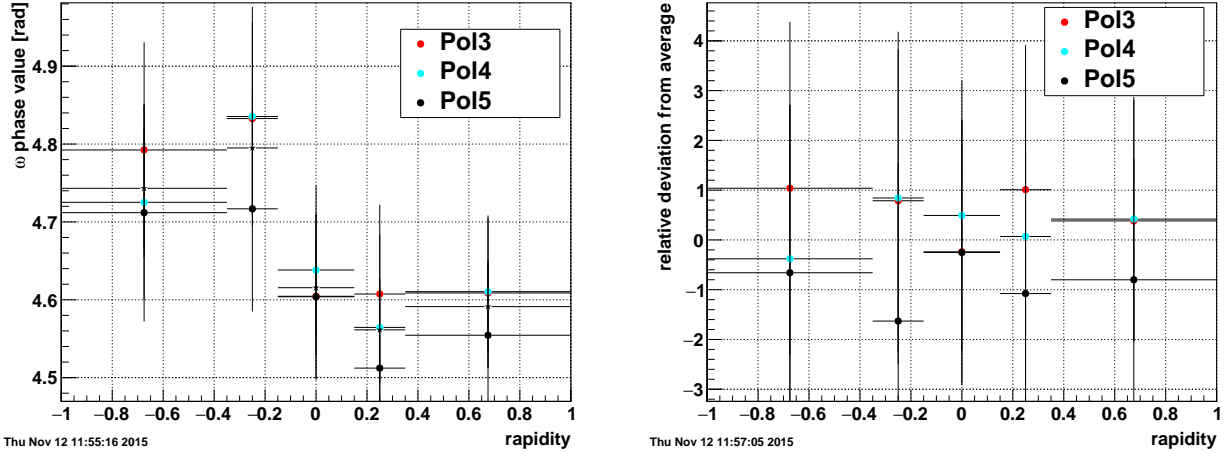


Figure 119: Left panel shows the phase of the ω mesons as extracted from mass fits in five rapidity bins. The black star markers correspond to the average in each bin. The other markers show the result of the fits for three descriptions of the fullChain correction as function of pion pair mass. The right panel shows the relative deviation from the average value in each rapidity bin. The biggest deviation is then considered as the systematic uncertainty for the ω phase related to the description of the mass corrections with polynomials.

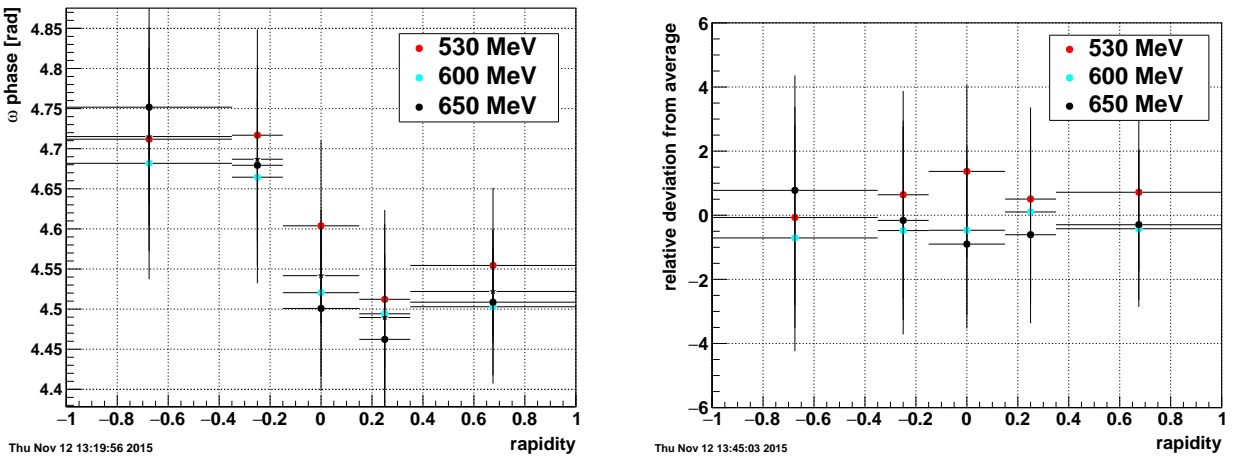


Figure 120: The left panel shows the phase of the ω mesons as extracted from mass fits in five rapidity bins. The black star markers correspond to the average in each bin. The other markers show the result of the fits for three values of the lower bound in the fits to the pion pair mass distribution. The right panel shows the relative deviation from the average value (in percent) in each rapidity bin. The biggest deviation is then considered as the systematic uncertainty for the ω phase related to the setting of lower bound in the fits.

The results of this study are summarized in table 19. From this table we can also pick the highest relative deviation from all rapidity bins and quote that number as the systematic uncertainty on the ω mesons extracted from the fit to the mass distribution integrated over rapidity. The phase will then be quoted as $\phi_\omega = 1.726 \pm 0.126(stat) \pm 0.08(syst)$ radians. We can also combine the statistical and systematic errors reading the highest relative deviation at the edge of the error bars and quote: $\phi_\omega = 1.726 \pm 0.148(stat + sys)$.

<i>rapidity</i>	ω phase Lower limit of fit	ω phase fullChain fit
-1., -0.35	0.75 %	1.0%
-0.35 -0.15	0.64%	1.6%
-0.15, 0.15	1.37%	0.5 %
0.15, 0.35	0.61%	1.1%
0.35, 1.	0.72%	0.8%

Table 19: Systematic uncertainties allocated to the B/A and C/A ratios. The fits to the pion pairs invariant mass are normally done from 600 MeV up to 1.3 GeV. Changing the lower limit does produce different values of the B/A, such changes ranged from 500, 550, 600 and 650 MeV. The mass fullChain corrections are used as smooth functions obtained from fits to embedding data. The choice of functions sets another systematic uncertainty and polynomials of third, fourth and fifth order were used to extract a systematic error.

10.6.4 Point-to-point uncertainties for Figure 4

Three systematic uncertainties related to track selection and particle identification were studied during the extraction of the rapidity distribution shown in Fig. 4. All three are extracted by generating data distributions with a set of two or three values for a particular parameter. The full chain corrections necessary to normalize the data are also extracted with the same parameter value. Relative deviations are calculated with respect to the distribution produced with the default value. The widest deviations are then listed in the table 20 in four coarse rapidity bins.

rapidity	PID cut	Fit to eff.	Number of track hits
-0.70, -0.5	8.%	0.25%	0.2%
-0.5, 0.	5.%	0.25%	0.05%
0., 0.5	5.%	0.25%	0.05%
0.5 - 0.7	8.%	0.25%	0.2%

Table 20: An estimate for three point-to-point systematic uncertainties identified in the generation of the rapidity distribution shown in Fig. 4 of the paper shown as a per-cent of the measured cross-section in four rapidity ranges.

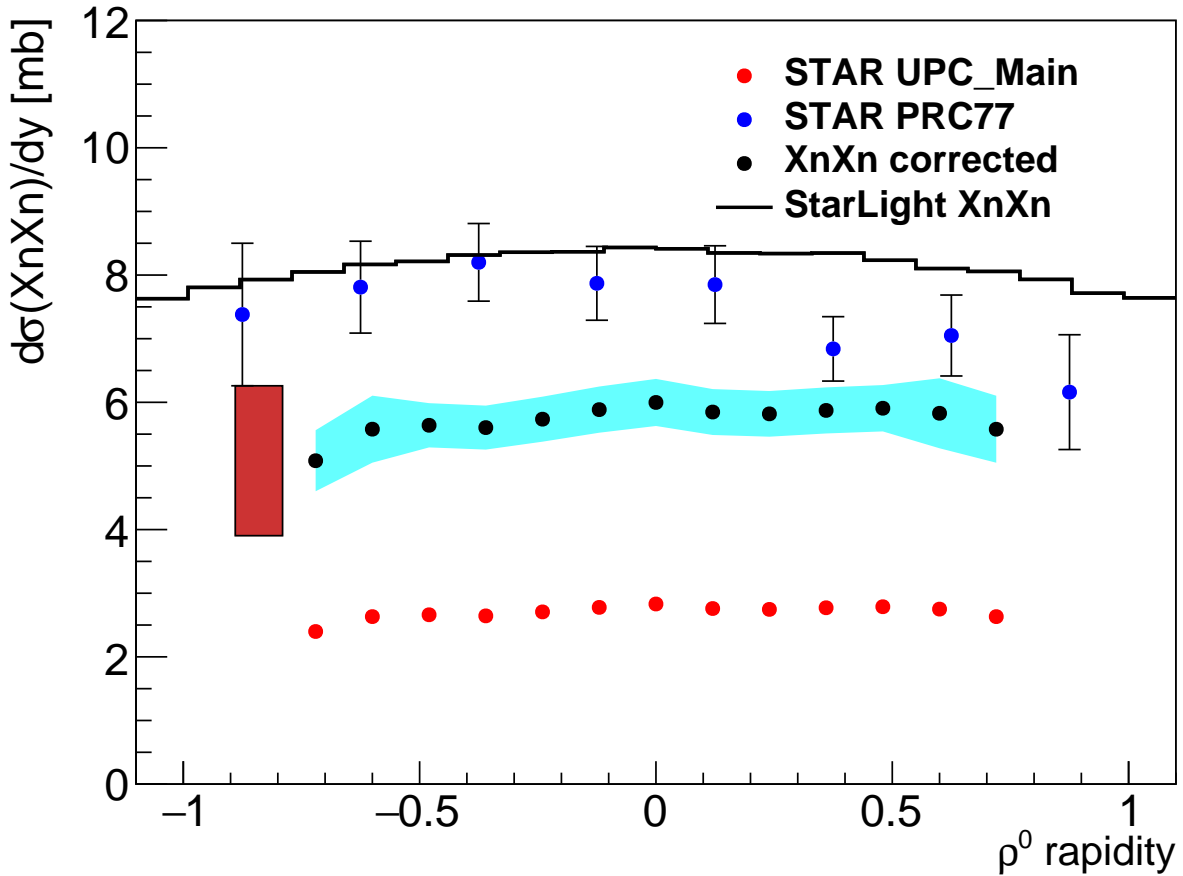


Figure 121: The red markers show the cross-section as function of rapidity distribution for exclusively photo-produced ρ^0 mesons reconstructed in events selected with the STAR UPC_Main trigger. Only their statistical errors are displayed and they are all smaller than the markers. The black points show the same distribution scaled up to the full XnXn cross-section. The magnitude of the scaling was obtained using the RELDIS event generator (see text for details [15]). Statistical errors are shown with black vertical lines. The sum in quadrature of all point-to-point systematic uncertainties identified for this measurement is shown with the cyan band. The sum in quadrature of all common systematic uncertainties ($\sim 17\%$) is shown with the red box at the left side of the figure. The blue markers show the previous STAR measurement [14]. The black histogram shows the rapidity distribution of XnXn STARLight events.

10.6.5 Point-to-point uncertainties for Figure 6

$-t_{\text{range}}[(GeV/c)^2]$	track sel.	pion PID	Incoherent comp.	sub.
0 - 0.02	0.2%	8%		0.5%
0.02 - 0.04	0.2%	8%		3.0%
0.04 - 0.1	0.2%	8%		8.5%

Table 21: An estimate for five point-to-point systematic uncertainties identified in the generation of the $-t$ distribution shown in Fig. 6 of the paper, listed as a per-cent of the measured cross-section in three $-t$ ranges.

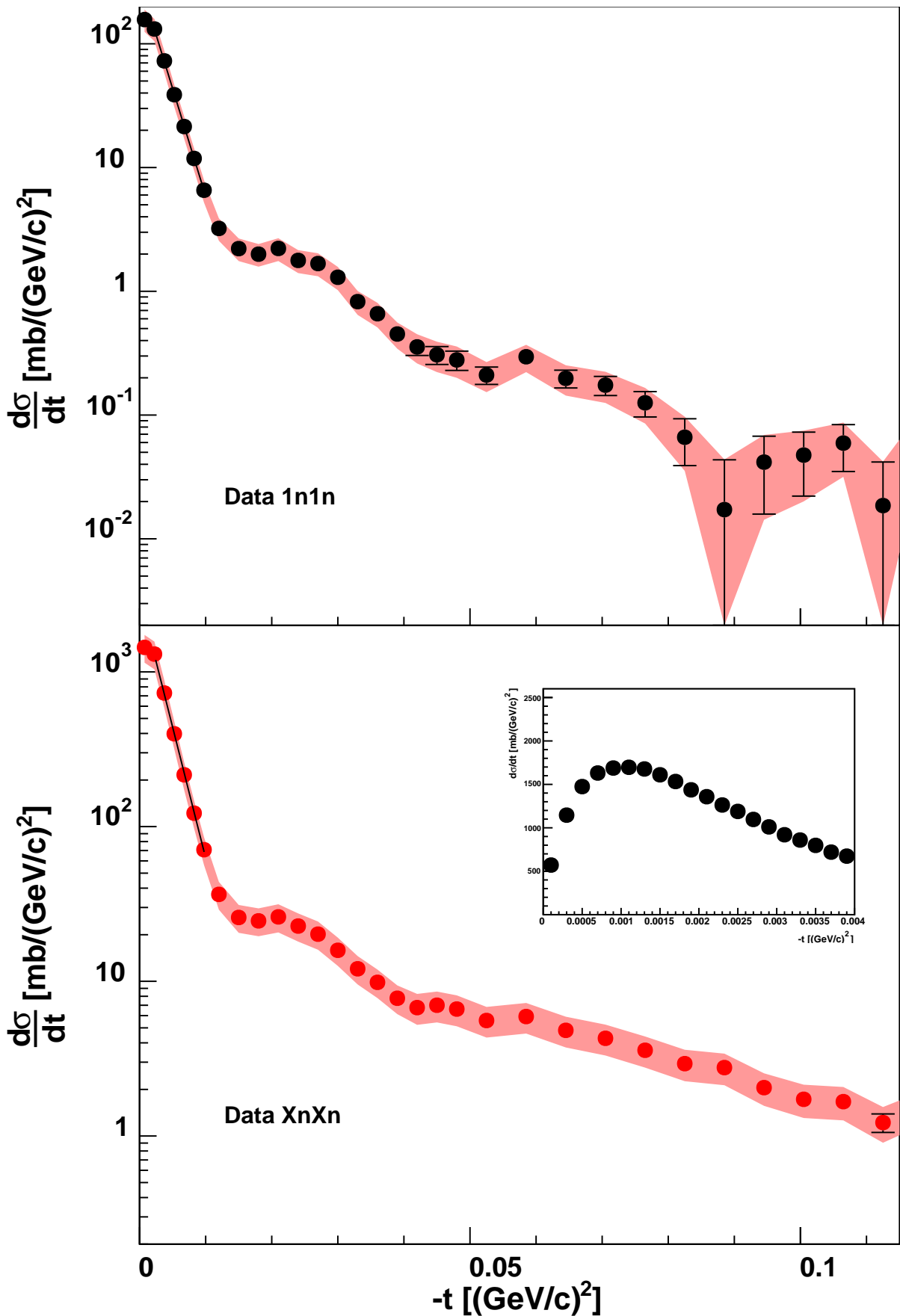


Figure 122: Fully normalized coherent diffraction pattern for ρ^0 mesons detected in exclusive XnXn events within a window in the vertex z coordinate of $|V_z| < 50$ cm. The filled band shows the sum in quadrature of all systematic uncertainties listed in table 21, the statistical errors are shown as vertical lines. The insert shows, with finner binning, the effects of the interference occurring in these UPC interactions as each ion is a source of ρ^0 mesons.

11 Appendix

11.1 Enhancing f2 and ρ' signal with pair p_T cuts

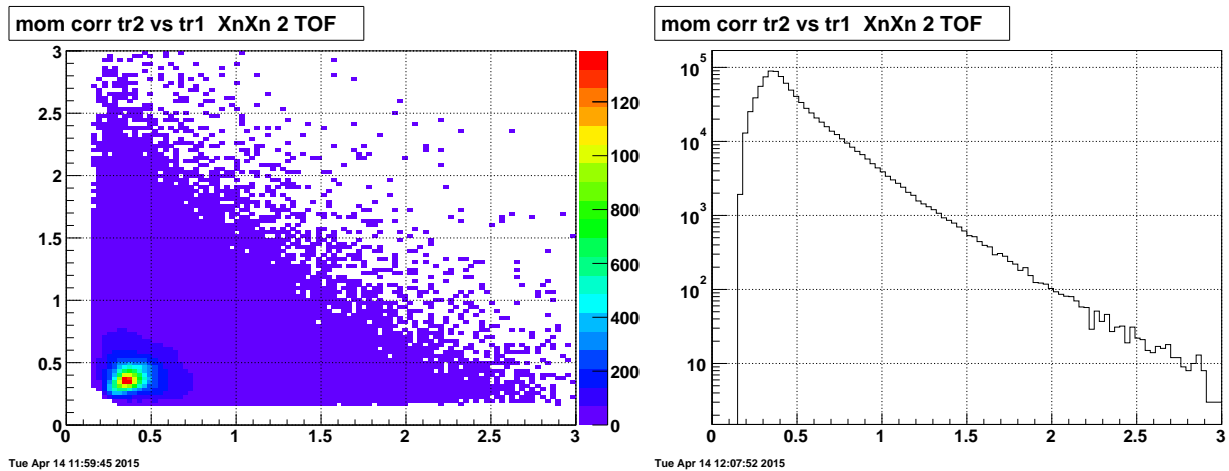


Figure 123: .

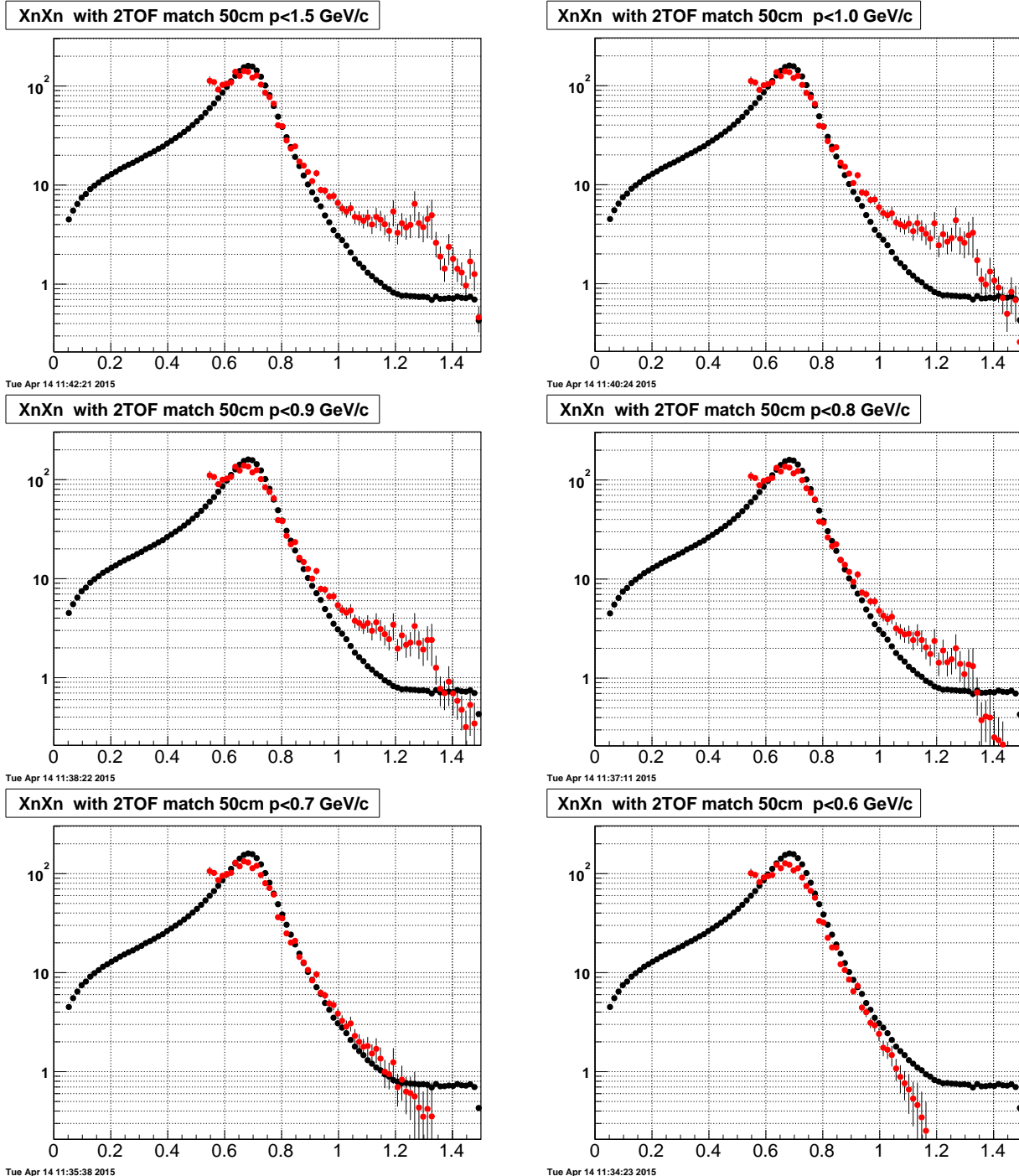


Figure 124: .

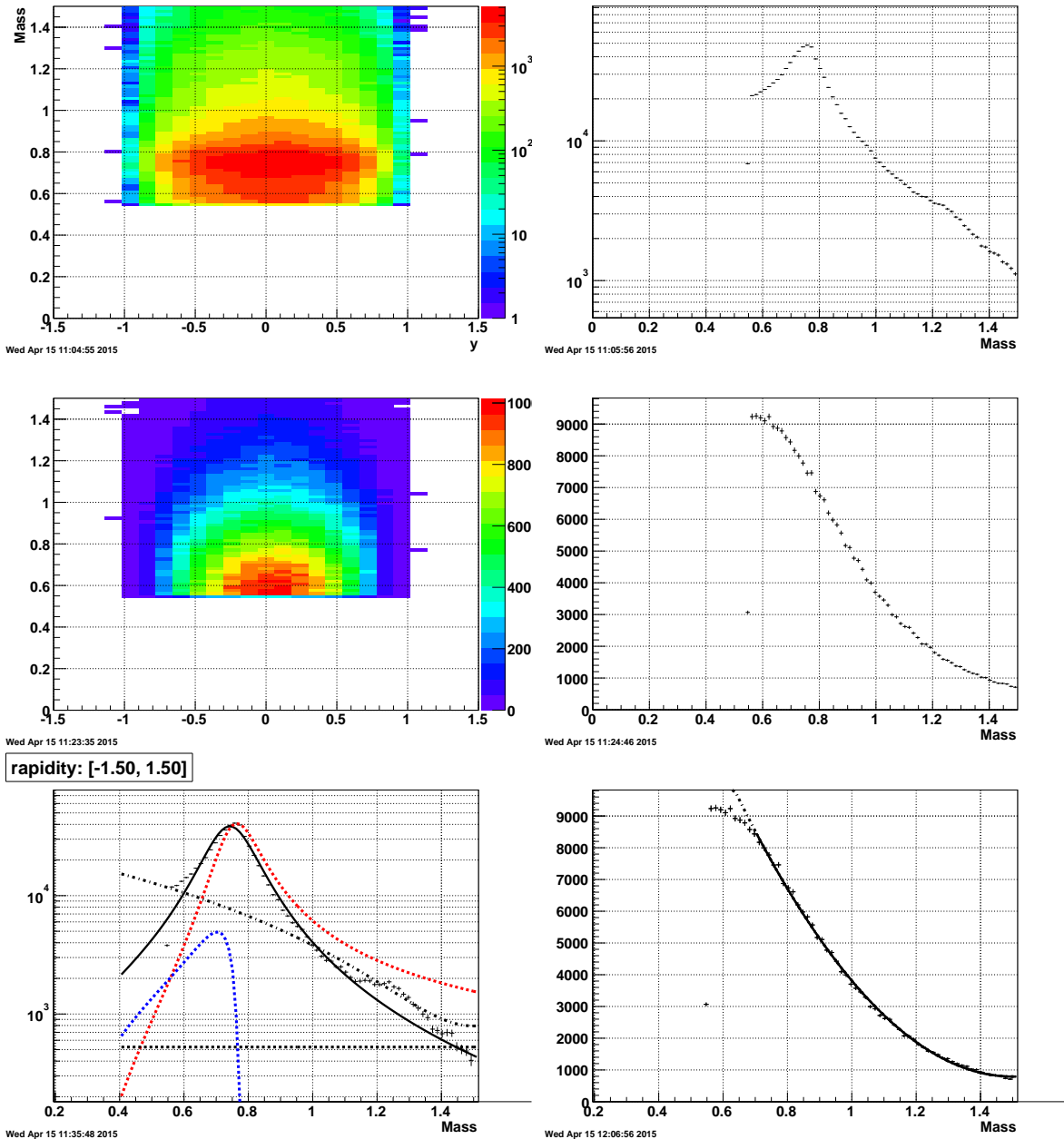


Figure 125: details about fits with cuts on the sum of pair momenta. No cut

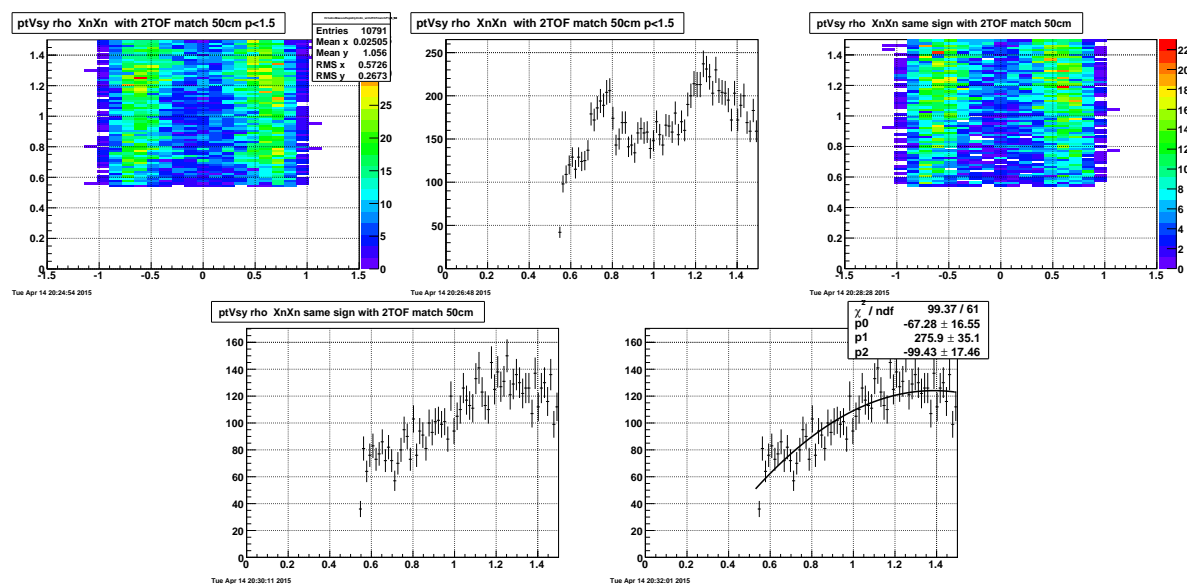


Figure 126: .

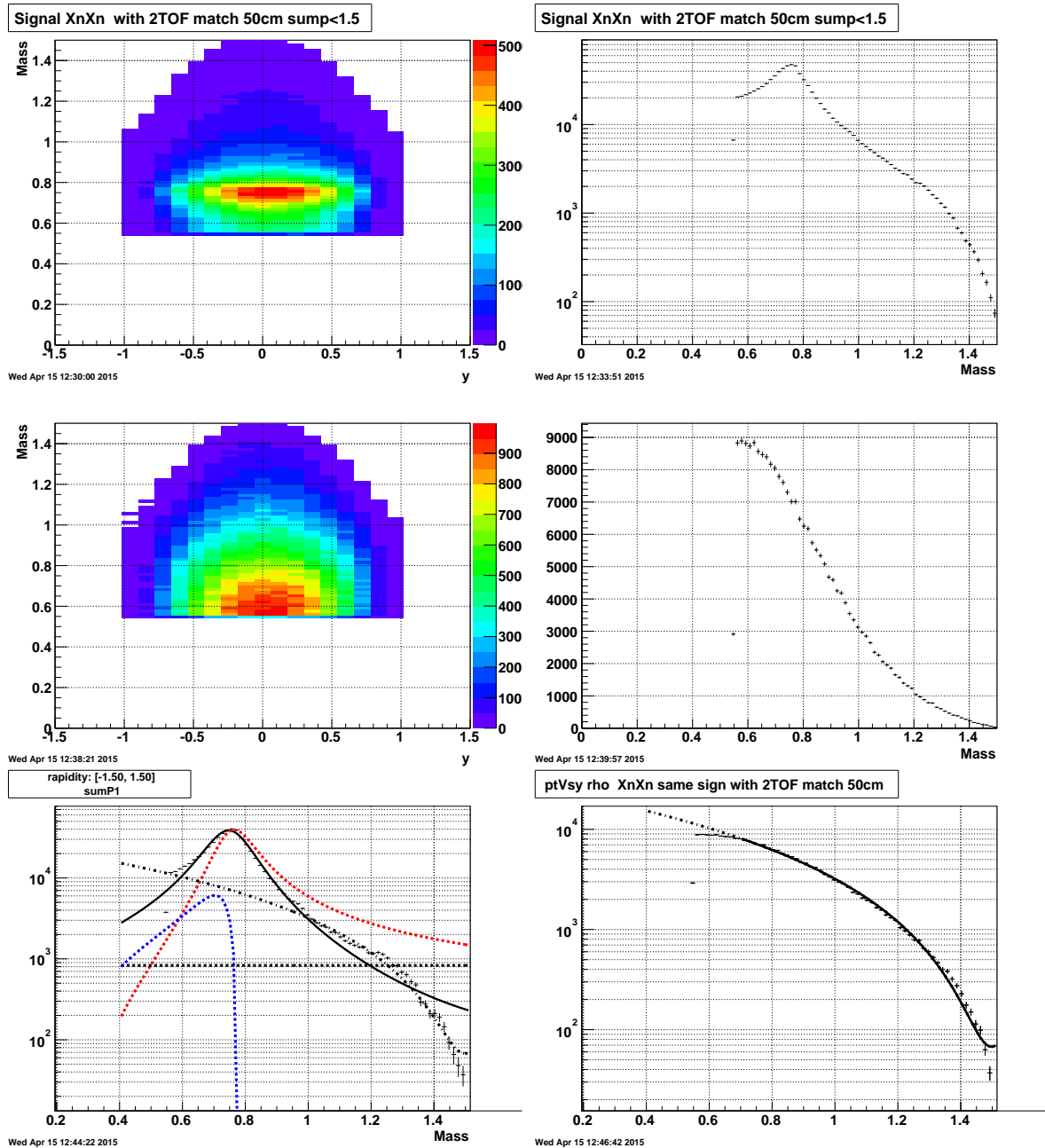


Figure 127: details about fits with cuts on the sum of pair momenta. $\text{sum}P < 1.5 \text{ GeV}/c$

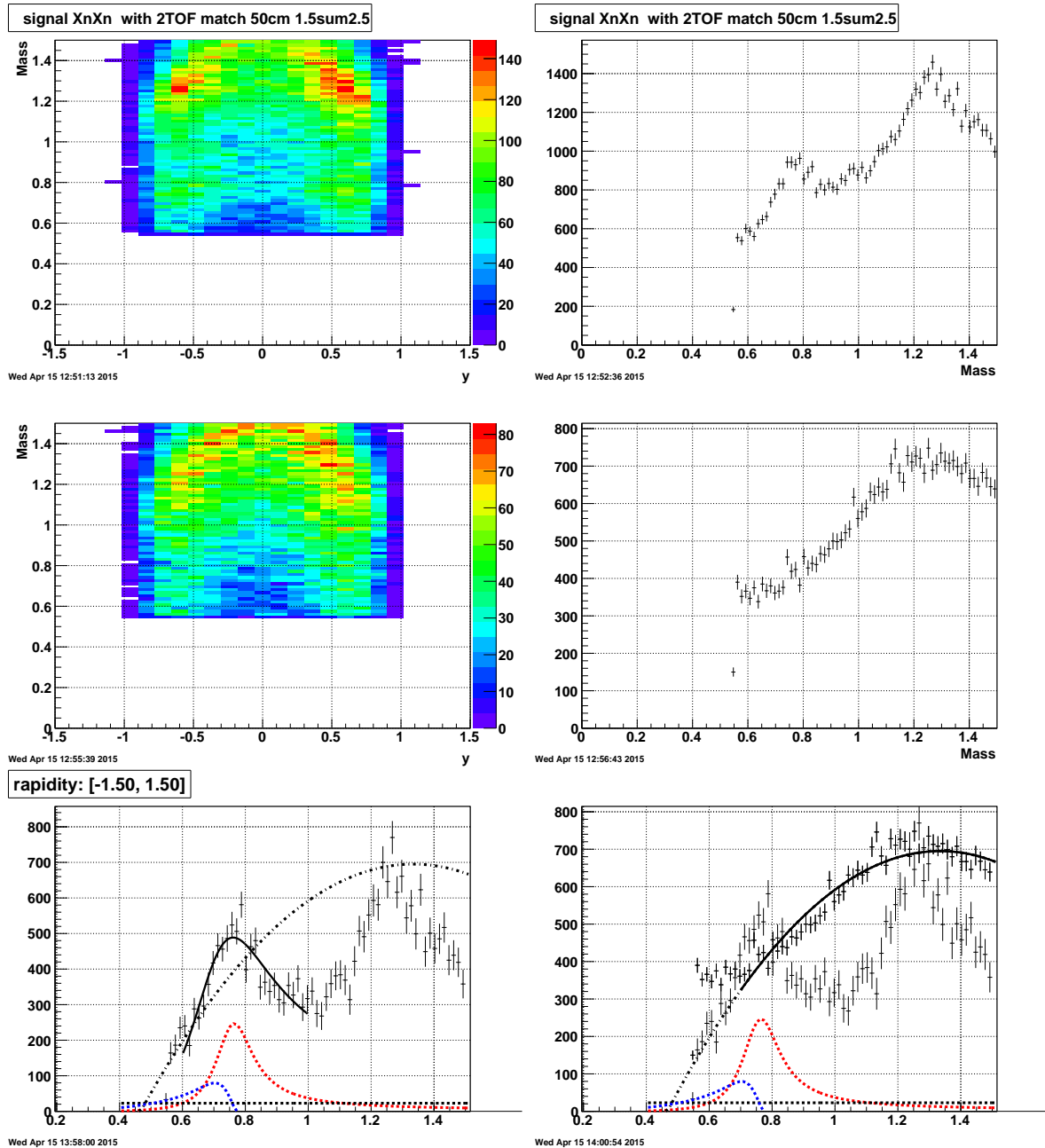


Figure 128: details about fits with cuts on the sum of pair momenta. sum $1.5 < P < 2.5 \text{GeV}/c$

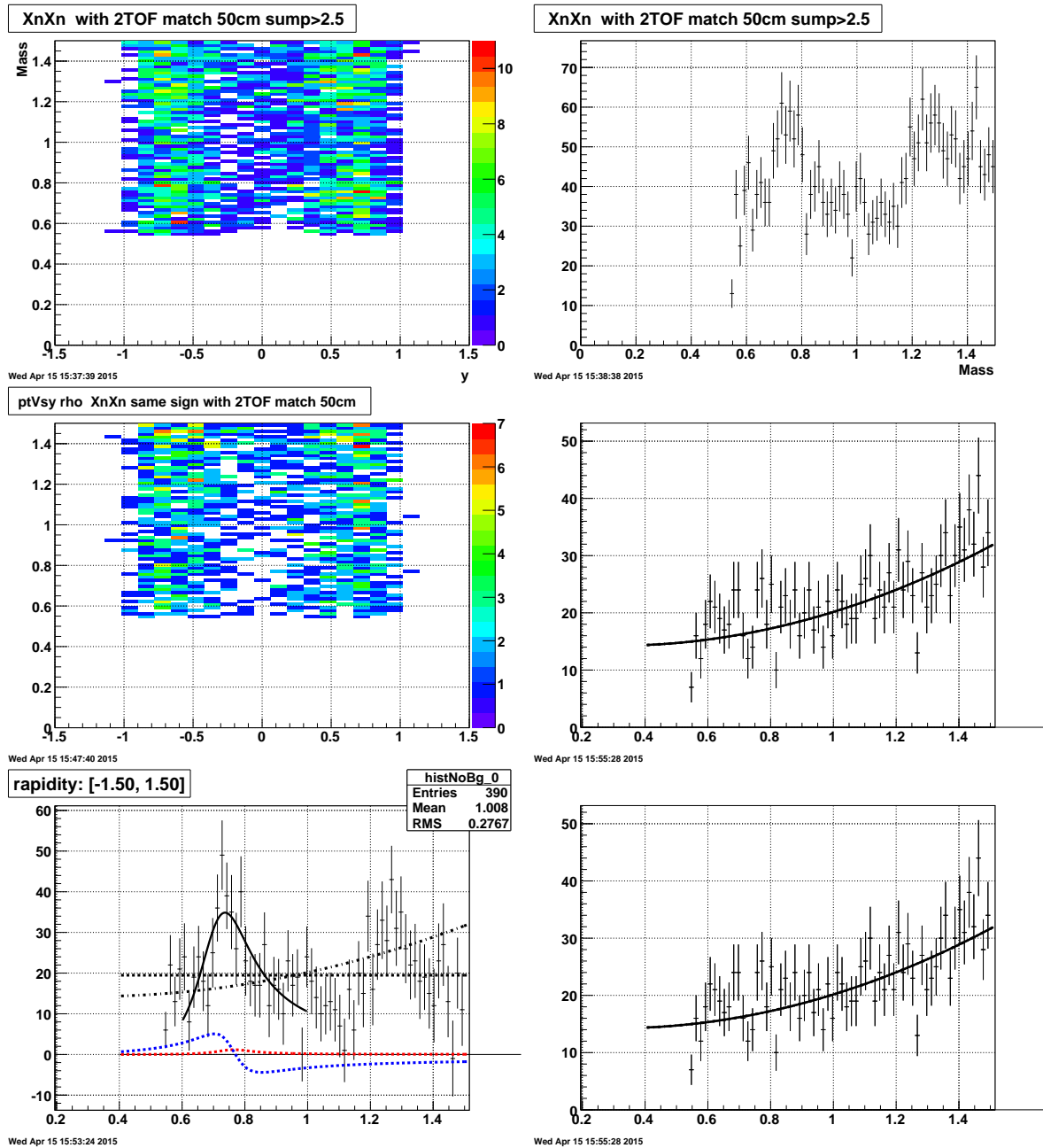


Figure 129: details about fits with cuts on the sum of pair momenta. sum $P > 2.5$

12 Appendix 2: Reconstruction efficiency (first embedding request)

A first embedding request was submitted to mix generated pion pairs from the decay of ρ^0 mesons generated by starlight into ZEROBIAS triggered events.:
<https://drupal.star.bnl.gov/STAR/starsimrequests/2011/sep/09/rho-meson-embedded-zerobias-data-upc-st>

At the time this request was submitted it was thought that the main purpose of such embedding was the extraction of the tracking efficiency of ρ^0 decayed pions in the STAR TPC using zerobias events as a good proxy of the 2010 run backgrounds. Further analysis forced us to realize that such embedding request suffered from too many drawbacks; the lack of vertex reconstruction and its absence of simulation of the TOF detector which is such an important part of the trigger of the UPC events. We present selected results from the first embedding request just as a sample of isolated tracking efficiencies and acceptance in the TPC.

A note has been prepared with detailed explanations of the steps in the analysis performed to extract tracking efficiencies for the pions as well as the mesons.

<http://www.star.bnl.gov/protected/pcoll/ramdebbe/embeddingEfficiency.pdf>

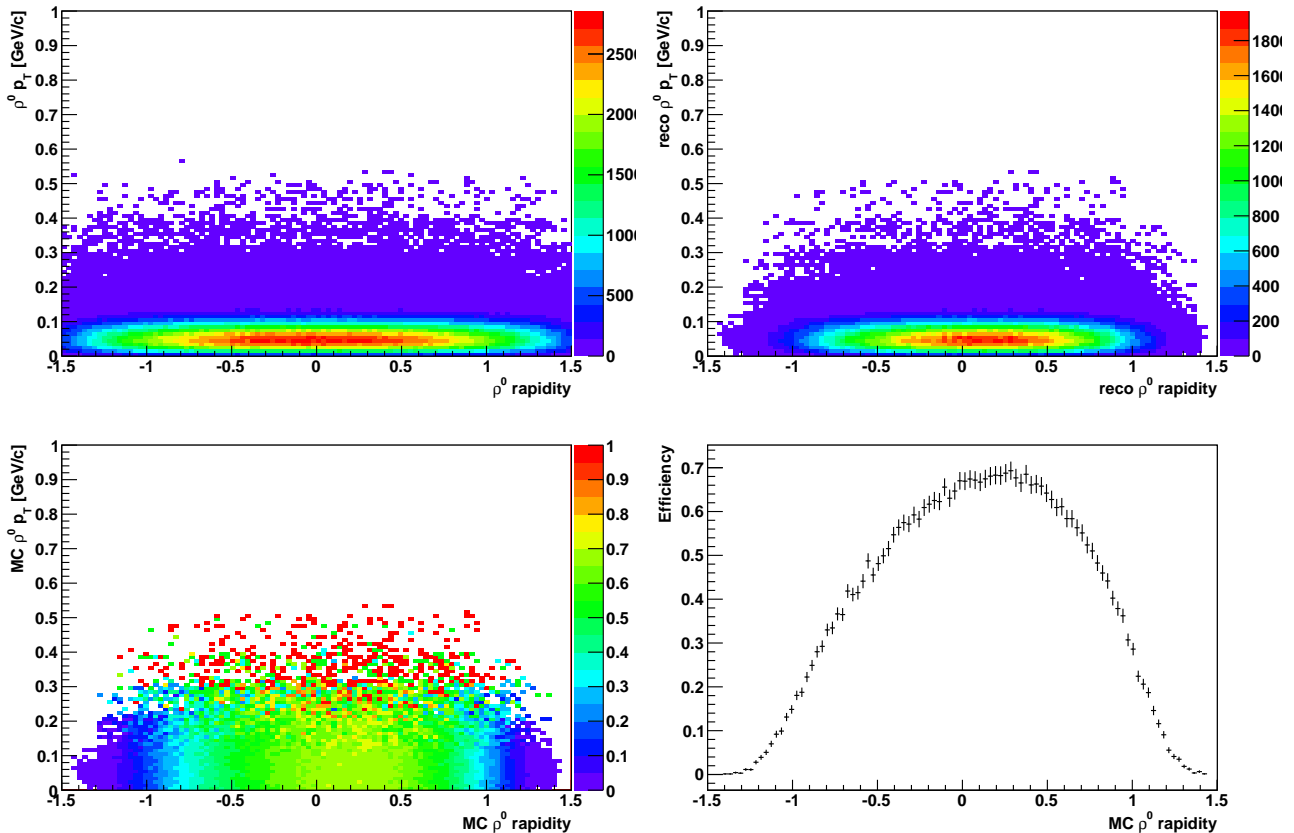


Figure 130: Efficiency for ρ^0 reconstruction in events with vertex in window: $|V_z| < 150\text{cm}$.

We also explored the possible changes in efficiency in the ρ^0 meson reconstruction if the vertex windows are modified. Figure 130 shows a summary of the calculation for the widest vertex window.

As seen in Fig. 131 the efficiencies do not change whenever they are calculated from narrower and narrower vertex windows. The left panel shows the efficiency for ρ^0 meson reconstruction and the right one the efficiency extracted for negative pions as function of pseudo-rapidity at $p_T=408\text{MeV}/c$ for all vertex windows.

Figure 132 shows that the reconstruction efficiency for ρ^0 decayed into a charged pion pair is constant as a function of the pair momentum.

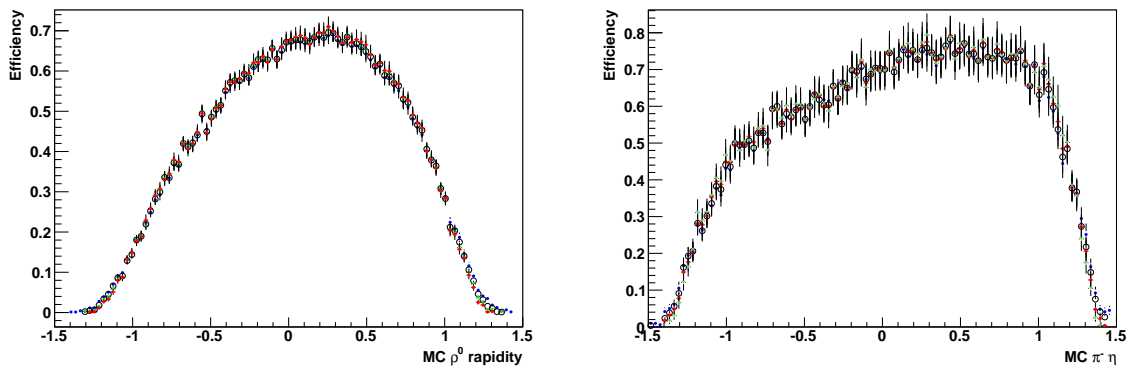


Figure 131: Left panel: efficiency for ρ^0 reconstruction as function of rapidity in events with all four vertex cuts. Right panel: efficiency for π^- reconstruction as function of its pseudo-rapidity extracted from events with all four vertex cuts.

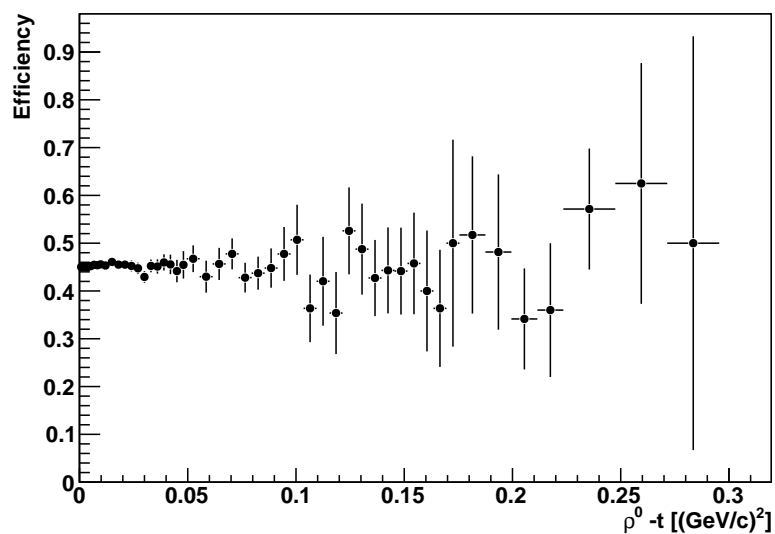


Figure 132: Efficiency for ρ^0 reconstruction as function of transverse momentum.

References

References

- [1] STAR note SN0447: Vernier scan technical note and preliminary result from 130 GeV AuAu collisions.
- [2] A. Baltz, *et al.*, Nucl. Instrum. and Methods, **A417** (1998) 1.
- [3] J. Nystrand and S. Klein, nucl-ex/9811007.
- [4] C. Adler, *et al.*, Phys. Rev. Lett. **89**, 272302 (2002).
- [5] B. I. Abelev *et al.* [STAR Collaboration], Phys. Rev. C **77** (2008) 034910 [arXiv:0712.3320 [nucl-ex]].
- [6] I. A. Pshenichnov, J. P. Bondorf, I. N. Mishustin, A. Ventura and S. Masetti, Phys. Rev. C **64**, 024903 (2001) [nucl-th/0101035].
- [7] S. R. Klein, arXiv:1502.06662 [nucl-ex].
- [8] Alvensleben, H. and others, Phys. Rev. Lett. **27**, 888 (1971)
- [9] J. Wu *et al.*, Nucl. Instrum. Meth. A **538**, 243-248 (2005).
- [10] STAR note SN0447: Vernier scan technical note and preliminary result from 130 GeV AuAu collisions.
- [11] A. Baltz, *et al.*, Nucl. Instrum. and Methods, **A417** (1998) 1.
- [12] J. Nystrand and S. Klein, nucl-ex/9811007.
- [13] C. Adler, *et al.*, Phys. Rev. Lett. **89**, 272302 (2002).
- [14] B. I. Abelev *et al.* [STAR Collaboration], Phys. Rev. C **77** (2008) 034910 [arXiv:0712.3320 [nucl-ex]].
- [15] I. A. Pshenichnov, J. P. Bondorf, I. N. Mishustin, A. Ventura and S. Masetti, Phys. Rev. C **64**, 024903 (2001) [nucl-th/0101035].
- [16] M. Klusek-Gawenda, M. Ciemala, W. Schafer and A. Szczurek, Phys. Rev. C **89**, no. 5, 054907 (2014) doi:10.1103/PhysRevC.89.054907 [arXiv:1311.1938 [nucl-th]].
- [17] K. A. Olive *et al.* [Particle Data Group Collaboration], Chin. Phys. C **38**, 090001 (2014). doi:10.1088/1674-1137/38/9/090001